University Of Nevada, Reno

SOURCE GRID INTERFACE OF WIND ENERGY SYSTEMS

A thesis submitted in partial fulfillment of the requirements for the degree of Master of Science in Electrical Engineering

by

Abhishek P. Chitnis

Dr. Andrzej M. Trzynadlowski, Thesis Advisor

May, 2014

UNIVERSITY OF NEVADA RENO

THE GRADUATE SCHOOL

We recommend that the thesis
prepared under our supervision by

ABHISHEK P. CHITNIS

entitled

Source Grid Interface of Wind Energy Systems

be accepted in partial fulfillment of the
requirements for the degree of

MASTER OF SCIENCE

Andrzej Trzynadlowski M. Trzynadlowski, Ph.D., FIEEE, Advisor

Sami M. Fadali, Ph.D., Committee Member

Dhanesh Chandra, Ph. D., Graduate School Representative

Marsha Read, Ph. D., Dean, Graduate School

May, 2014

ABSTRACT

Wind power is one of the most developed and rapidly growing renewable energy sources. Through extensive literature review this thesis synthesizes the existing knowledge of wind energy systems to offer useful information to developers of such systems. Any prototyping should be preceded by theoretical analysis and computer simulations, foundations for which are provided here.

The thesis is devoted to an in-depth analysis of wind energy generators, system configurations, power converters, control schemes and dynamic and steady state performance of practical wind energy conversion systems (WECS). Attention is mainly focused on interfacing squirrel cage Induction generators (SCIG) and doubly-fed induction generators (DFIG) with the power network to capture optimal power, provide controllable active and reactive power and minimize network harmonics using the two-level converter, as a power electronic converter.

Control of active and reactive power, frequency and voltage are indispensable for stability of the grid. This thesis focuses on two main control techniques, field oriented control (FOC) and direct torque control (DTC) for the SCIG. The dynamic model of induction generator is non-linear and hence for all types of control, the flux and the torque have to be decoupled for maintaining linearity between input and output for achieving high dynamic performance. FOC is used for decoupled control for rotor flux λr and electromagnetic torque ζe. The stator current is decomposed into flux and torque producing components and they both are controlled independently. FOC uses three feedback control loops generate gating signals for the converter. DTC also achieves high dynamic performance by decoupling of rotor flux and electromagnetic torque without the intermediate current loops. DTC asks for the estimation of stator flux and torque and like FOC has 2 branches which have flux and torque comparators. The errors between the set and the estimated value are used to drive the inverters. The two methods are valid for both steady and transient state. Their validity is confirmed by simulating the systems on MATLAB/Simulink platform and comparing them the results obtained by hand calculations.

Further DFIG's are introduced. The dynamic model is developed using the machines equivalent circuit and is expressed in the stationary, rotor and the synchronous reference frames for evaluating the performance of the machine. The stator of the DFIG is directly interfaced to the grid and by controlling the rotor voltage by a two level back-to-back converter the grid synchronization and power control is maintained. The DTC and the direct power control (DPC) methods are used to control the rotor side (RSC) and the grid side converter (GSC). The RSC generates the 3-ph voltages of variable frequency in order to control the generator torque and the reactive power exchanged between the stator and the grid. The GSC exchanges active power with the grid injected by the RSC with a constant frequency. The steady and transient behavior of the machine is investigated through simulations.

Dedication

This thesis is dedicated to my loving parents and grand-parents

Acknowledgements

I would like to express my appreciation to all those who gave me the possibility to complete this thesis. I wish to express my best gratitude and thanks to my adviser, Professor Dr. Andrezej Trzynadlowski, for his technical guidance, his intellectual support and encouragement of my thesis work. I am grateful for having the privilege to work with him and learn from his expertise in the past two years.

I would also like to thank Prof. Dr. Fadali and Prof. Dr. Chandra for being on my thesis committee.

I would like to thank all my colleagues of the power group at the University Of Nevada Reno especially to Fen Niu, Mehdi Farasat, Ekrem Karaman, Saman Arabali, Erik Chalko. I would also like to thank the new intern, Benedikt Bartenschalger, in the electric drives lab. We had many fruitful discussions during the past several years and I will always remember the time I shared with you.

Finally I want to thank my parents for everything they have done for me to make me reach where I am.

Fields of Study

Major Field: Electrical Engineering

Major Area of Specialization: Power Electronics. Control of Electric Drives

TABLE OF CONTENTS

Table of Figures

List of tables

ABBREVATIONS

WECS : Wind energy conversion system

VOC : Voltage oriented control

SCIG : Squirrel cage induction generator

DFIG : doubly-fed induction generator

WRSG : Wound rotor synchronous generator

PMSG : Permanent magnet synchronous generator

VAWT : Vertical axis wind turbine

HAWT : Horizontal axis wind turbine

DTC : Direct torque control

FOC : Field oriented control

DPC : Direct power control

PWM : Pulse width modulation

SV : Space vector

VSI : Voltage source inverter

CSI : Current source inverter

VSC : Voltage source converter

CSR : Current source converter

AC : Alternating current

DC : Direct current

MPPT : Maximum power point tracking

NPC : Neutral point clamped

IGBT : Insulated gate bipolar transistor

CHAPTER 1 Introduction

1.1 Motivation

Many forms of energy that we have grown dependent on are from non-renewable energy sources. This means that when the energy has been consumed, the supply has gone and cannot be replaced. An example of this is coal. Coal is a fossil fuel and is the largest source of energy for the generation of electricity worldwide. When coal has been mined and burnt, it cannot be replaced. Finding alternative energy sources will decrease our dependency on fossil fuels and other non-renewable energy sources [1] [2] .

Renewable energy is energy that comes from resources which are continually replenished such as sunlight, wind, rain, tides, waves and geothermal heat. That remains the most important advantage of renewable energy, which they are continually replenished, free of cost, and they are clean.

Renewable energy still has a long way to go in order to replace fossil fuels and become primary source of energy consumption but with rising climate change concerns, couples with high oil prices, peak oil things have definitely been moving in the right direction. Fossil fuels when burn, create harmful greenhouse gas emissions and our planet is already feeling the impact of climate change. By using renewable energy instead of fossil fuels we would significantly decrease the current levels of greenhouse gas emissions, and this would have positive environmental impact for our entire planet

The ever increasing demand for conventional energy sources has driven society towards the need for research and development of alternative energy sources. Many such energy sources, such as wind energy and photovoltaic are now well developed, cost effective and are being widely used, while others, such as fuel cells are in their advanced developmental stage. With rising fuel costs, increasing concerns for global climate change, and a growing worldwide demand for electricity, utilizing renewable energy sources such as solar and wind power becomes a necessity rather than a luxury [3].

Wind energy has some tremendous advantages over the conventional sources of energy. Wind power since it fueled by wind it's a clean fuel source. Wind energy does not pollute the air like power plants that rely on combustion of fossil fuels, such as coal or natural gas. Wind turbines do not produce atmospheric emissions that cause acid rain or greenhouse gasses. Wind energy is a domestic source of energy, since the nation's wind supply is abundant. Wind energy relies on the renewable power of the wind which is sustainable and cannot be completely used up. Wind is actually a form of solar energy; winds are caused by the heating of the atmosphere by the sun, the rotation of the earth, and the earth's surface irregularities. Due to extensive research wind energy is one of the cheapest renewable energy technologies available today, costing between 4 and 6 cents per kilowatt-hour[1] [2]. Wind turbines can be built on farms or ranches, thus benefiting the economy in rural areas, where most of the best wind sites are found. Farmers and ranchers can continue to work the land because the wind turbines use only a fraction of the land. Wind power plant owners make rent payments to the farmer or rancher for the use of the land [1] [2] [3] [4] .

The global energy consumption is increasing and the wind power generation is steadily rising and is being seen as a supplement and an effective alternative to large conventional power generation units. The power generated from wind energy systems needs to be fed into the grid and hence there is a need of an efficient interface between the wind energy systems and the grid. Power electronics serves as interface is necessary not only for the renewable energy source but also for its effects on the power system operation as the wind energy systems serve as an intermittent source of energy. The power electronics technology plays a very important role in the integration of renewable energy sources into the electrical grid, and it is widely used and rapidly expanding as these applications become more integrated with the grid systems. The technology used in the early developed wind turbines was based on a squirrel cage induction generator (SCIG) connected directly to the grid. This almost transfers the wind power pulsations to the electrical grid. There was no control of active and reactive powers which are key parameters to control frequency and voltage. This thesis, after conducting extensive literature review, explains how controlled active power, according to the grid requirements can be fed into the system.

1.2 Wind Energy

Even though the generation of electricity from modern wind turbines is now an established technology, many developments are yet to come; wind energy is an age old technology and known since 5000 BC. Continuous research and the oil crisis of the 1970s changed the energy picture of world by creating an interest in alternative energy sources like wind to generate electricity.

The first windmill to generate electricity was a system built in Cleveland, Ohio in 1888 by Charles F. Brush. The brush machine was a multi-bladed "picket-fence" rotor 17 meters in diameter. It was the first windmill to incorporate a step-up gearbox in order to turn a DC generator at an operational speed of 500 RPM. The brush machine showed some limitations like low speed, high solidity rotor for electricity production applications.

Extensive research took place from 1974 through mid-1980 in the United States due to the funding from the NSF (National Science Foundation) and DOE (Department of Energy) but due to low oil prices in the 1990's made the electricity generated from the wind uneconomical. The oil prices and interest in electricity generated by wind have always been connected with the lower the oil cost the lower the interest in wind energy and vice versa.

Today, wind-powered generators operate in every size range, from small turbines for battery charging to large, near-gigawatt-size offshore wind farms that provide electricity to national electric transmission systems. As of 2009 wind power provides 2% of worldwide electricity usage and worldwide there are 20000 wind turbines [4].

The main hurdle in front of wind energy is its cost competitiveness with its non-renewable counterparts. The technology requires a higher initial investment than fossil-fueled generators. Since usually good wind sites are often located in remote locations, far from cities where the electricity is needed, transmission lines must be built to bring the electricity from the wind farm to the city which considerably increases both power cost and complexity of the power network. Wind being an intermittent source of energy, the wind turbines does not always produce the same amount of power and sometimes they produce no power at all. Wind resource development may compete with other uses for land

and those alternative uses may be more highly valued than electricity generation. Some concern is raised over the noise produced by the rotor blades, aesthetic (visual) impacts, and sometimes birds have been killed by flying into rotors. Most of these problems have been resolved or greatly reduced through technological development or by properly siting wind plants [3].

1.2.1 Harnessing Power from Wind Energy

Power in the wind can be harnessed by using wind turbines. A wind turbine is a device that converts wind energy into mechanical energy in a process known as wind power. When this mechanical energy is used to produce electrical power, the system is known as wind power plant, if this wind turbine is used for purposes as grinding grain or pumping water, its known as windmill or wind pump. Wind turbines are classified into two types; Horizontal Axis Wind Turbine (HAWT) and Vertical Axis Wind Turbine (VAWT).

1.2.1.1 HAWT

In HAWT the spin axis is parallel to the ground as shown in the Figure 1.1. The HAWT sit atop towers to take advantage of the stronger and less turbulent wind at around 100 feet. The nacelle houses the generator and all other electrical circuitry at sufficient height to provide enough space for the rotor blade rotation and reach better wind conditions. The nacelle supports the rotor hub that holds the rotor blades and also houses the gearbox, generator and in some designs the power converters as well. The Industry, at this moment of time uses a three bladed configuration placed in front of the nacelle which is known as upward configuration [5].

HAWT offers the following advantages

- Access to stronger winds - The tall tower base allows access to stronger wind in sites with wind shear. In some wind shear sites, with every ten meters increase in the wind speed can increase by 20% and the power output by 34%.
- High efficiency since the blades always move perpendicularly to the wind, receiving power through the whole rotation in contrast to all vertical axis wind turbines
- Power Regulation by stall and pitch angle control at high wind speeds.

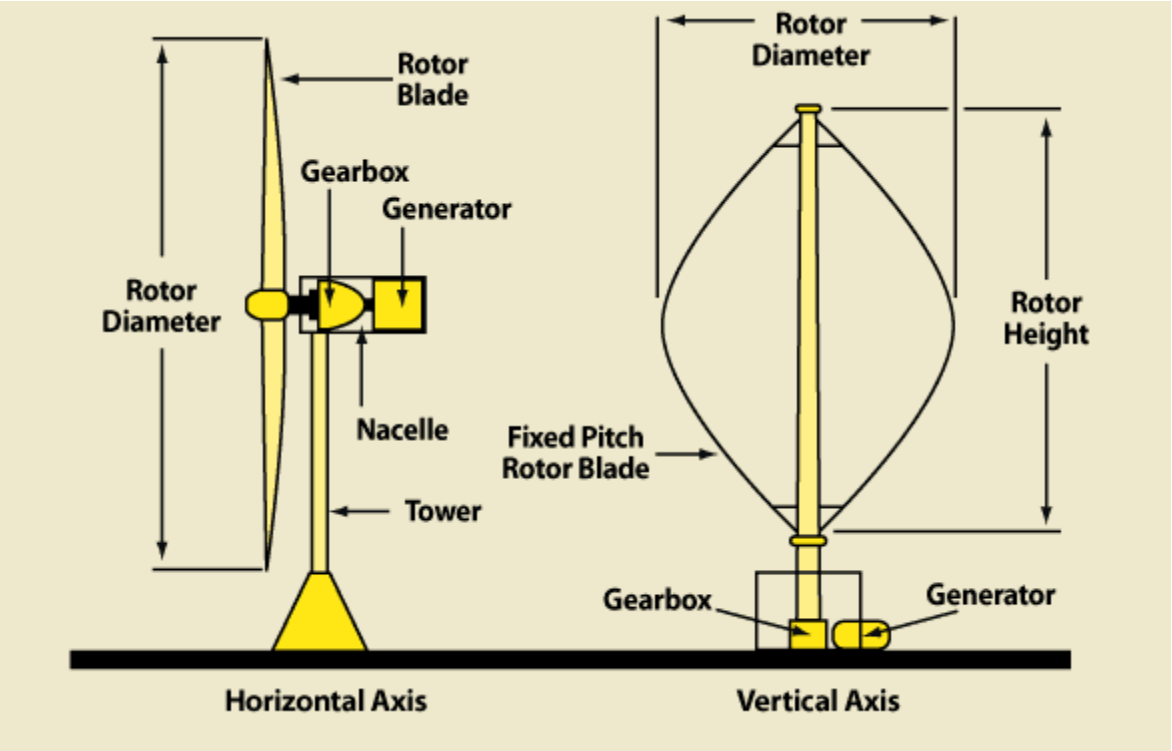

Figure 1.1. Horizontal-axis and vertical-axis wind turbines [6].

HAWT has the following disadvantages

- High construction cost - Massive tower construction is required to support the heavy blades, gearbox, and generator since components of a horizontal axis wind turbine are being lifted into position.
- Visual effects - Their height makes them obtrusively visible across large areas, disrupting the appearance of the landscape and sometimes creating local opposition.
- Wind turbulence effect -Downwind variants suffer from fatigue and structural failure caused by turbulence when a blade passes through the tower's wind shadow (for this reason, the majority of HAWTs use an upwind design, with the rotor facing the wind in front of the tower).
- Low and high wind speeds - HAWTs require an additional yaw control mechanism to turn the blades toward the wind when the wind speeds are less and they also require a braking or yawing device in high winds to stop the turbine from spinning and destroying or damaging itself [7] [8].

1.2.1.2 VAWT

In Vertical Axis Wind Turbine (VAWT) shown in the Figure 1.3. Savonius wind Turbinethe orientation of the spin is perpendicular to the ground [9]. The turbine rotor uses curves mounted airfoils. The generator and the gearbox and all the other assembly are normally placed in the base of the turbine on the ground as shown in the figure. The main advantages of this type of wind turbine are that it does not have to be pointed in the direction of the wind. This is a major advantage where the wind direction is highly variable or has turbulent winds. One of the major drawback is of the VAWT is it creates a drag when rotating into the wind. The VAWTs are difficult to mount on tower due to their way of arrangement and they are almost most of the times mounted at the bottom where wind speeds are low. However if the VAWT is mounted on a rooftop the building generally diverts the wind to the top and can double the wind speed at the turbine.

The rotor blades of VAWT have variety of designs like Darrieus wind turbine & Savonius wind turbine which have different shapes and number of blades.

Darrieus wind turbines are commonly called as “Eggbeater turbines” because they look like a giant eggbeater. They have good efficiency, but produce large torque ripple and cyclic stress on the tower which contributes to the poor reliability [5].

Figure 1.2. Darrieus wind turbines[9].

Figure 1.3. Savonius wind Turbine[9].

Savonius wind turbine is a drag type turbine and is hence less efficient but they perform well in the areas of turbulent wind and self-starting.

VAWT Advantages

- Yaw mechanisms are not needed since they can capture wind from any direction.
- Its location of the VAWT can be near the ground making it easier to maintain the moving parts.
- Lower wind startup speeds than the typical the HAWTs.
- Can be built at locations where taller structures are prohibited.
- Situated close to the ground can take advantage of locations where rooftops, mesas, hilltops, ridgelines, and passes funnel the wind and increase wind velocity.

VAWT Disadvantages

- Most VAWTs have a lower efficiency than a common HAWT [7], [8], mainly because of the additional drag that they have as their blades rotate into the wind.
- Having rotors located close to the ground where wind speeds are lower.
- Higher torque fluctuations and prone to mechanical vibrations [7], [8].

1.3 Wind Energy Technology

Wind power is the conversion of the wind energy into a useful form of energy such as electrical power etc. This technology is described in detail in this section.

1.3.1 Basics of Wind Energy Technology

A wind energy conversion system converts mechanical energy to electrical energy by using rotor blades. This energy is then transformed into electrical energy by a generator. This system is made up of several components, participating directly in the energy conversion process. There are also some other control circuits that assist the system to achieve this task in in reliably and efficiently.

A very important part of the wind energy conversion system is the wind captured by the blades and in this chapter we will discuss how to maximize the wind capture by the blades.

This will provide necessary insight on how the power output of a wind turbine can be regulated by adjusting the blade pitch angle or by controlling the generator torque or speed.

1.3.1.1 Nacelle

The nacelle of a wind turbine is the box-like component that sits atop the tower and is connected to the rotor [10]. The nacelle contains the majority of the approximately 8,000 components of the wind turbine such as the gearbox, generator, main frame, etc. The nacelle housing is usually made of fiberglass and protects the internal components from the environment. The nacelle cover is attached to the main frame, which also supports all the other components inside the nacelle. The main frames are large metal structures that must be able to withstand large fatigue loads [1] [3] [10].

1.3.1.2 Drivetrain

The heart of the wind turbine is its electricity generating system called the drivetrain shown in Figure 1.4 [11]. Inside the nacelle of a typical wind turbine, the rotor drives a large shaft into a gearbox, which steps up the revolutions per minute to a speed suitable for the electrical generator. A wind turbine gearbox must be robust enough to handle the frequent changes in torque caused by changes in the wind speed. The gearbox requires a lubrication system to minimize wear. Wind turbines being sold in the U.S. have either induction or permanent-magnet generators, depending on the model being sold. Induction generators are more common and require a gearbox as described in [1] [3].

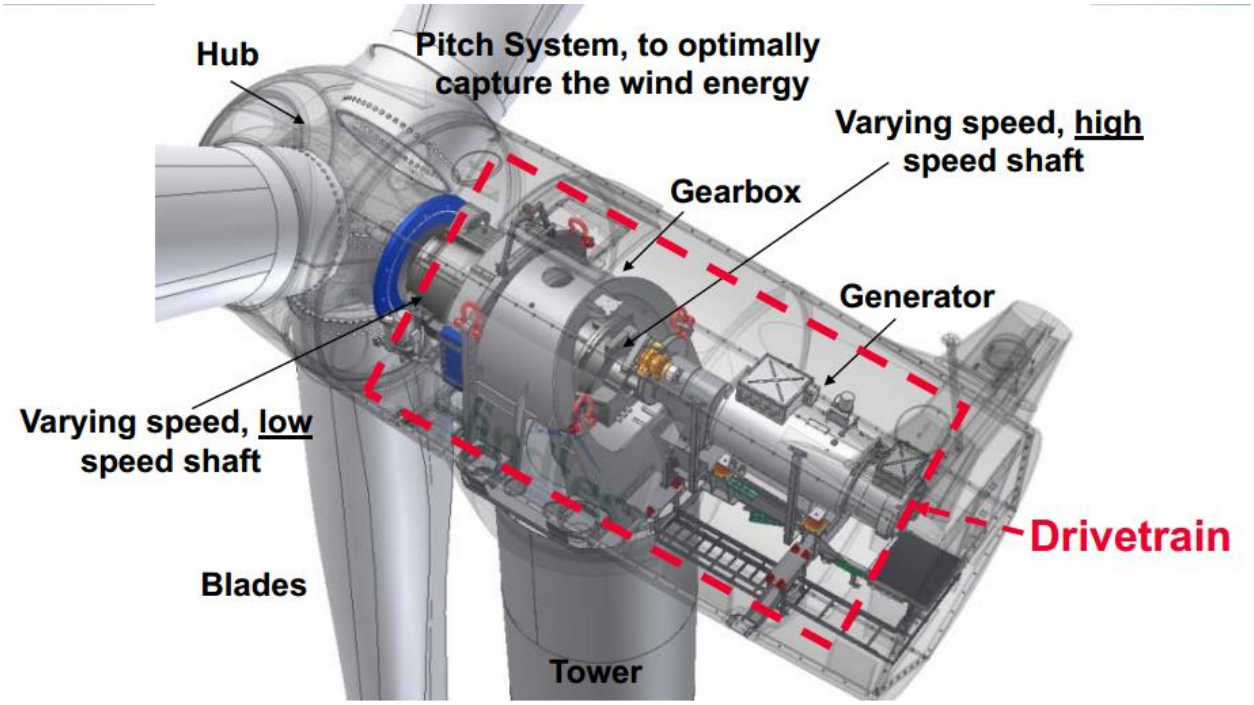

Figure 1.4. Structure of a drivetrain [11].

Some wind turbines avoid the gearbox completely and use a direct drive system. A direct drive system connects the rotor directly to a permanent-magnet generator. These turbines avoid the mechanical problems associated with a gearbox, but require extremely heavy and expensive generators that can produce electricity capable of supplying the grid.

1.3.1.3 Yaw

All turbines have a yaw drive system to keep the rotor facing into the wind and to unwind the cables that travel down to the base of the tower. The yaw drive system usually consists of an electric or hydraulic motor mounted on the nacelle which drives a pinion mounted on a vertical shaft through a reducing gearbox. The yaw drive system also has a brake in order to be able to stop a turbine from turning and stabilize it during normal operation [1] [3].

1.3.1.4 Control System

To control the functioning of the wind turbine, it is fitted with a number of sensors to read the speed and direction of the wind, the levels of electrical power generation, the rotor speed, the blades' pitch angle, vibration levels, the temperature of the lubricants and other variables. A computer processes the inputs to carry out the normal operation of the

turbine, with a safety system which can override the controller in an emergency. The control system protects the turbine from operating in dangerous conditions and ensures that the power generated has the proper frequency, voltage, and current levels to be supplied to the grid [1] [3].

1.4 Fundamentals of Wind Energy Control

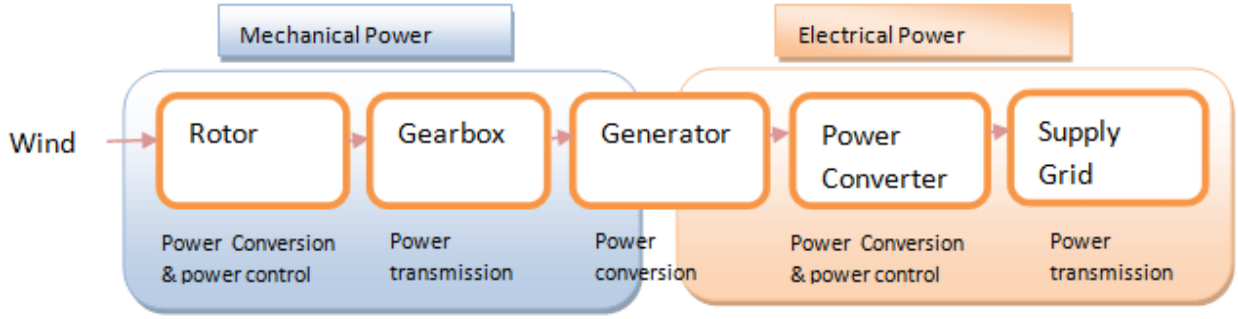

Figure 1.5. Conversion of wind energy to electrical energy.

The blades of the wind turbine rotor extract some of the flow from the moving air, convert it into rotational energy and deliver it via a mechanical drive unit to the rotor of a generator. The electrical energy from the generator is fed via a system of a switching and protection devices, lines and if necessary transformers to the grid, consumers or an energy storage device. The system is made up of several components that assist the system to achieve this task in a controlled, reliable, and efficient way.

Since the energy source for WECS is wind kinetic energy, wind plays a key role in several aspects of the conversion process. Hence we discuss a bit about relations of wind and the power captured by wind.

1.4.1.1 Turbine Blade

The turbine blade is the most distinctive and visible component of a wind turbine. It is responsible for transforming the wind kinetic energy into mechanical energy. The three bladed rotors considered the industry standard for large wind turbines. The one or two bladed turbines shown in the Figure 1.6. Wind turbine bladehave the advantage that their rotating speed is higher but they require a gearbox with lower gear ratio. On the other hand, they create significant acoustic noise [5].

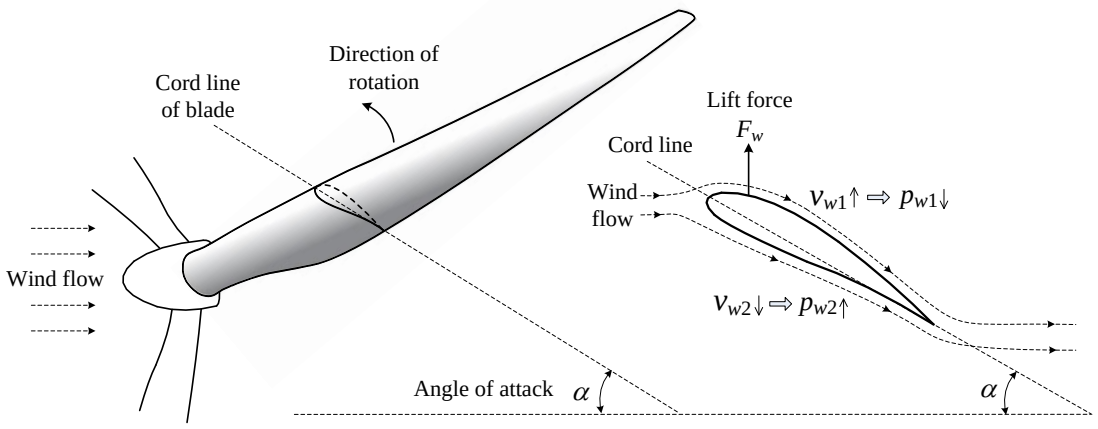

Figure 1.6. Wind turbine blade [5].

The principle of working of blade is that the airflow above it is faster than the airflow on the lower side and this creates a difference in pressure that results in a lift force on the blade. To control the lift we alter the angle of attack α, which is defined as the angle between the direction if the wind speed and the cord line of the blade. When this angle is zero no lift force or torque will be produced. The wind power captured by the blade and converted into mechanical power can be calculated by

$$P_M = \frac{1}{2}\rho A v_w^3 C_p$$

where ρ = air density

A = Rotor area swept

v_w^3 = wind speed

where C_p is the power coefficient of the blade. This coefficient has a theoretical maximum value of 0.59 according to Betz limit [12]. Observing the equation, we see that there are only three possibilities for increasing the power captured by a wind turbine: the wind speed, the power coefficient and the swept area.

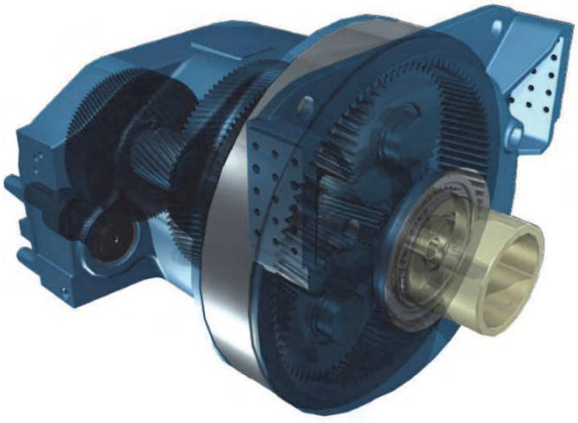

Figure 1.7. Gearbox used in wind turbines [12] .

Figure 1.8. SCIG [12]..

Figure 1.9. DFIG [12].

1.4.1.2 Gearbox

The rotor of a large three-blade wind turbine usually operates in a speed range from 6-20 rpm. This is much slower than a standard 4-5 pole wind generator with a rated speed of 1500 or 1600 for a 50Hz stator frequency and 1800 or 1200 rpm for a 60hz frequency. Therefore a gearbox shown in the Figure 1.7, is necessary to adapt the low speed of the turbine rotor to the high speed of the generator. The gearbox conversion ratio also known as the gear ration, is designed to match the high speed of generator with the low-speed turbine blades. It can be determined by

$$r_{gb} = \frac{n_m}{n_M} = \frac{\left((1-s) * 60 * f_s\right)}{P * n_M}$$

where n_m and n_M are the generator speeds and turbine speeds in rpm, s is the slip, f_s is the rated stator frequency.

In examining the functionality of and behavior of wind power plants, particular significance should be given to the generator as a source of load torque, depending on its situation and how it is coupled to the system. The generators used should

- Be simple to use
- Have a long useful lifetime

- Have a low maintenance outlay
- Have the lowest possible initial cost

Different type of generators have been used in wind energy systems over the years and these include the squirrel cage induction generators (SCIG) and doubly-fed induction generators (DFIG) and synchronous generator (SG) (wound rotor and permanent magnet) with power rating from a few kilo-watts to several megawatts.

The SCIG is simple and rugged in construction. It is relatively inexpensive and requires minimum maintenance. Traditional direct grid-connected wind energy systems which use SCIGs and operate at fixed speed are still available.

The DFIG is the current work horse of the wind industry, the stator is connected to the grid directly, while the rotor is interface with the grid through a power converter with reduced power capacity, the DFIG operates at about 30% above and below synchronous speed, sufficient for most wind speed conditions. It also has the ability to control the generator active side power and grid side reactive power control. The reduced-capacity converter is less expensive and requires less space, which makes the DFIG WECS popular in today's market [12].

1.4.1.3 Tip-Speed Ratio

The tip speed ration (TSR) is an important parameter in wind energy systems. It is defined as the ratio of the blade tip speed to the speed of the incoming wind, given by

$$\lambda_T = \frac{\omega_M r_T}{v_w}$$

where r_t is the radius of the turbine rotor (blade length), v_w is the wind speed, and ω_M is the rotating speed of the blade. Another important parameter is the power conversion efficiency C_p of the blade since the mechanical power is directly proportional to C_p

1.5 Thesis Outline

In this chapter we discuss the topologies of wind energy systems. First we discuss the most basic topology of the wind energy systems which are the single speed and the two-speed

types. Two-speed wind energy systems can be achieved by changing the number of poles of the generator or by simply using two generators. After that the variable wind energy systems are reviewed with stating some advantages. Their subtypes namely wound rotor Induction generator with external rotor resistance, squirrel cage induction generator with full capacity converters (two-level and three-level neutral point clamped). Some topologies using the permanent magnet synchronous generator interfaced with two-level and three-level converters and also with diode rectifier and the boost converters are explained. After that the actual power converters used in those wind energy systems are reviewed. The most important power converters namely AC-AC converters, both single phase and three phase, DC-DC converters, mostly boost converters, single channel, two channel and multi-channel topology. Next the most important type which is the voltage source converters are explained with the help of a three phase inverter and the pulse generation strategies such as sinusoidal pulse width modulation (SPWM), SPWM with the insertion of the third harmonic and the most important space vector pulse width modulation method. After the voltage source converters, the current source converters are reviewed and their switching strategies are explained. The current source converters will not be discussed further in this thesis. After discussing the power converts used in the wind energy systems, the control of the grid connected converter is studied in detail and reviewed with simulation study.

Chapter 3 introduces the wind energy systems with Induction generators. First and foremost the model of the Induction generator using state space is reviewed and studied in detail. The required Impedance matrices are obtained and the expression for developed torque is also obtained. The Park and Clarke transformation matrices are discussed. Next the control strategies are discussed. The most important control strategies for controlling induction generator based wind energy systems are field oriented control and the direct torque control. First the field oriented control (FOC) strategy is studied and discussed in detail and then the direct field oriented control is considered. The direct FOC is discussed and case studies are performed on the proposed strategy. Steady state and dynamic analysis is performed on the direct FOC control technique. After the direct FOC, the indirect FOC control technique is discussed. The complete control strategy is explained and case study for the steady state analysis of indirect FOC is presented and its simulation

waveforms are analyzed. Next the direct torque control (DTC) for the induction generator is discussed and its switching logic is studied and analyzed for the DTC scheme. The model for the flux and torque calculator is developed. Case studies are done to understand the steady and dynamic state analysis.

Chapter 4 introduces the doubly-fed induction generator (DFIG) based wind energy systems. Doubly fed Induction generator systems are the workhorse of the wind energy industry. Initially we discuss the principle of the DFIG is studied and the advantages of DFIG over the conventional induction generator and its use of DFIG in wind energy system is reviewed. The most important converter for the DFIG based systems which is the back to back converter is discussed and studied in depth. The back-to-back converter is modeled according to its parameters along with the grid side system, rotor side system and the DC link model. We also discuss two strategies that are similar to the SCIG based systems, sinusoidal pulse width modulation (SPWM), SPWM with insertion of third harmonic and the space vector pulse width modulation (SVPWM). Using the grid side system model the steady state and dynamic analysis are performed. The dynamic model of the DFIG is deviced and is used for the simulation study. The two models are presented, the $\alpha - \beta$ model and the $d - q$ model and once the modeling is done performance analysis is done in both the $\alpha - \beta$ reference frame and $d - q$ reference frame. After analyzing the dynamic model of the DFIG and analyzing it through case studies, vector control strategy for the DFIG based wind energy systems is then developed and discussed. Vector control is divided in three parts, the calculation of the current references, current control loops and the complete control system. Next the field oriented control strategy for the DFIG based systems is introduced. Direct control has two modules namely the direct torque control and the direct power control and both are developed and analyzed through case studies. In both strategies each block is thoroughly examined and its functionality is explained. Both the steady state and transient analysis is done for both modules of the direct control strategy.

CHAPTER 2 Wind Energy Configurations

2.1 Classification

A classification of the most common configurations is given in Figure 2-1. Wind turbines can be generally classified into fixed speed and variable speed turbines.

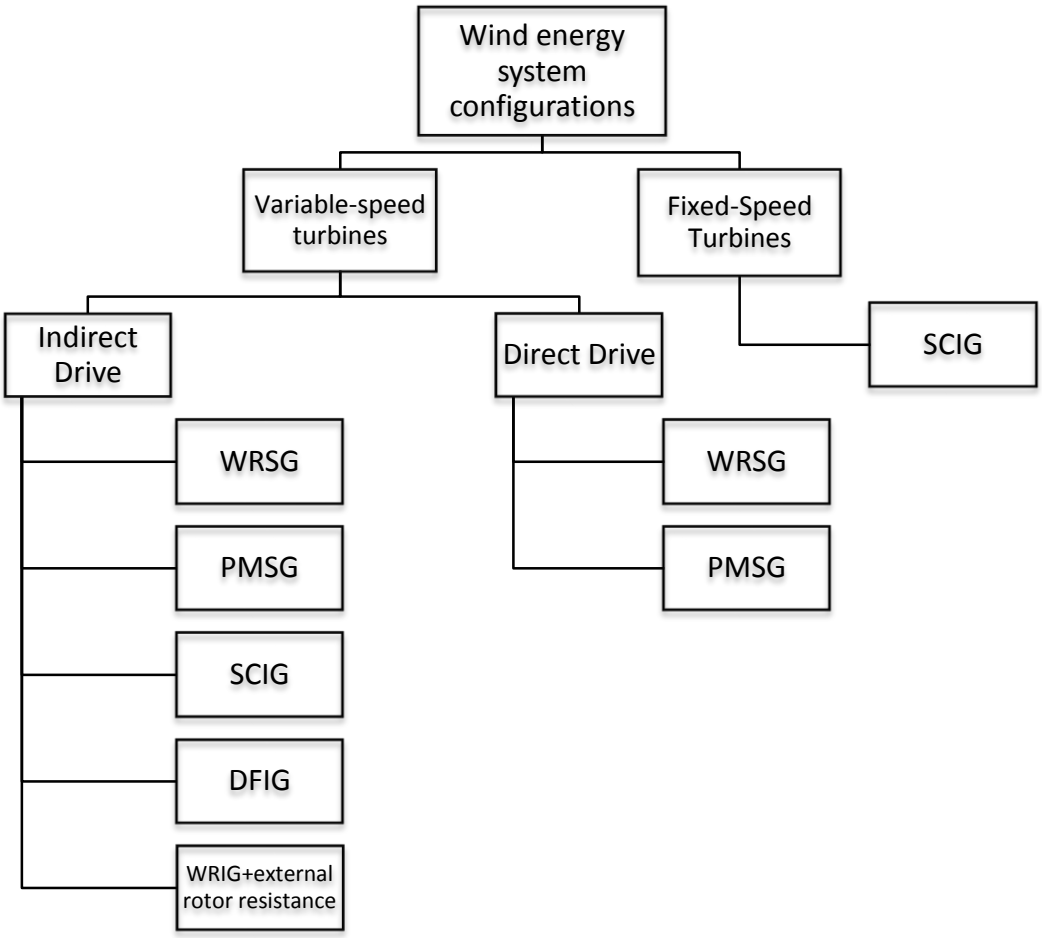

Figure 2.1. Classification of wind energy systems.

2.1.1 Fixed Speed

Fixed-speed turbines employ a squirrel-cage induction generator connected directly to the grid and thus do not need any power converter during normal operation.

2.1.1.1 Single Speed

A typical configuration for a high-power (megawatt), a fixed speed wind energy system is shown in the Figure 2.2.

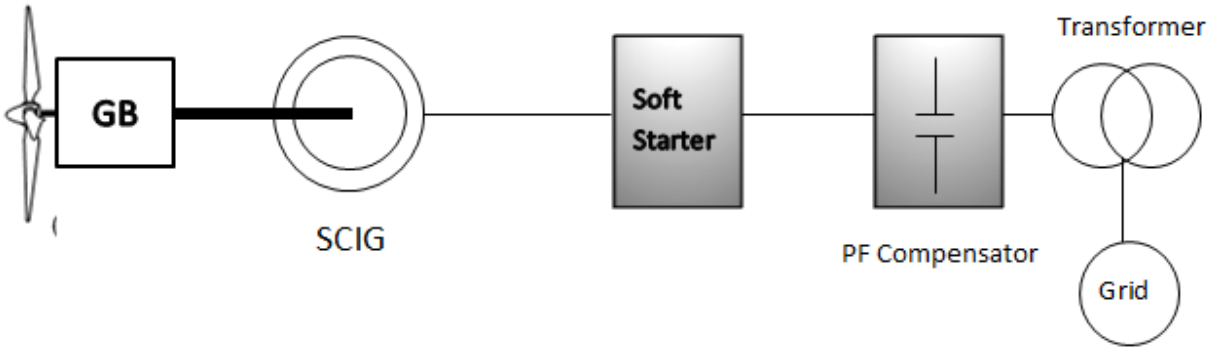

Figure 2.2. Single speed wind energy system.

The turbine is normally of horizontal-axis type with three rotor blades rotating at low speeds, like 15 rpm as the rated speed. Usually squirrel cage induction generators are used in the system.

To assist the startup of the turbine, a soft starter is used to limit the inrush current in the generator winding. The soft starter is basically a AC-AC converter which is discussed further in detail in the third and fourth chapters. Once the stator current is effectively limited the soft starter is bypassed by a switch and the WECS is then connected to the grid. Since the wind energy system does not need a power converter during normal operation, it is classified as WECS without power converters [5, 13-15].

2.1.1.2 Two Speed

To improve the energy conversion efficiency, two-speed SCIG wind energy systems have been developed

Two Speed Operation by Altering the Number of Poles [5, 13-15]

The development of induction generators with two sets of windings has allowed the number of poles within a single generator to be varied by connecting the windings together in different ways. A technique called pole amplitude modulation (PAM) is used. Switching

from a four pole to a six or eight pole configuration can introduce a speed reduction of one third or one half, respectively. The number of poles can be changed by reconfiguring the stator winding through appropriate parallel and series connection of the stator coils

Two Speed Operation by Two Generators [5, 13-15]

As discussed above the two-speed operation can also be obtained by having two separate generators mechanically coupled to a single shaft; one is a fully rated high speed generator and other is the low speed one. The selection of the generators is done by a switch. This approach requires two separate generators and a long drivetrain that needs special consideration for the coupling of both generators.

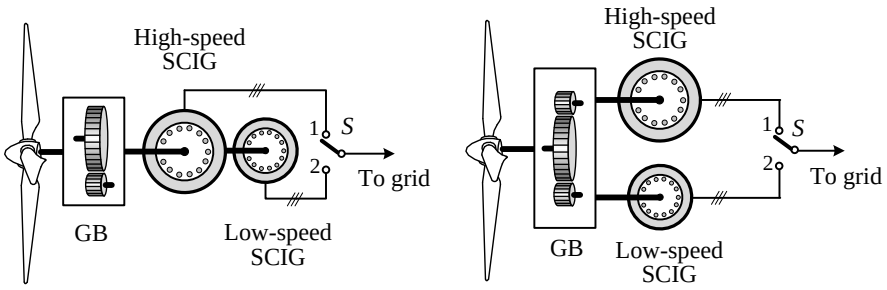

(a) Single-shaft configuration (b) Dual-shaft configuration

Figure 2.3. Two speed type of wind energy system [5].

The two-speed operation can also be obtained by using a split gearbox with two shafts. The two shafts have the same gear ratio and each shaft is connected to a separate SCIG. Similar to the single shaft technique the fully rated high speed generator is selected at high wind speeds, whereas a partially rated six – or eight- pole generator is switched on at low wind speeds.

The single- and dual shaft WECS configurations require two generators, which increases the cost and the weight of the system in addition to the added complexity in the mechanical components. Therefore they have limited practical applications [5, 13-15].

2.1.2 Variable Speed Wind Energy Systems

By interposing a frequency conversion between the generator and the network, it is possible to decouple the rotating speed of the generator and the turbine from the network frequency. Variable speed allows the rotor speed to vary and maximize the energy capture.

The variable-speed wind turbines can be divided into direct- and indirect-drive turbines. In the direct-drive turbines, low speed synchronous generators with a large number of poles are employed.

Advantages of Variable speed operation include:

- Below the rated wind speed, the rotor torque and hence the speed can be made to vary to maintain peak aerodynamic efficiency (C_p)
- The reduced rotor speed in low winds results in a significant reduction in aerodynamic generated noise
- The rotor can act as a flywheel, smoothing out the torque fluctuations before they enter the drive train.
- Direct control of the air-gap torque allows gearbox torque variations to be kept small
- Both active and reactive power can be controlled.
- Variable speed turbines will also give higher power quality due to the smoother output voltages they develop [5, 13-15].

2.1.2.1 WRIG with External Rotor Resistance

Figure 2-4 shows the simplified configuration for a variable speed WRIG system with a converter-controlled external rotor resistance. The external resistance is made adjustable by a converter composed of a diode bridge and IGBT chopper. The main advantage of this configuration compared to the WECS is the low cost and simplicity. The main disadvantage includes limited speed range, inability to control grid-side reactive power, and reduced efficiency due to the resistive loss.

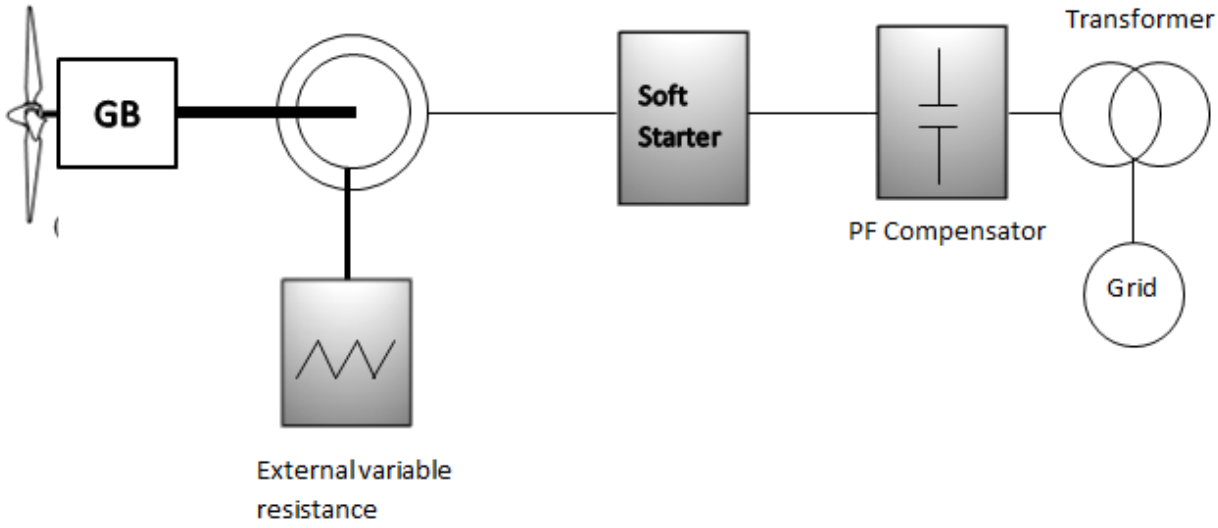

Figure 2.4. Wound rotor with external rotor resistance.

2.1.2.2 SCIG Wind Energy System with Full Capacity

The SCIG wind energy systems are briefly discussed below

Two Level Voltage Source Converters.

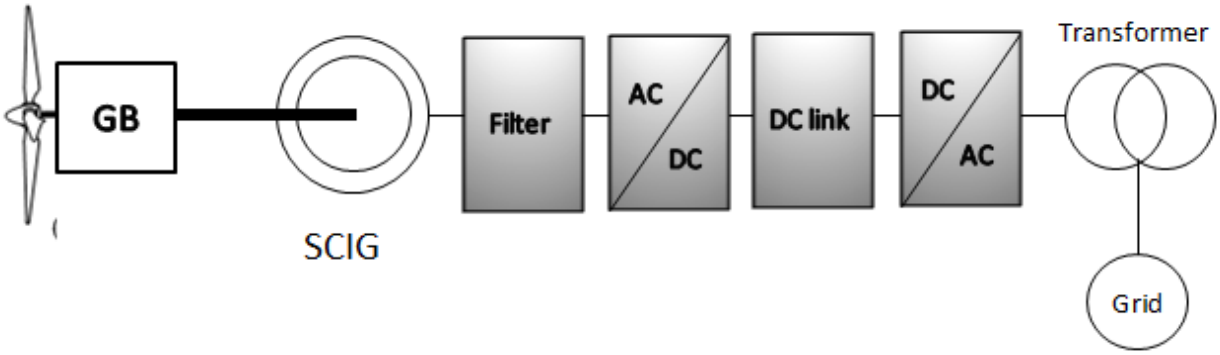

Figure 2.5. Wind energy system using a two level converter.

A typical voltage source converter configuration for SCIG wind energy systems is shown in the Figure 2.5. In this topology of converter we use a two level voltage source rectifier (VSR) and voltage source inverter (VSI) using IGBT devices. A DC link capacitive filter links the two converters which have the same topology.

An alternative approach to the parallel converter channels is shown in the Figure 2.6 where three converters are used in parallel for a megawatt IG wind turbine. Each converter

channel is mainly composed of two level VSC's in a very popular back-to-back configuration with harmonic filters.

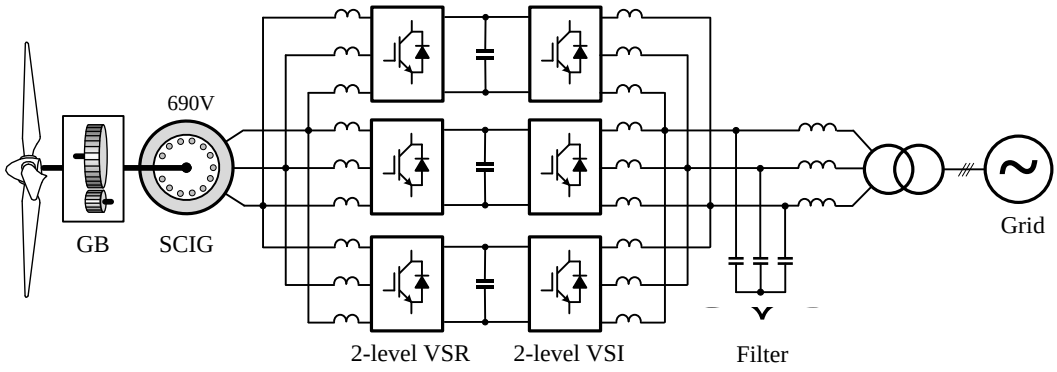

Figure 2.6. Wind energy system using parallel converters [5].

This arrangement yields better efficiency. For example, at low wind speeds when the system delivers a small amount of power to the grid at low wind speeds, one out of two converter channels can be turned off leading to higher efficiency. Also if one channel fails, the other two can continue to operate under certain conditions [5, 13-15].

Three Level Neutral Point Converters

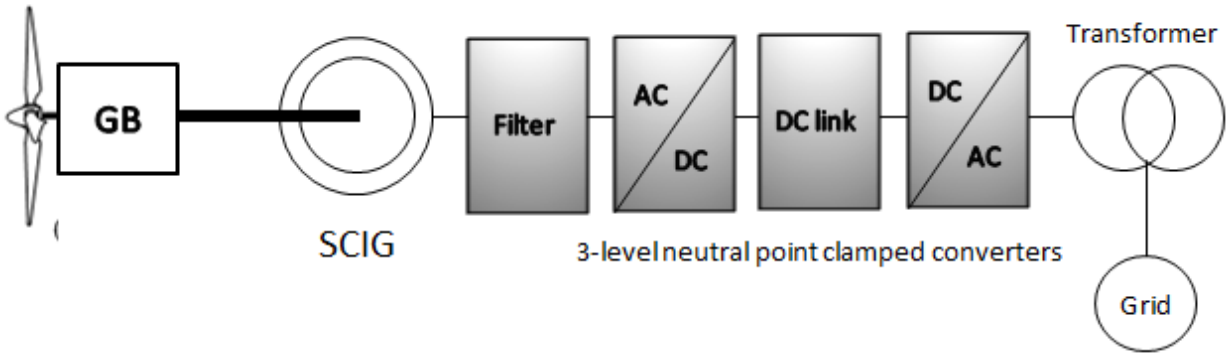

Figure 2.7. Wind energy system using three level neutral point converters.

Low-voltage converters provide cost effective solutions at lower power levels. Figure 2.7 shows a MV wind turbine that employs a full-capacity converter system with a MV generator. Here again two back-to-back connected three-level neutral point clamped (NPC) converters are used. The switching devices employed in these converters are high voltage IGBT, IGCT of 4.5 kV to 6.5 kV. The switching frequency used is around a few hundred hertz

(mainly to reduce switching losses). The Neutral Point Clamped converters have found wide application in commercial medium -voltage SG WECS [5, 16].

2.1.2.3 Variable Speed Synchronous Generator Systems

Synchronous generators have many more configurations than the induction generators WECS due to the following facts

- The synchronous generators provides the rotor flux by itself through permanent magnets or rotor field winding. Thus diode rectifiers can be used as the generator-side converters, which is impossible in the SCIG WECS.
- It is easier and more cost effective for the synchronous generator to have multiple pole and multiple phase configurations.

With two-level VSC and Three-level NPC Converters –

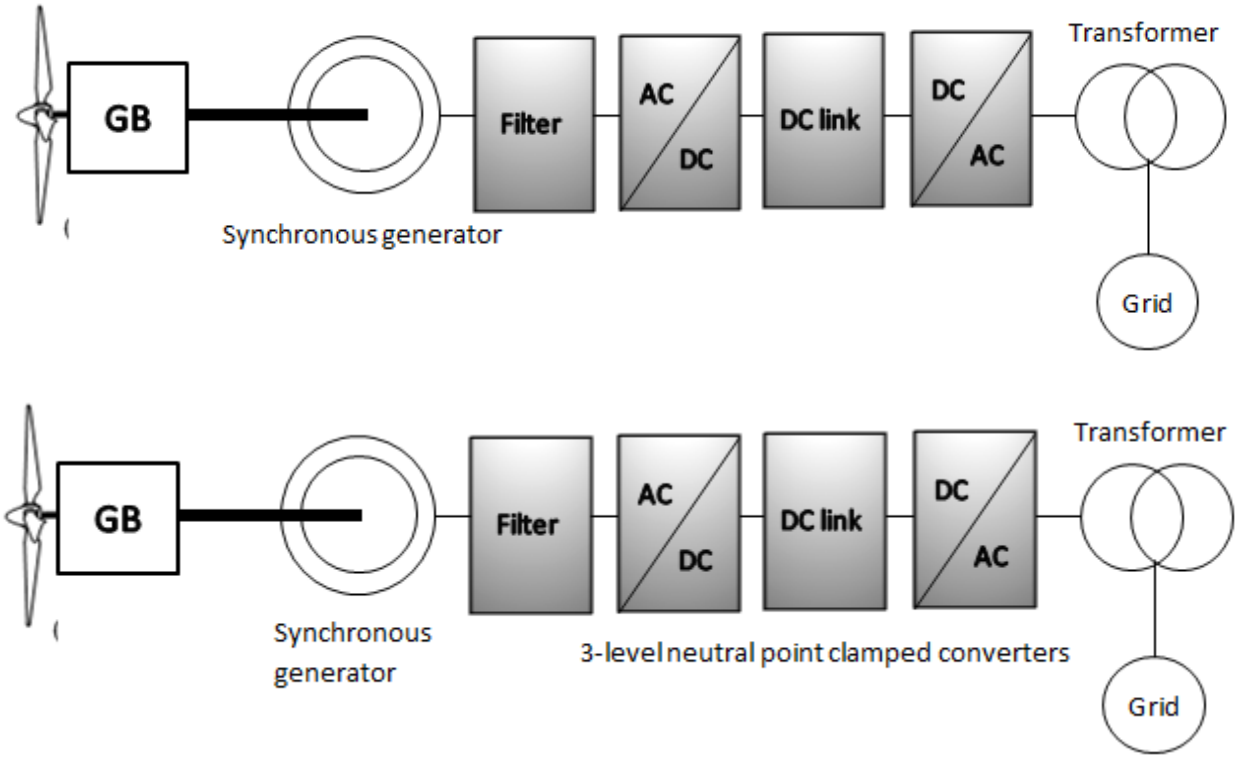

Figure 2.8. Wind energy systems with 2-level and 3-level converters.

A typical configuration for SG wind energy systems with full capacity converters is shown in Figure 2.8 where a back-to-back converter is employed. In low voltage wind energy systems three-level NPC are used in medium voltage turbines. Not all wind energy systems need a gearbox instead a low-speed generator with high number of poles is employed and the gearbox is eliminated.

With PWM Current Source Converters

Figure 2.9 shows a typical configuration for a medium-voltage SG wind energy system using current source converter

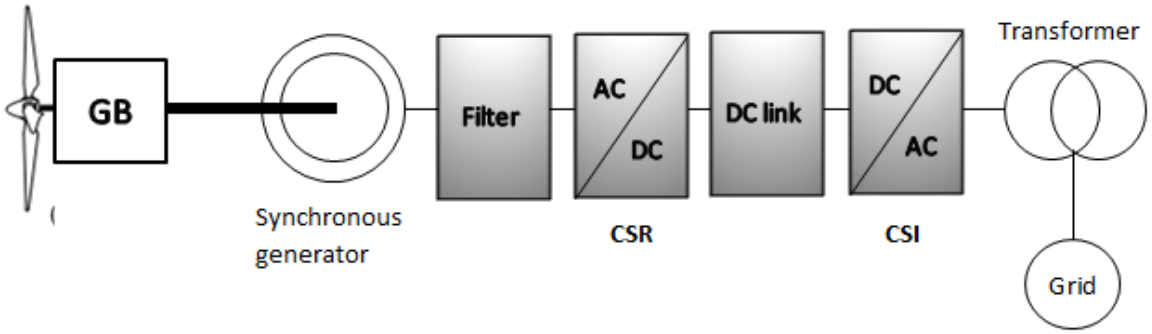

Figure 2.9. Wind energy systems with current source rectifiers.

2.1.2.4 With Diode Rectifier and DC-DC Converter

Wind energy system topologies using diode rectifiers and DC-DC converters are discussed below.

Using Multichannel Boost Converter

The two-level voltage source converter can be replaced by a diode rectifier and a boost converter as shown in Figure 2.10. This type of converter topology cannot be used with SCIG wind energy systems since induction generators need external excitation. The diode rectifier converts variable generator voltage to a DC voltage, which is boosted to a sufficiently high level for the inverters which ensures maximum capture power to the grid.

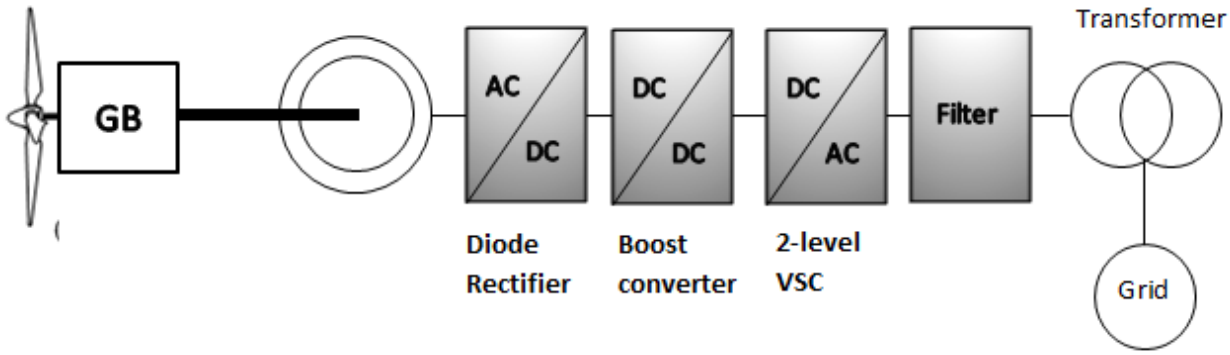

Figure 2.10. Wind energy systems with diode rectifier and boost converter.

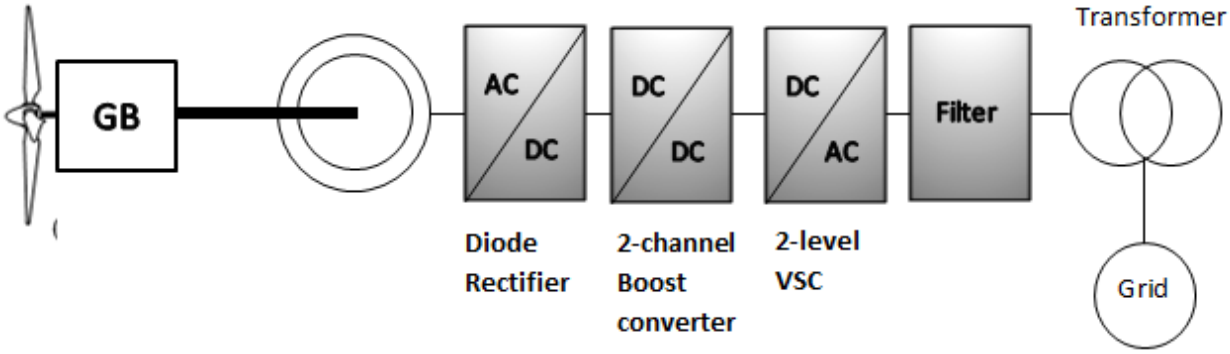

Figure 2.11. Wind energy systems with diode rectifier and 2-channel boost converter.

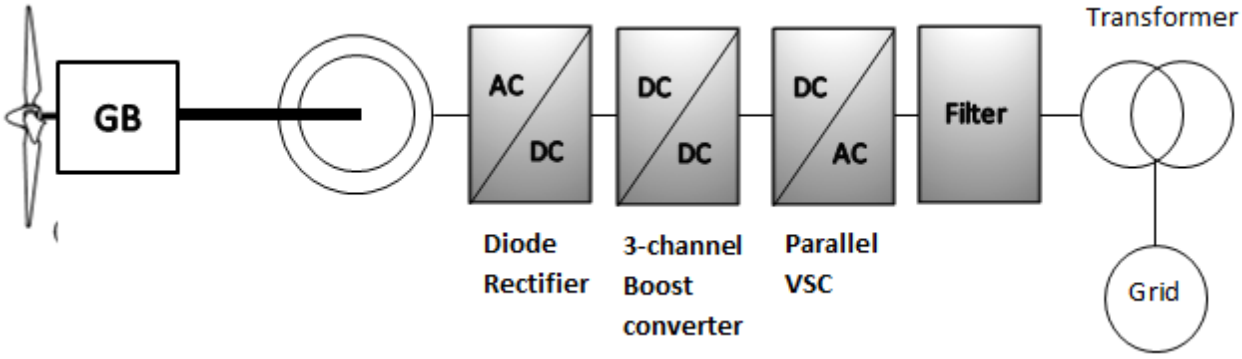

Figure 2.12. Wind energy systems with two diode rectifiers and 3-channel boost converter.

Another alternative WECS configuration using a six-phase generator with a multichannel boost converter is shown in Figure 2.12 where the output of the generator is rectified by

two diode bridge rectifiers. To increase the power rating, a three-channel interleaved boost converter and two paralleled three-phase inverters are used [5, 16, 17].

Using Multilevel Boost Converters

One more configuration for the diode boost inverter is shown in Figure 2.13 where a three level boost converter is used. A three level boost converter is realized by combining two single-boost converters connected in cascade. This alternative configuration has found application with a power rating upto 1.2 MW.

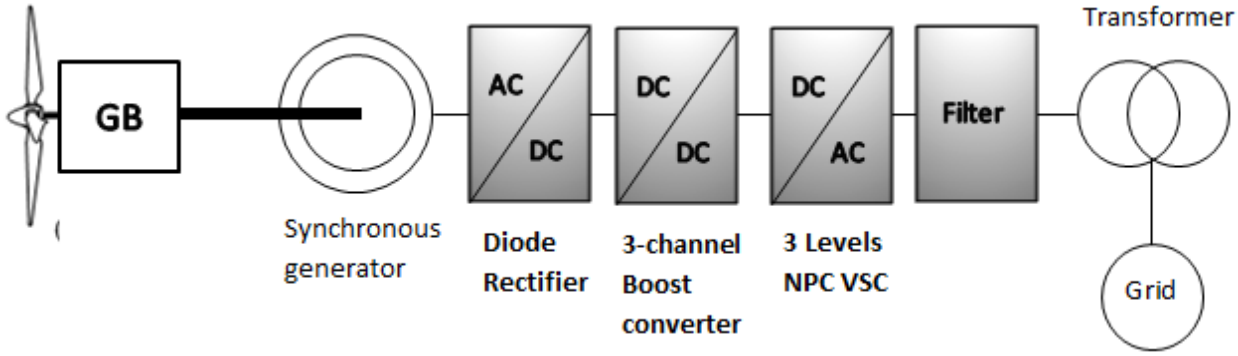

Figure 2.13. Wind energy systems with 3-level boost converter and 3-level NPC converter.

A topology of this configuration for the medium voltage wind turbines is shown in Figure 2.13 where a three level boost converter and a three-level NPC inverter using both IGCT and IGBT. The additional benefit of this topology is that the neutral point voltage can be effectively controlled by boost converters and there is no need of complex control scheme for the NPC inverter to balance the neutral point voltage [18].

With Diode Rectifier and Buck Converter

The dual of the voltage source converter is the current source converter and a CSC configuration with a diode rectifier and a buck converter can be deduced from the VSC configuration and as we saw that the one major difference is that the boost converter used in the VSC topology is replaced by the Buck converter. The topology is shown in Figure 2.14

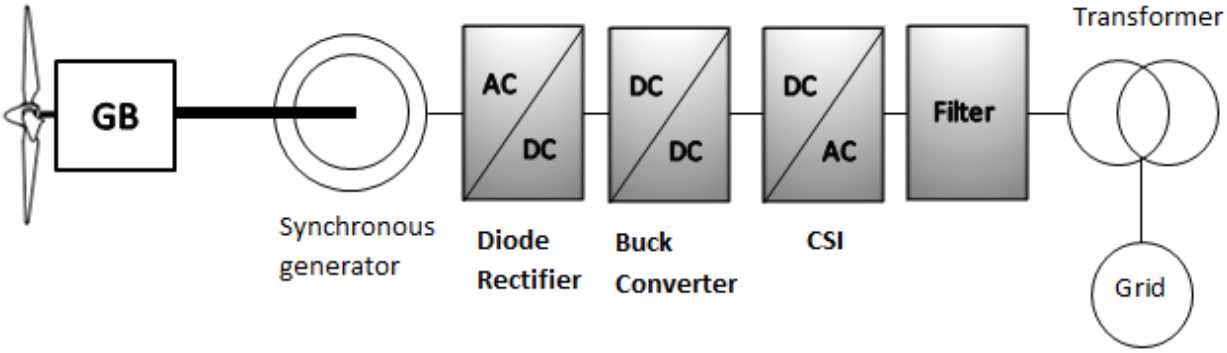

Figure 2.14. Wind energy systems with diode rectifier, buck converter and a current source inverter.

The buck converter is the obvious choice for this topology because it needs an output inductor, which can serve as the DC link inductor needed by the CSC. By controlling the duty cycle of the buck converter and modulation index and delay angle of the inverter, the generator-side active power, the DC link current, and grid-side reactive power can be controlled. This topology is a reliable, simple, cost-effective solution. The drawback of this strategy is that the stator current contains higher total harmonic distortion (THD) due to the use of the diode rectifier[19].

2.1.2.5 With Distributed Converters for Multi Winding Generators

The multi winding generator approach is shown in Figure 2.15 where a six-phase generator is used and the power is delivered to the grid through distributed converter channels. Each converter channel is composed of two-level voltage source converters and filters. Since the two sets of the stator windings are insulated, there is no circulating current between the two converter channels can be connected to the same transformer windings. With proper design of the switching schemes of the two inverters, the grid side harmonic performance of the system can be further improved by the phase-shifting transformer.

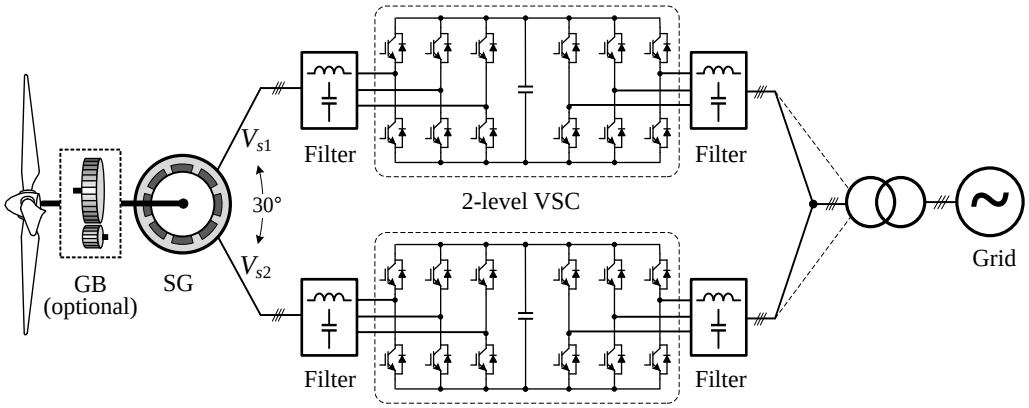

Figure 2.15. Wind energy systems with distributed converters with multi-winding generators [5].

Another example for the multiwinding generator is shown in the figure where the generator has six sets of three-phase windings, and each winding feeds the wind power to the grid through a power converter channel. The system configuration is the same as that with the six-phase generator except that there are no pulse displacements between the stator voltages of different windings. Although this type of topology has been designed at higher cost, this configuration has found practical application due to its advantages [5, 20].

2.1.2.6 With Multiple Generators

A recent configuration with four synchronous generators and distributed power converter is shown in Figure 2.16. The system uses a distributed gearbox with multiple high speed shafts that drive four independent generators. Each generator is interfaced to the grid via a converter channel composed of a diode bridge rectifier and two-level voltage source converters. Since the power is divided among four distributed converters, the wind turbine can reach multi-megawatt power range without using paralleled switching devices or converters [21].

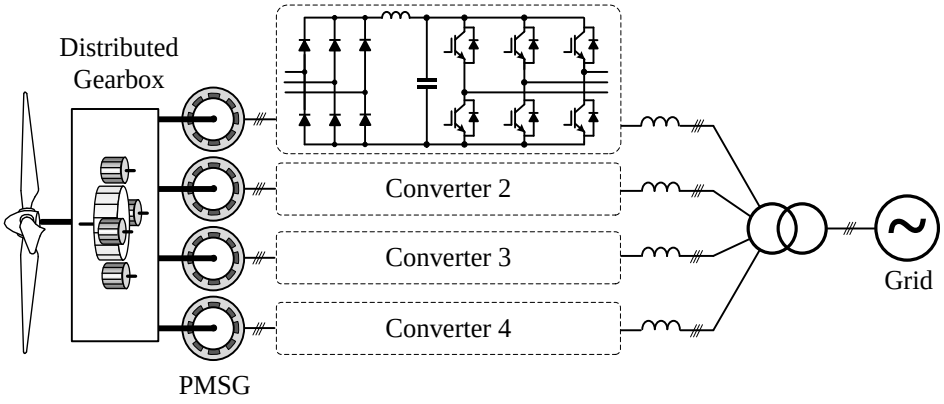

Figure 2.16. Wind energy systems with multiple generators [16].

The main advantage of this configuration is the high power density achieved by the distributed gearbox of and multiple generator system which leads to light and distributed nacelle and reduces transportation and installation costs. The use of a diode rectifier and standard two-level converter makes this a cost effective solutions [21].

2.2 Power Converters Used in Wind Energy Systems

Renewable energy sources can be classified as sustained or intermittent. Intermittent sources include wind and photovoltaic energy sources, whose randomly varying output makes power electronic converters a vital and unavoidable part. Power electronics are needed to interface a renewable energy source efficiently with the power grid for power conditioning, voltage boosting, and control the flow of the power.

Power converters are widely used in wind energy conversion systems (WECS). In fixed-speed WECS, the converters are used to reduce the inrush current and torque oscillations during start-up, whereas in variable-speed WECS they are employed to control the speed/torque and also active/reactive power to the grid.

Figure 2.17 shows the fixed speed wind turbine based WECS. If an Induction machine is used as the generator, its speed is almost constant varying only a little within a limit of the machine slip.

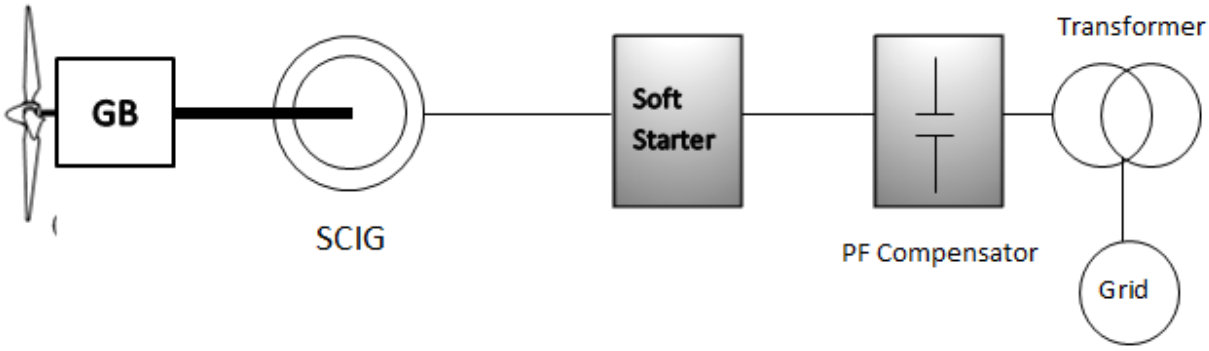

Figure 2.17. Fixed speed wind energy system with a soft starter.

The generator is driven via a gearbox and typically through a transformer). Here a soft starter is employed to reduce the inrush of current caused by transients that take place at the moment when the generator is connected to the grid. The soft starter is essentially an AC voltage controller using SCR devices[5].

Maximum power point requires a variable turbine speed. This means that the frequency of the generator voltage is changing and hence a frequency converter is needed between the generator and the transformer.

Figure 2.18 shows a variable speed WECS using squirrel cage induction generator (SCIG) or synchronous generator (SG's) where a back-to-back type converter configuration with two identical PWM converters is used. The converters can either be voltage source converters (VSC's) or current source converters (CSC).

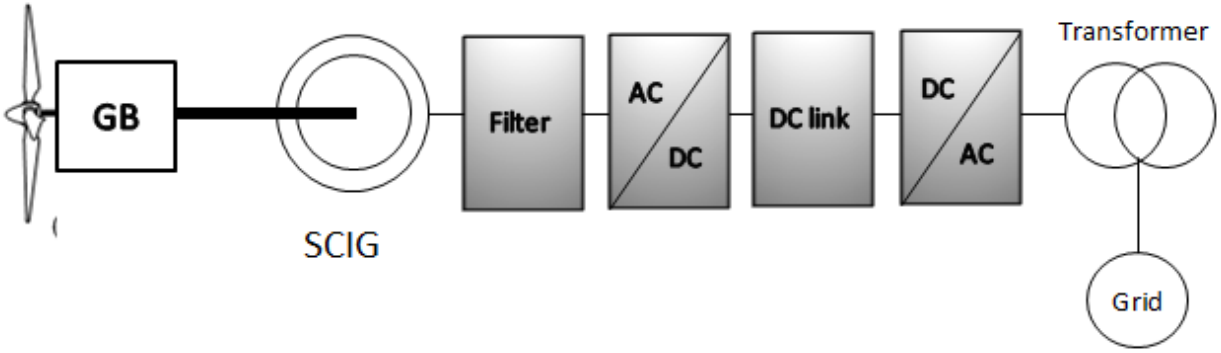

Figure 2.18. Variable speed WECS with back-to-back PWM converters.

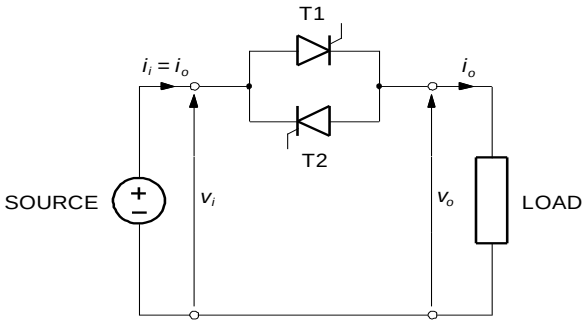

Figure 2.19. Single phase AC voltage controllers [24].

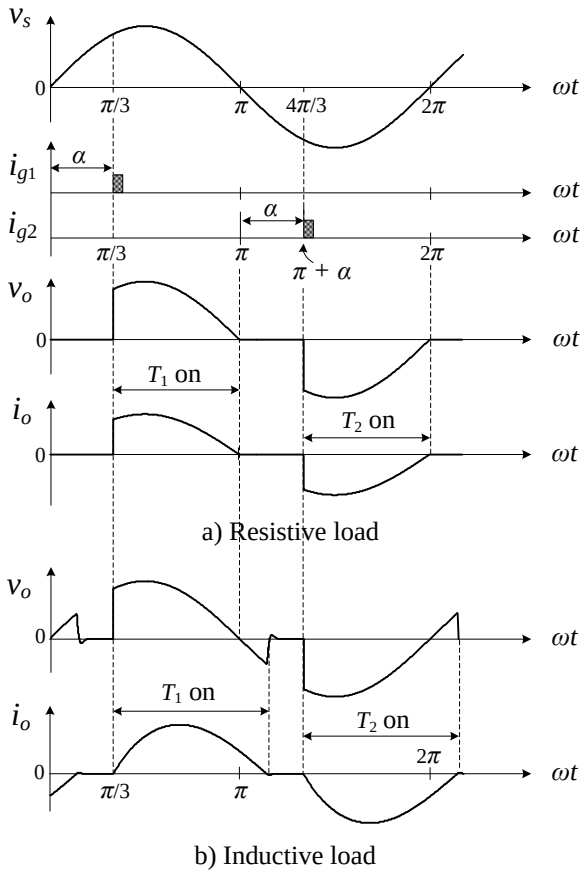

Figure 2.20. Waveforms for inductive and resistive load [5].

We study different power converter topologies for WECS which include AC-AC converters, DC-DC boost converters, two level voltage source converters, three-level neutral point clamped (NPC) and PWM current source converters [16, 22, 23].

2.2.1 AC Voltage Controllers

A power electronic AC to AC converter, in generic form, accepts electric power from one system and converts it for delivery to another ac system with waveforms of different amplitude, frequency, and phase. They are single-or three-phase types depending on their power ratings. The AC-AC converters employed to vary the rms voltage across the load are

known as ac voltage controllers or ac regulators. In other words, AC voltage controllers are employed when a fixed ac voltage must be adjusted. AC-AC controllers provide voltage control without frequency control.

2.2.1.1 Single Phase AC Voltage Converters

A simplified circuit of the AC voltage controller is shown in the Figure 2.19. It is composed of a pair of SCR thyristors antiparallel between the power supply and the load. A Triac is used instead of the two-anti parallel-connected SCR's when the low-power converters are used.

For a resistive load, the rms value of the voltage can be found from

$$V_o = V_s\left(1 - \frac{\alpha}{\pi} + \frac{sin2\alpha}{2\pi}\right)^{\frac{1}{2}} \qquad 2.1$$

The waveforms for a resistive load are as follows are shown in Figure 2.19.

For and Inductive load and firing angle $\alpha = 60$ we can see that the thyristor T_1 will not be turned when the supply voltage v_s falls to zero at $\omega t = 180$. This is due to the lagging inductive load current flowing through T_1, which is not zero yet at $\omega t = 180$. It can be noted that if α is smaller than the load power factor angle ϕ , then the output voltage v_o of the controller will be exactly equal to the supply voltage v_s and thus v_o is no longer adjustable[22-24].

For a pure Inductive load the rms value of the output voltage v_o of the controller can be calculated by

$$V_o = \begin{cases} V_s & for\ 0 \le \alpha < \frac{\pi}{2} \\ V_s\left(2 - \frac{2\alpha}{\pi} + \frac{sin2\alpha}{\pi}\right) & for\ \frac{\pi}{2} \le \alpha < \pi \end{cases} \qquad (2.2)$$

2.2.1.2 Three Phase AC Voltage Controllers

Several configurations of the three phase converter are possible but her we will only consider the fully controlled topology which is shown in Figure 2.21. Considering a pure

resistive load for the controller, one thyristor in each of the two legs is turned on at one point of time and hence because of those voltages v_{ab}, v_{bc}, v_{ca} is applied to the load.

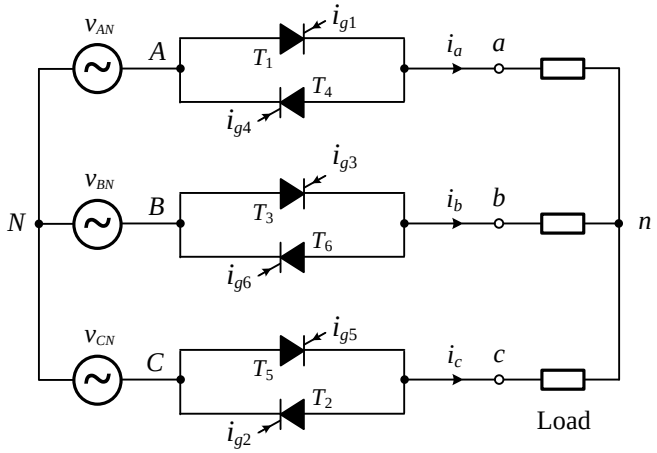

Figure 2.21. Three phase AC voltage controllers [16].

The waveforms of the line to line voltages can be obtained by $v_{ab} = v_{an} - v_{bn}, v_{bc} = v_{bn} - v_{cn}$, $v_{ac} = v_{an} - v_{cn}$

2.2.1.3 Interleaved Boost Converters

The most basic form of DC-DC converters is the buck converter or the step down chopper. A chopper is basically a DC-DC converter with adjustable average output voltage and current which lower than or equal to its DC source. The DC supply source is alternatively connected or disconnected with the DC source. In contrast to these choppers are the step-up choppers produces an output voltage with a fixed average value which is higher than the input voltage.

The functions of dc-dc converters are:

- to convert a dc input voltage VS into a dc output voltageV_o;
- to regulate the dc output voltage against load and line variations;
- to reduce the ac voltage ripple on the dc output voltage below the required level;
- to provide isolation between the input source and the load (isolation is not always required);

- to protect the supplied system and the input source from electromagnetic interference (EMI)

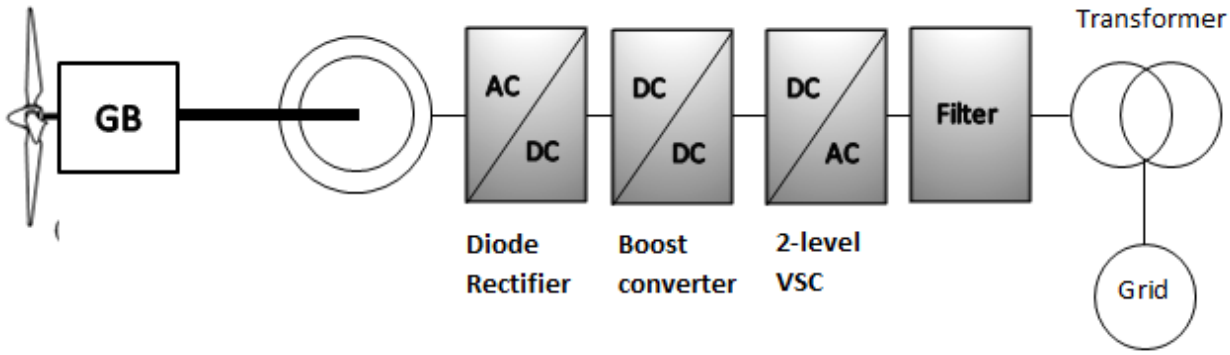

Figure 2.22. Variable speed WECS with DC/DC boost converter.

The DC-DC boost converter is one of the topologies often used in synchronous generator based wind energy system. We can see that the converter is placed between the diode rectifier and the inverter of the main system. The boost converter along with the PWM inverter functions mentioned above serve two main functions: tracking maximum power from the wind and boosting DC voltage to an appropriate value of the inverter. The advantages of the increased frequency are lower input current ripple and output voltage ripple, faster dynamic response, and better power handling capability. IGBT's are preferred over the MOSFET as the primary switching device [17].

Single Channel Boost Converter

The typical circuit diagram of a single phase boost converter is as shown in Figure 2.23. It is basically composed of a switch, a diode, DC inductor, and filter capacitor C. When the switch is turned on the diode is reverse biased and the energy is supplied to the inductor and stored. When the switch is open the diode becomes forward biased and the energy stored in the inductor is released through the diode which becomes forward biased. The operation of the converter can be divided into two operating modes: continuous-current mode (CCM) and discontinuous-current mode (DCM). As the name suggests that in continuous current the inductor current never falls to zero [16].

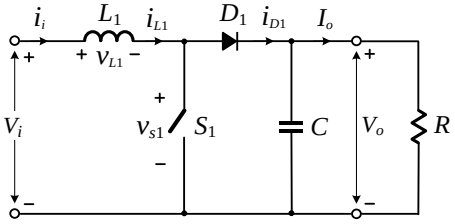

Figure 2.23. Single channel boost converter [5].

For a single channel boost converter

$$V_i t_{on} = (V_o - V_i) t_{off} \tag{2. 3}$$

from which

$$\frac{V_0}{V_i} = \frac{1}{1 - D} \tag{2. 4}$$

where 'D' is the duty cycle
t_{on} and t_{off} are the ON and OFF times respectively
The relationship between the converter input current I_i and the output current I_o is

$$\frac{I_o}{I_i} = 1 - D \tag{2. 5}$$

Under light load conditions, the load current is low and so is the current in the inductor L_1. The energy store in the inductor during the ON period may not be sufficient to maintain its current during the OFF period. Hence the inductor current reaches zero before the end of the OFF period and becomes discontinuous. The converter is thus said to be operating in the discontinuous mode.

Two-Channel Boost Converter

The topology for a two-channel interleaved boost converter is shown in Figure 2.24. There are two parallel converter channels in the circuit both composed of inductor, switch and diode. They both share the same filter capacitor.

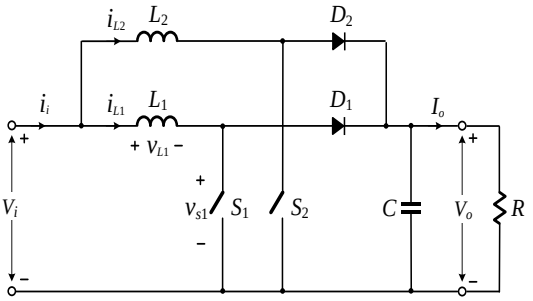

Figure 2.24. Two-channel boost converter [16].

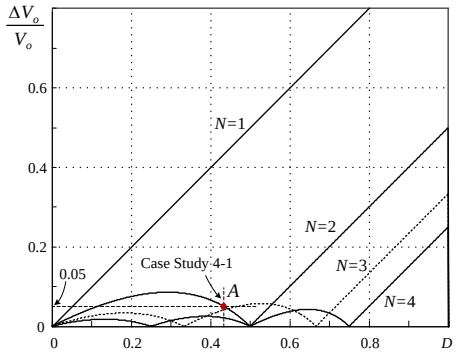

Figure 2.25. Input current ripple [16].

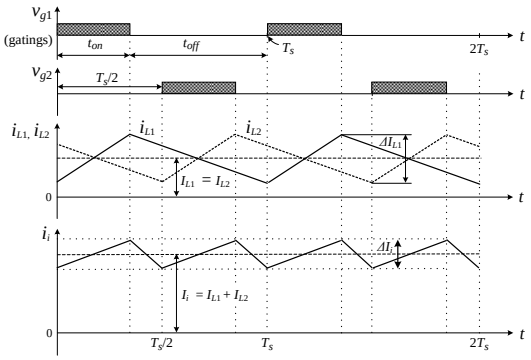

Figure 2.26. Analysis of input current ripple in a two channel interleaved converter [16].

The gating signals for both the switches are identical but shifted by $\frac{360^o}{N} = 180^o$ where N is the number of parallel channels. The total input current i_i, which is the sum of the two inductor currents i_{L1} and i_{L2} has the following properties.

- The average DC component of the input current (I_i) is twice that of the individual inductor ($I_i = I_{L1} + I_{L2}$). Since the input and output voltages for the parallel converters are the same, each channel handles only half of the total power of the load.
- The peak-to-peak input current ripple ΔI_i is smaller than that in the individual channels due to the use of interleaved technique and this helps to reduce the volume of the input filter.
- The frequency of the input ripple current is twice that of the individual channels. In other words, the equivalent switching frequency of the interleaved converter is twice that of each channel.

The ***Input Current Ripple*** in Figure 2.25 shows a very interesting characteristics when the duty cycle is varied from about 0.35 to 0.5 the ripples in the two inductor currents i_{l1} and i_{L2} cancel each other and do not reappear in i_i, that is, $\Delta I_i = 0$.

The Output Voltage Ripple

One of the main benefits of the interleaved converters is the reduction of the output ripple. In the two channel converter, the two parallel converters share the same capacitor ***C*** which makes the analysis a bit tedious. Figure 2.26 shows the results for the relative output voltage ripple voltage for the two channel converter (assuming that the converter operates in the steady state). The relative voltage ripple for the single channel converter is also shown in the figure [17, 22-24].

2.2.1.4 Voltage Source Converters

This is probably the most widely used converter in the wind power industry. Figure 2.27 shows a simplified diagram for a three-phase, two-level voltage source converter. The converter is composed of six switches which mostly are IGBT's or IGCT's depending on the power rating of the converter.

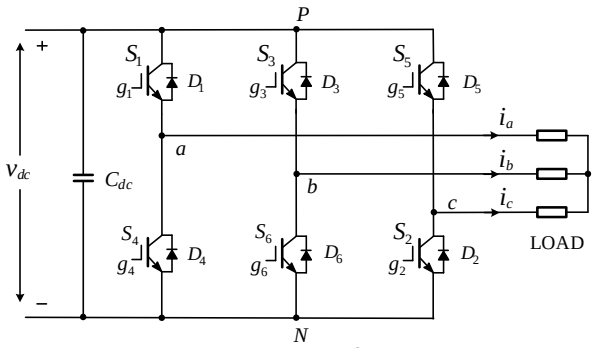

Figure 2.27. Three phase VSC – converter topology [5].

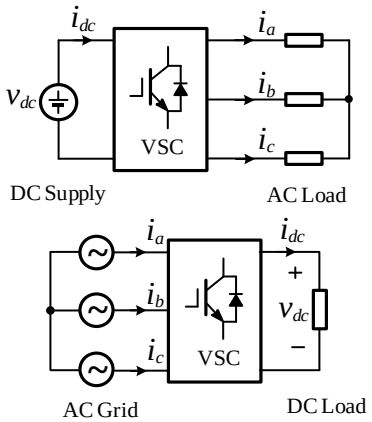

Figure 2.28. VSC in inverter and rectifier mode [5].

When the converter transforms a fixed DC voltage to a three-phase AC voltage with a variable magnitude and frequency for an AC load it is called an inverter as shown in part

(b) of the Figure 2.28.When the converter transforms a AC grid voltage with fixed magnitude and frequency to and adjustable DC voltage for DC load it is called a Rectifier shown in part c. In either of the cases the power flow is bidirectional. In WECS this converter is used as a grid side converter. We are going to see the PWM schemes for the two level converters.

In our converter topology the voltages denoted by V_a, V_b and V_c. They can attain a value of $+0.5\,V_{dc}$ when the upper switch is operating and $-0.5\,V_{dc}$ when the lower switch is operating. Consider the phase voltages applied to the as V_{AN}, V_{BN}, V_{CN} as shown in the detailed version of the three phase inverter [5, 17, 22].

The relation between leg voltage and switching signals are

$$V_k = S_k V_{dc}\ ; k \in A, B, C \tag{2. 6}$$

Where $S_k = 1$ when the upper power switch is 'ON' and $S_k = 0$ when the lower switch is 'ON'

Sinusoidal PWM

If v_{ma} , v_{mb} , v_{ca} are the three-phase modulating waveforms and v_{cr} is the triangular carrier signal, then the operation of the switches is determined by comparing the modulating waves with the carrier wave. The waveform is shown in Figure 2.29. The fundamental-frequency component in the inverter output voltage can be controlled by the amplitude-modulation index

$$m_a = \frac{\hat{V}_m}{\hat{V}_{cr}} \tag{2. 7}$$

where $\hat{V}_m$ and $\hat{V}_{cr}$ are the peak values of the modulating and carrier waves, respectively. The frequency modulation index is

$$m_f = \frac{f_{cr}}{f_m} \tag{2. 8}$$

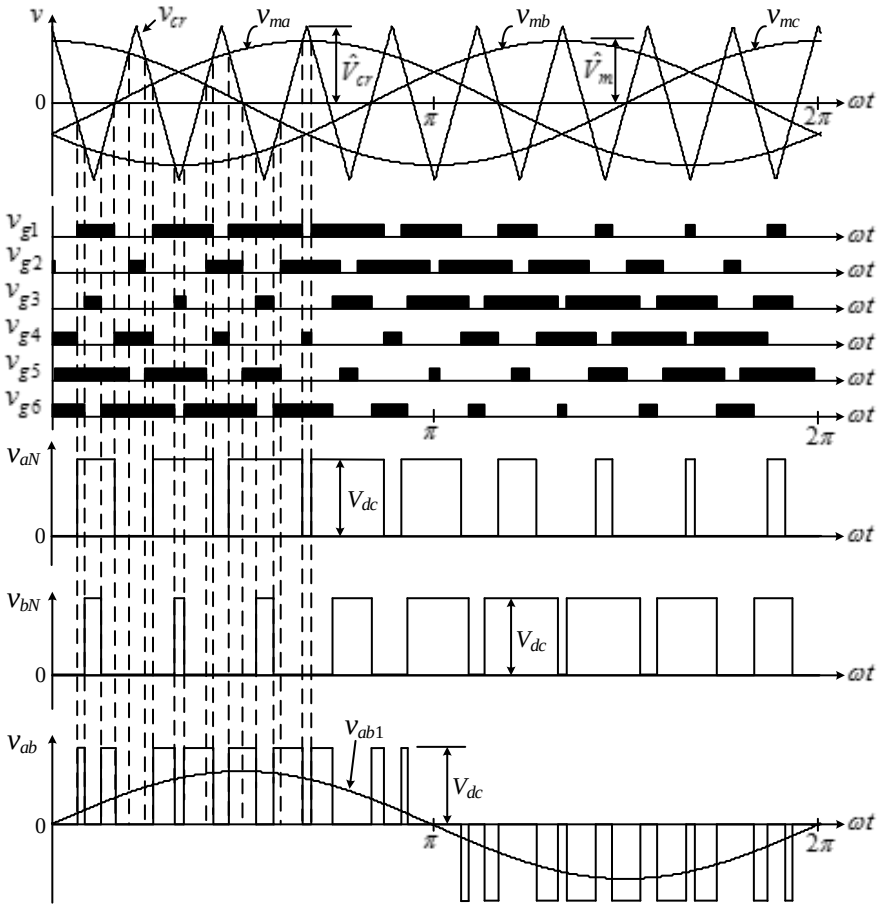

Figure 2.29. Sinusoidal pulse width modulation (SPWM) [16].

When $v_{ma} > v_{cr}$ the upper switch in the inverter leg a is turned on and the other switch is always OFF. Similarly when $v_{ma} < v_{cr}$ the lower switch is ON and the other switch is complementary of that and the resultant voltage v_{aN} will be zero.

Since v_{aN} has only two levels, this converter is often called a two-level converter. Once we have v_{aN} , v_{bN} , v_{cN} we can calculate the inverter line to line voltage by $v_{ab} = v_{aN} - v_{bN}$. The switching frequency can be found from $f_{SW} = f_{cr} = f_m * m_f$.

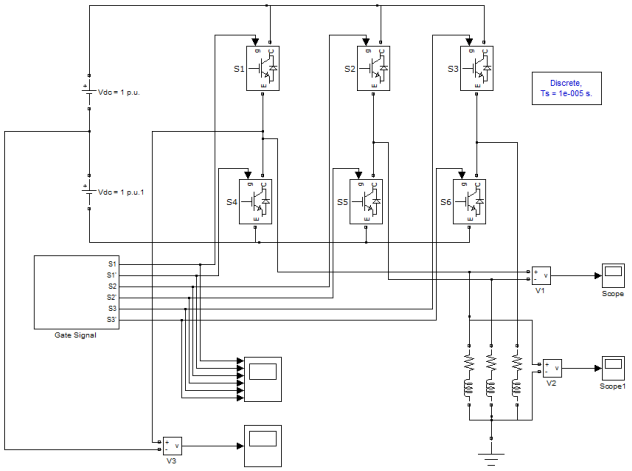

Figure 2.30. MATLAB/SIMULINK model for Sinusoidal PWM.

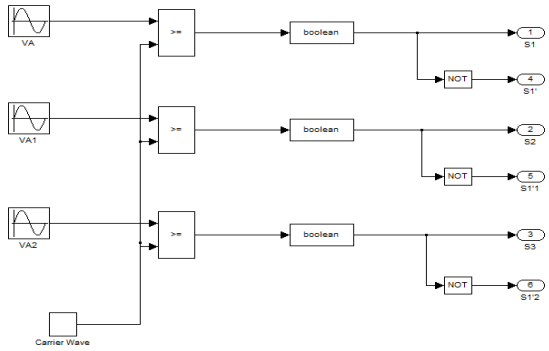

Figure 2.31. Block diagram for Sinusoidal PWM.

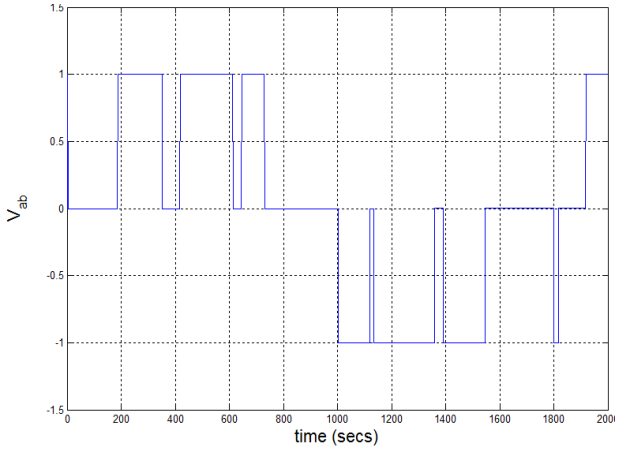

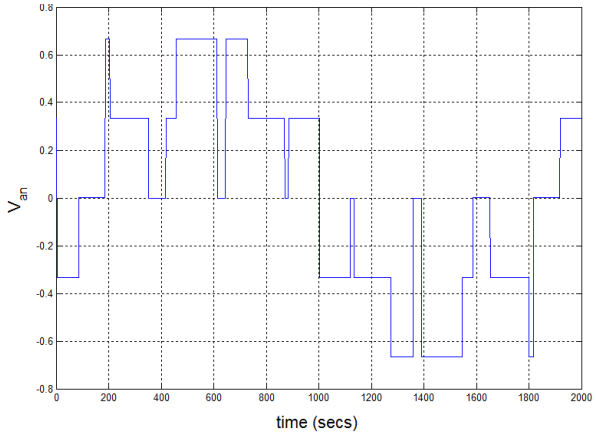

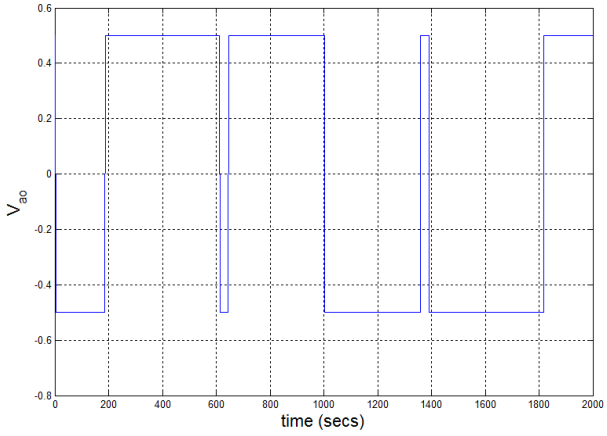

Figure 2.32. Output voltage waveform for SPWM

Third-harmonic Injection Carrier-based PWM

The output voltage using the SPWM is limited to 0.5 V_{dc}. If the SPWM technique is used in motor drive applications, the available voltage may not be sufficient to run the motor at a rated condition. In this situation, the machine needs to be derated and a reduced torque is produced. To enhance the output voltage from the PWM inverter using carrier based scheme, third-harmonic injection, shown in Figure 2.33 in the modulating scheme is done. It is shown that by adding an appropriate third harmonic component of the modulating signal in the fundamental modulating signal leads to a reduction in the peak of the resultant modulating signal, Hence the reference value of the resulting modulated signals can be increase beyond $0.5V_{dc}$ and that leads to the higher output voltage at the inverter. The injected third-harmonic component in the modulated signal or reference leg voltages cancels out in the legs and does not appear in the output phase voltages. Thus the output voltage does not contain the undesired low-order harmonics. The optimal level of the third-harmonic injection can be determined by considering the modulating signals:

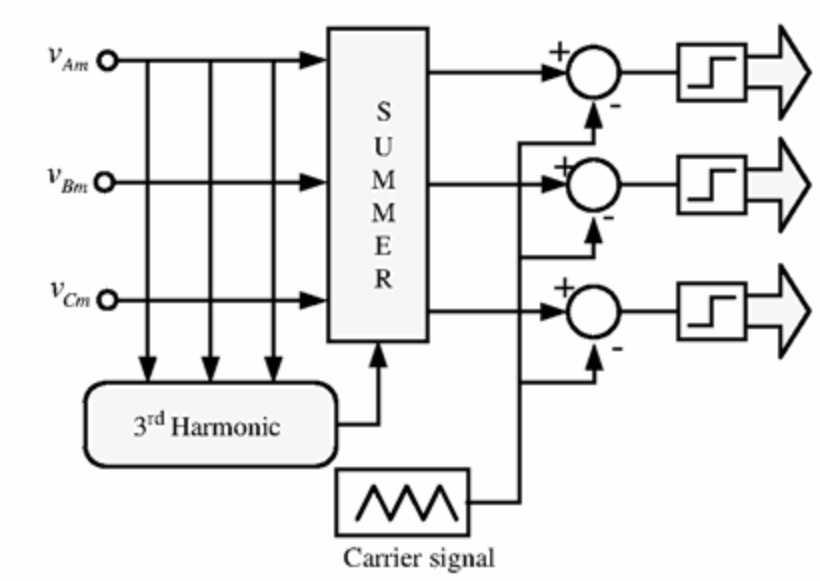

Figure 2.33. PWM with 3rd harmonic injection.

$$V_{Am} = V_{m1}\sin(wt) + V_{m3}\sin(3wt) \tag{2. 9}$$

$$V_{Bm} = V_m \sin\left(wt - \frac{2\pi}{3}\right) + V_{m3}\sin(3wt) \tag{2. 10}$$

$$V_{Cm} = V_m \sin\left(wt + \frac{2\pi}{3}\right) + V_{m3}\sin(3wt) \quad (2.11)$$

For the SPWM without harmonic injection, the fundamental peak magnitude of the output voltage is $0.5V_{dc}$. It is noted that the third harmonic has no effect on the value of the reference waveform when $= (2k+1)\frac{\pi}{3}$, since $\sin(3(2k+1)\frac{\pi}{3})$ for all odd k. Thus the third harmonic is chosen to make the peak magnitude of the reference equation occur where the third harmonic is zero.

The reference voltage reaches a maximum when

$$\frac{dv_{am}}{dwt} = V_{m1}\sin(wt) + V_{m3}\sin(3wt) = 0 \quad (2.12)$$

which yields

$$V_{m3} = -\frac{1}{3}V_{m1}\cos(\tfrac{\pi}{3}) \text{ for } wt = \frac{\pi}{3} \quad (2.13)$$

$$V_{m1} = \frac{0.5V_{dc}}{\sin(\frac{\pi}{3})} \text{ for } wt = \frac{\pi}{3} \quad (2.14)$$

$$V_{m3} = -\frac{1}{3}V_{m1}\cos(\tfrac{\pi}{3}) \text{ for } wt = \frac{\pi}{3} \quad (2.15)$$

Therefore, we have

$$V_{m1} = \frac{0.5V_{dc}}{\sin(\frac{\pi}{3})} \text{ for } wt = \frac{\pi}{3} \quad (2.16)$$

Thus the output fundamental voltage is increase by 15.47% of the value obtainable using simple SPWM by injecting $1/6^{th}$ third harmonic originally.

Space Vector Modulation

Space vector modulation is one of the real time modulation schemes used for the digital control of voltage source converters.

Switching States

We will denote the switches' "ON" state, where the switch is closed as 1 and the switches' "OFF" state where the switch is open as 0. As indicated in the table the switching state O denotes that the upper switch in leg is ON and the switching state X means that the lower

switch in the leg is ON and the inverter terminal voltage is zero due to the conduction of the lower switch [25].

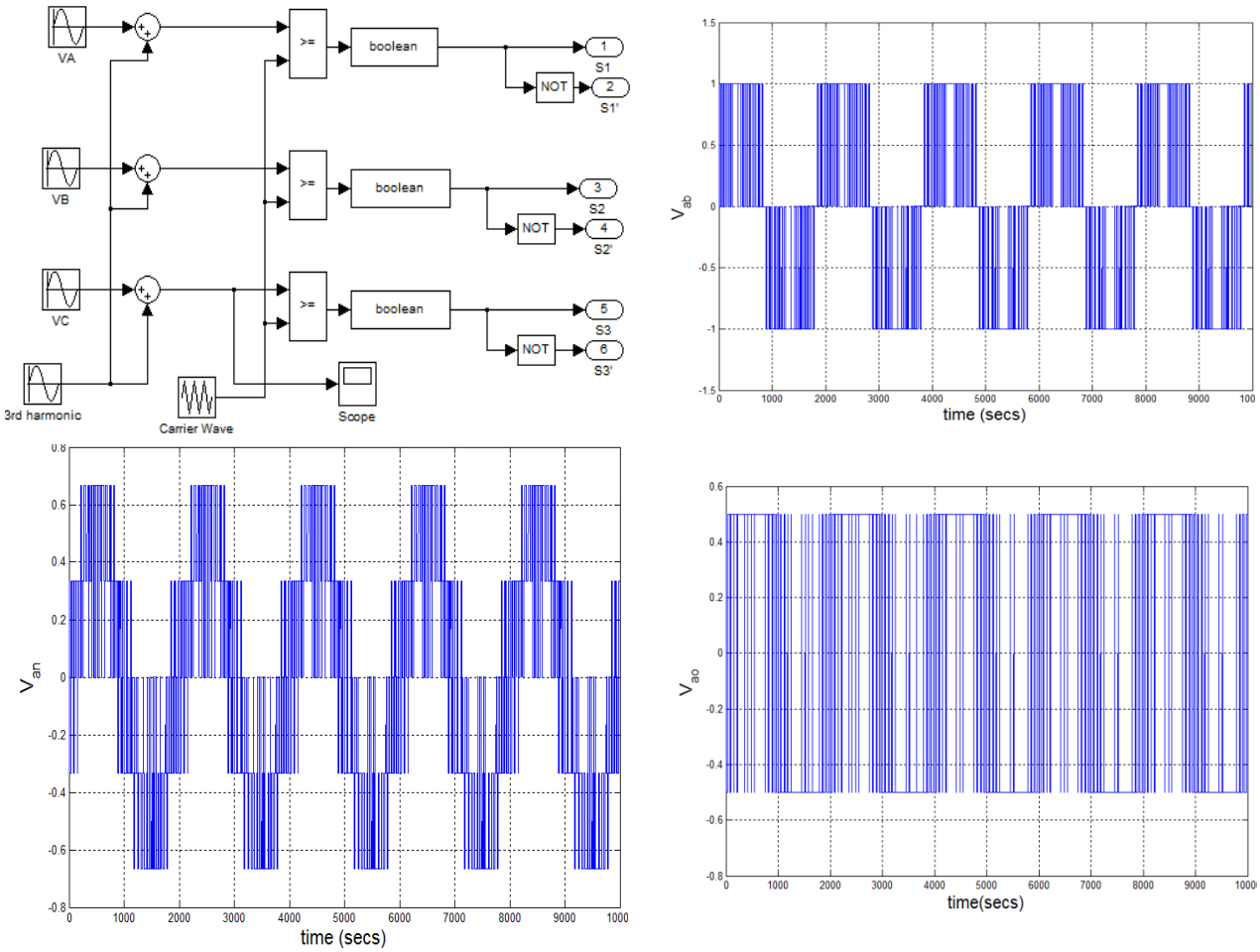

Figure 2.34. Pulse generation for the 3rd harmonic injection PWM scheme and Output voltage waveforms of a 3rd harmonic injection PWM scheme.

Table 1. Switching state in a 2-level VSC

Switching state	Leg a			Leg b			Leg c		
	S_1	S_4	V_{aN}	S_3	S_b	V_{bN}	S_5	S_2	V_{cN}
O	1	0	V_{dc}	1	0	V_{dc}	1	0	V_{dc}
X	0	1	0	0	1	0	0	1	0

The eight possible combinations of switching states in the two-level inverter are listed in the Table 1. Switching state in a 2-level VSC

Space Vectors

The active and zero switching states can be represented by active and zero space vectors, respectively as shown in the Figure 2.35, where there are six active vectors $\overrightarrow{V_1}$ to $\overrightarrow{V_6}$ form a regular hexagon with six equal sectors (I to VI). The zero vector lies in the center of the hexagon.

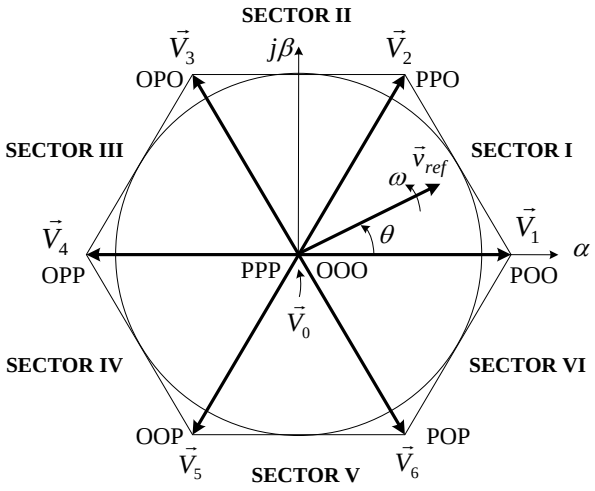

Figure 2.35. Space vector diagram [5].

Table 2. Space vectors, switching states, and on-states switches

Space Vector		Switching state	On-State Switch	Vector definition
Zero Vector	$\overrightarrow{V_0}$	[111] [000]	S_1, S_3, S_5 S_4, S_6, S_2	$\overrightarrow{V_0} = 0$
Active vector	$\overrightarrow{V_1}$	[100]	S_1, S_6, S_2	$V_1 = \frac{2}{3} V_{dc} e^{j0}$
	$\overrightarrow{V_2}$	[110]	S_1, S_3, S_2	$V_2 = \frac{2}{3} V_{dc} e^{\frac{j\pi}{3}}$
	$\overrightarrow{V_3}$	[010]	S_4, S_3, S_2	$V_3 = \frac{2}{3} V_{dc} e^{\frac{j2\pi}{3}}$
	$\overrightarrow{V_4}$	[011]	S_4, S_3, S_5	$V_4 = \frac{2}{3} V_{dc} e^{\frac{j3\pi}{3}}$
	$\overrightarrow{V_5}$	[001]	S_4, S_6, S_5	$V_5 = \frac{2}{3} V_{dc} e^{\frac{4j\pi}{3}}$
	$\overrightarrow{V_6}$	[101]	S_1, S_6, S_5	$V_6 = \frac{2}{3} V_{dc} e^{\frac{5j\pi}{3}}$

Assuming balanced operation of the inverter, we have

$$v_a(t) + v_b(t) + v_c(t) = 0 \tag{2.17}$$

where v_a , v_b , v_c are the instantaneous load phase voltages. It is possible to transform the three phase variables to two phase variables through park's transform

$$\begin{bmatrix} v_\alpha(t) \\ v_\beta(t) \end{bmatrix} = \frac{2}{3}\begin{bmatrix} 1 & -\frac{1}{2} & -\frac{1}{2} \\ 0 & \sqrt{\frac{3}{2}} & -\sqrt{\frac{3}{2}} \end{bmatrix}\begin{bmatrix} v_a(t) \\ v_a(t) \\ v_a(t) \end{bmatrix} \tag{2.18}$$

A space vector generally expressed in terms of two phase voltages in the $\alpha\beta$ frame

$$v(t) = v_\alpha(t) + j\, v_\beta(t) \tag{2.19}$$

Substituting

$$\bar{v}(t) = \frac{2}{3}\,[v_a(t)e^{j0} + v_b(t)e^{j2\pi/3} + v_c(t)e^{j4\pi/3}] \tag{2.20}$$

where $e^{jx} = \cos x + j\sin x$ and $x = 0, \frac{2\pi}{3}\ or\ \frac{4\pi}{3}$. For the active switching state [100], the generated load phase voltages are

$$v_a(t) = \tfrac{2}{3}\,V_{dc}\,, v_b(t) = -\tfrac{1}{3}\,V_{dc} \text{ and } v_c(t) = -\tfrac{1}{3}\,V_{dc} \tag{2.21}$$

The corresponding space vector, denoted as $\overrightarrow{V_1}$, can be obtained by substituting eqn (2.21) into (2.20)

$$\overrightarrow{V_1} = \frac{2}{3}V_{dc}e^{jo} \tag{2.22}$$

The zero vector $\vec{V}_0$ has two switching states [111] and [000], one of which is redundant and these are used to minimize switching frequency of the inverter. The zero and active vectors do not move in space and are referred to as stationary vectors. The reference vector $\vec{v}_{ref}$rotates at an angular velocity

$$\omega = 2\pi f \tag{2.23}$$

where f is the fundamental frequency of the inverter. The angular displacement between $\vec{v}_{ref}$ and the α-axis of the $\alpha - \beta$ frame can be obtained by

$$\theta(t) = \int_0^t \omega(t)dt + \theta_0 \tag{2.24}$$

For a given magnitude and position, v_{ref} can be synthesized by three nearby stationary vectors, based on which the switching states of the inverter can be selected and the gate signals can be generated. When v_{ref} passes through the sectors one by one, different sets of switches will be turned on or off [5, 26].

Switching Sequence

When the space vectors are selected the next time is to arrange the switching sequence. The switching sequence should satisfy two requirements

- The transition from one switching state to the next involves only two switches in the same inverter leg, one being switched on and the other switched off
- The transition of $\vec{v}_{ref}$ moving from one sector to the next requires minimum number of switchings.

Figure 2.36 shows a typical seven-segment switching sequence and inverter output voltage waveforms for $\vec{v}_{ref}$ in sector 1 where $\vec{v}_{ref}$ is synthesized by $\vec{V}_1, \vec{V}_2, \vec{V}_0$.

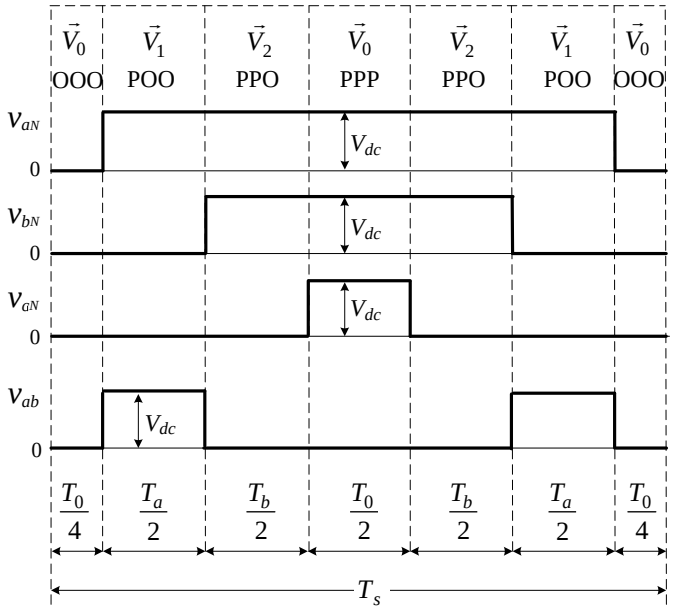

Figure 2.36. Seven-segment switching sequence for $\vec{V}_{ref}$ in sector I [5].

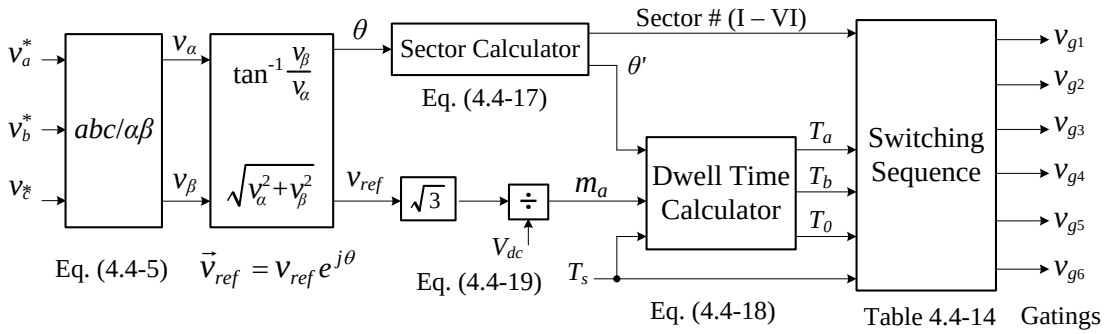

Figure 2.37. Block diagram for computer simulation and real time digital implementation of the SVM algorithm[5].

SIMULINK Implementation of the SVPWM Scheme

The simulated waveforms for the inverter output voltage and the load current are seen in Figure 2.38. The inverter operates under the condition of $f_1 = 60\ hz, f_{\text{sw}} = 1980$ hz , and $m_a = 0.8$ with a rated three-phase inductive laod. It can be obeserved from the wave for m that the inverter line-to-line voltage v_{ab} is not symmetrical; therefore it contains even-order harmonics such as 2nd, 4ht, 8th and 10th, in addition to odd-order harmonics. The total harmonic distortion (THD) of v_{ab} is 56.1%.

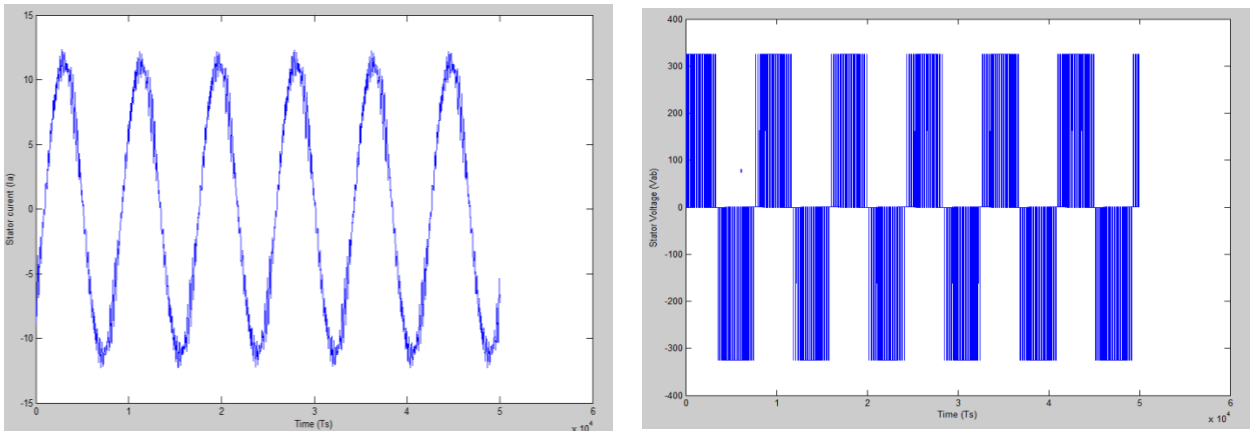

Figure 2.38. Inverter output waveforms produced by SVM scheme with f_1=60 hz, f_{sw} = 1980 hz , and m_a=0.8.

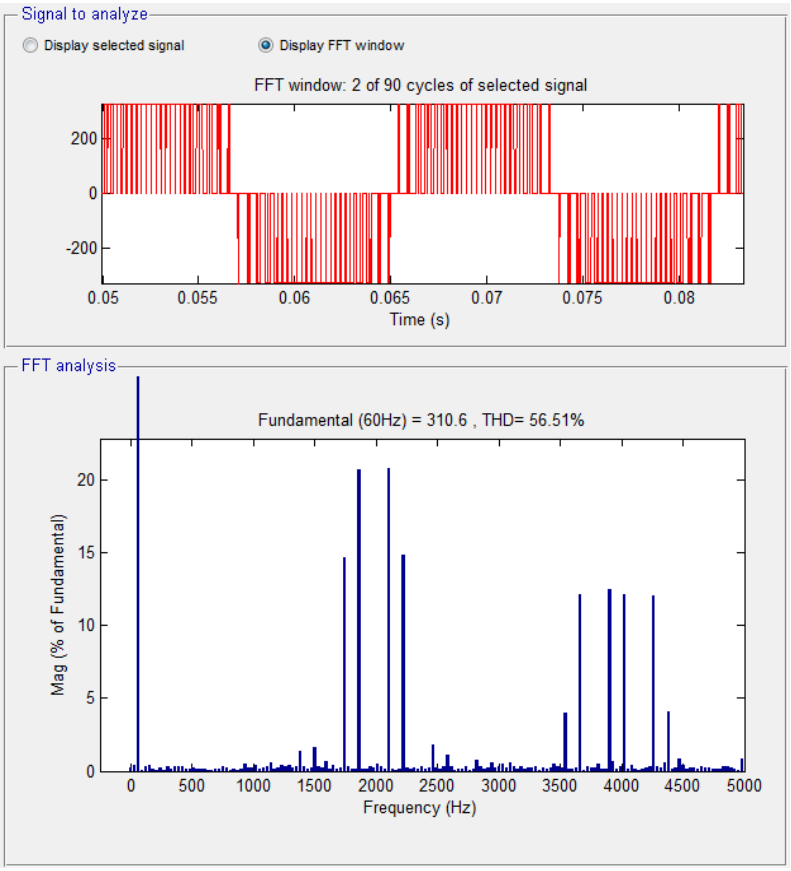

Figure 2.39. Harmonics spectrum.

2.2.1.5 Multi-Level Inverters

The three phase voltage source converter (two-level) is by far the most common DC-AC power converters in practice. Recently multi-level inverters have gained a lot of interest. Multi-level inverters offer better performance than two level inverters but they are more complex and costly.

These multi-level inverters can be classified as 3, 4, and 5 level inverter of these the three level inverter the neutral point clamped (NPC) inverter has found with practical applications. The main features of the NPC include reduced THD in its output voltages in comparison to the two-level inverter.

Three Level Neutral Point Converter

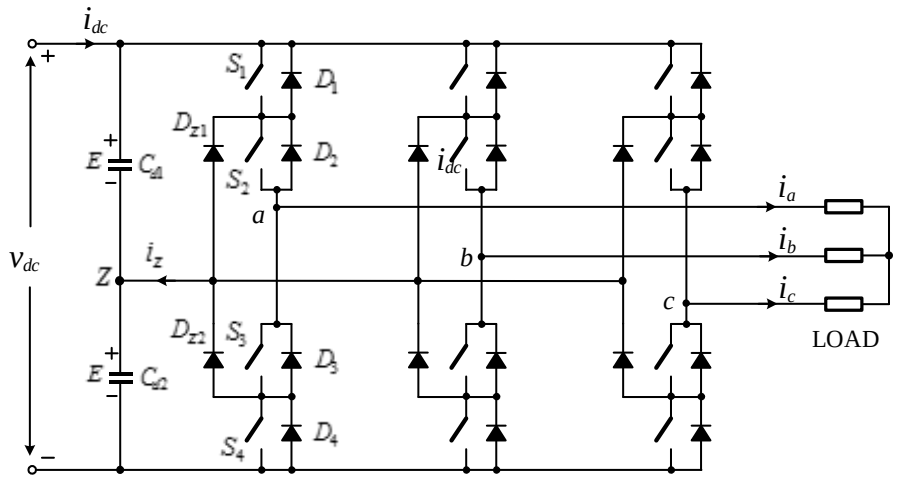

Figure 2.40. 3-level NPC inverter [5].

Figure 2.40 shows the simplified diagram of the NPC converter. The obvious difference from the 2-level inverter and the NPC converter is that NPC has four active switches in each leg with four antiparallel diodes. In practice either an IGBT or IGCT can be employed as a switching device. On the DC side a DC bus capacitor is split into two providing a neutral point. The operating states of the switches of the NPC are represented in the Table 3.

Table 3. Switching states in a NPC.

Switching state	Device Switching states (Phase a)				Inverter terminal voltage
	S_1	S_2	S_3	S_4	V_{aZ}
O	1	1	0	0	E
X	0	1	1	0	0
Y	0	0	1	1	$-E$

Switching state O means that the upper two switches in leg a are ON and the inverter voltage v_{aN} is $+E$ where as Y indicates that lower two switches conduct leading to $v_{aN} = -E$. The switching state X indicates that the inner two switches $S_2$and S_3 are ON and the v_{aN} is clamped to zero through the clamping diodes. Figure 2.42 shows the line-to-line voltage waveform is obtained. The inverter terminal voltages v_{aN}, v_{bN}, v_{cN} are three phase balanced with a phase shift of 120^o. The line-to-line to voltage can be found from $v_{ab} = v_{aN} - v_{bN}$).[17, 22, 24, 26].

Space Vector Modulation

Taking all the three phases into account, the inverter has a total of 27 combinations if switching states (3^3 – even though the converter has 4 switches in one leg only three are use). The principle of the space vector modulation for the NPC, shown in the Figure 2.41 is the same for the two-level but the implementation is complicated. The simulation waveforms and the harmonic analysis are shown in Figure 2.42 and Figure 2.43. The only difference is that now for any given position in space the reference vector $\vec{v}_{ref}$ can be synthesized by three vectors [27].

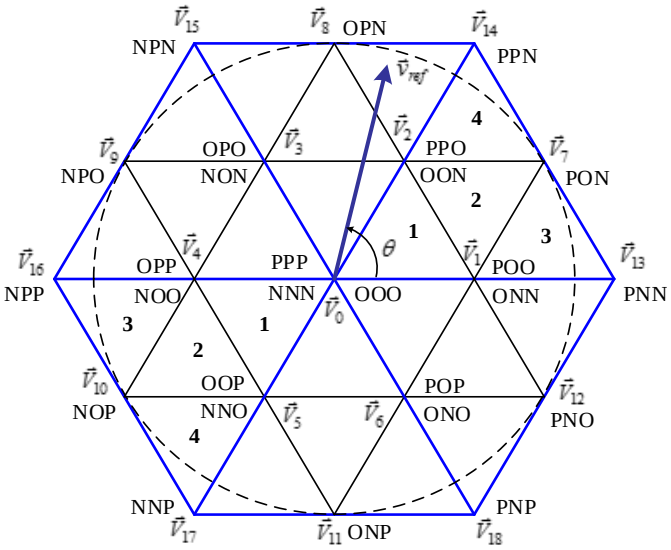

Figure 2.41. Space vector diagram [5].

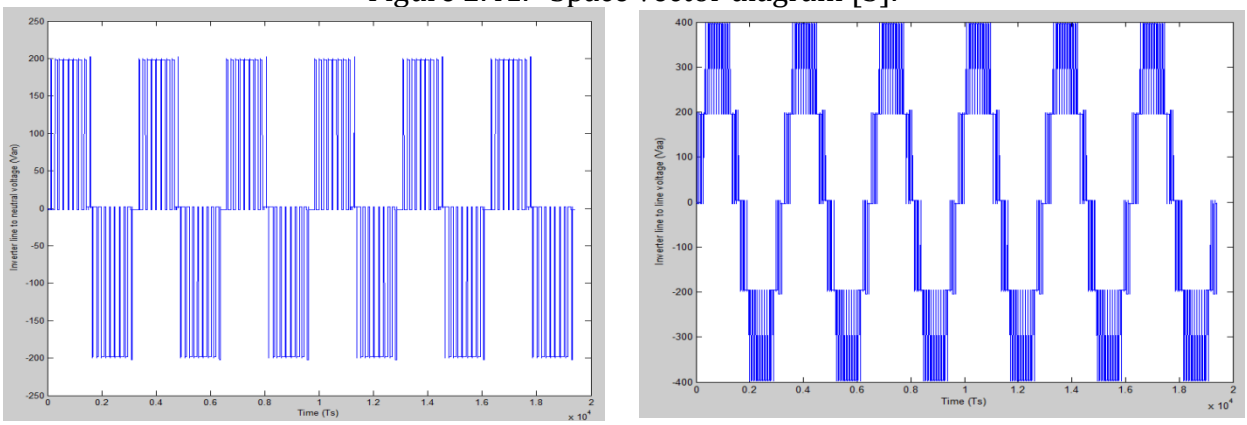

(a) (b)

Figure 2.42. Simulated voltage waveforms of the NPC inverter (f_1=60hz, T_s=0.1sec, f_{sw}=1080 hz and m_a=0.8) (a) Line-to-neutral voltage, (b) line-to-line voltage.

(a)

(b)

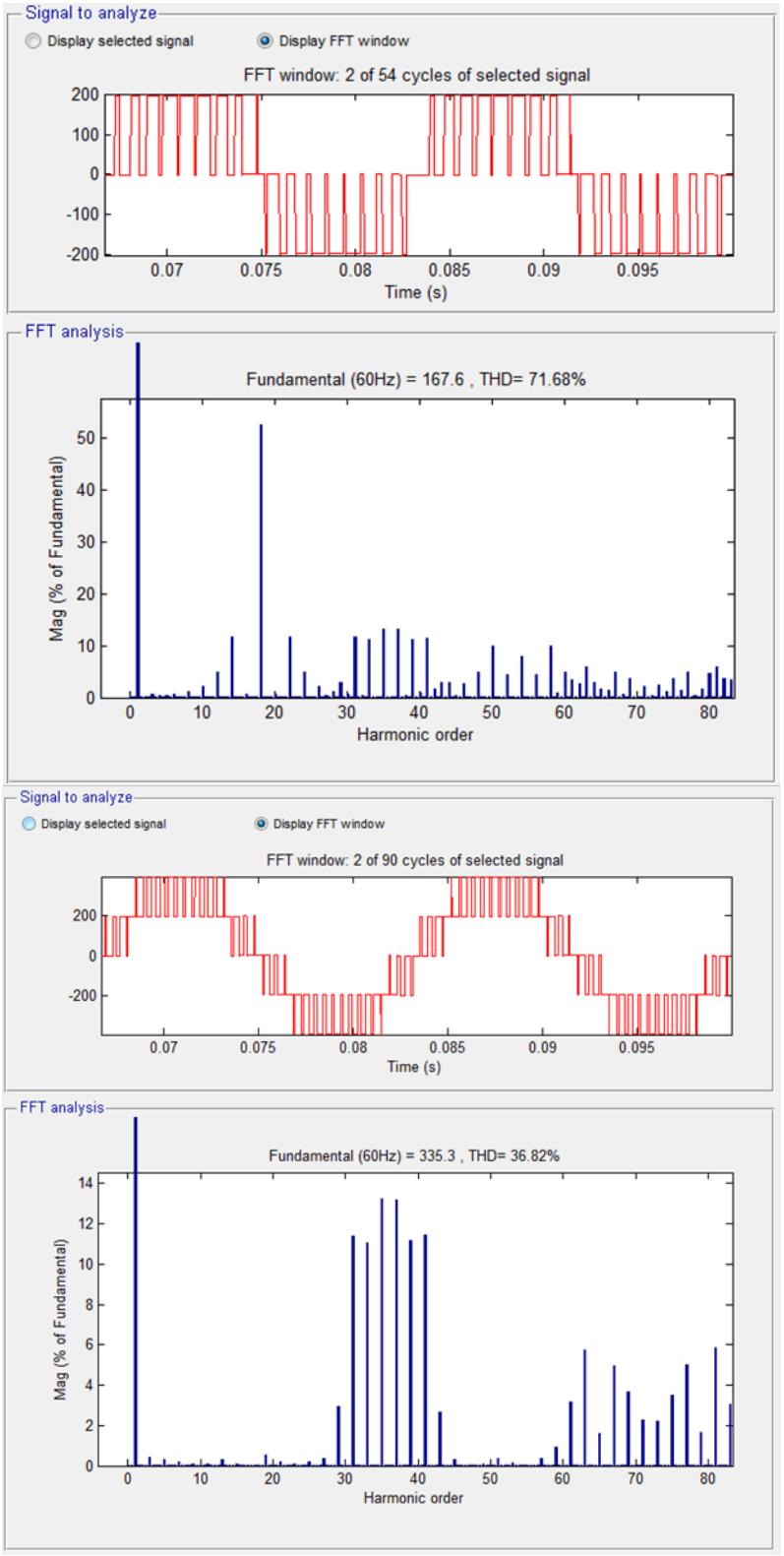

Figure 2.43. Harmonic spectrum of (a) Line-to-neutral voltage, (b) line-to-line voltage..

2.2.1.6 Current Source Converters

The freewheeling diodes used in the voltage source converters become redundant if an inverter is supplied from a DC current source instead of a voltage source. Then the current entering any leg of the inverter cannot change its polarity and therefore through the semiconductor switches.

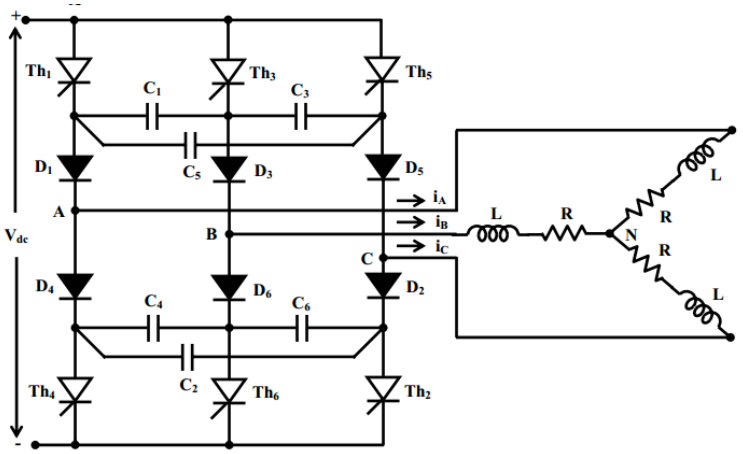

Figure 2.44. Three phase current source inverter [28].

The absence of the freewheeling diodes reduces the size and weight of the circuit and further increases the reliability of the current-source inverter. The practical current source consists of a controlled rectifier and Inductive DC link.

Figure 2.44 shows the typical simplified current source converter. Here in CSC's the simultaneous conduction of both the switches in an inverter leg is allowed then, $2^6 = 64$ states of the inverter are possible and six switching variables, one for each switch can be defined. The switching patter design for the CSI should generally satisfy two conditions: (1) the DC current i_{dc}should be continuous and (2) the inverter PWM i_{aw} should be defined. In other words there are only two switches conducting: one in the top half of the bridge and the other in the bottom half [17, 22, 24, 26].

Harmonic Elimination PWM Method

With only one switch turned ON the continuity of the DC current is lost and if more than two switches are ON simultaneously, the PWM currenti_{aw} is not defined by the switching pattern. Selective harmonic elimination (SHE) is and offline modulation scheme, which is

able to eliminate a number of low-order unwanted harmonics in the PWM inverter current i_{aw} . Figure 2.45 shows a typical SHE waveform. There are five pulses per half cycle with five switching angles in the first 180^o. However the first two angles, θ_1 and θ_2 are independent. Given these two angles, all the other switching angles can be calculated.

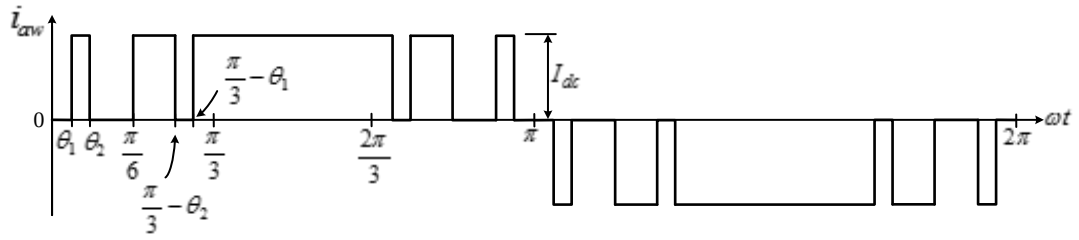

Figure 2.45. Selective harmonic elimination scheme (SHE) [5].

The two switching angles give two degrees of freedom which can be used to eliminate two harmonics in i_{aw} without modulation index control or eliminate one harmonic and provide an adjustable modulation index m_a. The first option is preferred since the adjustment if i_{aw} is normally done by varying i_{dc}. The number of harmonics is then given by $k = \frac{N_p-1}{2}$.

To determine the switching angles such as θ_1 and θ_2 for harmonic elimination, Fourier analysis used to obtain set of nonlinear equations. These equations can be solved by numerical methods [16, 26].

Space Vector Modulation (SVM)

In addition to the SHE scheme, the current source inverter can also be controlled by space vector modulation (SVM)

Space Vectors

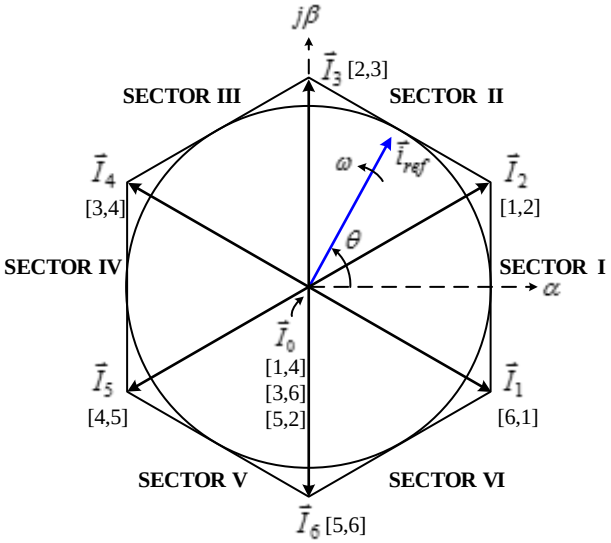

Figure 2.46. Space vectors [5].

Switching States

As stated earlier the PWM switching pattern, given in the Table 4 for the CSI must satisfy the constraint that only two switches in the inverter conduct at any time instant, on in the top half of the CSI bridge and the other in the bottom half.

The space vector diagram for the CSI is as shown where $\vec{I}_1$ to $\vec{I}_6$ are active vectors and $\vec{I}_0$is the zero vector. As seen for the VSC, the active vectors form a hexagon with six equal sectors, whereas the zero vector $\vec{I}_0$ lies at the center of the hexagon. Assuming that operation of the inverter is balanced

$$i_{aw}(t) + i_{bw}(t) + i_{cw}(t) = 0 \tag{2. 25}$$

Table 4. Switching states of CSI.

TYPE	Switching state	ON state	Inverter PWM '*i*'			Space Vector
			i_{aw}	i_{bw}	i_{cw}	
Zero states	$(1,4)$ $(3,6)$ $(5,2)$	S_1, S_4 S_3, S_6 S_5, S_2	0	0	0	$\vec{I}_o$
Act states	$(6,1)$	S_6, S_1	I_{dc}	$-I_{dc}$	0	$\vec{I}_1$
	$(1,2)$	S_1, S_2	I_{dc}	0	$-I_{dc}$	$\vec{I}_2$
	$(2,3)$	S_2, S_3	0	I_{dc}	$-I_{dc}$	$\vec{I}_3$
	$(3,4)$	S_3, S_4	$-I_{dc}$	I_{dc}	0	$\vec{I}_4$
	$(4,5)$	S_4, S_5	$-I_{dc}$	0	I_{dc}	$\vec{I}_5$
	$(2,6)$	S_2, S_6	0	$-I_{dc}$	I_{dc}	$\vec{I}_6$

where $i_{aw}(t), i_{bw}(t),\ i_{cw}(t)$ are the instantaneous PWM output currents in the inverter phases $a\ , b, c$. These three phase currents can be transformed into two-phase currents in the $\alpha\beta$ frame

$$\begin{bmatrix} i_\alpha \\ i_\beta \end{bmatrix} = \frac{2}{3}\begin{bmatrix} 1 & -\frac{1}{2} & -\frac{1}{2} \\ 0 & \sqrt{\frac{3}{2}} & -\sqrt{\frac{3}{2}} \end{bmatrix}\begin{bmatrix} i_{aw}(t) \\ i_{bw}(t) \\ i_{cw}(t) \end{bmatrix} \tag{2. 26}$$

A current-space vector can be generally expressed in terms of the two phase currents as

$$\bar{\imath}(t) = \ i_\alpha + j i_\beta \tag{2. 27}$$

substituting (2. 27) in (2. 27)

$$\bar{\imath}(t) = \frac{2}{3}\ [i_{aw}(t)e^{j0} + \ i_{bw}(t)e^{j2\pi/3} + \ i_{cw}(t)e^{j4\pi/3}] \tag{2. 28}$$

where $e^{jx} = \cos x + j\sin x$ and $x = 0, \frac{2\pi}{3}\ or\ \frac{4\pi}{3}$. For the active switching state [100], the generated load phase voltages are

$$i_{aw}(t) = I_{dc}\ , i_{bw}(t) = -\ I_{dc} \text{ and } i_{cw}(t) = 0 \tag{2. 29}$$

The corresponding space vector, denoted as $\vec{I}_1$,can be obtained

$$\overrightarrow{I_1} = \frac{2}{\sqrt{3}} I_{dc} e^{j(-\pi/6)} \tag{2. 30}$$

Similarly 5 other vectors can be derived and the active vectors can be expressed as

$$\overrightarrow{I_1} = \frac{2}{\sqrt{3}} I_{dc} e^{j((k-1)\frac{\pi}{3} - \frac{\pi}{6})} \tag{2. 31}$$

PWM Current Source Rectifier

The Figure 2.47. PWM current-source rectifiershows a PWM current source rectifier (CSR) in a wind energy conversion system. Like the current source inverter (CSI), the PWM

rectifier a filter capacitor C_r to assist the commutation of switching devices and filter out current harmonics. Both the selective harmonic elimination (SHE) and space vector modulation (SVM) can be used for the CSR.

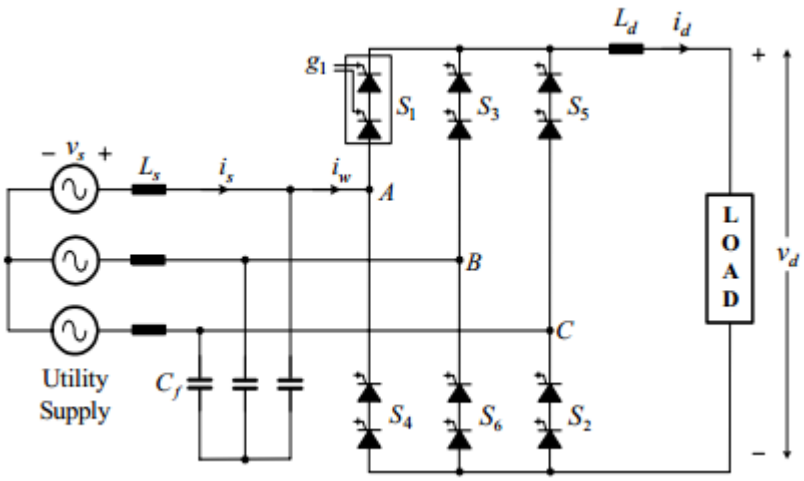

Figure 2.47. PWM current-source rectifier [29].

The DC output voltage v_{dc} of the rectifier can be adjusted by two methods: modulation index m_a control and delay angle (α) control. The operating principle of delay angle control is the same as that of phase-controlled SCR rectifiers.

The input active power of the rectifier can be expressed as

$$P_{ac} = 3V_{a1}I_{aw1}cos\alpha \tag{2.32}$$

where $V_{a1}$the fundamental-frequency rms phase is input voltage and I_{aw1} is the PWM input current of the rectifier. The delay angle α is defined as the angle between V_{a1} and I_{aw1}, respectively. The DC output power is given by

$$P_{dc} = V_{dc}I_{dc} \tag{2.33}$$

2.2.1.7 Control of Grid Connected Inverter

Most commercial wind turbines today deliver the generated power to the electric grid through power converters and hence the gird side inverter is the most important device in the power conversion system. It is desirable to send optimal power to the grid with

controllable power factor or voltage and to have harmonic performance satisfying the system grid. The grid side inverter, as a main component, must possess these features.

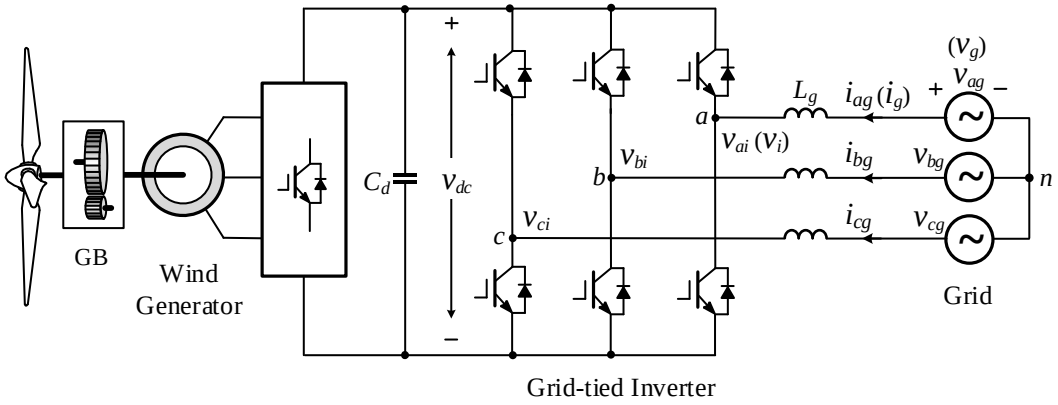

Figure 2.48. Grid tied Inverter [5].

A typical grid connected inverter for wind energy applications is shown in Figure 2.48. Grid tied Inverter where a two level converter is used in inverter mode.

If the wind energy system is simplified to a system shown in figure where the wind turbine, generator and is replaced by a battery in series with a small resistance that represents the losses in the system. The active power transmitted to the grid can be calculated by

$$P_g = 3\, V_g I_g cos\varphi_g \tag{2. 34}$$

where φ_g is $\angle\overrightarrow{V_g} - \angle\overrightarrow{I_g}$

It is often expected by the grid operator that a wind energy system provide a controllable reactive power to the grid to support the grid voltage in addition to the active power production [5, 30].

Voltage Oriented Control (VOC)

The grid connected inverter can be controlled by various schemes and one of these schemes is voltage oriented control. The control algorithm is implemented in the grid voltage synchronous frame, where all the variables are of DC components in the steady state. This facilitates the design and control of the inverter.

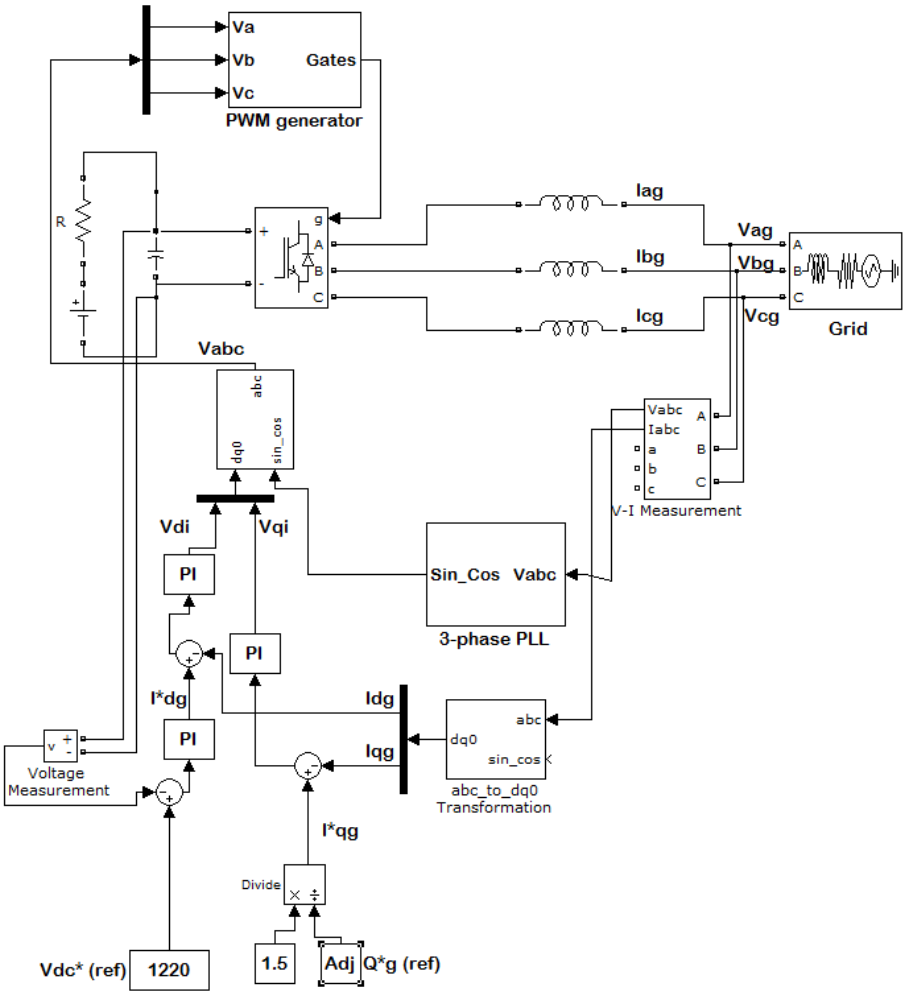

Figure 2.49. Simulation model of voltage oriented control.

To realize the VOC, the grid voltage is measured and its angle θ_g is detected for the voltage orientation and this angle is used for transformation of variables from abc frame to the dq synchronous frame or vice versa. Assuming that the grid voltages, v_{ag}, v_{bg}, v_{cg} are three phase balanced sinusoidal waveforms, θ_g can be obtained from

$$\theta_g = \tan^{-1}\frac{v_\beta}{v_\alpha} \tag{2.35}$$

and v_α and v_β can be obtained by the abc to $\alpha\beta$ transformation

$$v_\alpha = \frac{2}{3}\left(v_{ag} - \frac{1}{2}v_{bg} - \frac{1}{2}v_{cg}\right) = v_{ag} \tag{2.36}$$

$$v_\beta = \frac{2}{3}\left(\frac{\sqrt{3}}{2}v_{bg} - \frac{\sqrt{3}}{2}v_{cg}\right) = \frac{\sqrt{3}}{3}(v_{ag} + 2v_{bg}) \quad (2.37)$$

In practical systems digital filters or phase locked loops (PLL's) are used for detection of θ_g by filtering out the harmonics. There are three feedback control loops in the system: two inner current loops for the accurate control of the dq-axis currents i_{dg} and i_{qg}, and one outer DC voltage feedback loop for the control of DC voltage v_{dc}. In the VOC scheme, the three-phase line currents in the abc stationary frame i_{ag}, i_{bg} and i_{cg} are transformed to the two phase currents i_{dg} and i_{qg} in the dq synchronous frame, which are the active and reactive components of the three-phase line currents and the independent control of these two components provides an effective means of independent control of system active and reactive power [5, 30-32].

To achieve the VOC control, the d-axis of the synchronous frame is aligned with the grid voltage vector, therefore $(v_{dg} = v_g)$, and the resultant q-axis voltage v_{qg} is then equal to zero. Now the active and reactive power can be calculate by

$$P_g = \frac{3}{2}(v_{dg}i_{dg} + v_{dg}i_{qg}) = \frac{3}{2}v_{dg}i_{dg} \quad (2.38)$$

$$Q_g = \frac{3}{2}(v_{qg}i_{dg} - v_{dg}i_{qg}) = -\frac{3}{2}v_{dg}i_{qg} \quad (2.39)$$

The q-axis current reference i_{qg}^* can then be obtained from

$$i^* = -\frac{Q_g^*}{-1.5v_{dg}} \quad (2.40)$$

where Q_g^* is the reference for the reactive power.

The d-axis current reference i_{dg}^*, which represents the active power of the system, is generated by the PI controller for DC voltage control. When the inverter is operated in steady state, the DC voltage v_{dc} of the inverter is kept constant at a value set by its reference $v^*{}_{dc}$. Neglecting the losses in the inverter

$$P_g = \frac{3}{2} v_{dg} i_{dg} \tag{2. 41}$$

As we know that the power flow between the inverter system is bidirectional, the control system will automatically switch between two operating modes. The average DC voltage V_{dc} of the inverter is set by its reference v_{dc}^* and is kept constant by the PI controller[5, 30-32].

$$V_{dc}^* = \frac{\sqrt{6} V_{a1}}{m_a} \tag{2. 42}$$

where V_{a1} is the rms value of the fundamental frequency component.

The operation of the grid tied inverter with VOC is analyzed through a case study. We have considered a 2.3MW/690 V grid tied inverter. This inverter is controlled with a VOC scheme as shown in the Figures 2.50 to 2.53. The DC reference voltage is set to 1220V.

The waveforms show the phase-a grid voltage v_{ag} , the phase-a current and the space angle θ_g. When $\overrightarrow{v_g}$ rotates in space, θ_g and v_{ag} varies from zero to 2π periodically. When θ_g is equal to zero, v_{dg} reaches its peak. The transient current and voltage waveforms also can be seen. The inverter initially delivers rated active power to the grid and zero reactive power. We can see the current waveform for the $d-$ axis current, i_{dg} because the $q-$ axis current, i_{qg} is zero.

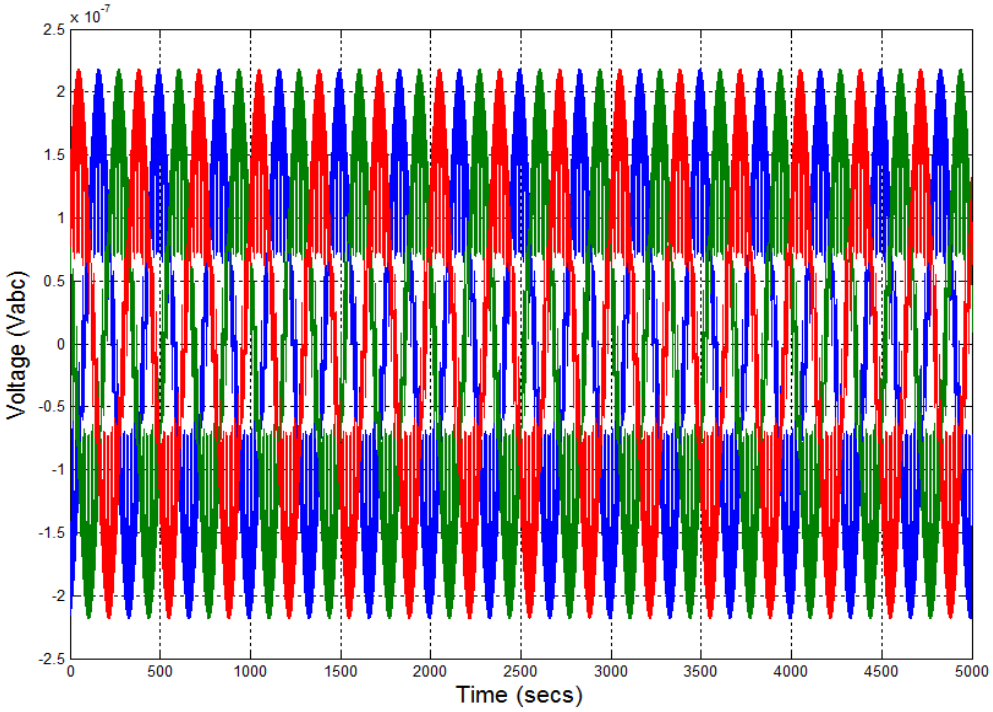

Figure 2.50. *abc* grid voltages.

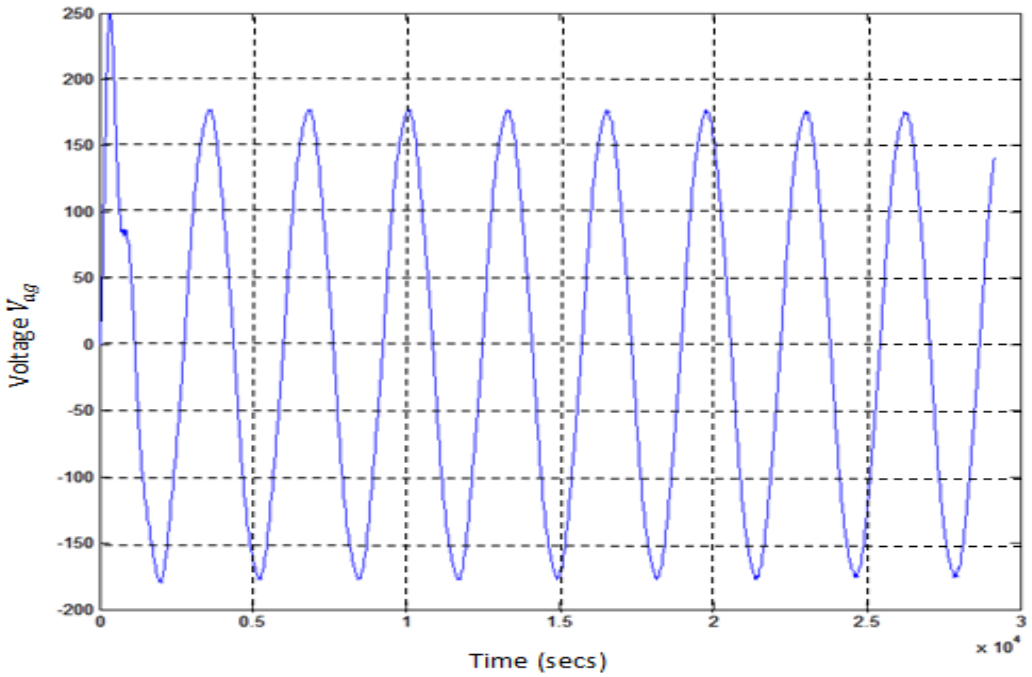

Figure 2.51. Phase-*a* grid voltage.

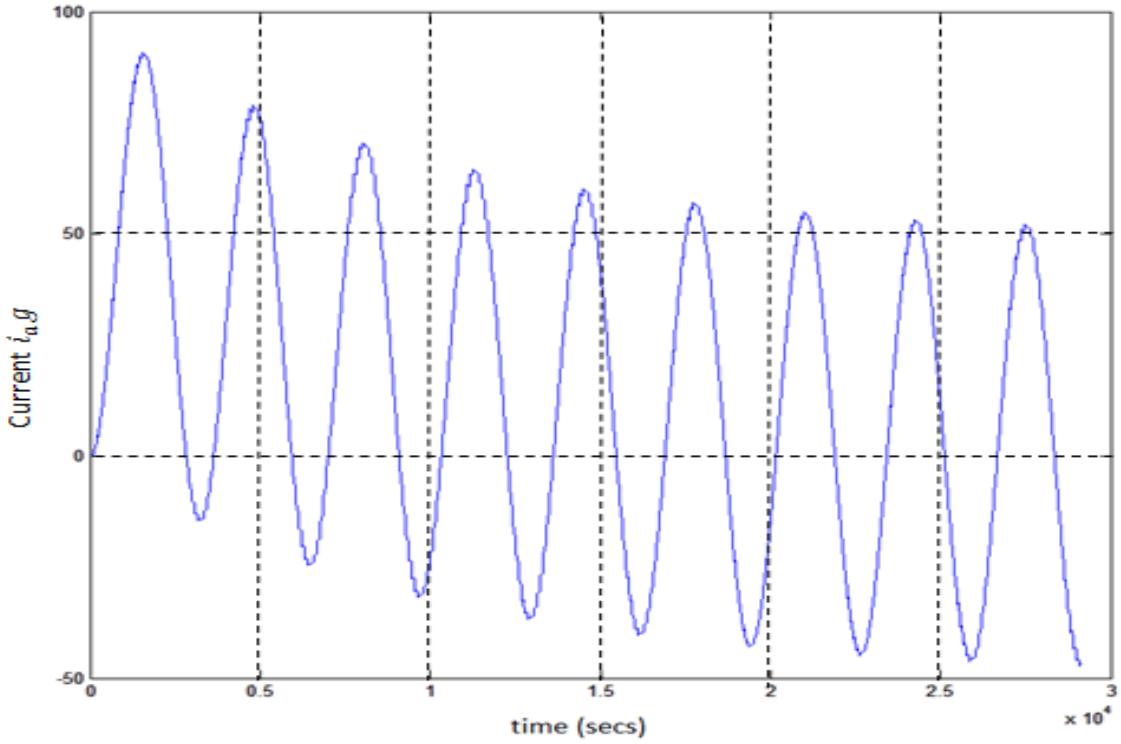

Figure 2.52. Phase-*a* grid current.

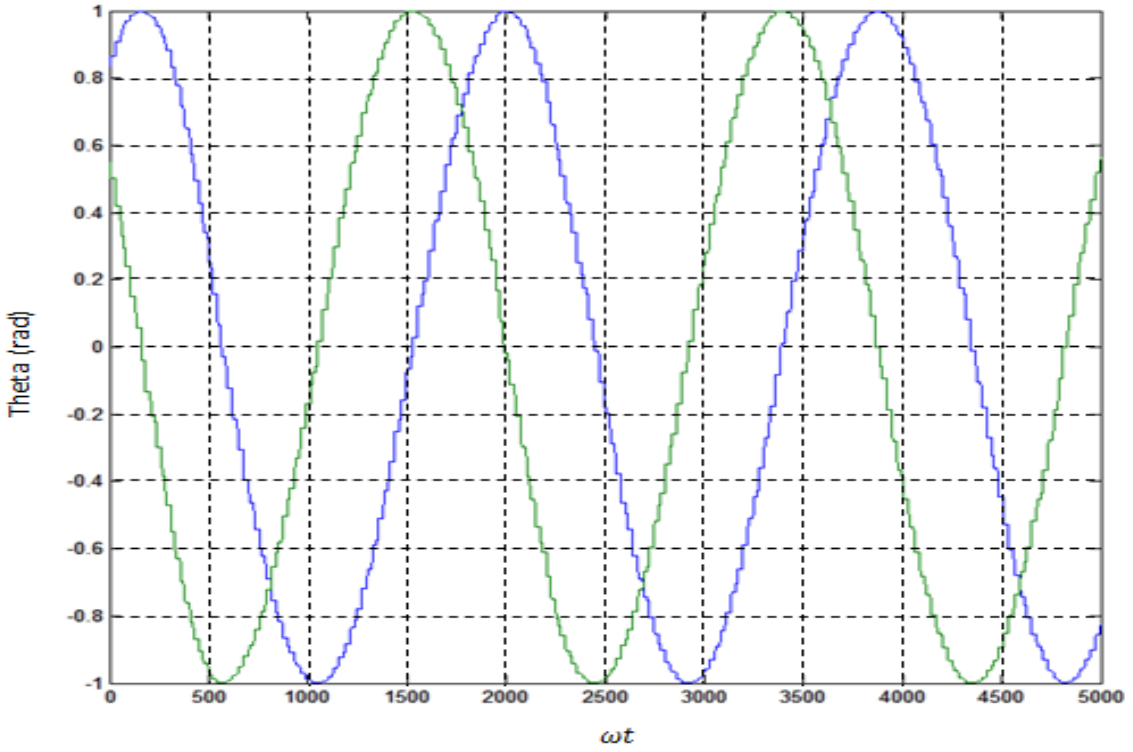

Figure 2.53. theta – angle.

Reducing the battery voltage to such an extent that the active power to the grid is reduced to 0.8pu (i.e 80 percent of the rated power), leads to the reduction of the $d-$axis current (the $q-$axis current remains unchanged) and also the magnitude of the phase-a grid current i_{ag} is reduced, but kept out of phase with the voltage.

The state equations for the grid-side circuit of the inverter in the abc stationary reference are expressed as

$$\frac{di_{ag}}{dt} = (v_{ag} - v_{ai})/L_g \tag{2. 43}$$

$$\frac{di_{ag}}{dt} = (v_{bg} - v_{bi})/L_g \tag{2. 44}$$

$$\frac{di_{ag}}{dt} = (v_{cg} - v_{ci})/L_g \tag{2. 45}$$

Transforming the equations into the dq synchronous reference frame

$$\frac{di_{ag}}{dt} = \frac{v_{dg} - v_{di} + \omega_g L_g i_{qg}}{L_g} \tag{2. 46}$$

$$\frac{di_{qg}}{dt} = \frac{v_{qg} - v_{qi} + \omega_g L_g i_{dg}}{L_g} \tag{2. 47}$$

where ω_g is the speed of the synchronous reference frame and $\omega_g L_g i_{qg}$ and $\omega_g L_g i_{dg}$ are the induced speed voltage s due to the transformation of the three-phase inductance L_g.

Observing the equations (2. 48) and (2. 49) we understand that the derivative of the d-axis line current i_{dg} is related to both d-axis and q-axis variables, as in the q-axis current i_{qg}. This indicates that the system is cross-coupled, which may lead to difficulties in controller design and to solve this problem we can implement decoupled controller.

$$\frac{di_{ag}}{dt} = \frac{\left(k_1 + \frac{k_2}{s}\right)\left(i_{dg}^* - i_{dg}\right)}{L_g} \tag{2. 50}$$

$$\frac{di_{qg}}{dt} = \frac{\left(k_1 + \frac{k_2}{s}\right)\left(i_{qg}^* - i_{qg}\right)}{L_g} \tag{2. 51}$$

Equations (2. 52) and (2. 53) indicate that the control of the d-axis grid current is decoupled, involving only the d-axis components, as is the q-axis currents i_{qg}.

2.3 Summary

This chapter introduces various topologies of wind energy systems based on Induction generator, permanent magnet synchronous generators and double fed induction generators. An overview of these systems is presented in this chapter. These systems include the basic single speed, two speed and the more advanced and the practical variable speed systems. All these three system are explained with the respective generators.

After this, the power electronics systems used in the wind energy systems is explained in detail. The power electronics systems include AC voltage controllers, DC-DC converters and the most important of all, the voltage source converter (rectifier and inverter). The AC voltage converters are basically used as soft started, to reduce the heavy in-rush current while starting of the Induction generators. The DC-DC converters explained are used as buck or boost converters in the wind energy systems. The three phase voltage source converter which is used in every wind energy systems is explained in detail. The switching strategies for the VSC such as sinusoidal pulse width modulation (SPWM), sinusoidal pulse width modulation with insertion of the third harmonic and the widely used space vector pulse width modulation (SVPWM) technique are discussed in detail with their control strategies. The converters and their strategies are analyzed through computer simulations.

Further the grid connected inverter and the control strategy for the grid connected inverter, voltage oriented control is explained. The control strategy is analyzed by simulating the converter using a 2 MW induction generator. The same control strategy is used in later chapters

CHAPTER 3 Wind Energy Systems with Induction Generators

3.1 Introduction

The induction generator with its lower maintenance demands and simplified controls, appears to be a good solution for wind energy generating operations. Because of its simplicity, robustness and small size per generated KW the induction generator is favored for wind power plants. Standing alone the maximum power does not go above 15kW, but when connected to the grid or to other sources it can reach upto 100kW and custom made wound-rotor schemes enable even higher power.

The interfacing the squirrel cage induction generator is not recommended because it transmits all the fluctuations and transients to the grid. The voltage and the frequency and the reactive power must be adjusted according to the grid in order to transmit the power from the renewable source to the grid. In squirrel cage induction generators (SCIG) wind energy conversion systems, full converters are needed to adjust speed of the generator in order to extract maximum power available from wind. A typical configuration of the wind energy system employing a SCIG is shown in figure [5].

3.2 State Space Modeling Of The Induction Generator

Induction machines can be either Induction generators or Induction motors, both are described by the same set of voltage and torque equations. Steady state model of the induction generator neglects electrical transients due to load changes and stator frequency variations. Such variations arise in applications involving variable-speed drives. Variable-speed drives are converter-fed from finite sources, which unlike the utility supply, are limited by switch ratings and filter sizes. Thus, we need to evaluate dynamics of converter-fed variable-speed drives to assess the adequacy of the converter switches and the converters for a given generator and their interaction to determine the excursions of currents and torque in the converter and generator. Thus, the dynamic model considers the

instantaneous effects of varying voltages/currents, stator frequency and torque disturbance. The transient phenomenon is difficult to model from an operational point of view and the impact of self-excitation is more pronounced in generators with a heavier load [33].

Transient state analysis of the Induction generator uses Park's transformation. The Parks transform specifies a two phase primitive machine with fixed stator windings and rotating rotor windings to represent fixed stator windings (direct axis) and pseudo-stationary rotor windings (quadrature axis).

The following system of equations describe the dynamic behavior of the induction machine

$$\begin{Bmatrix} V_s^{abc} \\ V_r^{abc} \end{Bmatrix} = \begin{bmatrix} V_s^{abc} & 0 \\ 0 & V_r^{abc} \end{bmatrix} \begin{Bmatrix} i_s^{abc} \\ i_r^{abc} \end{Bmatrix} + \frac{d}{dt} \begin{Bmatrix} \lambda_s^{abc} \\ \lambda_r^{abc} \end{Bmatrix} \tag{3. 1}$$

V_s^{abc} – Stator winding's voltage vector

V_r^{abc} – Rotator winding's voltage vector

i_s^{abc} – Stator winding's current vector

i_r^{abc} – Rotator winding's current vector

λ_s^{abc} – Stator winding's flux vector

λ_r^{abc} – Rotator winding's flux vector

The relationship between the fluxes and rotor and stator currents is given by

$$\begin{Bmatrix} \lambda_s^{abc} \\ \lambda_r^{abc} \end{Bmatrix} = \begin{bmatrix} L_{ss}^{abc} & L_{sr}^{abc} \\ L_{rs}^{abc} & L_{rr}^{abc} \end{bmatrix} \begin{Bmatrix} i_s^{abc} \\ i_r^{abc} \end{Bmatrix} \tag{3. 2}$$

where each term is either a 3-dimensional matrix or a three dimensional vector. Then the vectors can be written as

$$v_s = \begin{pmatrix} v_{sa} \\ v_{sb} \\ v_{sc} \end{pmatrix}, v_r = \begin{pmatrix} v_{ra} \\ v_{rb} \\ v_{rc} \end{pmatrix}, i_s = \begin{pmatrix} i_{sa} \\ i_{sb} \\ i_{sc} \end{pmatrix}, i_r = \begin{pmatrix} i_{ra} \\ i_{rb} \\ i_{rc} \end{pmatrix} \tag{3. 3}$$

and the impedance matrices are

$$r_s^{abc} = \begin{bmatrix} r_s & 0 & 0 \\ 0 & r_s & 0 \\ 0 & 0 & r_s \end{bmatrix} \tag{3. 4}$$

$$r_r^{abc} = \begin{bmatrix} r_r & 0 & 0 \\ 0 & r_r & 0 \\ 0 & 0 & r_r \end{bmatrix} \tag{3. 5}$$

$$L_{ss}^{abc} = \begin{bmatrix} L_{ls} + L_{ss} & L_{sm} & L_{sm} \\ L_{sm} & L_{ls} + L_{ss} & L_{sm} \\ L_{sm} & L_{sm} & L_{ls} + L_{ss} \end{bmatrix} \tag{3. 6}$$

$$L_{rr}^{abc} = \begin{bmatrix} L_{lr} + L_{rr} & L_{rm} & L_{rm} \\ L_{rm} & L_{lr} + L_{rr} & L_{rm} \\ L_{rm} & L_{rm} & L_{lr} + L_{rr} \end{bmatrix} \tag{3. 7}$$

$$L_{sr}^{abc} = \{L_{rs}^{abc}\}^t = \begin{bmatrix} \cos(\theta_r) & \cos\left(\theta_r + \frac{2\pi}{3}\right) & \cos\left(\theta_r - \frac{2\pi}{3}\right) \\ \cos\left(\theta_r - \frac{2\pi}{3}\right) & \cos\theta_r & \cos\left(\theta_r + \frac{2\pi}{3}\right) \\ \cos\left(\theta_r + \frac{2\pi}{3}\right) & \cos\left(\theta_r - \frac{2\pi}{3}\right) & \cos\theta_r \end{bmatrix} \tag{3. 8}$$

and hence torque on the rotor shaft

$$T_m = \frac{P}{2}[i]^t \frac{\delta[L(\theta_r)]}{\delta(\theta_r)}[i] \tag{3. 9}$$

where:

P- number of poles of the Induction machine

T- Torque of the Induction machine

$$L(\theta_r) = \begin{bmatrix} L_{ss} & L_{sr} \\ L_{rs} & L_{rr} \end{bmatrix} \tag{3. 10}$$

Equation (3. 9) expresses the torque developed by the induction machine at any time, depending on the instantaneous currents circulating in each one of the six windings, and the separation angle between the stator winding and rotor winding [33, 34] . Since

$L_{ss}\ and\ L_{rr}$ are not dependant on θ_r the derivative of those terms is zero, and after simplification of the equation can be written as

$$T_m = \frac{P}{2}\begin{Bmatrix} i_s^{abc} \\ i_r^{abc} \end{Bmatrix}^t \begin{bmatrix} 0 & N_{sr} \\ N_{rs} & 0 \end{bmatrix} \begin{Bmatrix} i_s^{abc} \\ i_r^{abc} \end{Bmatrix} where, \tag{3. 11}$$

$$N_{sr}^{abc} = -L_{sr}\begin{bmatrix} \sin(\theta_r) & \sin\left(\theta_r + \frac{2\pi}{3}\right) & \sin\left(\theta_r - \frac{2\pi}{3}\right) \\ \sin\left(\theta_r - \frac{2\pi}{3}\right) & \sin(\theta_r) & \sin\left(\theta_r + \frac{2\pi}{3}\right) \\ \sin\left(\theta_r + \frac{2\pi}{3}\right) & \sin\left(\theta_r - \frac{2\pi}{3}\right) & \sin(\theta_r) \end{bmatrix} \tag{3. 12}$$

Since the rotor windings of the SCIG are short circuited, the only part of the generator connected to the grid is the stator and because of this we get $v_r^{abc} = 0$. Therefore

$$\begin{Bmatrix} V_s^{abc} \\ V_r^{abc} \end{Bmatrix} = \begin{bmatrix} r_s^{abc} & 0 \\ 0 & r_r^{abc} \end{bmatrix} \begin{Bmatrix} i_s^{abc} \\ i_r^{abc} \end{Bmatrix} + \frac{d}{dt}\begin{Bmatrix} \lambda_s^{abc} \\ \lambda_r^{abc} \end{Bmatrix} \tag{3. 13}$$

Parks transformation is basically a mathematical transformation used for the analysis of three phase circuits. In case of balanced three phase circuits, Park's transform reduces the three phase AC quantities to two phase DC quantities and the calculations can be carried out on these imaginary quantities before inverse transforming to recover the actual three-phase AC results. But before transforming the three phase stationary axes to synchronous rotating reference frame we need to transform these axes to two axis stationary frame by Clarke's transformation. Clarke's transformation allows us to change the 3-dimenstionsystem to 2-dimension system($abc\ to\ \alpha\beta$). The transformation is as follows

$$\begin{Bmatrix} \alpha \\ \beta \end{Bmatrix} = \frac{2}{3}\begin{bmatrix} 1 & -\frac{1}{2} & -\frac{1}{2} \\ 0 & \frac{\sqrt{3}}{2} & -\frac{\sqrt{3}}{2} \end{bmatrix} \begin{Bmatrix} a \\ b \\ c \end{Bmatrix} \tag{3. 14}$$

Park's transformation describes rotation of a stationary system

$$\begin{Bmatrix} d \\ q \end{Bmatrix} = \begin{bmatrix} -\sin(\theta_r) & \cos(\theta_r) \\ \cos(\theta_r) & \sin(\theta_r) \end{bmatrix} \begin{Bmatrix} \alpha \\ \beta \end{Bmatrix} \tag{3.15}$$

The Parks transform can be directly used to convert the three phase stationary axes to two phase synchronous rotating reference frame. These equations are actually a "shortcut" for Clarke and Park transformation [35, 36].

$$x^{abc} = T^{-1}(\theta)x^{gdo} \text{where}, T^{-1}(o) = \begin{bmatrix} \cos(\theta) & \sin(\theta) & 1 \\ \cos\left(\theta - \frac{2\pi}{3}\right) & \sin\left(\theta - \frac{2\pi}{3}\right) & 1 \\ \cos\left(\theta + \frac{2\pi}{3}\right) & \sin\left(\theta + \frac{2\pi}{3}\right) & 1 \end{bmatrix} \tag{3.16}$$

3.3 Control Schemes For SCIG WECS

The main control schemes for SCIG wind energy systems are direct and indirect field oriented control (FOC) and direct torque control (DTC). We analyze the steady state and dynamic state performance of the Induction generator drive.

3.3.1 Direct Field Oriented Control

Field orientation is basically stator flux, air-gap flux and rotor flux orientation. Field oriented control is the decoupled control of the rotor flux λ_r and the electromagnetic torque T_e of the generator to achieve high dynamic performance. Rotor flux orientation is achieved by aligning the *d*-axis of the synchronous reference frame with the rotor flux vector λ_r .

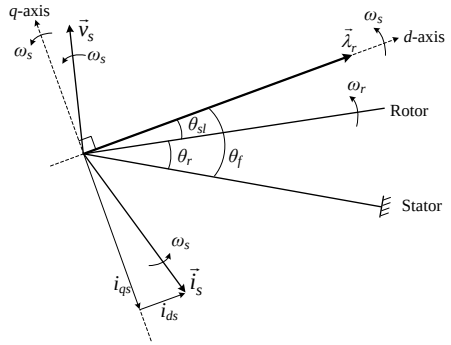

Figure 3.1. Rotor flux field oriented control (d-axis is aligned with λ_r) [5].

Therefore the flux components are

$$\lambda_{qr} = 0 \tag{3. 17}$$

$$\lambda_{dr} = \sqrt{(\lambda_r)^2 - \left(\lambda_{qr}\right)^2} = \lambda_r \tag{3. 18}$$

Substituting the above equation in the torque equation gives

$$T_e = K_T \lambda_r i_{qs} \tag{3. 19}$$

where $K_T = (\frac{3PL_m}{3L_r})$.

The stator current i_s can be resolved into two components along the d-q axis. The d-axis current i_{ds} is the flux producing current whereas the q axis current i_{qs} is the torque producing current and hence in filed oriented control i_{ds} is normally kept constant and i_{qs} is controlled independently. Another key factor in rotor flux oriented control is to accurately determine the rotor flux angle θ_f. If the angle is obtained through the measurement of generator terminal voltages and currents the method is known as direct field oriented control and if the angle is obtained from

$$\theta_t = \theta_r + \theta_{si} \tag{3. 20}$$

where θ_r and θ_{sl} are the measured rotor position angle and calculated slip [16, 37].

Figure 3.1 shows a typical block diagram of a direct FOC for SCIG wind energy systems. To implement direct FOC the rotor flux magnitude λ_r and its angle θ_f are identified by the rotor flux calculator based on the measured stator voltages (v_{as} and v_{bs}) and currents ($i_{as}$and i_{bs}).

There are three feedback loops: one for the rotor flux linkage λ_r, one for the d-axis stator current i_{ds} and another for the q-axis stator current i_{qs}. For the rotor flux control, the measure λ_r is compared to the reference flux λ_r^* and the error is fed to a PI controller. The output of the PI regulator yields i_{ds}^*. The torque reference can be generated by the maximum power point tracking scheme. From all the known values

$$i_{qs} = \frac{T_e}{k_T \lambda_r} \tag{3. 21}$$

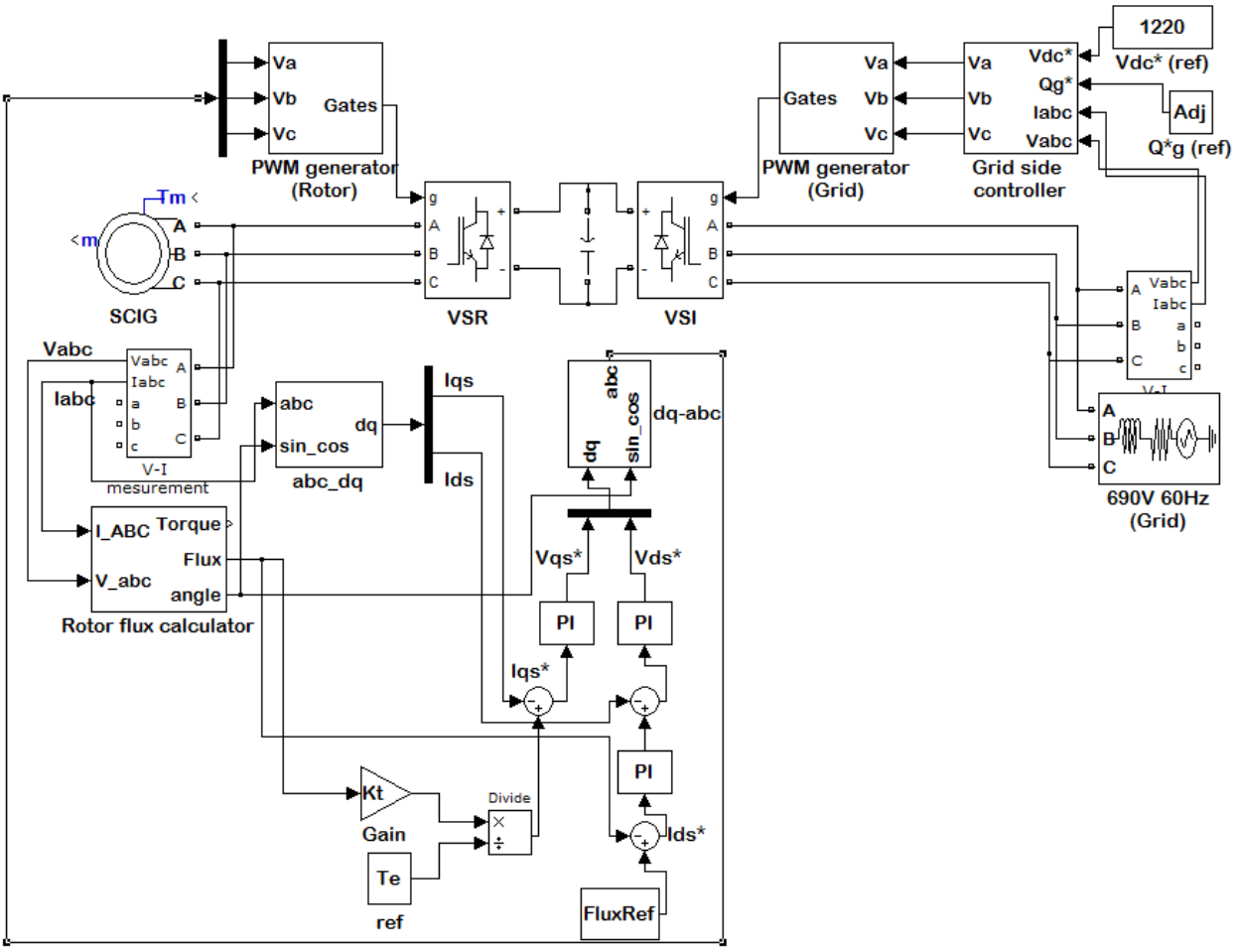

Figure 3.2. Direct field oriented control model with rotor flux orientation.

The feedback dq-axes stator currents i_{ds} and i_{qs} are compared with the references and the errors are sent to PI regulators to generate v_{ds}^* and v_{qs}^* and these dq-axes voltages are transformed to three phase stator voltages v_{as}^* , v_{bs}^* and v_{cs}^* in the stationary frame through the dq/abc transformation block. Both the carrier based modulation or the space vector modulation techniques which we discussed in the Section 2.2.1.4 can be used to generate gating signals for the rectifier [24, 38-40].

3.3.2 Rotor Flux Calculator

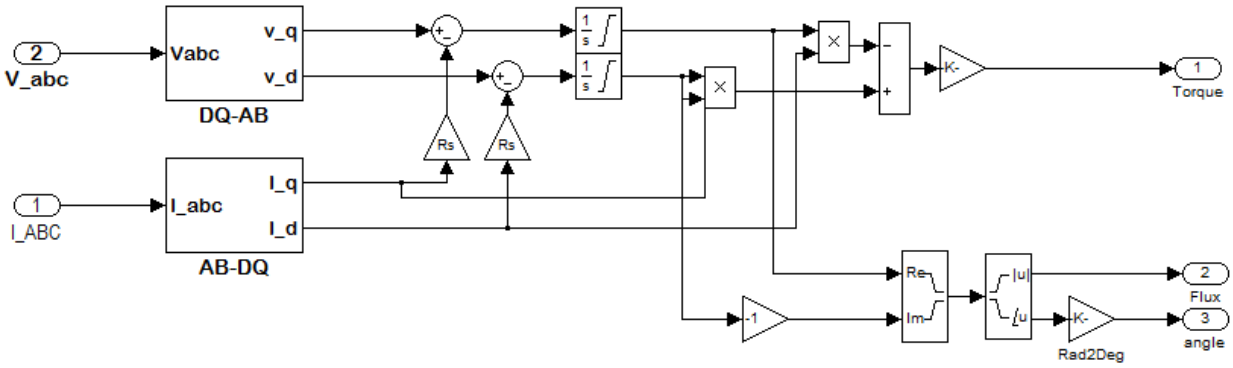

Figure 3.3. Simulation model of the rotor flux calculator.

3.3.3 Dynamic and steady state Analysis of Direct FOC WECS

The speed of the turbine is increased from zero to its rated value by wind, at which the step rotor flux reference is applied. The rotor flux starts to build to build up, and when it reaches a rated value a step torque reference is applied. The wind energy system then delivers its rated power to the grid at the rated wind speed.

After the start-up transients of the generator, when the wind is at its rated speed the wind energy system starts operating in steady state. Included are the waveforms for the phase-a PWM stator voltage v_{as}, the fundamental-frequency stator voltage v_{as1} , stator current i_{as}, phase-a rotor flux linkage λ_{ar} and dq- axis stator currents shown in Figure 3.4 to Figure 3.7).

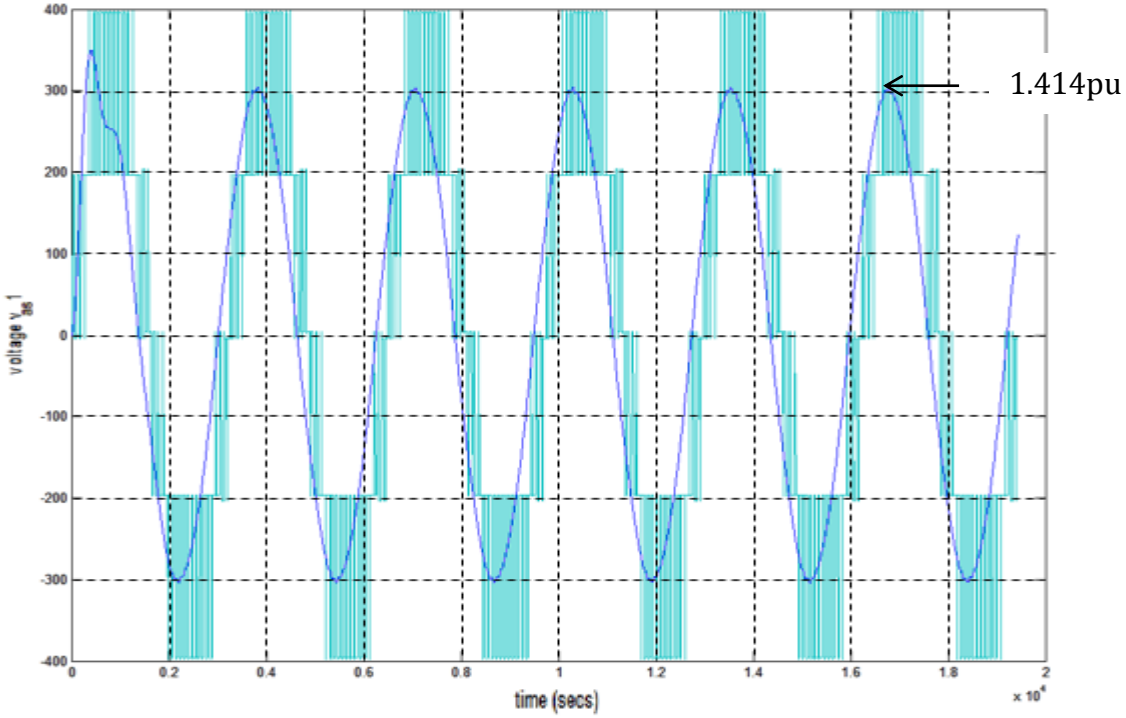

Figure 3.4. Fundamental frequency stator voltage v_{as1}.

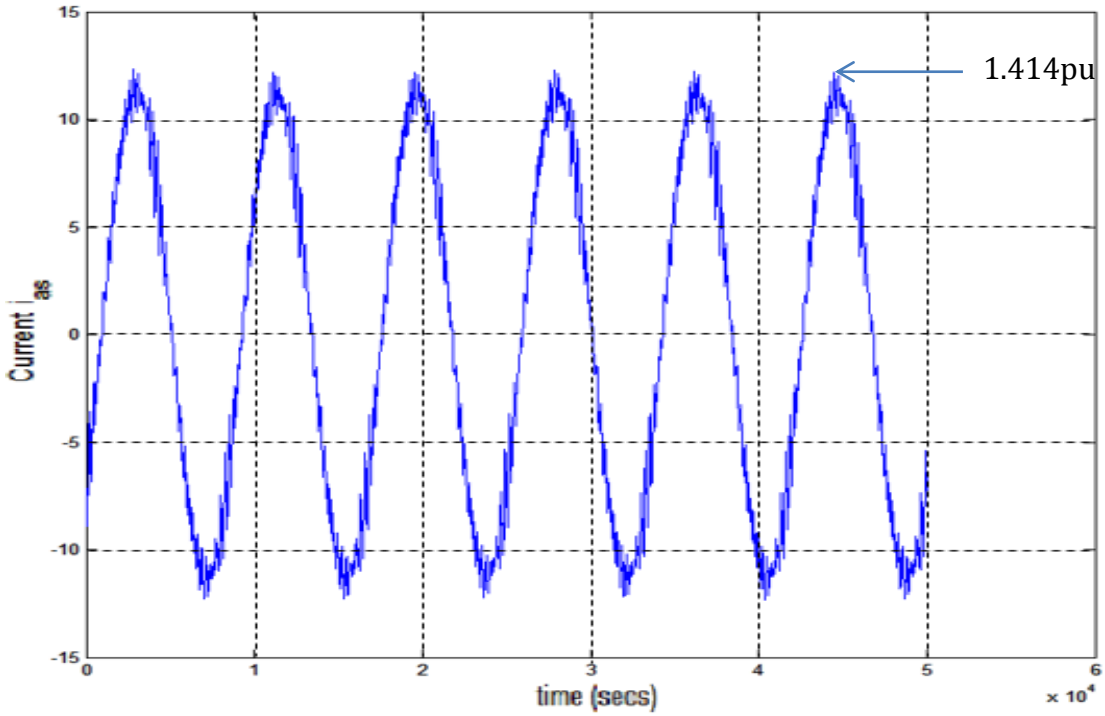

Figure 3.5. Stator current i_{as}.

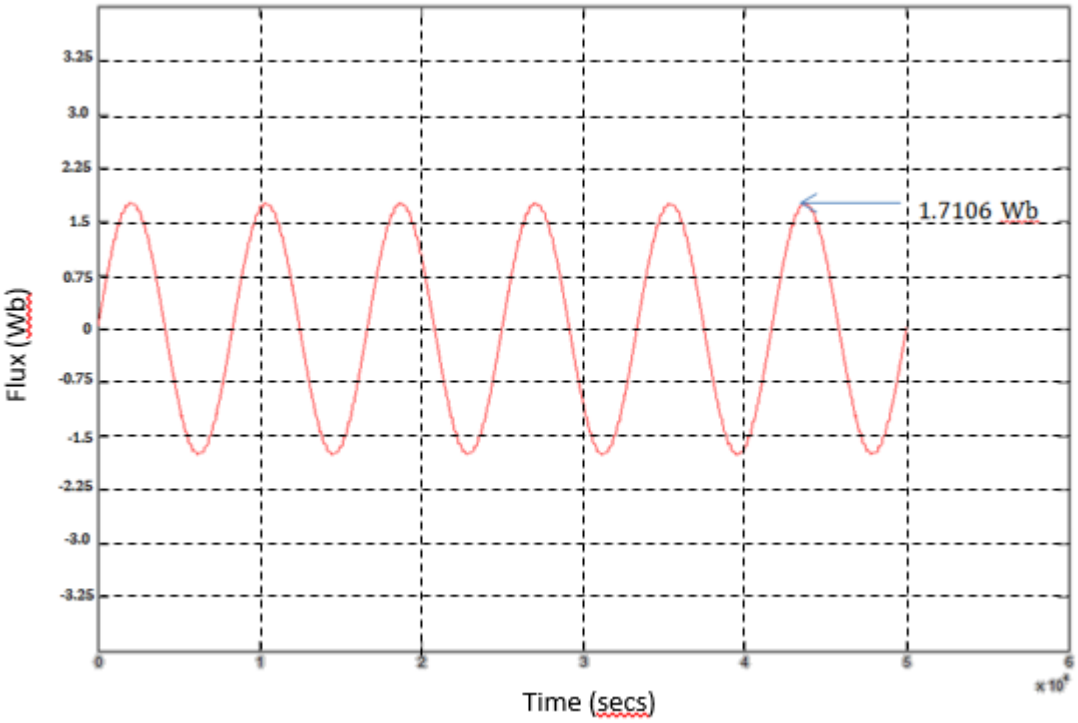

Figure 3.6. Phase-a flux linkage λ_{ar}.

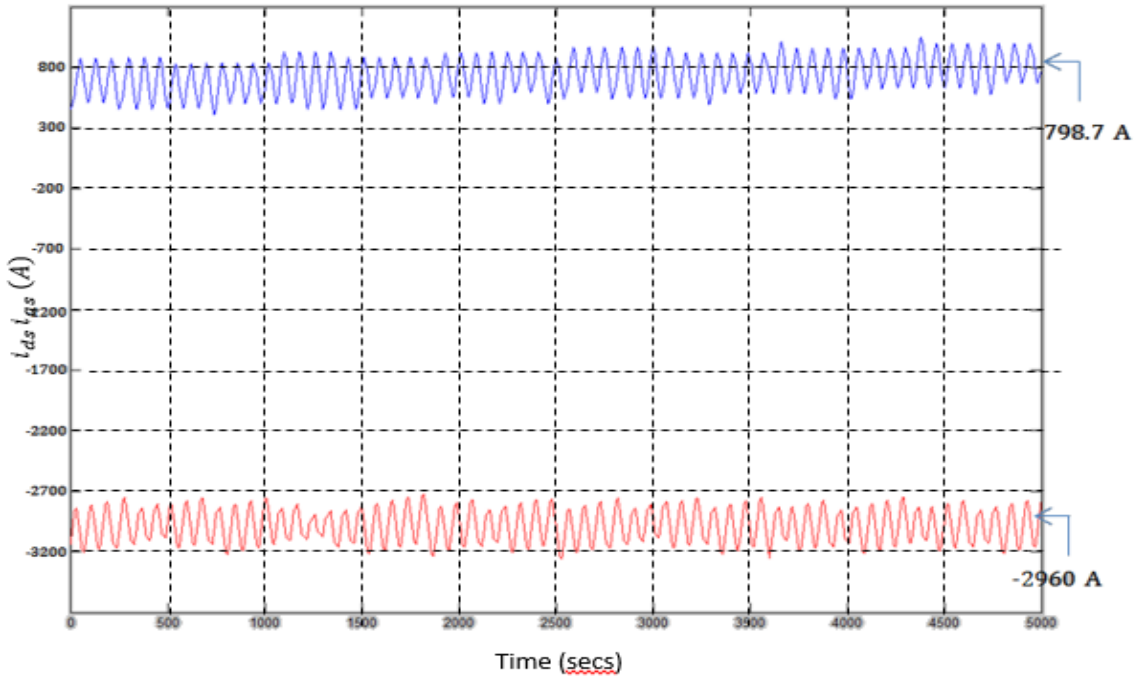

Figure 3.7. dq-axis stator currents

With the rated parameters (given in appendix), the input impedance is

$$\overline{Z}_s = \frac{R_s + jX_{ls} + jX_m}{\left(\frac{R_r}{s} + jX_{ls}\right)} = 0.1838\angle 152°6\ \Omega \tag{3. 22}$$

The rms and the peak values of the stator current are

$$\overline{I_s} = \frac{V_s}{Z_s} = 2168\angle -152.6^{o} \tag{3. 23}$$

$$i_s = \sqrt{2} \times 2168 = 3066\ \text{A} \tag{3. 24}$$

The rotor current can be found from

$$\bar{I}_r = \frac{jX_m\bar{I}_s}{jX_m + (\frac{R_r}{s} + jX_{lr})} = 2030.8\angle -167.6^{o} \tag{3. 25}$$

The magnetizing flux linkage is calculated by

$$\overline{\Lambda}_m = (\overline{I_s} - \bar{I}_r)L_m = 1.2168\angle -83.9^{o}\text{Wb} \tag{3. 26}$$

The rms rotor flux linkage is

$$\overline{\Lambda}_r = \overline{\Lambda}_m - L_{lr}\bar{I}_r = 1.2096\angle -77.7^{o} \tag{3. 27}$$

The peak rotor flux is then given by

$$\lambda_r = \sqrt{2}\overline{\Lambda}_r = 1.7106\ \text{Wb} \tag{3. 28}$$

The dq–axes stator currents (rms) can be determined by using the phasor diagram for the steady state operation of the generator

$$I_{ds} = I_s\cos(\angle\bar{I}_s - \angle\bar{\Lambda}_r) = 2168(-74.9^{o}) = 564.8\text{A} \tag{3. 29}$$

$$I_{qs} = I_s\sin(\angle\bar{I}_s - \angle\bar{\Lambda}_r) = 2168(-74.9^{o}) = -2093\text{A} \tag{3. 30}$$

The current peak values are given by

$$i_{ds} = \sqrt{2}\, I_{ds} = 798.7 \text{ A} \tag{3.31}$$

$$i_{qs} = \sqrt{2}\, I_{qs} = -2960 \text{ A} \tag{3.32}$$

The theoretical results are confirmed by the simulation results shown above.

DYNAMIC ANALYSIS

In this analysis, the transients of a 2.3 MW/690V SCIG wind energy systems caused by a step change in wind speeds is investigated. We assume that the wind speed increases from 8.4m/sec to 12m/sec. The system is initially operating with a rotor speed of 0.7 (wind speed of 8.4 m/sec) and we analyze the system transients when wind speed suddenly increase to 12 m/sec. Initially the system operates at 0.7 pu rotor speed, at which the mechanical torque T_m is -7222.6 Nm (generating mode). The electromagnetic torque produced by the generator T_e contains ripple caused by harmonics in the stator current, but its average value is -7222.6 Nm which is equal to T_m.

When the wind speed suddenly increases to 12 m/sec, the turbine mechanical torque T_m is instantly increased from -72226 Nm to -14,740 Nm shown in Figure 3.8 but the mechanical speed of the generator cannot change instantly as shown in Figure 3.9 and hence the T_e^* produced by the MPPT scheme remains constant and hence the generator electromagnetic torque remains unchanged shown in Figure 3.10.

After T_m has increased the difference between T_m and T_e accelerates the generator and the rotor speed increases accordingly. After a period of time the system reaches the steady state. With the rated wind speed, the generator operates under the rated conditions with the rated torque and the rated stator current. The waveforms of the dq – axis stator currents, i_{ds} and i_{qs}, are also given in the Figure 3.11. With the rotor flux feedback control, the $d-$ axis stator current i_{ds} is kept constant during the transients which in turn makes the rotor flux λ_r constant. The stator currents ($i_{ds} = 801.4$ A and $i_{qs} = -1452.4$ A) correlate with the steady state analysis done in the Section 3.3.3.

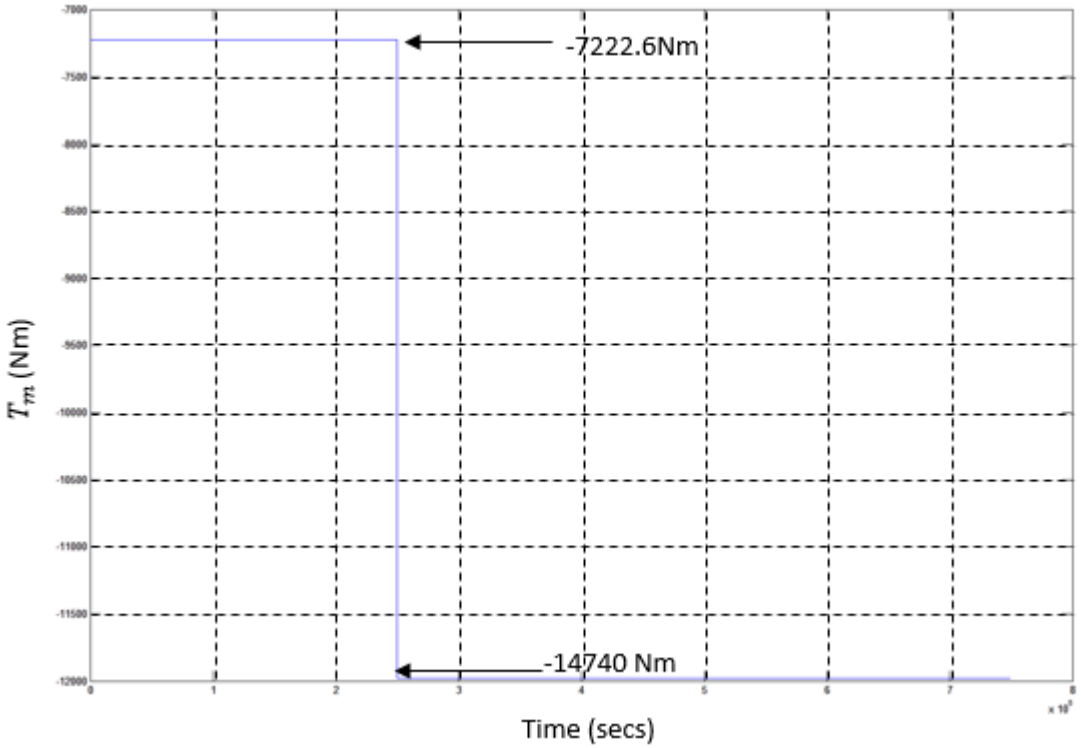

Figure 3.8. Mechanical torque.

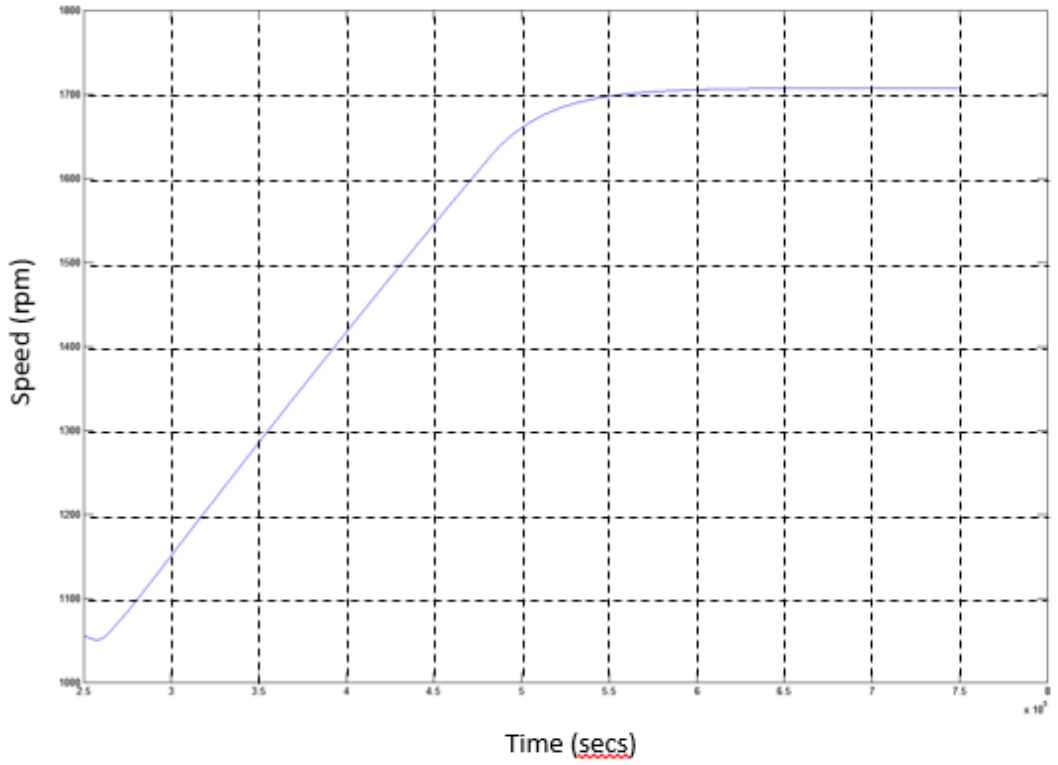

Figure 3.9. Rotor speed.

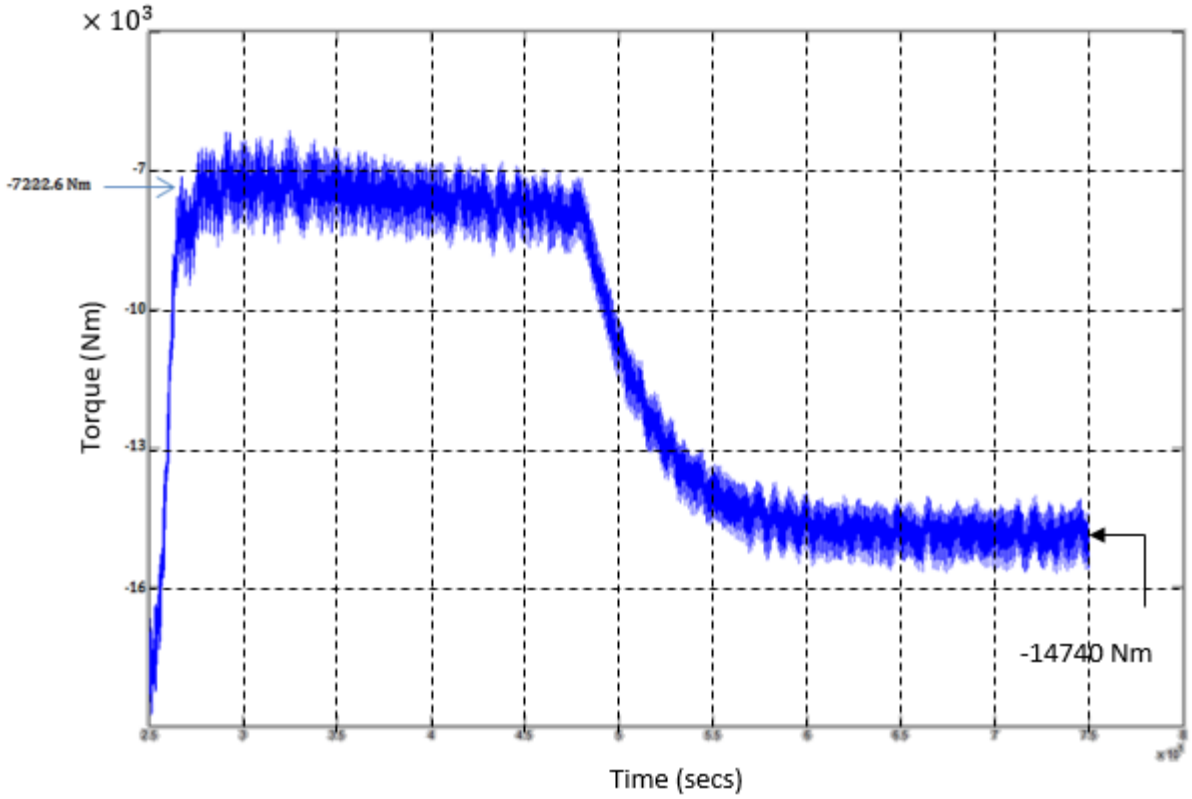

Figure 3.10. Electromagnetic torque.

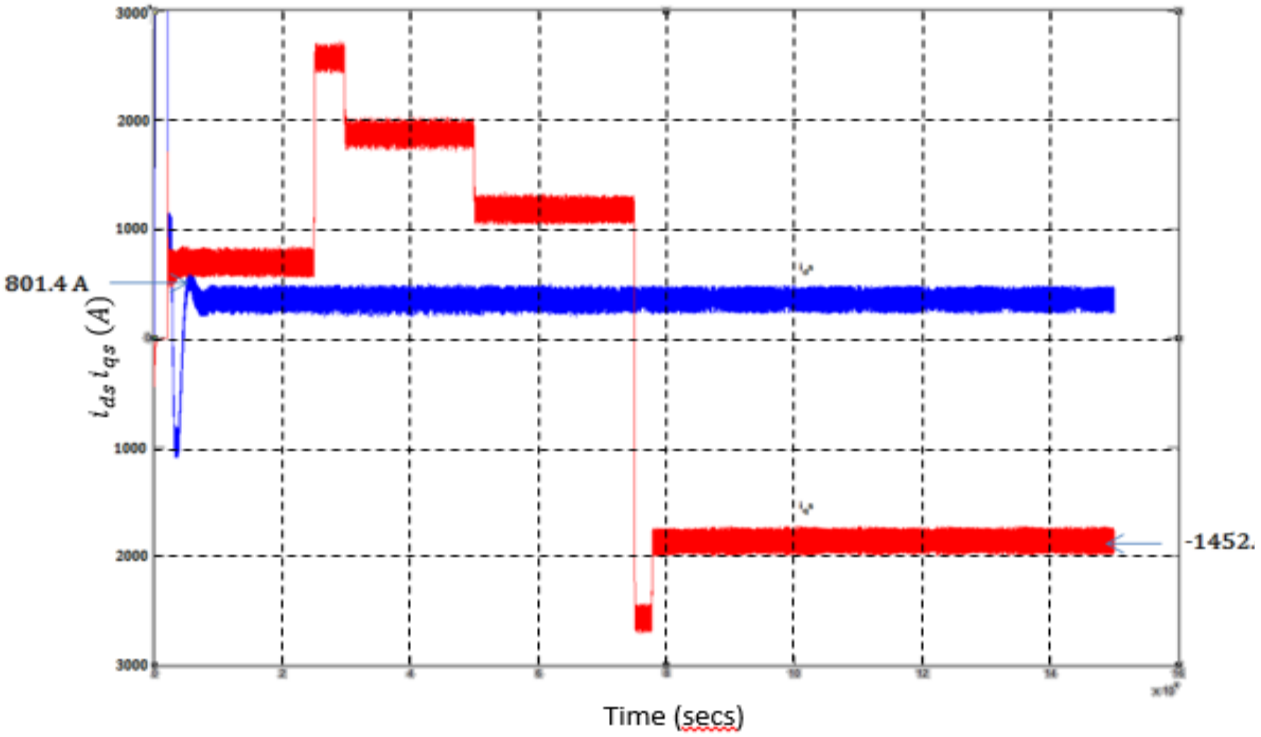

Figure 3.11. i_{ds} and i_{qs} currents.

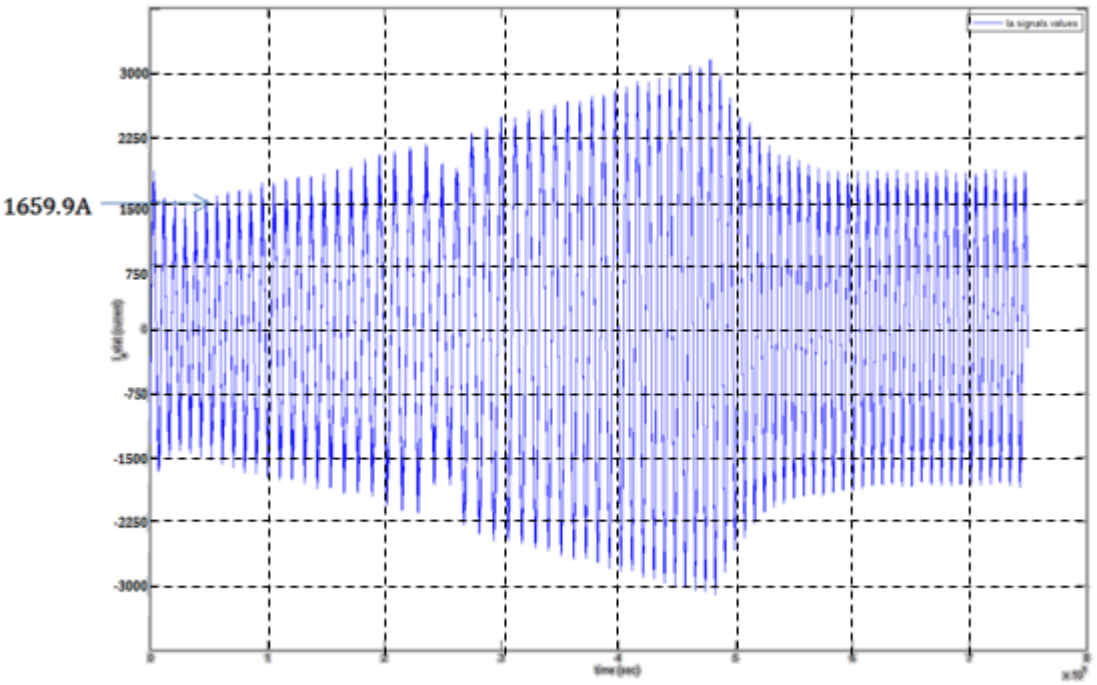

Figure 3.12. Stator current.

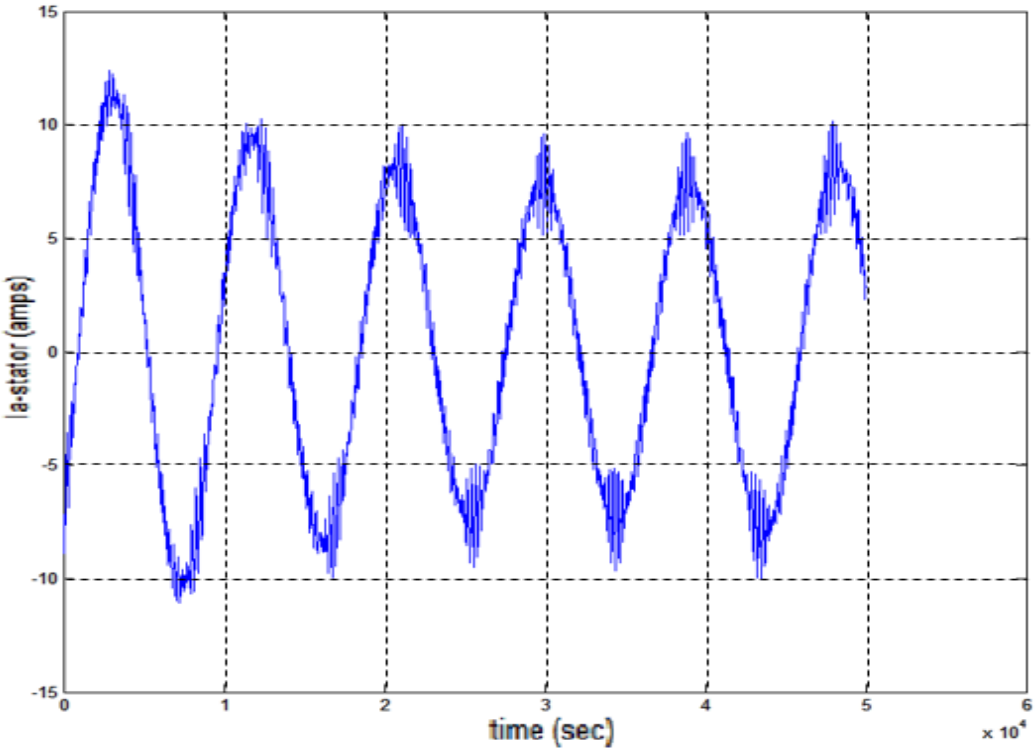

Figure 3.13. Phase-*a* stator current.

3.3.4 Indirect Field Oriented Control

Indirect Field oriented control is same as the direct FOC with only difference is the method of obtaining the rotor flux angle. In Indirect FOC the rotor flux angle can be obtained from

$$\theta_f = \int (w_r + w_{sl})dt \tag{3. 33}$$

where $\omega_r$the measured rotor speed and ω_{sl} is the calculated slip frequency

The slip frequency is obtained by [42]

$$W_{sl} = \frac{L_m}{t_r X_r} iqs \tag{3. 34}$$

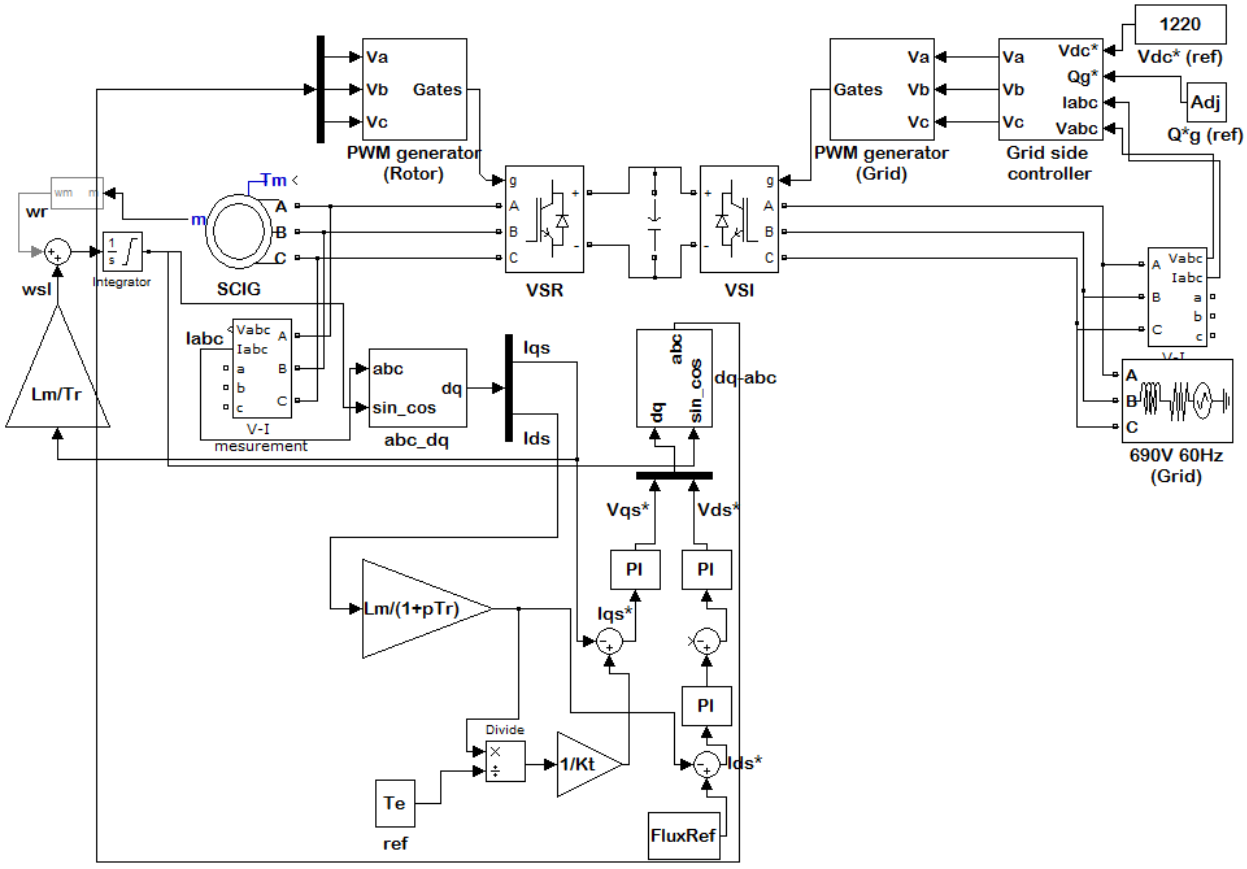

Figure 3.14. Indirect field oriented control for an SCIG wind energy system.

A typical block diagram of the SCIG wind energy system with indirect FOC is shown in the Figure 3.14. Observing the figure we can see that the rotor flux angle θ_f for field orientation

is obtained by measuring the rotor speed ω_r and calculating the slip frequency ω_{sl}. Similar to the Direct FOC scheme there are are three feedback loops: one for the rotor flux linkage λ_r, one for the d-axis stator current i_{ds}, another for the q-axis stator current i_{qs}[43, 44]. The rotor flux reference λ_r^* is set at a rate value and the actual rotor flux can be obtained from

$$\lambda_r = \frac{L_m}{(1 + pt_r)} \times ids \tag{3. 35}$$

The torque reference T_e^* is generated by the MPPT block and the q-axis current reference i_{qs}^* can be obtained from the torque equation [45-47]

$$i_{qs}^* = \frac{1}{K_T \lambda_r} T_e^* \tag{3. 36}$$

3.3.4.1 Steady State Analysis of the Indirect FOC SCIG Wind Energy System

We consider the same Induction generator 2.3 MW/690 V SCIG wind energy system. The rotor flux λ_r is kept constant at its rated value of 1.711 Wb by the FOC scheme. The d – axis current can be calculated by

$$i_{ds} = \frac{\lambda_r}{L_m} = 801.4 \text{ A} \tag{3. 37}$$

The turbine mechanical torque is given by

$$T_m = T_{mR} \times 0.7^2 = -14{,}740 \times 0.7^2 = -7{,}222.6 \text{ kNm} \tag{3. 38}$$

The q-axis current is calculated by

$$i_{ds} = \frac{\lambda_r}{L_m} = 801.4 \text{ A} \tag{3. 39}$$

$$i_{qs} = \frac{2L_r}{3PL_m} \frac{T_e}{\lambda_r} = -1450.2 \text{ A} \tag{3.40}$$

The peak stator current can then be obtained by

$$i_s = \sqrt{i_{ds}^2 + i_{qs}^2} = 1659.9 \text{ A} \tag{3. 41}$$

The above calculated i_{ds}, i_{qs} and i_s are essentially the same as those obtained by simulations.

The slip frequency can be determined by

$$\omega_{sl} = \frac{R_r L_m}{L_r \lambda_r} i_{qs} = -1.2137 \text{ rad/sec} \tag{3. 42}$$

The stator frequency can be found from

$$\omega_s = \omega_r + \omega_{sl} = 220.4 \text{ rad/sec} \tag{3. 43}$$

From which the slip is

$$s = \frac{\omega_{sl}}{\omega_s} = -5.588 \times 10^{-3} \tag{3.44}$$

The rms values if the stator current is expressed as

$$\bar{I}_{S=\frac{i_s}{\sqrt{2}\angle 0^o}} = 1171.6 \angle 0^o \tag{3. 45}$$

with the generator impedance of

$$\overline{Z_s} = R_s + jX_s + \frac{jX_m}{\frac{R_r}{s} + jX_{lr}} = 0.2349 \angle 144.9^o \tag{3. 46}$$

The rms stator voltage can be calculated by

$$\overline{V_s} = \overline{I_s}\,\overline{Z_s} \tag{3. 47}$$

The magnetizing flux is

$$\overline{\Lambda}_r = \overline{\Lambda}_m - L_{lr}\bar{I}_r = 1.2096 \angle 61.1^o \tag{3. 48}$$

The rms rotor flux linkage can be obtained by

$$\overline{\Lambda}_r = \overline{\Lambda}_m - L_{lr}\overline{I_r} = 1.2096 \angle 61.1^o \text{Wb} \tag{3. 49}$$

The angle between the stator and rotor voltage flux is

$$\theta_2 = \varphi - \theta_1 = 83.8^o \tag{3.50}$$

From which

$$\begin{cases} v_{ds} = \sqrt{2}V_s \cos\theta_2 = 42.0\ V \\ v_{qs} = \sqrt{2}V_s \sin\theta_2 = 386.9\ V \end{cases} \tag{3.51}$$

3.4 Direct Torque Control

The electromagnetic torque developed by an Induction generator is expressed as

$$T_e = \frac{3P}{2}\frac{L_m}{\sigma L_s L_R}\lambda_s \lambda_r \sin\theta_T \tag{3.52}$$

where λ_s and λ_r are the magnitude of the stator and rotor flux vectors $\overrightarrow{\lambda_r}$ and $\overrightarrow{\lambda_s}$ and θ_T is the angle between the two vectors, also known as the torque angle. The essence of the direct torque control is to control the electromagnetic torque of the generator by adjusting the torque angle θ_T while keeping the magnitude of the stator flux at rated value. If the stator flux is kept at its rated value, the rotor flux of the generator is almost constant, and the torque can be directly controlled by θ_T .[48]

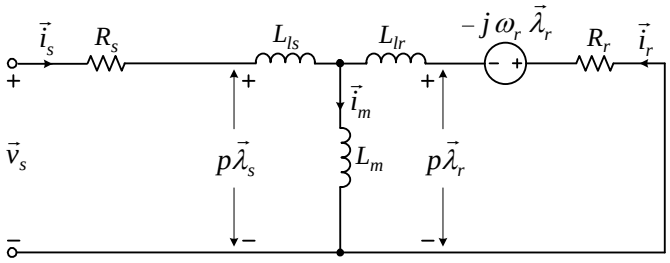

Figure 3.15. SCIG dynamic model [44].

Referring to the Figure 3.15, the stator flux relates the stator voltage by

$$p\vec{\lambda}_s = \overline{V}_s - R_s\vec{\imath}_s \tag{3.53}$$

From (3. 53) it is seen that the derivative of the stator flux reacts instantly to the changes in $\overrightarrow{v_s}$. The stator voltage $\overrightarrow{v_s}$is, the pulse-width modulated output voltage in the rectifier, which can be controlled by the reference vector $\vec{v}_{ref}$ in the space vector modulation and since it is managed by the switching states of the rectifier, a proper selection of switching states, we can adjust magnitude and the angle of $\overrightarrow{\lambda_s}$. [49, 50]

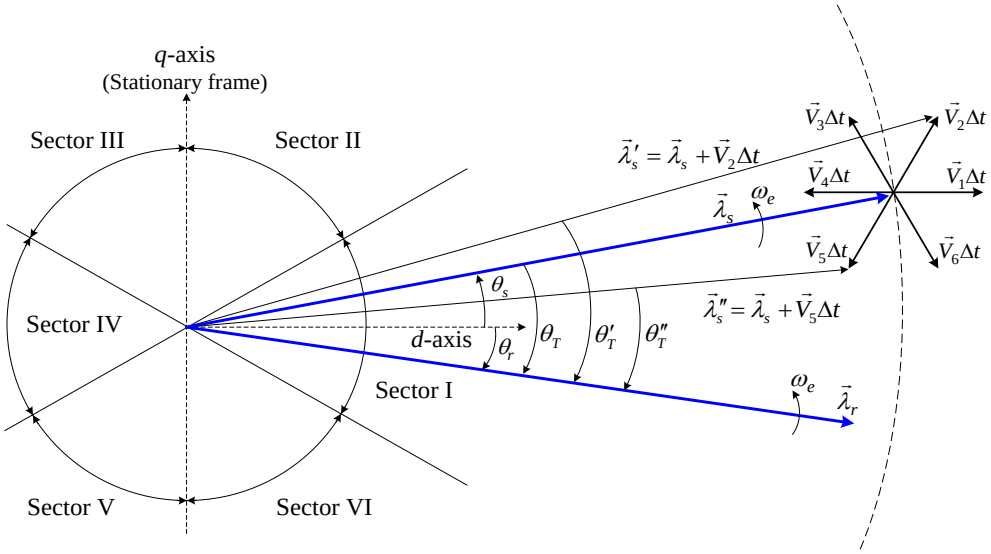

Figure 3.16. Principle of direct torque control [16].

The direct torque control method implemented for a two level VSC is shown in the Figure 2.25. Input current ripple [16].The *dq*- plane for the stator flux $\overrightarrow{\lambda_s}$ is divided into six sectors, I to VI. The stator flux $\overrightarrow{\lambda_s}$ falls in sector I and its angle θ_s is referenced to the *d*-axis of the stationary reference frame. In wind energy system the induction machine acts in a generating mode and the torque angle θ_T is negative, and resultant torque T_e is negative which is in the case of induction generators. The torque angle can be determined from

$$\theta_T = L\vec{\lambda}_s - L\vec{\lambda}_r = \theta_s - \theta_r \tag{3. 54}$$

Examining the effect of the voltage vectors of the rectifier $\overrightarrow{V_0}$ to $\overrightarrow{V_6}$ on $\overrightarrow{\lambda_s}$ and θ_T. Assuming that $\overrightarrow{\lambda_s}$ and θ_T are initial stator flux and the torque angle, a voltage vector $\overrightarrow{V_2}$ is selected then the stator flux will become $\overrightarrow{\lambda_s}' = \overrightarrow{\lambda_s} + \overrightarrow{V_2}\Delta t$ leading to an increase in flux magnitude of the stator flux magnitude and torque angle ($\lambda_s' > \lambda_s \; and \; \theta_T' > \theta_T$). If for example

voltage vector $\overrightarrow{V_5}$ is selected, $\overrightarrow{\lambda_s}$ will change to $\overrightarrow{\lambda_s}'' = \overrightarrow{\lambda_s} + \overrightarrow{V_5}\Delta t$ causing a decrease in flux magnitude and the torque angle ($\lambda_s'' < \lambda_s \; and \; \theta_s'' < \theta_T$). Similarly the choice of vectors $\overrightarrow{V_3}$ and $\overrightarrow{V_6}$ can bring about increase or decrease in the stator flux magnitude and torque angle [51, 52].

3.4.1 DTC Scheme and the Switching Logic

Figure 3-17 shows the typical block diagram of a DTC controlled Induction generator WECS. The direct torque control is realized by the rectifier whereas the DC link voltage and the grid side reactive power are achieved by the gird side converter. The stator flux and the electromagnetic torque are controlled separately to achieve good dynamic performance. The stator flux reference λ_S^* is compared to the calculated stator flux λ_s , and the error $\Delta\lambda_s$ is sent to the flux comparator (FC) and similarly the torque reference T_e^* is compared with the calculated torque T_e and their difference ΔT_e is sent to the torque comparator (TC) [52-54].

Both flux (two output levels, $x_T = +1, and -1$) and torque comparators (three output levels, $x_T = +1, 0, and -1$), shown in Figure 3.17, are hysteresis type. +1 output level requests a increase in λ_s and θ_T, -1 requests a decrease in λ_s and θ_T.

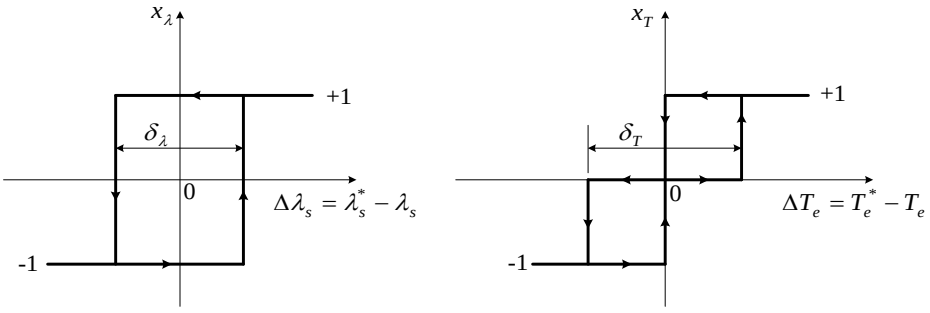

(a) Flux comparator (b) Torque comparator

Figure 3.17. Characteristics of hysteresis comparators.

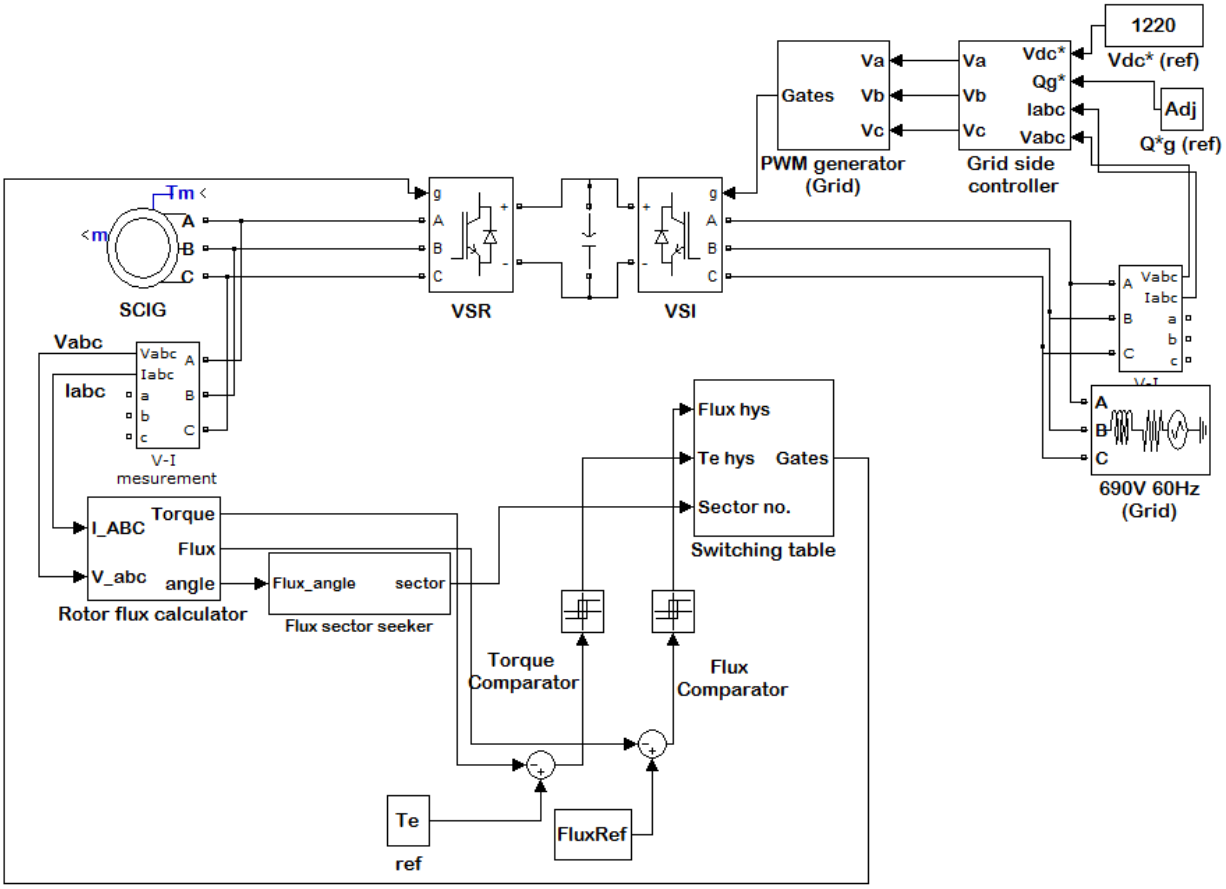

Figure 3.18. DTC model for an SCIG wind energy system.

The Table 5 shows the switching pattern for the stator flux reference rotating in the counterclockwise direction.

Input variables are $x_A(FC)\ output, x_T(TC) output$ and the sector number and the output variables are the rectifier voltage vectors. The The output of the comparators dictate which voltage vector should be selected. For eg x_A is +1 and x_T and -1 then there is an increase in the stator flux and decrease in the torque angle therefore either $\overrightarrow{V_6}$ *or* $\overrightarrow{V_1}$ can be selected. If x_A is +1 and x_T and +1 then there is an increase in the stator flux and increase in the torque angle therefore either $\overrightarrow{V_2}$ can be selected.

When the output of the comparator is zero, the zero vector $\overrightarrow{V_0}$ can be selected. The zero vector helps in reducing the switching frequency of the converter and smoothing out the voltage ripple [52-54].

Table 5. Converter switching pattern according to voltage vector selection

Comparator o/p		**Sector**					
x_A	x_T	**I**	**II**	**III**	**IV**	**V**	**VI**
+1	+1	$\vec{V}_2$ 110	$\vec{V}_3$ 010	$\vec{V}_4$ 011	$\vec{V}_5$ 001	$\vec{V}_6$ 101	$\vec{V}_1$ 100
	0	$\vec{V}_0$ 111	$\vec{V}_0$ 000	$\vec{V}_0$ 111	$\vec{V}_0$ 000	$\vec{V}_0$ 111	$\vec{V}_0$ 000
	-1	$\vec{V}_6$ 101	$\vec{V}_1$ 100	$\vec{V}_2$ 110	$\vec{V}_3$ 010	$\vec{V}_4$ 011	$\vec{V}_5$ 001
-1	+1	$\vec{V}_3$ 010	$\vec{V}_4$ 011	$\vec{V}_5$ 001	$\vec{V}_6$ 101	$\vec{V}_1$ 100	$\vec{V}_2$ 110
	0	$\vec{V}_0$ 000	$\vec{V}_0$ 111	$\vec{V}_0$ 000	$\vec{V}_0$ 111	$\vec{V}_0$ 000	$\vec{V}_0$ 111
	-1	$\vec{V}_5$ 001	$\vec{V}_6$ 101	$\vec{V}_1$ 100	$\vec{V}_2$ 110	$\vec{V}_3$ 010	$\vec{V}_4$ 011

3.4.2 Stator Flux and Torque Calculator

The stator flux vector can be expressed as

$$\bar{\lambda}_s = \lambda d_s + j\lambda qs \tag{3.55}$$

$$= \int (V_{ds} - R_s i_{ds})dt + j\int (V_{qs} - R_s i_{qs})dt \tag{3.56}$$

From which its magnitude and the angle are

$$\sqrt{\lambda_{ds}^2 + \lambda_{qs}^2} \tag{3.57}$$

$$\theta_s = \tan^{-1}\left(\frac{\lambda_{qs}}{\lambda_{ds}}\right) \tag{3.58}$$

The developed electromagnetic torque can be calculated by [55]

$$T_e = \frac{3P}{2}(\lambda_{ds} i_{qs} - \lambda_{qs} i_{ds}) \tag{3.59}$$

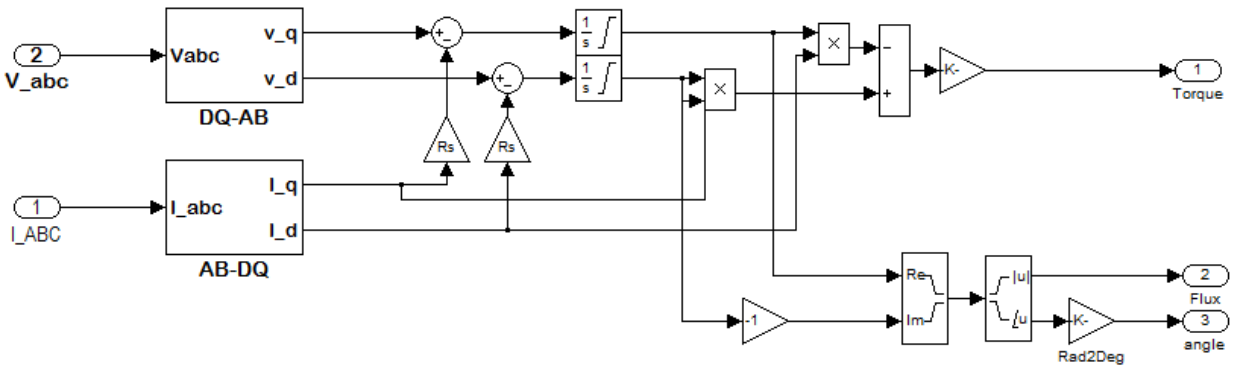

Figure 3.19. Simulink block diagram of the flux/torque calculator for use in DTC scheme.

3.4.3 Steady State and Transient State Analysis of SCIG WECS with DTC

Transient Analysis

For transient analysis, we simulate the conditions when the wind speed changes from 8.4m/sec to 12 m/sec so that the rotor speed changes from the 0.7 pu to 1.0 pu. To ensure accurate control a PI controller is added to the torque control loop.

The following Figures 3.20 to Figure 3.27. Stator flux.are the simulated waveforms for the DTC wind energy system when the wind speed changes from 8.4 m/sec to 12m/sec. The waveforms include the rotor mechanical speed ω_m, generator mechanical torque T_m, electromagnetic torque T_e , phasor- a stator current and phase-a stator voltage v_{as}. Comparing with the FOC scheme for transient analysis, we can observe that the dynamic performance of the DTC WECS is similar.

To further study the performance, the waveforms of the stator flux $\lambda_s$is given in Figure 3.27. Stator fluxThe stator flux contains some ripples but its average value is kept constant by its reference λ_s^*. During the transient process caused by the step changes in wind speed, the stator flux remains constant by the DTC scheme. The rotor flux has very little ripple due to the filtering effect of the stator and rotor leakage inductances. When the rotor speed is at 0.7 pu (when the wind speed is 8.4m/sec), the rotor flux is 1.7406 Wb but as the rotor speed increases from 0.7 pu to 1.0 pu, the rotor flux reduces to 1.5006 Wb. Since the stator

flux is held constant the variation of the rotor flux is minimal (only 0.24 Wb). The above values are verified by the steady state analysis done in the next case study.

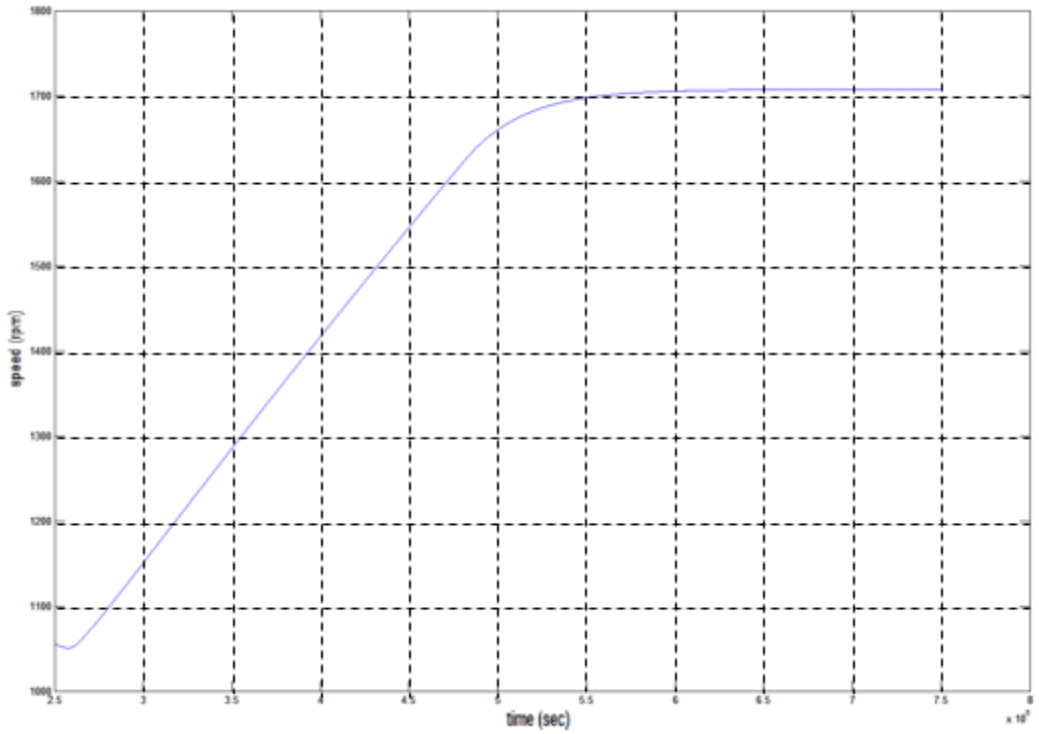

Figure 3.20. Rotor speed.

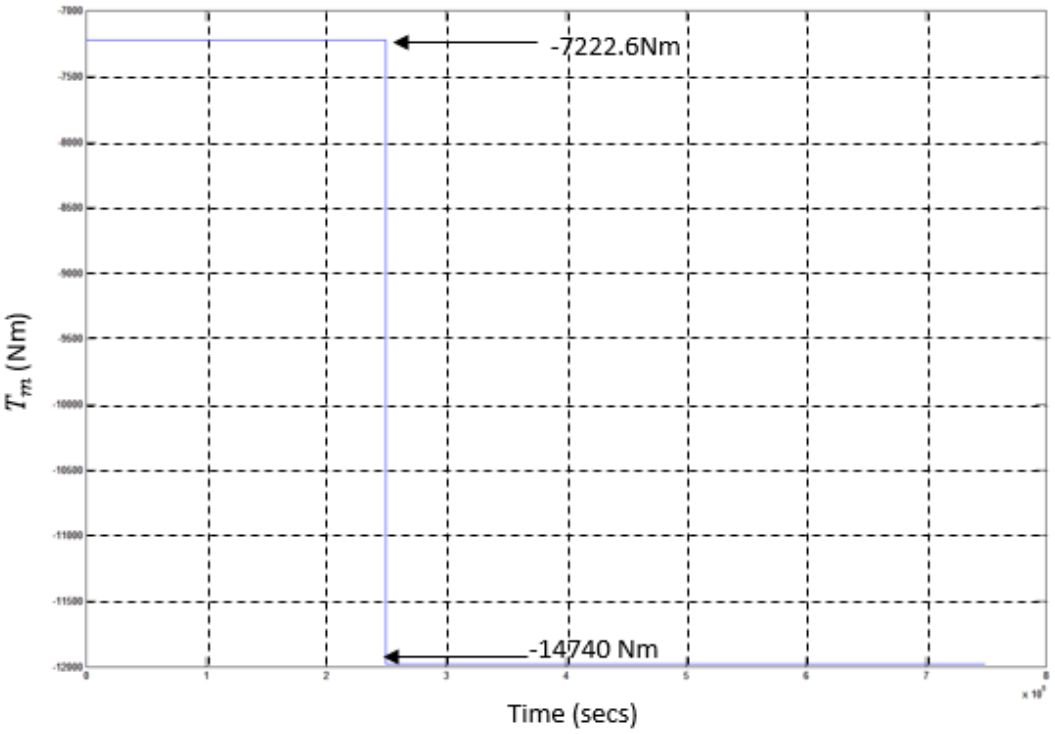

Figure 3.21. Mechanical torque.

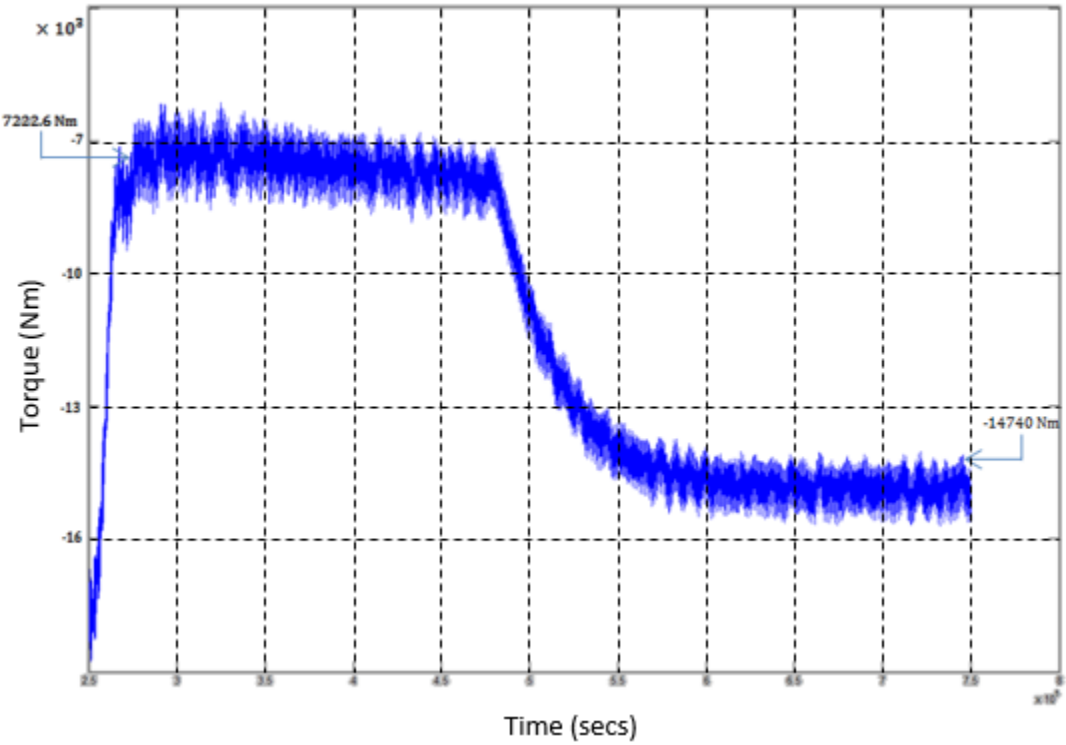

Figure 3.22. Electromagnetic torque.

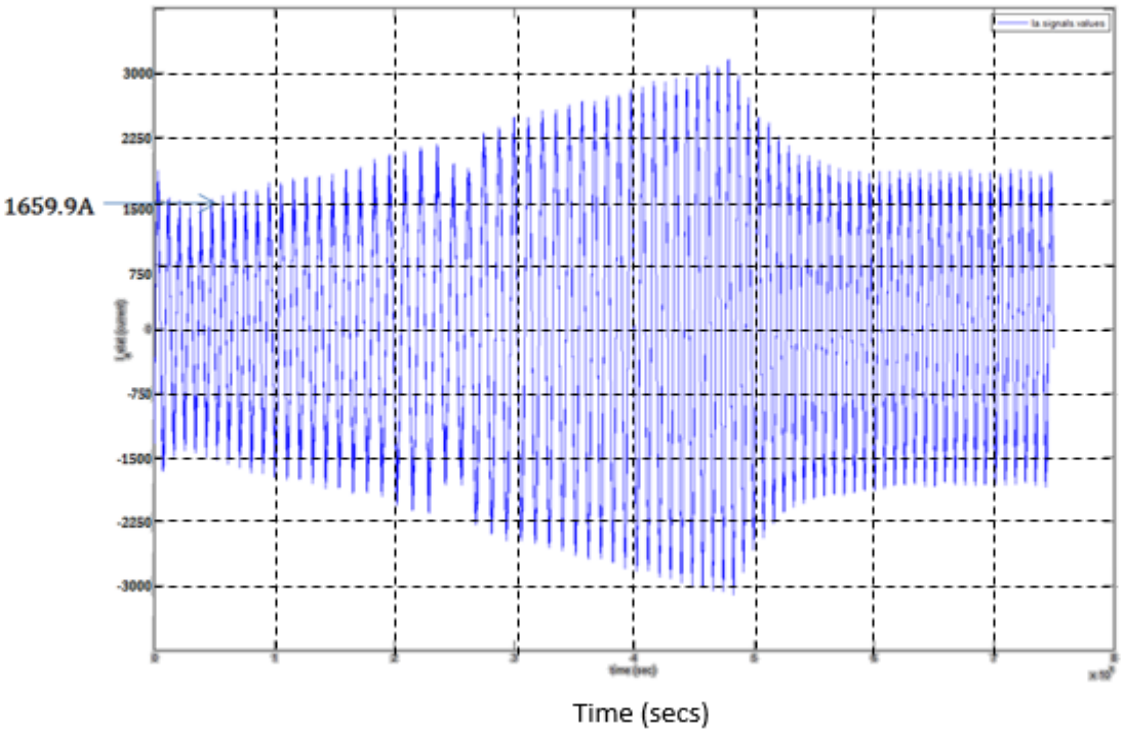

Figure 3.23. Stator current.

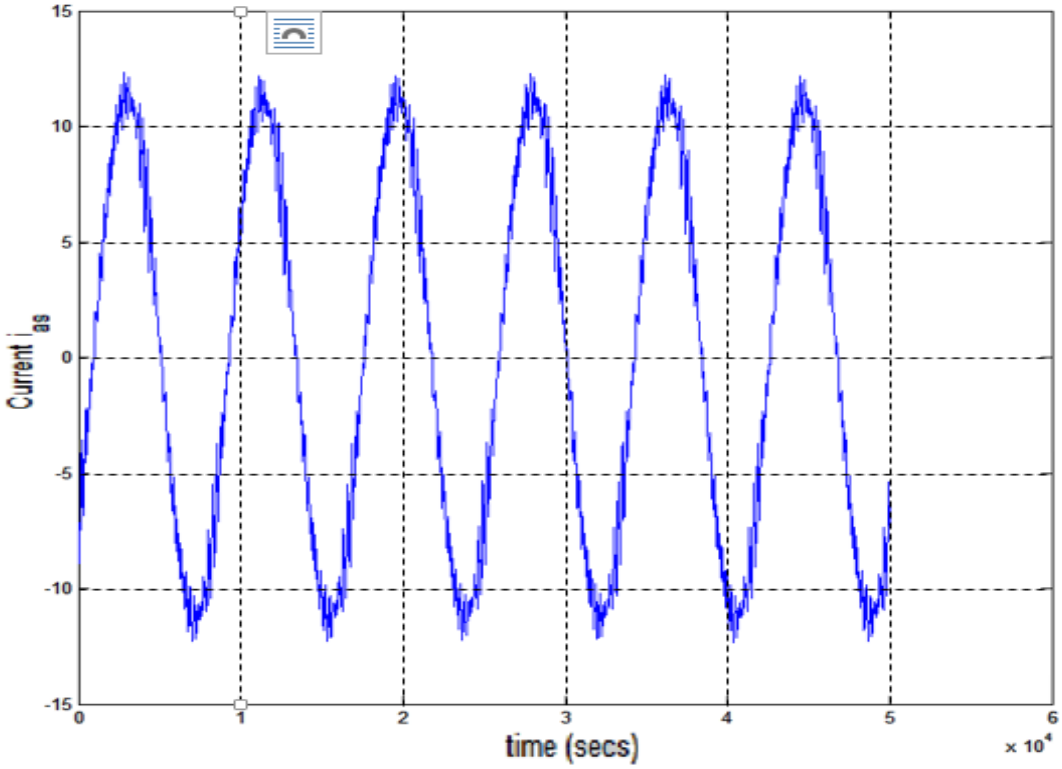

Figure 3.24. phase-*a* stator current.

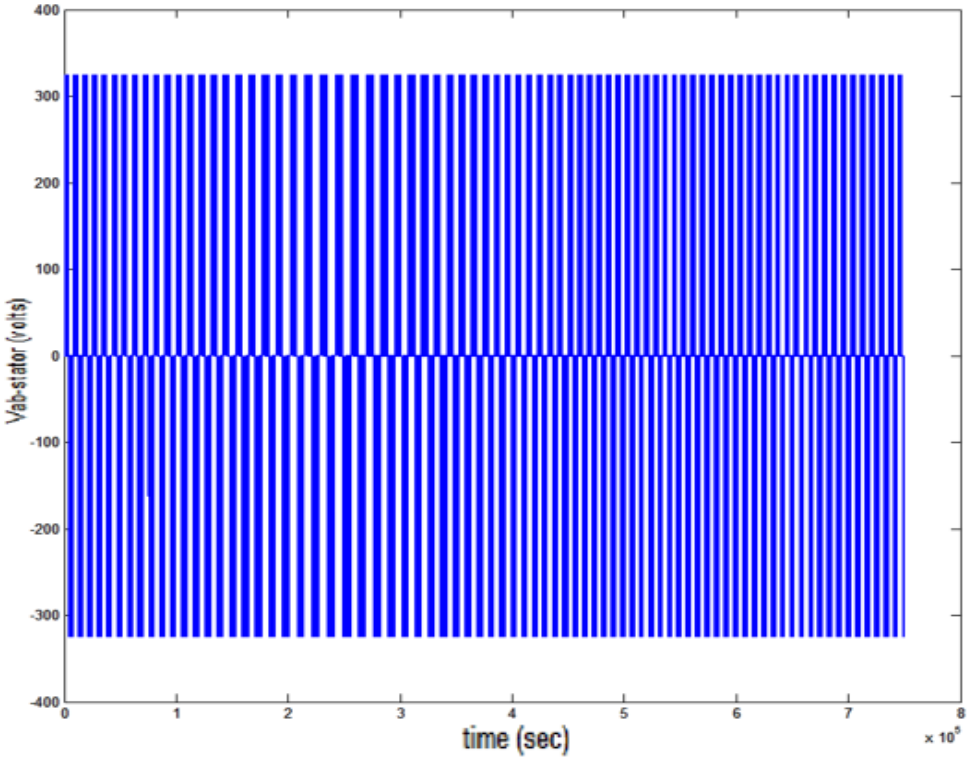

Figure 3.25. Stator voltage.

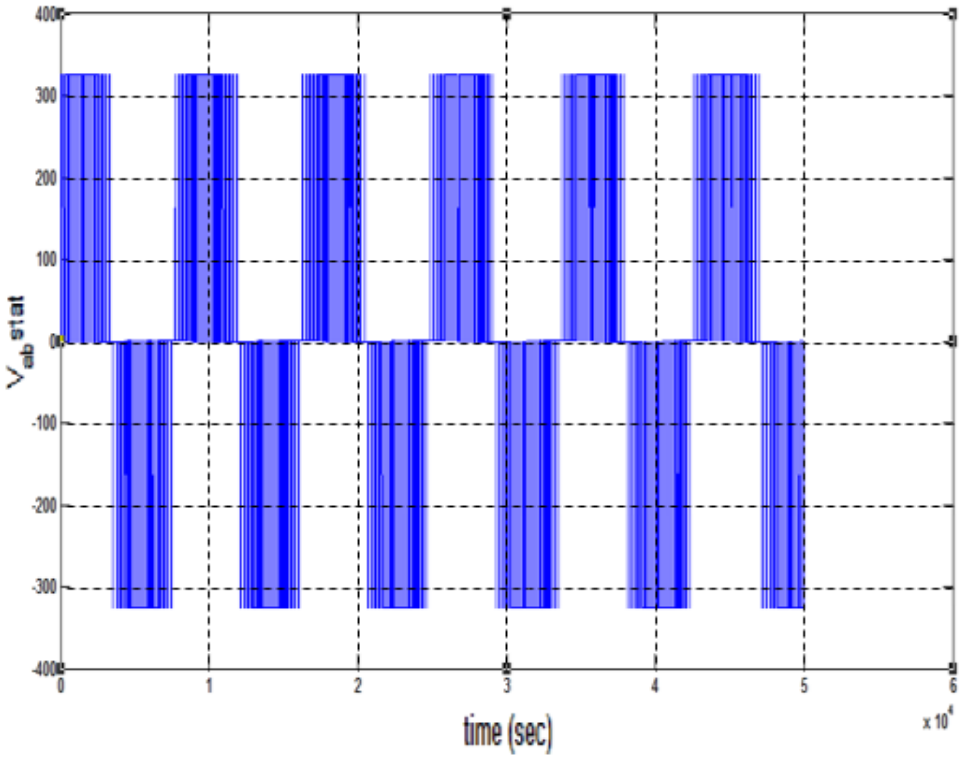

Figure 3.26. V_{as}rectifier PWM input voltage.

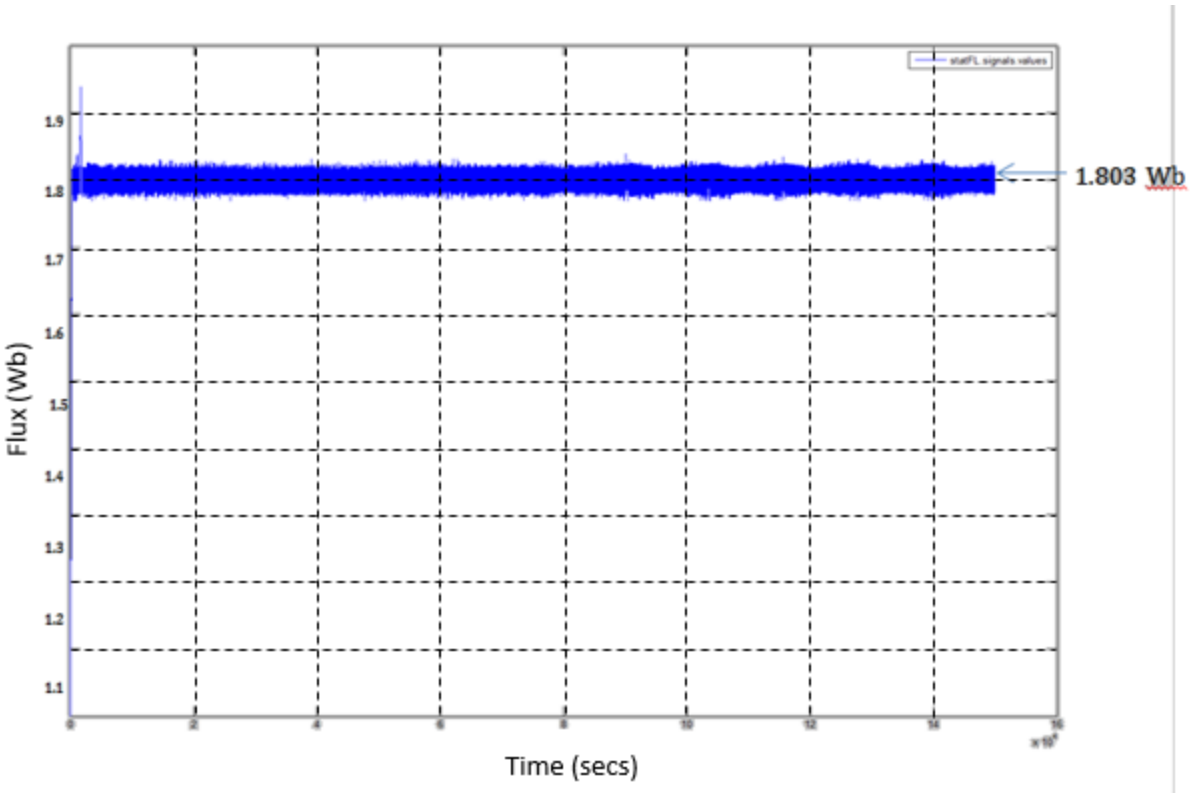

Figure 3.27. Stator flux.

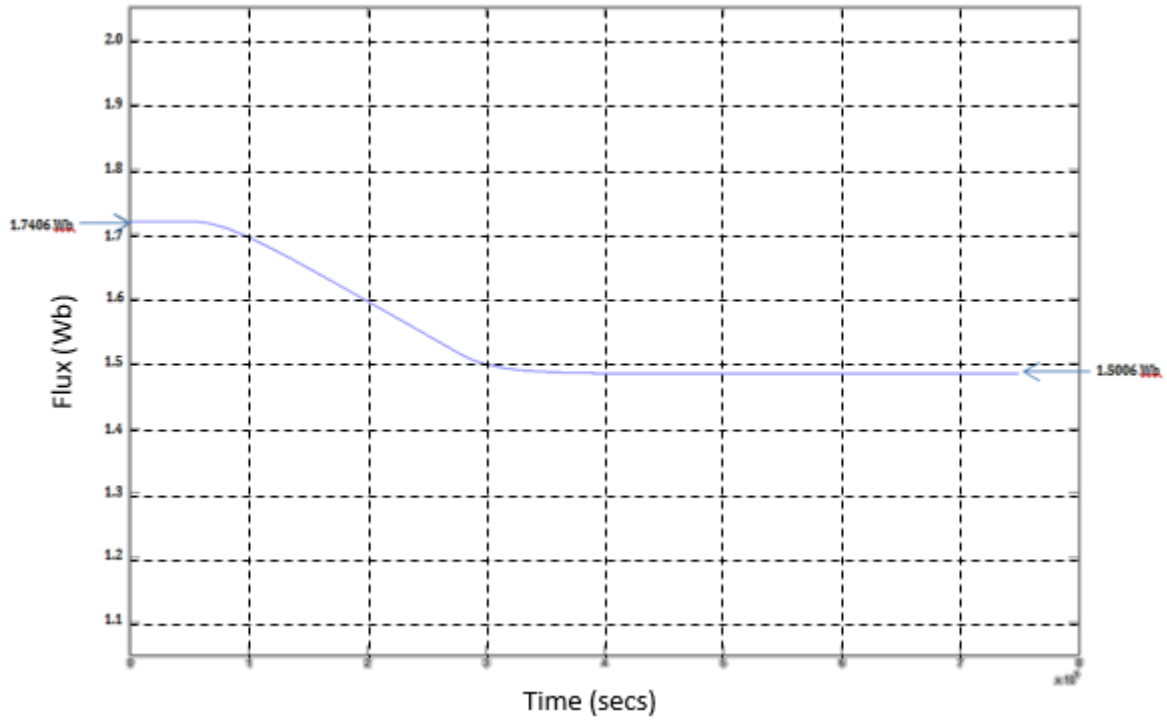

Figure 3.28. Rotor flux.

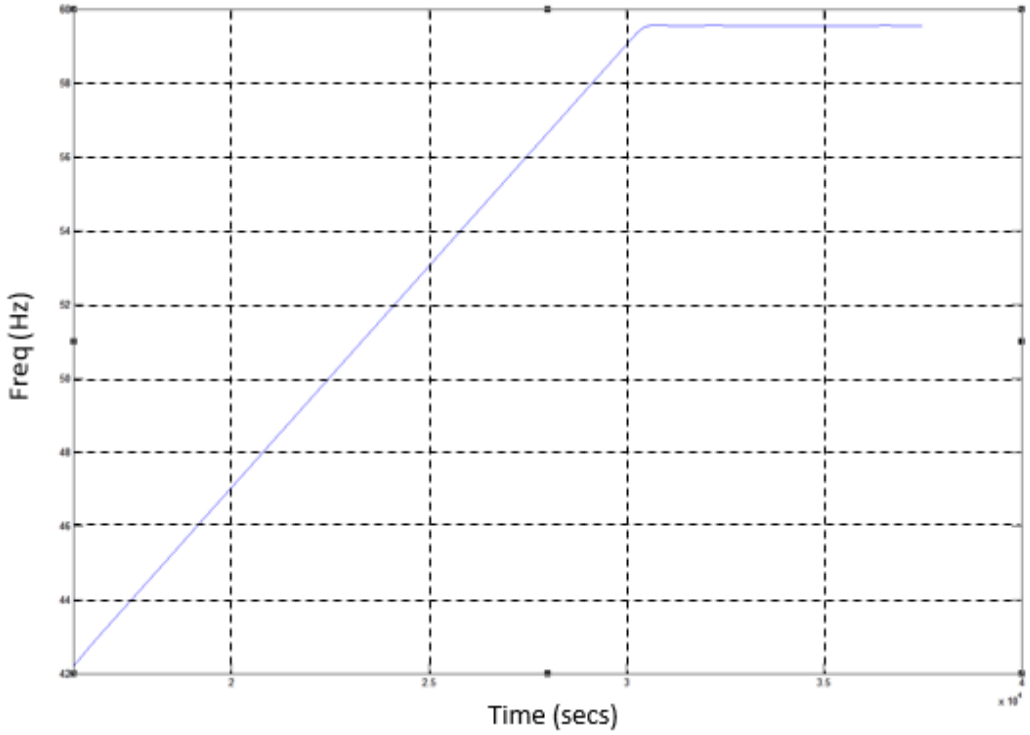

Figure 3.29. Frequency.

With direct torque control, the stator flux is kept at the rated value set by its reference, that is,

$$\lambda_s = \lambda_s^* = \sqrt{2} \times 1.2748 = 1.803 \text{ Wb} \tag{3.60}$$

For a given generator speed of 0.7 pu, the generator mechanical torque is

$$T_m = T_m R \times \omega_m^2 = -14{,}740 \times 0.7^2 = -7222.6 \text{ N. m} \tag{3.61}$$

With the rate stator flux, the q −axis current of the generator is

$$i_{qs} = \frac{2T_e}{3P\lambda_s} = -1335.4 \text{ A} \tag{3.62}$$

The slip frequency ω_{sl} is determined by

$$(T_r\sigma)^2\omega_{sl}^2 - \frac{(1-\sigma)T_r\lambda_s}{L_s i_{qs}}\omega_{sl} + 1 \tag{3.63}$$

From which we get

$$\omega_{sl} = -1.1895\frac{\text{rad}}{s} \ (0.1893 \text{ Hz}) \tag{3.64}$$

The d −axis current is calculated by

$$i_{ds} = \frac{\left(\lambda_s + \sigma L_s T_r \, \omega_{sl} i_{qs}\right)}{L_s} = 955.4 \text{ A} \tag{3. 65}$$

The stator frequency is

$$\omega_s = \omega_r + \omega_{sl} = 220.48 \text{ rad/sec} \tag{3. 66}$$

The rms stator current is then obtained by

$$\bar{I}_s = \frac{\sqrt{i_{ds}^2 + i_{qs}^2}}{\sqrt{2}} = 1161.1 \angle 0^{\text{o}} \tag{3. 67}$$

With the rated parameters (given in appendix), the input impedance is

$$\overline{Z}_s = \frac{R_s + jX_{ls} + jX_m}{\left(\frac{R_r}{s} + jX_{ls}\right)} = 0.2412 \angle 144.3^{\text{o}} \ \Omega \tag{3. 68}$$

The rms stator voltage is calculated as

$$V_s = \bar{I}_s \, \bar{Z}_s = 280.0 \angle 144.3^{\text{o}} \text{V} \tag{3. 69}$$

The rotor current can be found from

$$\bar{I}_r = \frac{jX_m \bar{I}_s}{jX_m + (\frac{R_r}{s} + jX_{lr})} = 978.0 \angle -29.8^{\text{O}} \text{ A} \tag{3. 70}$$

The magnetizing flux linkage is calculated by

$$\overline{\Lambda}_m = (\overline{I}_s - \bar{I}_r) L_m = 1.2325 \angle -57.2^{\text{o}} \text{Wb} \tag{3. 71}$$

The rms rotor flux linkage is

$$\overline{\Lambda}_s = \overline{\Lambda}_m - L_{ls} \bar{I}_s = 1.2748 \angle 54.4^{\text{o}} \tag{3. 72}$$

The peak rotor stator flux is then given by

$$\lambda_s = \sqrt{2} \overline{\Lambda}_s = 1.806 \text{ Wb} \tag{3. 73}$$

which is equal to its reference λ_s^*

The rms rotor flux linkage is

$$\bar{\Lambda}_r = \bar{\Lambda}_m - L_{ls}\bar{I}_r = 1.2308 \angle 60.2^{o} \tag{3. 74}$$

and its peak value is

$$\lambda_r = \sqrt{2}\bar{\Lambda}_r = 1.5006 \text{ Wb} \tag{3. 75}$$

The calculated values for the stator flux λ_s (1.806 Wb) , rotor flux λ_r (1.5006 Wb) at the rotor speed of 0.7 pu match well with the simulated results shown in the Figure 3.27 and Figure 3.28.

On further verification, the generator electromagnetic torque can be calculated by

$$T_e = \frac{3P}{2}\frac{L_m}{sL_sL_r}\lambda_s\lambda_r = -7222.6 \text{ N. m} \tag{3. 76}$$

The calculated results are confirmed by the simulation results of FiguresFigure 3.20. Rotor speed. Figure 3.27. Stator flux.

3.5 Summary

This chapter provides a state-space model of the induction generator and the model is used for computer simulation. The state space model is based on the equivalent circuit of the generator. The generator is described by developing the voltage and the torque equations.

Further the vector control schemes namely the field oriented control and the direct torque control techniques are introduced. There are two types of field oriented control namely the direct field oriented and the indirect field oriented control. The strategies basically remain the same, the only difference is the determination of the rotor flux angle. The two control strategies are explained and examined through understanding of the block diagram and observing the torque equations. Both the strategies are simulated in steady and dynamic conditions and simulation results demonstrate that they work well in both the conditions. A theoretical analysis was also done for the steady state operation and it was seen that the values obtained theoretical calculations and the simulation results match.

Along with FOC, a direct torque control technique was developed. The functionality of the block was explained. It was seen how the torque can be controlled by modifying the rotor

flux by simply adjusting the torque angle. The technique for inserting the voltage vectors is explained further to explain how the voltage vectors change the magnitude of the rotor flux vector. The control strategy for inserting the voltage vector the and the switching pattern of the converter is developed and analyzed through steady and dynamic state analysis and simulation results prove that this strategy works well during both operations. Similar to FOC, theoretical calculations are done for the steady state and it was seen that they match with the simulation results.

CHAPTER 4 Doubly Fed Induction Generator Based Wind Energy Systems

4.1 Introduction

Doubly-fed electric machines are basically electric machines that are fed ac currents into both the stator and the rotor windings. Most of the doubly-fed Induction machines used in industry are of wound rotor type. Doubly-fed induction machines have found great use in today's wind power generation industry.

Doubly-fed induction generators (DFIGs) are by far the most widely used type of doubly-fed electric machine, and are one of the most common types of generator used to produce electricity in wind turbines because of the numerous advantages over other types of generators when used in wind turbine technology.

The primary advantage of doubly-fed induction generators when used in wind turbines is that they allow the amplitude and frequency of their output voltages to be maintained at a constant value, regardless of the wind speed. Because of this, doubly-fed induction generators can be directly connected to the ac power network without the use of bulky and costly power converters and remain synchronized at all times with the ac power network. Other advantages include the ability to control the power factor (e.g., to maintain the power factor at unity), while keeping the power electronics devices in the wind turbine at a moderate size [56].

4.2 Principle of Doubly fed Induction generators

In a conventional three-phase synchronous generator, when an external source of mechanical power (i.e., a prime mover) makes the rotor of the generator rotate, the static magnetic field created by the dc current fed into the generator rotor winding rotates at the same speed (n_{Rotor}) as the rotor. As a result, acontinually changing magnetic flux passes through the stator windings as the rotor magnetic field rotates, inducing an alternating

voltage across the stator windings. Mechanical power applied to the generator shaft by the prime mover is thus converted to electrical power that is available at the stator windings.

In conventional (singly-fed) induction generators, the relationship between the frequency f_{Stator} of the ac voltages induced across the stator windings of the generator and the rotor speed n_{Rotor} is expressed using the following equation

$$f_{Stator} = \frac{(n_{Rotor} * N_{Poles})}{120} \quad (4.1)$$

Using the above equation (4.1), we can determine that when (n_{Rotor}) of the generator rotor is equal to generator synchronous speed n_S, the frequency f_{Stator} of the AC voltages across the stator windings is equal to frequency $f_{Network}$ of the AC power system.

The same operating principles apply in a doubly-fed induction generator as in a conventional (singly-fed) induction generator. The only difference is that the magnetic field created in the rotor is not static (as it is created using three-phase ac current instead of dc current), but rather rotates at a speed $n_{\phi,rotor}$ proportional to the frequency of the ac currents fed into the generator rotor windings. This means that the rotating magnetic field passing through the generator stator windings not only rotates due to the rotation of the generator rotor, but also due to the rotational effect produced by the ac currents fed into the generator rotor windings. Therefore, in a doubly-fed induction generator, both the rotation speed n_{Rotor} of the rotor and the frequency f_{rotor} of the ac currents fed into the rotor windings determine the speed $n_{\phi,stator}$ of the rotating magnetic fieldpassing through the stator windings, and thus, the frequency f_{stator} of the alternating voltage induced across the stator windings [56, 57].

Thus when the magnetic field at the rotor rotates in the same direction as the generator rotor, the rotor speed n_{rotor} and the speed $n_{\phi,rotor}$ of the rotor magnetic field (proportional to f_{rotor}) add up. The frequency f_{stator} of the voltages induced across thestator windings of the generator can thus be calculated using the following equation:

$$f_{Stator} = \frac{n_{Rotor} * N_{Poles}}{120} + f_{Rotor} \quad (4.2)$$

Conversely, when the magnetic field at the rotor rotates in the direction opposite to that of the generator rotor, the rotor speed $n_{Rotor}$and the speed $n_{\phi,stator}$of therotor magnetic field subtract from each other. The frequency $f_{Stator}$of the voltages induced across the stator windings of the generator can thus be calculated using the following equation:

$$f_{Stator} = \frac{n_{Rotor} * N_{Poles}}{120} - f_{Rotor} \tag{4. 3}$$

In other words, the frequency f_{stator} of the AC voltages produced at the stator of DFIG increases with the $n_{\phi,stator}$ and f_{Rotor} of the AC currents fed into the machine rotor.

The primary reason for using a doubly-fed induction generator is generally to produce three-phase voltage whose frequency f_{stator} is constant, i.e., whose frequency f_{stator} remains equal to the frequency $f_{network}$of the ac power network to which the generator is connected, despite variations in the generator rotor speed n_{Rotor}caused by fluctuations of the mechanical power provided by the prime mover (e.g., a wind turbine rotor) driving the generator. To this end, the frequency $f_{rotor}$of the ac currents fed into the rotor windings of the doubly-fed induction generator must be continually adjusted to counteract any variation in the rotor speed n_{rotor}caused by fluctuations of the mechanical power provided by the prime mover driving the generator.

The frequency $f_{rotor}$of the ac currents that must be fed into the doubly-fed induction generator rotor windings to maintain the generator output frequency f_{stator}at the same value as the frequency $f_{network}$of the ac power network depends on the rotation speed of the generator rotor n_{rotor} and can be calculated using the following equation

$$f_{rotor} = f_{network} - \frac{n_{Rotor} * N_{Poles}}{120} \tag{4. 4}$$

Thus, we conclude that if the speed of the rotor is equal to the synchronous speed the frequency f_{rotor} that needs to fed will be 0hz and thus the machine would operate as conventional three phase synchronous machine.

When the generator rotor speed n_{rotor}decreases below the nominal synchronous speed n_s, the frequency $f_{rotor}$of the ac currents that need to be fed into the generator windings

increases accordingly and is of positive polarity. Thus indicates that the phase sequence of the three-phase ac currents fed into the rotor windings must make the rotor magnetic field rotate in the same direction as the generator rotor.

Similarly, when the generator rotor speed n_{rotor}increases above the nominal synchronous speed n_s, the frequency $f_{rotor}$of the ac currents that need to be fed into the generator windings increases accordingly and is of negative polarity. Thus indicates that the phase sequence of the three-phase ac currents fed into the rotor windings must make the rotor magnetic field rotate in the direction opposite to that of the generator rotor[56-58].

4.2.1 DFIG used in Wind Turbines

In variable-speed wind turbines, the rotation speed of the wind turbine rotor is allowed to vary as the wind speed varies. This precludes the use of asynchronous generators in such wind turbines as the rotation speed of the generator is quasi-constant when its output is tied directly to the grid. The same is true for synchronous generators which operate at a strictly constant speed when tied directly to the grid. This is where doubly-fed induction generators come into play, as they allow the generator output voltage and frequency to be maintained at constant values, for any generator rotor speed and any wind speed. As seen in the Section 4.1, this is achieved by feeding ac currents of variable frequency and amplitude into the generator rotor windings. By adjusting the amplitude and frequency of the ac currents fed into the generator rotor windings, it is possible to keep the amplitude and frequency of the voltages (at stator) produced by the generator constant, despite variations in the wind turbine rotor speed (and, consequently, in the generator rotation speed) caused by fluctuations in wind speed. This also allows operation without sudden torque variations at the wind turbine rotor, thereby decreasing the stress imposed on the mechanical components of the wind turbine and smoothing variations in the amount of electrical power produced by the generator. Using the same means, it is also possible to adjust the amount of reactive power exchanged between the generator and the ac power network. This allows the power factor of the system to be controlled (e.g., in order to maintain the power factor at unity). Finally, using a doubly-fed induction generator in

variable-speed wind turbines allows electrical power generation at lower wind speeds than with fixed-speed wind turbines using an asynchronous generator [58-60].

4.3 Back-to-Back Power Electronic Converter for DFIG Based Wind Turbines

4.3.1 Introduction

The broadly employed wind turbine is supplied by the rotor with a back-to-back converter also known as a reversible or a bidirectional converter as shown in Figure 4.1. In this section we discuss about the back to back converter emphasizing the grid side rather than the rotor side.

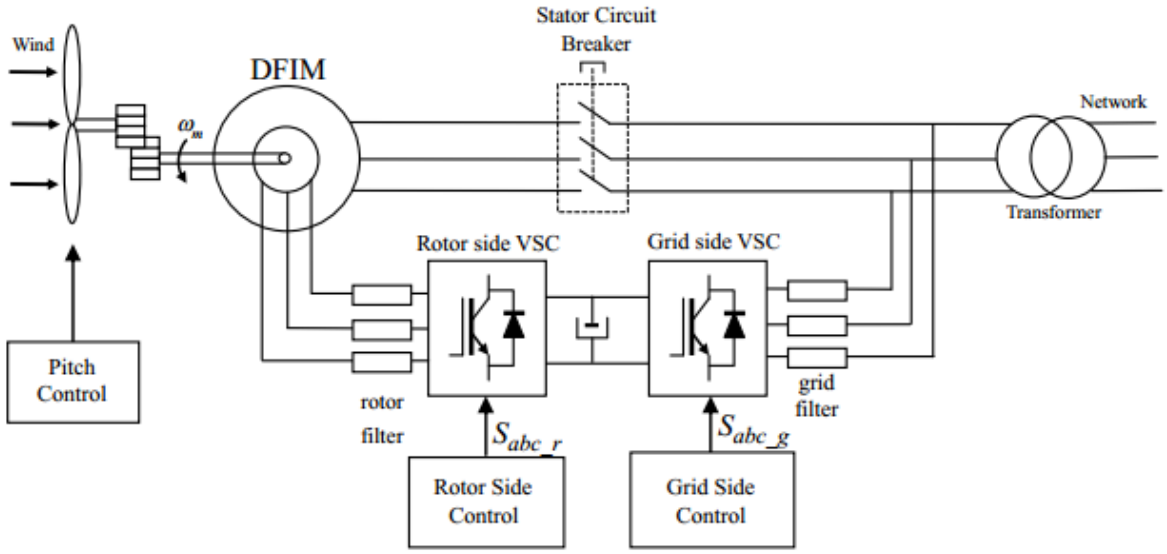

Figure 4.1. System configuration of the DFIG based wind turbine [61].

First there is a need to study the two level voltage source converters, examining its model and presenting different pulse generating possibilities for its controlled switches. Then newer and emerging topologies are studied. After this we discuss the control of grid side converter[62].

4.3.2 Back-to-Back Converter Based on a Two-Level Topology

The two-level converter is the most widely used converter in the industry and this section discuss the back-to-back converter based on the two level topology.

4.3.2.1 Grid Side System

The grid side system is composed by the grid side converter, grid side filter and the grid voltage as shown in Figure 4.2. The grid side converter is modeled by ideal bidirectional switches. The exchange of power can be DC to AC or AC to DC. Here the controlled semiconductor is an Insulated Gate Bipolar Transistor (IGBT). The grid side filter is composed of at least three inductances which forms a link between the converter and the grid voltage. In some cases each inductance is accompanied by one capacitor. The grid voltage is generally supplied through a transformer and this AC voltage is balances and sinusoidal under normal conditions[63].

Converter Model

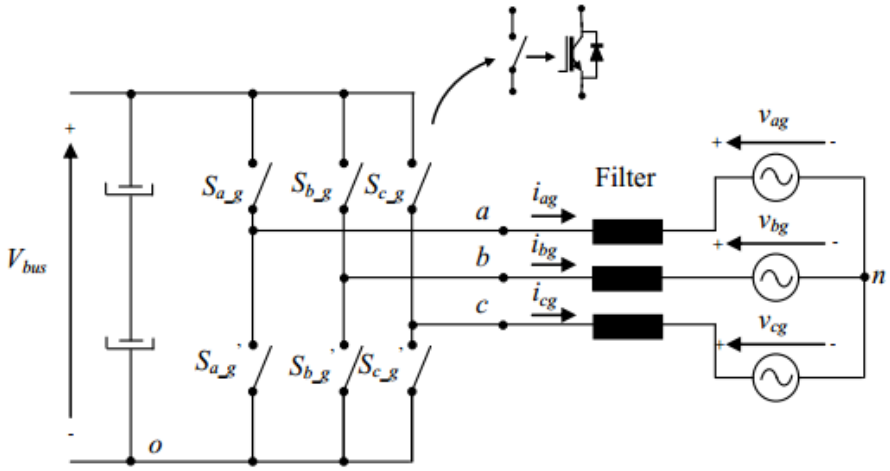

Figure 4.2. Simplified converter, filter and grid model [61].

We will model the two-level converter by ideal switches which provide power flow in both the directions. The command of the switches is done by signals S_{a_g} , S_{b_g} , S_{c_g} . Under Ideal conditions

$$S'_{a\_g} = \overline{S_{a\_g}} \tag{4. 5}$$

$$S'_{b\_g} = \overline{S_{b\_g}} \tag{4. 6}$$

$$S'_{c\_g} = \overline{S_{c\_g}} \tag{4. 7}$$

This means that in a leg of the converter, it is not possible to have conduction in both the switches. Thus by different combinations of S_{a_g} , S_{b_g} , S_{c_g} it is possible to create AC output voltages with fundamental component of different amplitude and frequency [60, 62, 64].

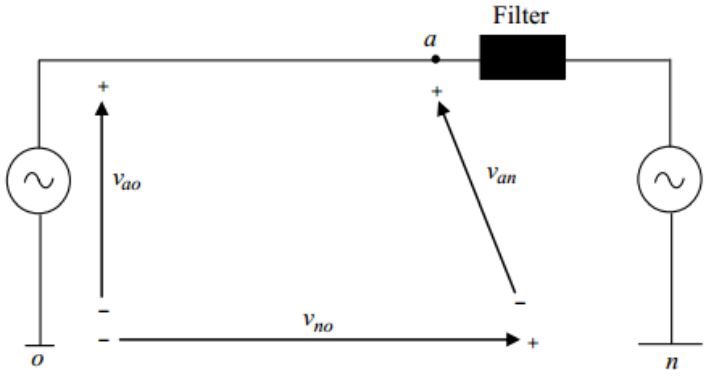

Figure 4.3. Simplified equivalent single-phase grid circuit (a phase).

From the Figure 4.3 the following voltage relationships are true

$$v_{jn} = v_{jo} - v_{no} \tag{4. 8}$$

The voltage between the neutral point (n) and the negative point of the DC bus is needed, so assuming a three phase grid system that holds, we have

$$v_{an} + v_{bn} + v_{cn} = 0 \tag{4. 9}$$

Substituting the (4.9) into (4.8) the last expression yields

$$v_{no} = \frac{1}{3}(v_{ao} + v_{bo} + v_{co}) \tag{4. 10}$$

Substituting the equation (4. 11) in (4. 12) we get,

$$v_{an} = \frac{2}{3}v_{ao} - \frac{1}{3}(v_{bo} + v_{co}) \tag{4. 13}$$

$$v_{bn} = \frac{2}{3}v_{bo} - \frac{1}{3}(v_{ao} + v_{co}) \tag{4. 14}$$

$$v_{cn} = \frac{2}{3}v_{co} - \frac{1}{3}(v_{bo} + v_{ao}) \tag{4. 15}$$

4.3.2.2 Rotor Side System

The rotor side converter that supplies the DFIG, in general terms, is equal to the grid side converter shown in the Section 4.2.3.1 as shown in the Figure 4.4. In this case also a two level VSC feeds the rotor and between the rotor and the converter we have a $\frac{dv}{dt}$filter to protect the machine from the harmful effects of the converter like capacitive leakage currents and bearing currents.

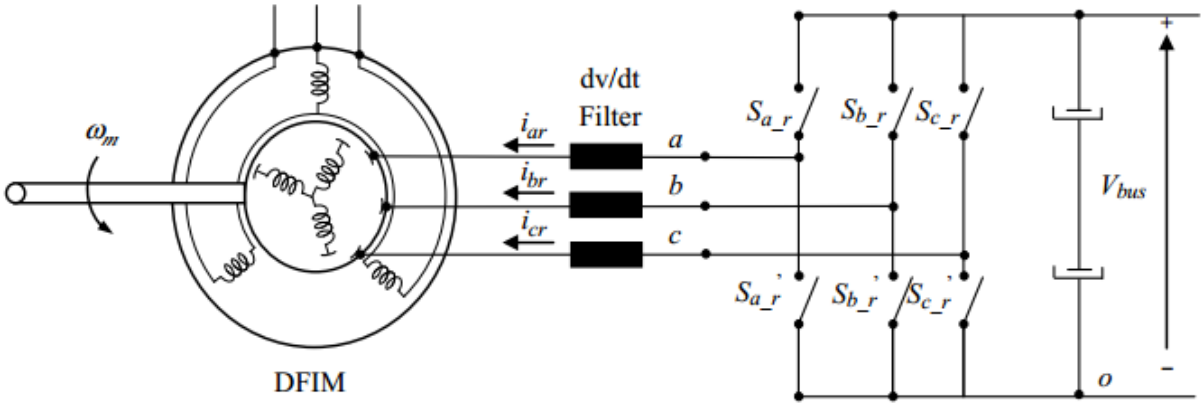

Figure 4.4. Rotor side converter and the $\frac{dv}{dt}$ filter [61].

The $\frac{dv}{dt}$filter tries to attenuate the step voltages in rotor terminals of the machine, coming from the converter. The three main factors are that determine how harmful the effects are on the machine which the $\frac{dv}{dt}$filter tends to reduce and they are the type of voltage steps generated by the converter, the characteristics and length of cable used for connected the converter and the machine and also the characteristics of the machine. To reduce the voltages at the terminals of the motor, we locate a resistance and an inductance in parallel at the output of the converter. The filter is generally composed of two passive elements, the resistance damps the reflection in the cable and the inductance is necessary for reducing the voltage drop. The filter whose objective is to couple the input impedance of the motor

with the impedance are normally located at the terminals of the motor and it is possible to locate a RC or an RLC filter[65].

4.3.2.3 DC Link

The DC part of the back-to-back converter is typically called the DC link and using thanks to the energy in the capacitor, it tries to maintain a constant voltage in its terminals. It is the linkage between the grid side and the rotor side converter. Figure 4.5 shows the simplified diagram of the DC link system composed of a capacitor in parallel with a high resistance. The DC bus voltage is dependent on the current through the capacitor[66]

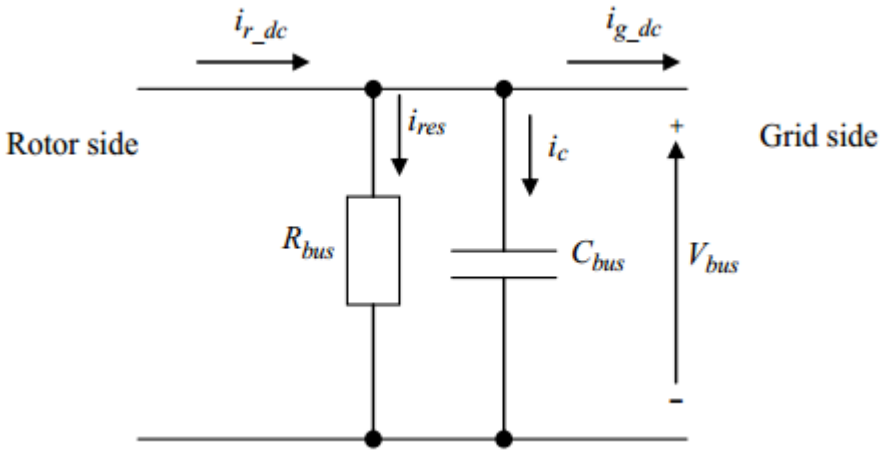

Figure 4.5. DC link system.

$$V_{bus} = \frac{1}{C_{bus}} \int i_c dt \tag{4. 16}$$

The current through the capacitor can be found by

$$i_c = i_{r\_dc} - i_{g\_dc} - i_{res} \tag{4. 17}$$

where

i_{res} = current through the resistance

i_{g_dc} = DC current flowing from the DC link to the grid

i_{r_dc} = DC current flowing from the rotor to the DC link

These currents can be calculate as follows

$$i_{g\_dc} = S_{a\_g} i_{ag} + S_{b\_g} i_{bg} + S_{c\_g} i_{cg} \quad (4.18)$$

$$i_{r\_dc} = -S_{a\_r} i_{ar} - S_{b\_r} i_{br} - S_{c\_r} i_{cr} \quad (4.19)$$

The current through the resistance

$$i_{res} = \frac{V_{bus}}{R_{bus}} \quad (4.20)$$

4.3.2.4 Pulse Generation of the Controlled Switches

The commands for the controlled semiconductors of the two-level converter can be generated according to different laws using three modulation techniques

- Sinusoidal pulse width modulation (PWM) technique
- Sinusoidal pulse width modulation (PWM) technique with injection of third harmonic
- Space vector modulation (SVM) technique [25, 32]

We can apply all the techniques to both rotor and grid side converters

4.4 Control of Grid Side Systems

We develop two models for the grid side system: a steady state model and a dynamic model based on space vector theory. The control strategy developed using these models.

4.4.1 Steady State Modeling of the Grid Side System

The power flow normally calculates the grid variables rather than those of the converter. The active and the reactive powers calculated are

$$P_g = V_{ag} I_{ag} cos\varphi \quad (4.21)$$

$$Q_g = V_{ag} I_{ag} sin\varphi \quad (4.22)$$

4.4.2 Dynamic Modeling of the Grid Side System

In this section the grid side systems is represented in space vector form as this representation serves as the mathematical basis for dynamic modelling of the grid side system.

4.4.2.1 $\alpha\beta$ Model

By applying the space vector notation to the abc modeling equations, it is possible to represent the electric equations in $\alpha\beta$ components [57, 60, 64].

We have

$$v_{\alpha f} = R_f i_{\alpha g} + \frac{L_f d i_{\alpha g}}{dt} + v_{\alpha g} \tag{4. 23}$$

$$v_{\beta f} = R_f i_{\beta g} + \frac{L_f d i_{\beta g}}{dt} + v_{\beta g} \tag{4. 24}$$

A compact version, referred to a stationary reference frame,

$$\overrightarrow{v_f^s} = R_f \overrightarrow{i_g^s} + \frac{L_f d\overrightarrow{i_g^s}}{dt} + \overrightarrow{v_g^s} \tag{4. 25}$$

where

$$\overrightarrow{v_f^s} = v_{\alpha f} + j v_{\beta f} \tag{4. 26}$$

$$\overrightarrow{v_g^s} = v_{\alpha g} + j v_{\beta g} \tag{4. 27}$$

$$\overrightarrow{i_g^s} = i_{\alpha g} + j i_{\beta g} \tag{4. 28}$$

The schematic representation of the resulting electric circuit is depicted in Figure 4.6

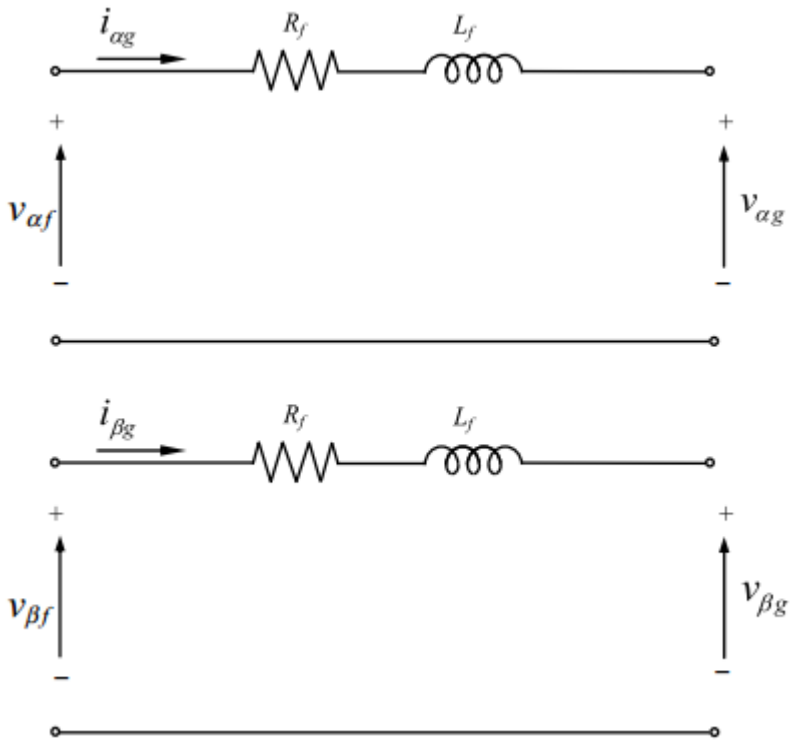

Figure 4.6. $\alpha\beta$ model of the grid side system.

4.4.2.2 *dq* Model

Similarly the dq equations can be derived (rotating frame)

$$\overrightarrow{v_f^a} = R_f \overrightarrow{i_g^a} + \frac{L_f d\overrightarrow{i_g^s}}{dt} + \overrightarrow{v_g^a} + j\omega_a L_f \overrightarrow{i_g^a} \tag{4. 29}$$

with dq componenets,

$$\overrightarrow{v_f^a} = v_{df} + jv_{qf} \tag{4. 30}$$

$$\overrightarrow{v_g^s} = v_{dg} + jv_{qg} \tag{4. 31}$$

$$\overrightarrow{i_g^s} = i_{dg} + ji_{qg} \tag{4. 32}$$

Therefore, by decomposing into dq components, the basic equations for vector orientation are obtained [57, 60, 64]:

$$v_{df} = R_f i_{dg} + \frac{L_f di_{dg}}{dt} + v_{dg} + \omega_a L_f i_{dg} \tag{4. 33}$$

$$v_{qf} = R_f i_{qg} + \frac{L_f di_{qg}}{dt} + v_{qg} - \omega_a L_f i_{qg} \quad (4.34)$$

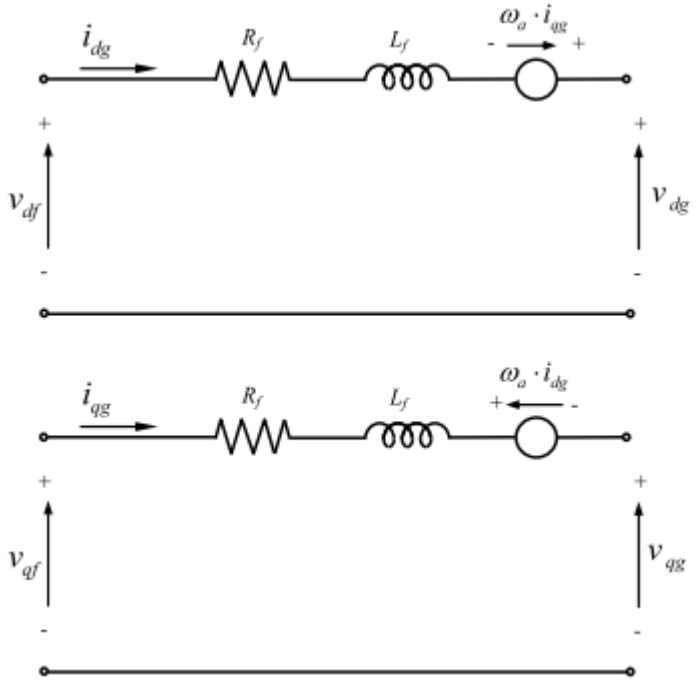

Figure 4.7. *dq* model of the grid side system.

4.4.2.3 Alignment of the *dq* Reference Frame:

Expressions (4.31) and (4.32) are the *dq* equations of the electric system rotating at a speed of ω_s, which is equal to the angular speed of the grid voltage. The *d*-axis of the rotating frame is aligned with the grid voltage space vector $\vec{v}_g^a$.

The resulting *dq* components of the grid voltage yield

$$v_{dq} = |\vec{v}_g^a| \quad (4.35)$$

$$v_{qg} = 0 \quad (4.36)$$

$$\omega_a = \omega_s \quad (4.37)$$

$$\theta_g = \omega_s t \quad (4.38)$$

Therefore,

$$v_{df} = R_f i_{dg} + \frac{L_f di_{dg}}{dt} + v_{dg} - \omega_s L_f i_{dg} \quad (4.39)$$

$$v_{qf} = R_f i_{qg} + \frac{L_f di_{qg}}{dt} + \omega_s L_f i_{qg} \quad (4.40)$$

This grid voltage alignment simplifies the voltage equations of the system and the active and reactive power computations. Thus the active and reactive powers exchanged with the grid are calculated

$$P_g = \frac{3}{2}\left(v_{dg} i_{dg} + v_{qg} i_{qg}\right) \quad (4.41)$$

$$Q_g = \frac{3}{2}\left(v_{dg} i_{dg} - v_{qg} i_{qg}\right) \quad (4.42)$$

By considering equations (4.33) and (4.34) the power calculation can be simplified to

$$P_g = \frac{3}{2} v_{dg} i_{dg} \quad (4.43)$$

$$Q_g = -\frac{3}{2} v_{qg} i_{qg} \quad (4.44)$$

Equations (4.41) and (4.42) we show that the dq components and the active and reactive powers have been decoupled. Thus the d-axis current i_{dg} is responsible for P_g and the q-axis current is responsible for the Q_g.

The active and reactive power calculated in the terminals if the converter is not the same as the power in the grid terminals. They are calculated as follows

$$P_f = \frac{3}{2}\left(v_{df} i_{df} + v_{qf} i_{qf}\right) \quad (4.45)$$

$$Q_f = \frac{3}{2}\left(v_{df} i_{df} - v_{qf} i_{qf}\right) \quad (4.46)$$

Substituting the value of v_{df} and v_{qf} from equations (4. 39) and (4. 40) and assuming a steady state, the first derivatives of the dq components are zero, we find

$$P_f = \frac{3}{2}\left(R_f |\vec{i}|^2 + v_{dg} i_{dg}\right) \quad (4.47)$$

$$Q_f = \frac{3}{2}\left(L_f \omega_s |\vec{\imath}|^2 - v_{dg} i_{dg}\right) \tag{4. 48}$$

We can see from the equations (4.45) and (4.46) that the converter also provides the active and the reactive power of the filter. In the converters' power expression, the power part assumed by the filter also appears.

4.4.3 Vector Control of the Grid Side System

The grid side converter is in charge of controlling part of the power flow of the DFIM. The power generated by the wind turbine is partially delivered through rotor of the DFIM and it also flows through the DC link and finally is transmitted by the grid side converter to the grid. A general power flow diagram is shown in the Figure 4.8.

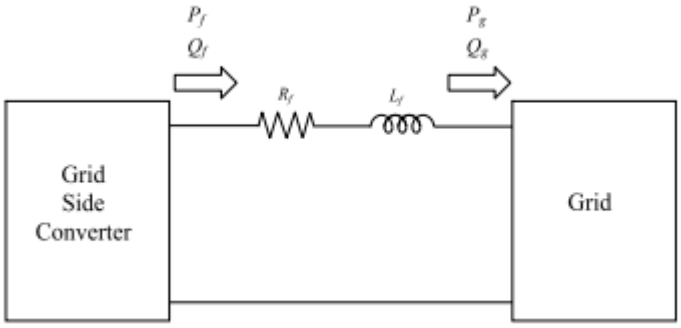

Figure 4.8. Power flow diagram.

Similar to the grid side converter of the SCIG, the pulses for the controlled switches of the 2L-VSC, that is the output voltage of the converter, are generated in order to control the DC bus voltage of the DC link and the reactive power exchange with the grid. This is done by strategy called gird voltage oriented vector control (GVOVC). Since the active power through the rotor must cross the DC link and is then transmitted to grid, maintaining the DC bus voltage is mandatory. So this DC bus voltage must be maintained at a constant level[25, 32].

Similarly the reactive power exchanged with the grid Q_g, can be controlled. It can take different values depending on the current through the rotor side converter and the grid side converter. Generally a sensorless strategy is not adopted, the control magnitudes

which are measured are the stator currents and voltages with the DC link voltage. From the V_{bus} and Q_g references the strategy generates for the control of switches as shown in the Figure 4.9.

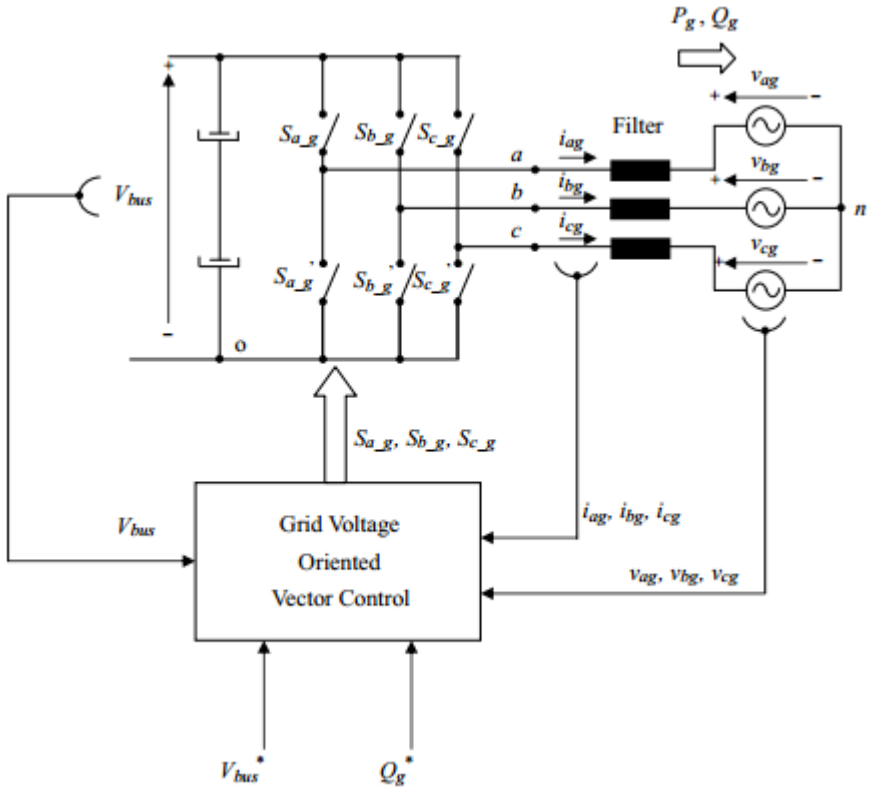

Figure 4.9. Grid side system control [61].

As shown in the Figure 4.10 block diagram the modulator generates the controlled pulses from the switches from the references for the grid side converter v_{af}^*, v_{bf}^* and v_{cf}^*. The modulator can be based on any of the schemes mentioned before in this thesis.

The grid side controller was simulated under steady state conditions and the simulation results are shown in Figures 11-16. The figures show the Grid voltages, *abc* grid side currents, *dq* grid side currents, Grid side converter output voltage, Power exchange with the grid, DC bus voltage.

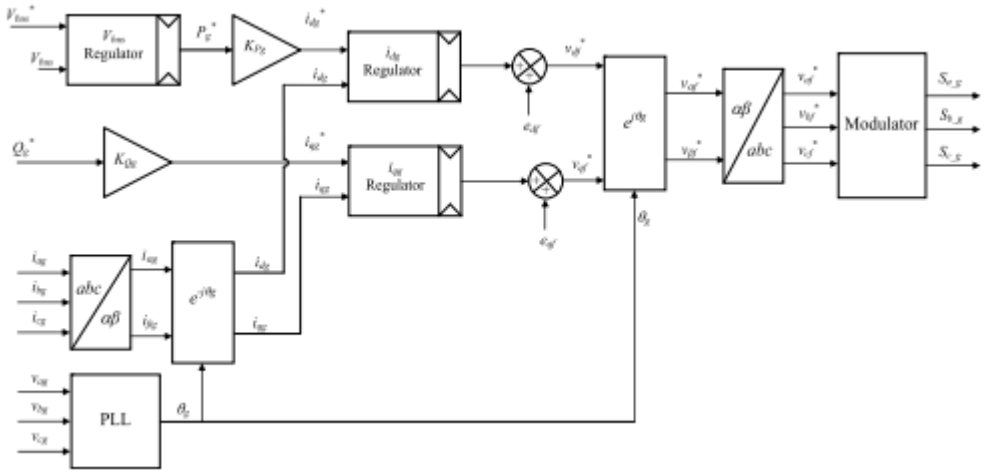

Figure 4.10. Grid voltage oriented vector control (GVOVC) block diagram [61].

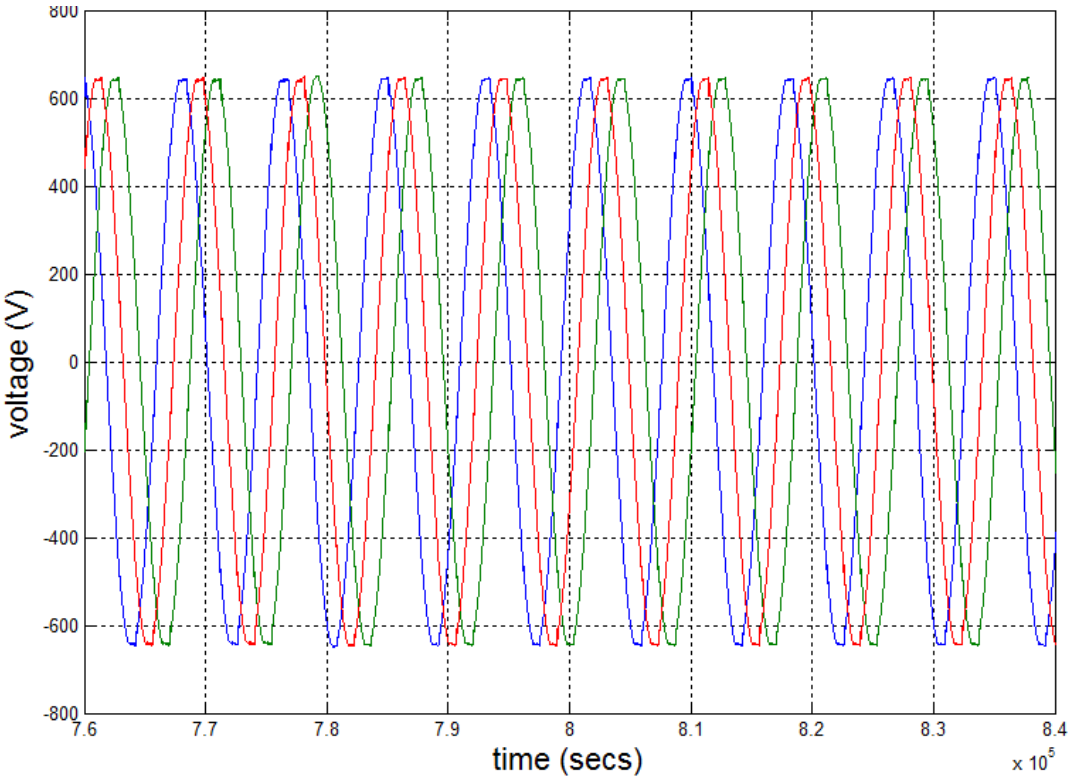

Figure 4.11. Grid voltages.

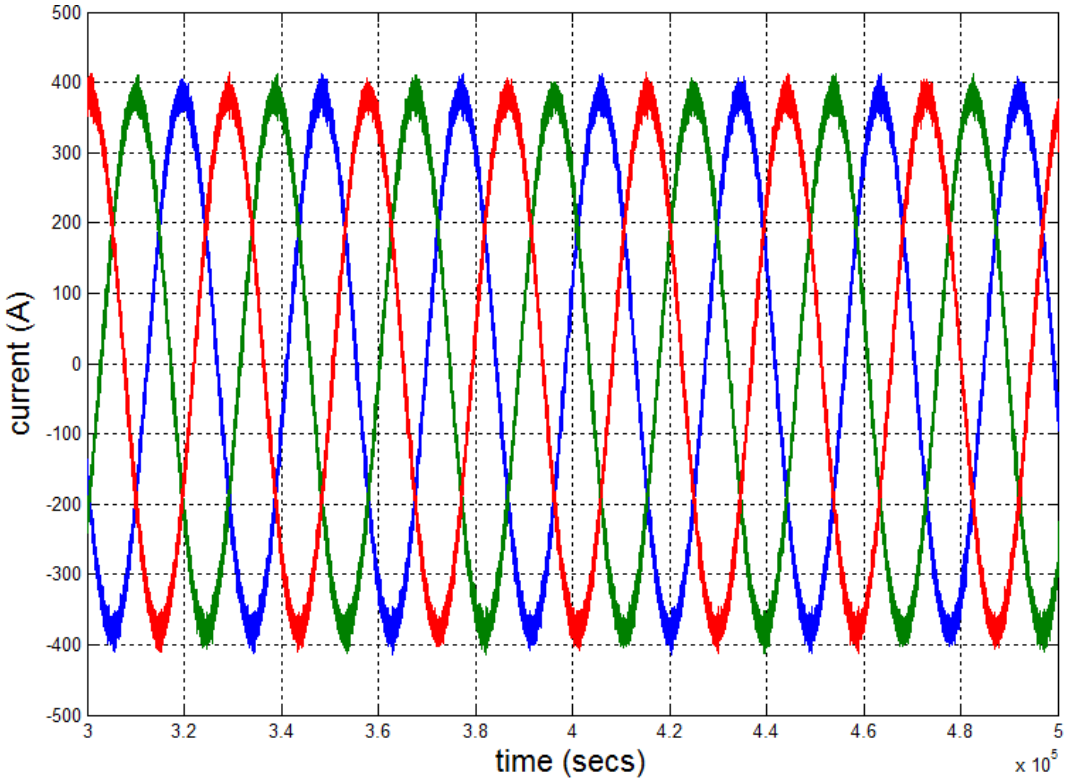

Figure 4.12. *abc* grid side currents.

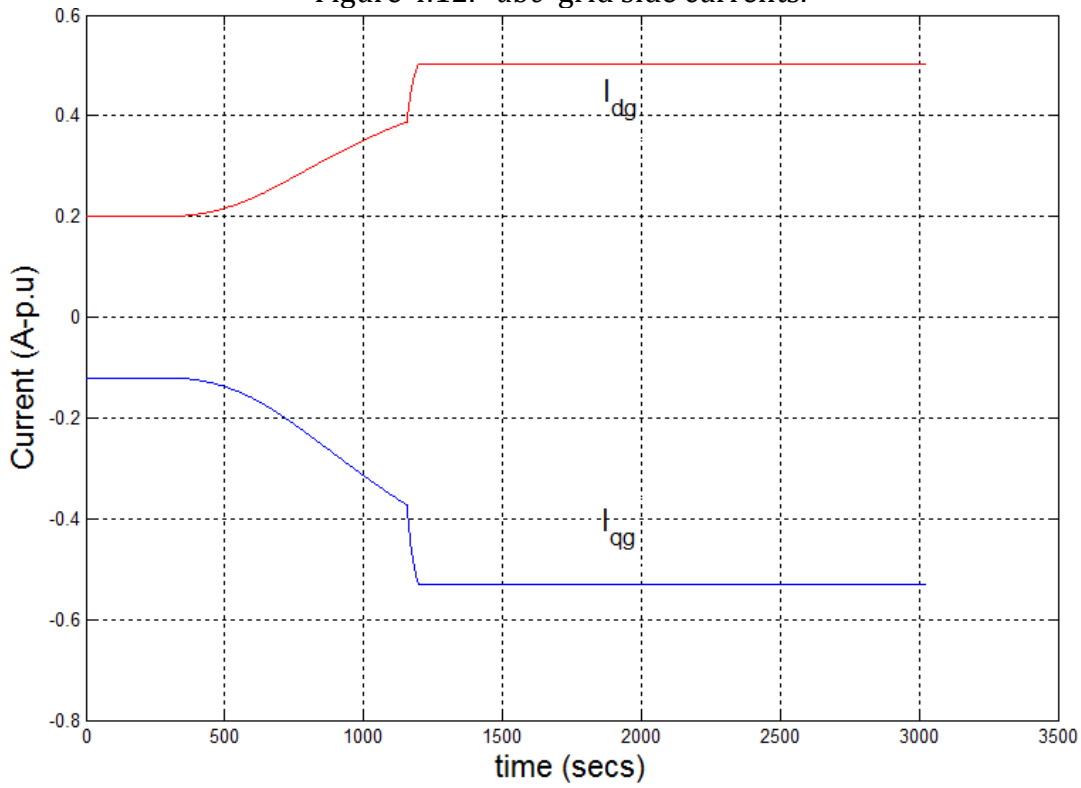

Figure 4.13. *dq* grid side currents.

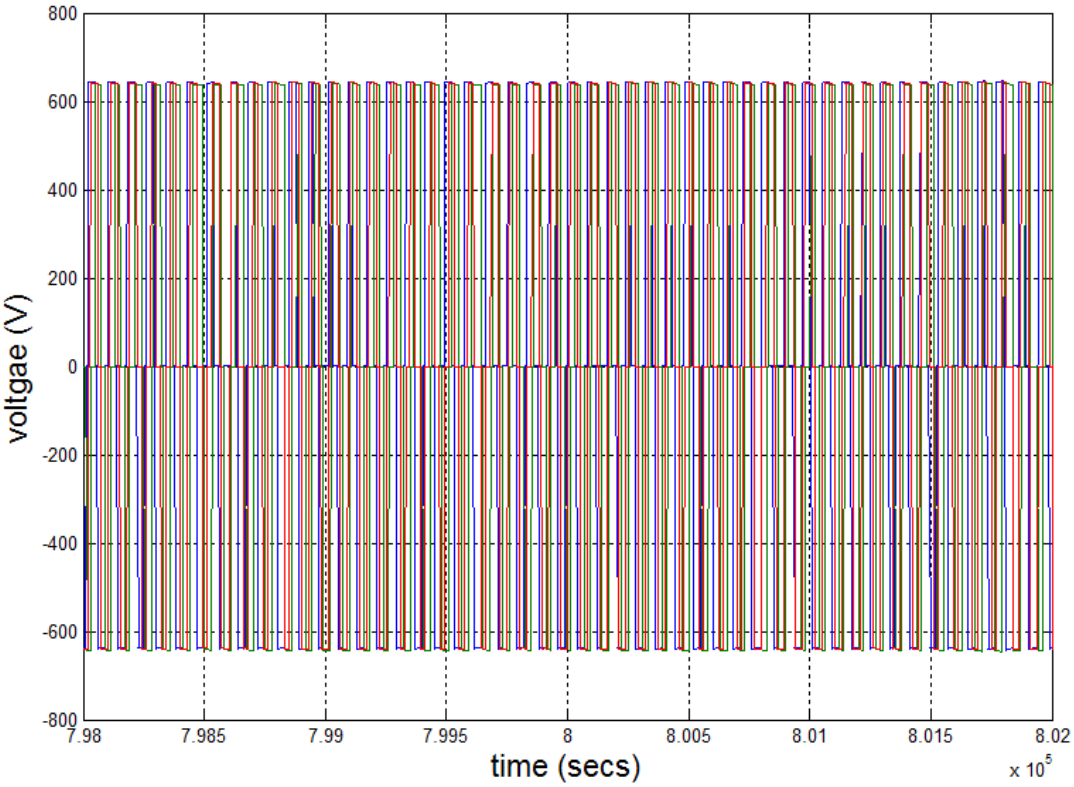

Figure 4.14. Grid side converter output voltage.

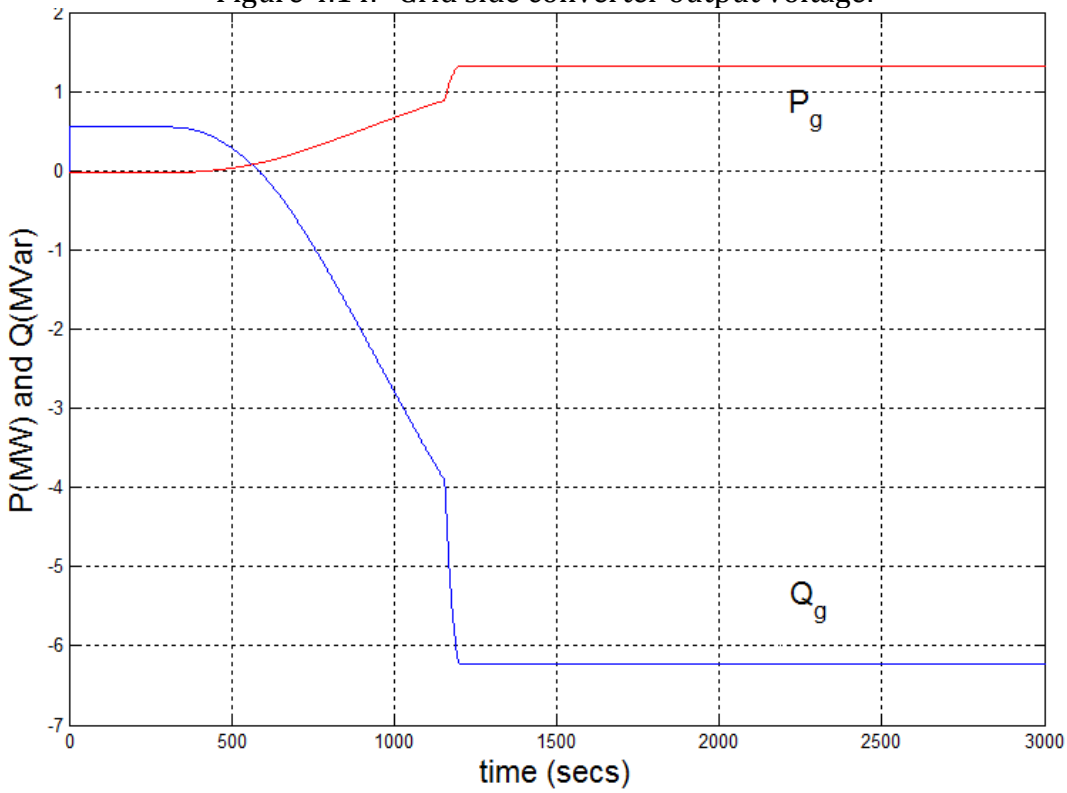

Figure 4.15. Power exchange with the grid.

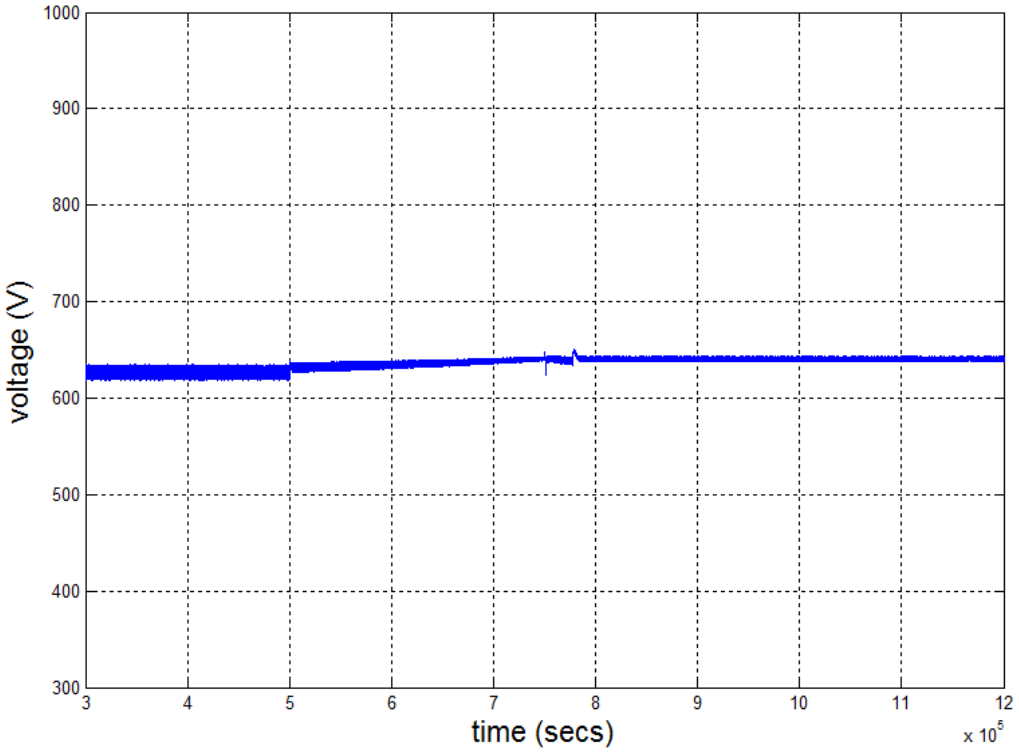

Figure 4.16. DC bus voltage.

4.4.3.1 Performance Analysis of the DFIG in $\alpha\beta$ Reference Frame

The DFIG reaches a steady state depending upon stator and rotor voltages injected into the machine as well as load torque. A case study is done to see how the machine behaves during hyper-synchronous operation.

Figure 4.17 shows the operation of the DFIG in the $\alpha\beta$ reference frame generator operation of a 2 MW DFIG, at hypersynchronous and subsynchronous speeds. The figures show (a) Stator voltages, (b) Stator voltages (zoomed), (c) Stator voltages $\alpha\beta$, (d) Rotor voltages, (e) Rotor voltages (zoom), (f) *abc* stator currents, (g) Rotor voltage $\alpha\beta$, (h) *abc* stator currents (zoom), (i) *abc* rotor currents, (j) *abc* rotor currents (zoom), (k) rotor flux, (l) speed , (m) torque.

First operating point:

$$T_{em} = -7400N.mQ_s = 1.1\ MVARQ_r = 80\ KVAR$$

$\Omega_m = 2100\frac{rev}{min} P_s = -1.2\ MW P_r = -0.5\ MW$

Seecond operating point:

$\Omega_m = 900 \frac{rev}{min} P_s = -1.2\ MW P_r = -0.45\ MW$

$T_{em} = -7400N.mQ_s = 1.1\ MVAR Q_r = -0.19\ KVAR$

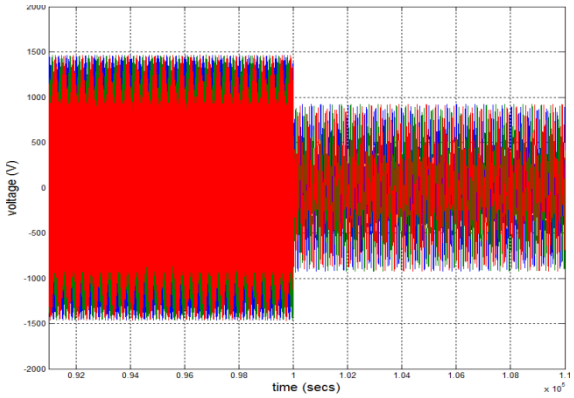

(a)

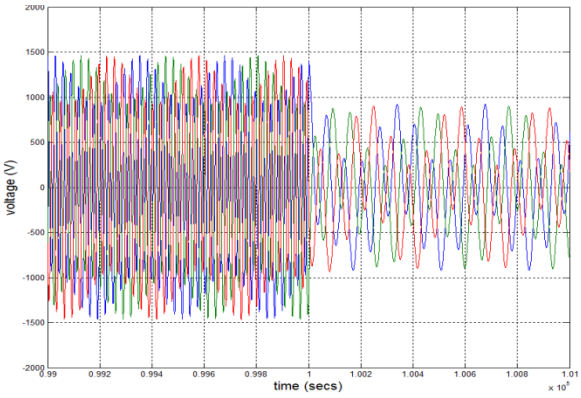

(b)

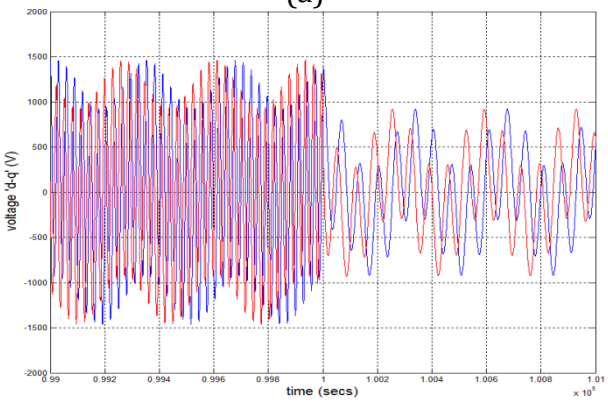

(c)

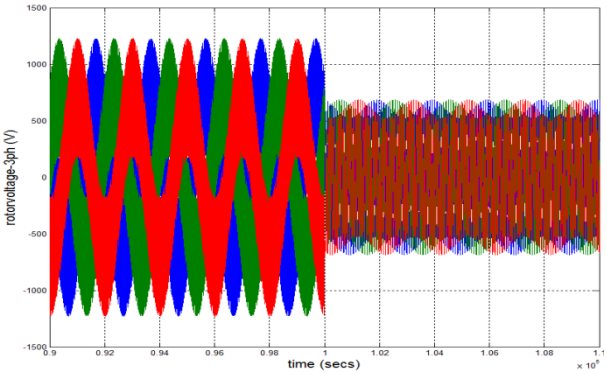

(d)

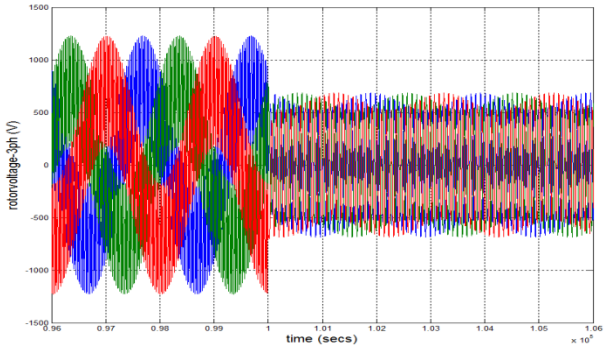

(e)

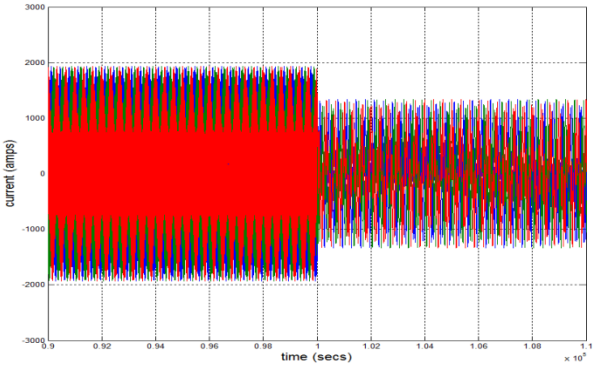

(f)

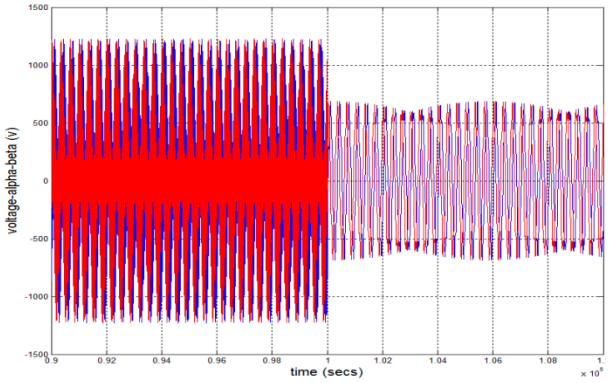
voltage-alpha-beta (v)
time (secs)

(g)

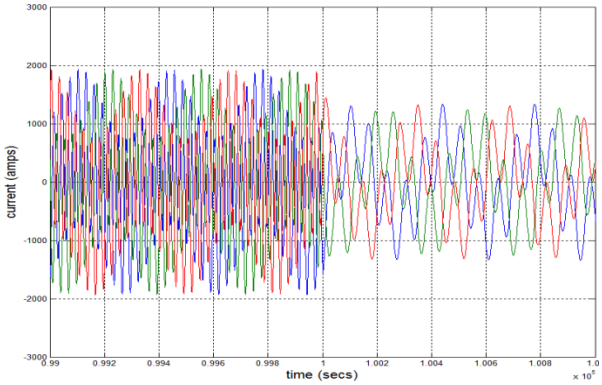
current (amps)
time (secs)

(h)

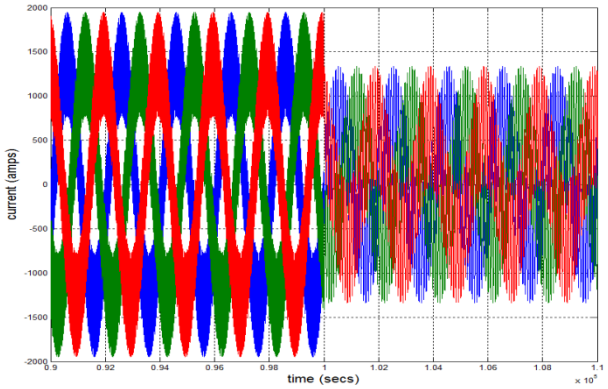
current (amps)
time (secs)

(i)

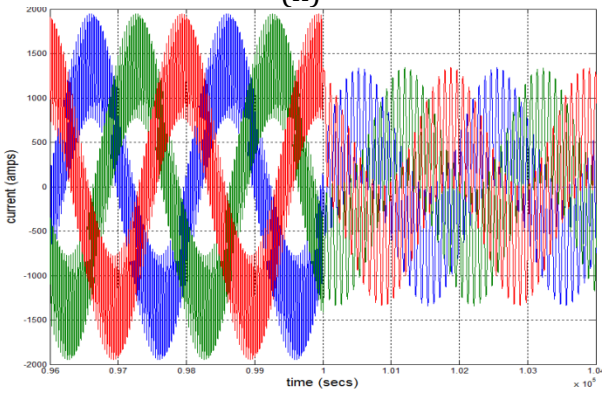
current (amps)
time (secs)

(j)

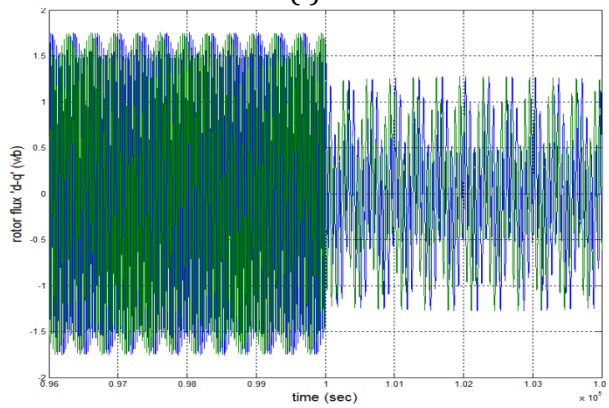
rotor flux 'd-q' (vb)
time (sec)

(k)

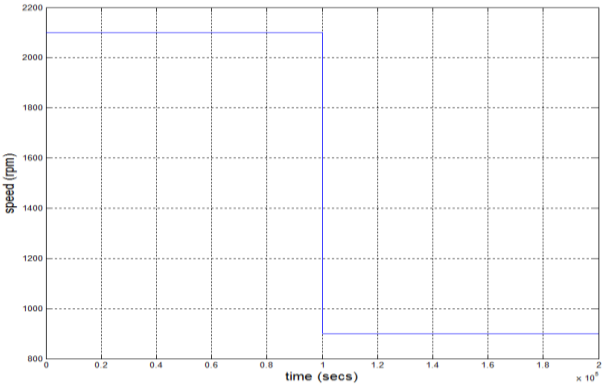
speed (rpm)
time (secs)

(l)

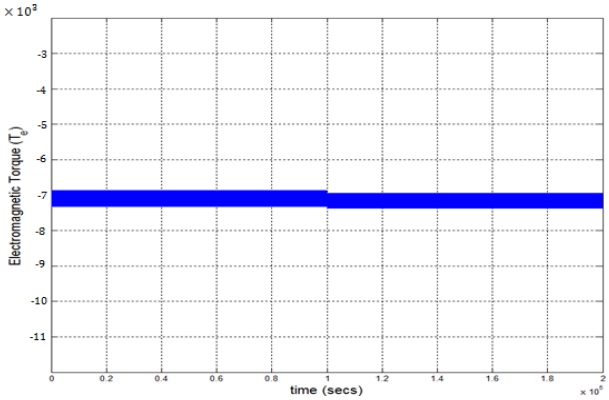

(m)

Figure 4.17. Generator operation of a 2 MW DFIG, at hypersynchronou speeds and subsynchronous: (a) Stator voltages, (b) Stator voltages (zoomed), (c) Stator voltages $\alpha\beta$, (d) Rotor voltages, (e) Rotor voltages (zoom), (f) *abc* stator currents, (g) Rotor voltage $\alpha\beta$, (h) *abc* stator currents (zoom), (i) *abc* rotor currents, (j) *abc* rotor currents (zoom), (k) rotor flux, (l) speed , (m) torque.

4.4.3.2 Performance Analysis of the DFIG in DQ $(rotor)$ Reference Frame

Figure 4.18 shows the operation of the DFIG in the DQ $(rotor)$ reference frame generator operation of a 2 MW DFIG, at hypersynchronous and subsynchronous speeds. The figures show (a) Rotor voltages (zoom) (b) Stator voltages, (c) rotor voltages , (d) Stator voltages DQ, (e) *abc* Rotor current (zoom) , (f) *abc* rotor currents, (g) *abc* stator currents, (f) Rotor flux, (i) Stator flux (j) torque

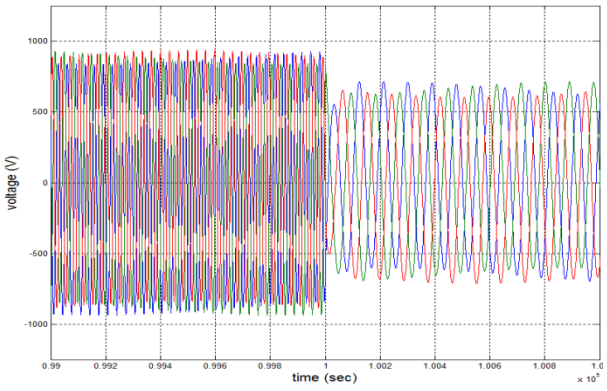

(a)

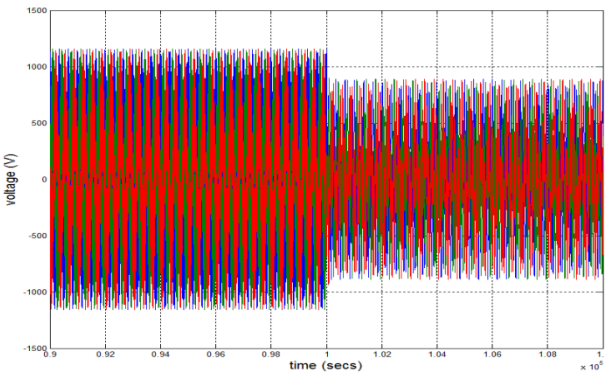

(b)

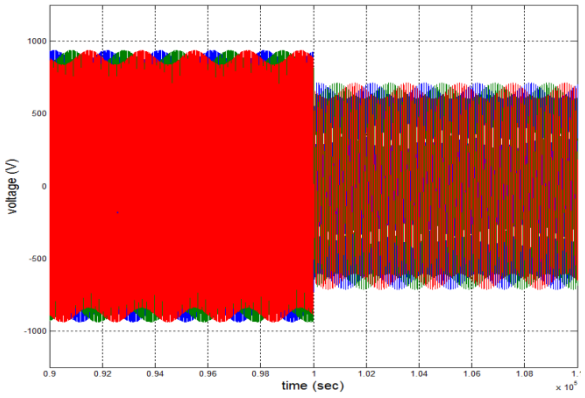
voltage (V)
time (sec)

(c)

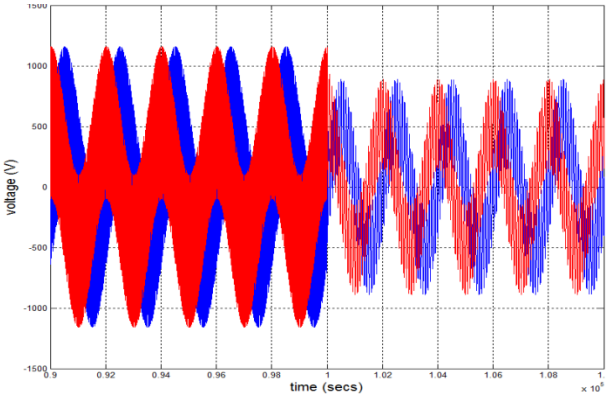
voltage (V)
time (secs)

(d)

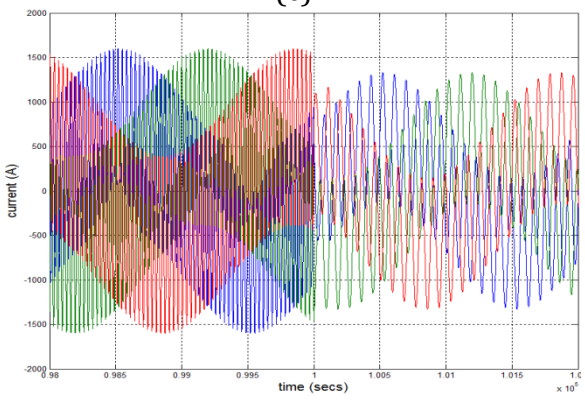
current (A)
time (secs)

(e)

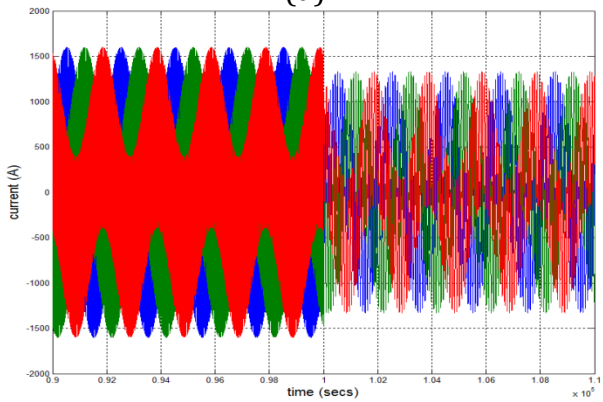
current (A)
time (secs)

(f)

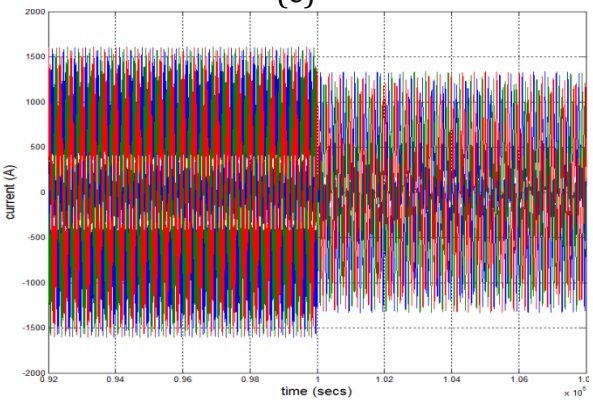
current (A)
time (secs)

(g)

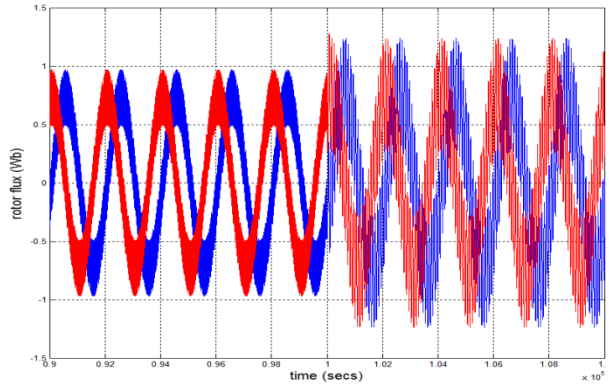
rotor flux (Wb)
time (secs)

(h)

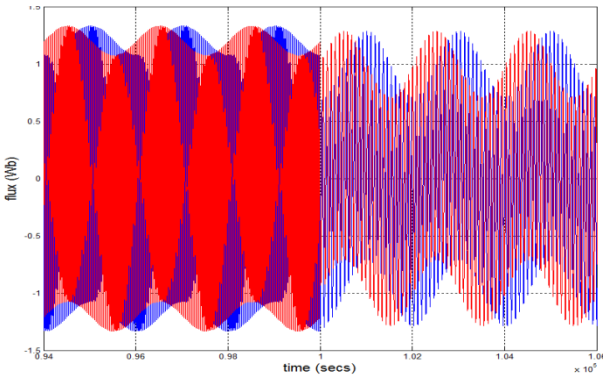
flux (Wb)
time (secs)

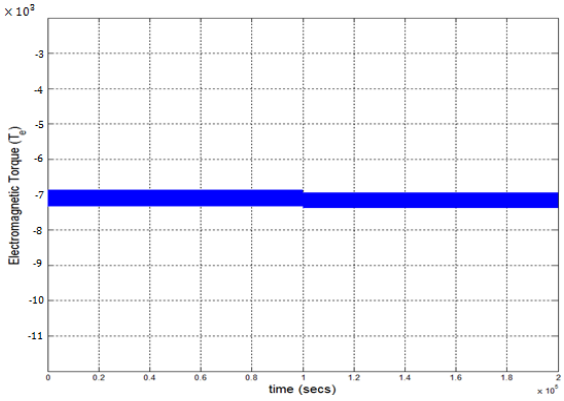
Electromagnetic Torque (Te)
time (secs)

(i) (j)

Figure 4.18. Generator operation of a 2 MW DFIG, at hypersynchronou speeds and subsynchronous: (a) Rotor voltages (zoom) (b) Stator voltages, (c) rotor voltages , (d) Stator voltages DQ, (e) *abc* Rotor current (zoom) , (f) *abc* rotor currents, (g) *abc* stator currents, (f) Rotor flux, (i) Stator flux (j) torque.

4.4.3.3 Performance Analysis of the DFIG in dq ($synchronous$) Reference Frame.

Figure 4.19 shows the operation of the DFIG in the DQ ($rotor$) reference frame generator operation of a 2 MW DFIG, at hypersynchronous and subsynchronous speeds. The figures show (a) *abc* stator voltages (zoom) (b) Stator flux, (c) *abc* Rotor voltages, (d) Rotor voltages DQ, (e) Stator Flux *dq* , (f) *abc* rotor currents, (g) *abc* stator currents, (f) Rotor flux, (i) Speed (j) torque

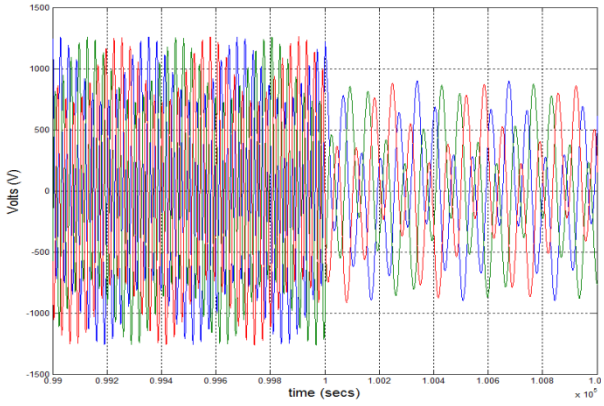

(a)

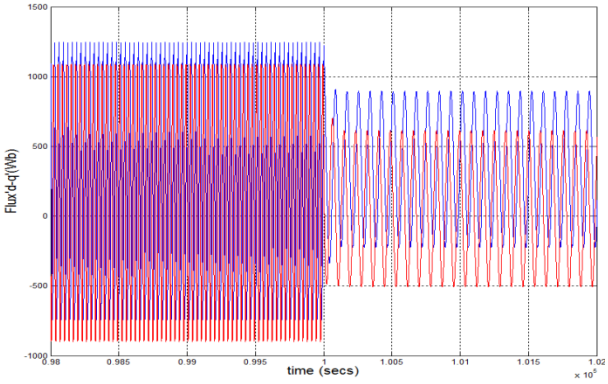

(b)

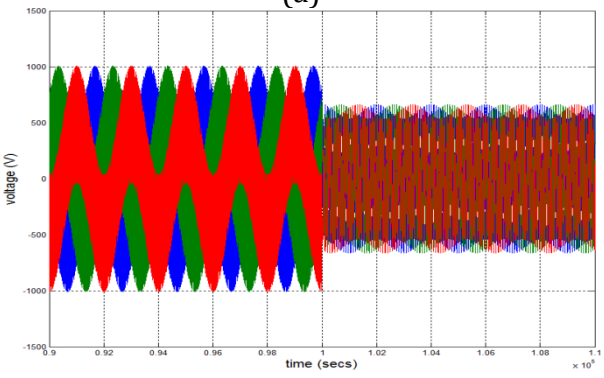

(c)

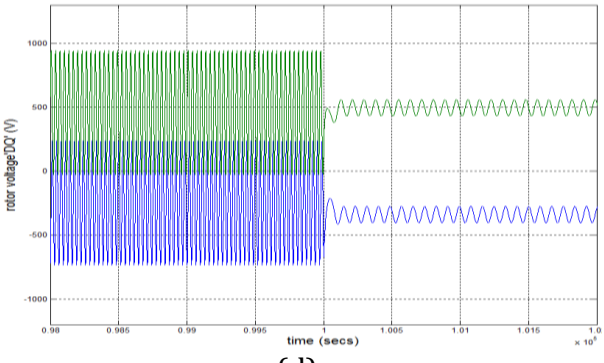

(d)

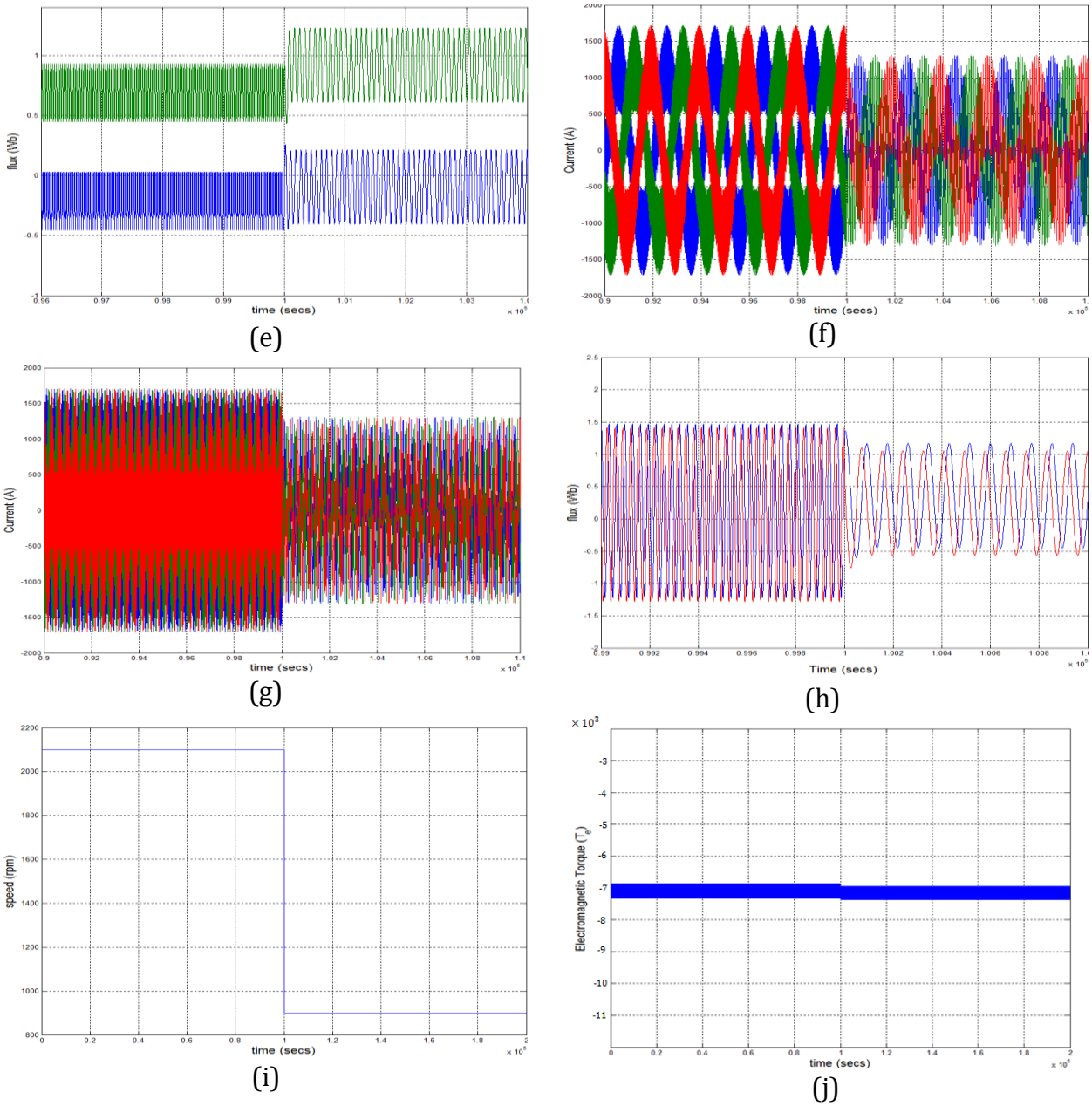

Figure 4.19. Generator operation of a 2 MW DFIG, at hypersynchronou speeds and subsynchronous: (a) *abc* stator voltages (zoom) (b) Stator flux, (c) *abc* Rotor voltages, (d) Rotor voltages DQ, (e) Stator Flux *dq* , (f) *abc* rotor currents, (g) *abc* stator currents, (f) Rotor flux, (i) Speed (j) torque.

4.4 Vector Control of DFIG based Wind Energy Systems

Control plays a very important role in drives and consequently in wind turbine technology. Control of the DFIG when generating energy in a wind turbine is unavoidable as we have

seen throughout the thesis. Control maintains magnitudes of torque, active and reactive power, and also magnitudes related to the grid side converter such as reactive and DC bus voltage. Also control, together with the modulator is in charge of generating the converter switch pulses.

Initially we are going to study the vector control technique (a.k.a field oriented) and later on in the chapter the direct control technique. We have already seen Vector Control in this chapter when we applied it to the control of the grid side converter.

4.4.1 Calculation of the Current References

The generic expressions can be simplified by using a reference frame aligned with the stator flux. Under this orientation, the relationship between the current and the fluxes will be

$$i_{ds}L_s + i_{dr}L_m = \psi_s \tag{4.49}$$

Using these equations, the relationship between the rotor and the stator current can is obtained

$$i_{qs}L_s + i_{qr}L_m = 0 \tag{4.50}$$

In steady state the stator flux is proportional to the grid voltage, $\hat{V}_g$

$$i_{ds} = \frac{\psi_s}{L_s} - \frac{L_m}{Ls}\, i_{dr} \tag{4.51}$$

Thus, when orienting the direct axis with the stator flux, the direct axis aligns with the qudrature axis. Therefore the stator active and reactive powers are

$$i_{qs} = -\frac{L_m}{Ls}\, i_{dr} \tag{4.52}$$

Combining these equations with the above equations, we get

$$v_{ds} = 0 \tag{4.53}$$

$$v_{qs} = \hat{V_g} \approx \omega_s \psi_s \tag{4.54}$$

Thus we can see that the under stator flux orientation the active and reactive powers are decoupled and can be controlled by the rotor currents[67].

$$P_s = -\frac{3}{2}\hat{V}_g \frac{L_m}{Ls}\, i_{qr} \tag{4.55}$$

$$Q_s = \frac{\frac{3}{2}\hat{V}_g\, \psi_s}{L_s} - \frac{\frac{3}{2}\hat{V}_g L_m}{L_s} i_{dr} = \frac{\frac{3}{2}\hat{V}_g{}^2}{\omega_s L_s} - \frac{\frac{3}{2}\hat{V}_g L_m}{L_s} \tag{4.56}$$

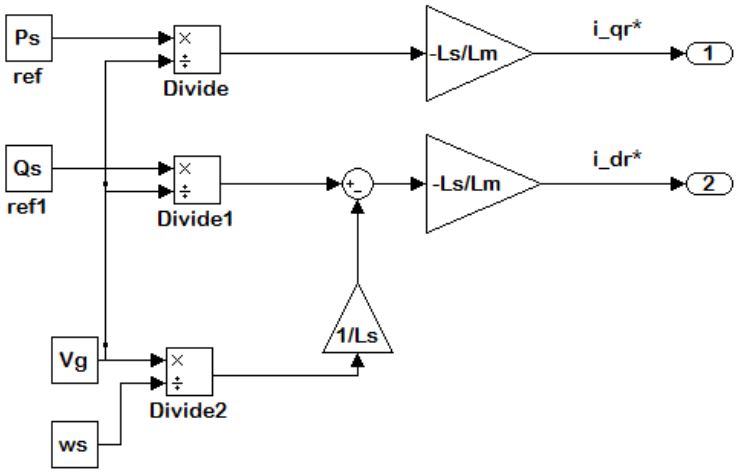

Figure 4.20. Simulink model for calculation of current references.

These relationships are not completely exact, since the effect of stator resistance has been neglected. To correct this error, two outer power loops are added, the first loop regulates the active power by means of the direct current i_{dr}, and the second loop regulates the reactive power by means of the direct current. The electromagnetic torque generated by the generator is

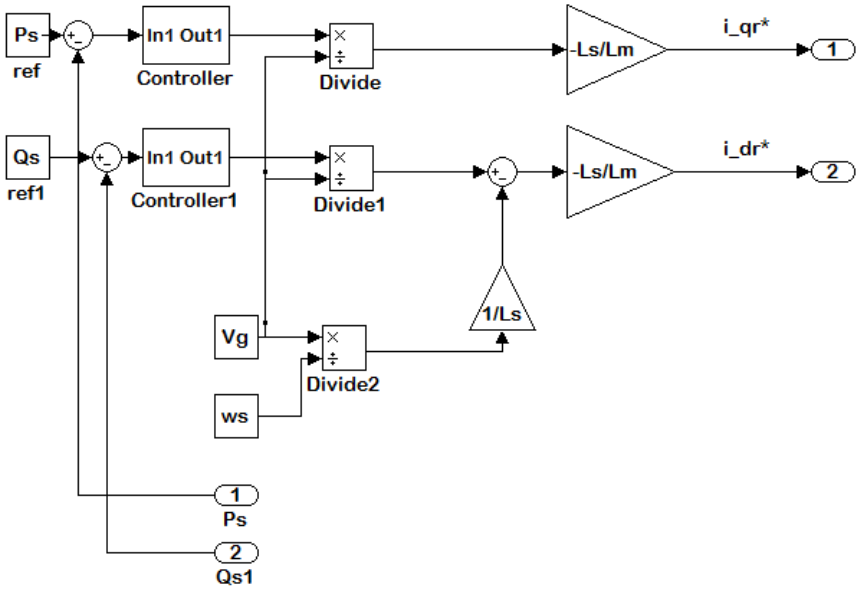

Figure 4.21. Reference calculation model including external power loops.

$$T_{em} = \frac{3}{2}\, p \frac{L_m}{L_s}\, (\psi_{qs} i_{dr} - \psi_{ds} i_{qr}) \tag{4.57}$$

Under stator flux orientation this expression is

$$T_{em} = \frac{3}{2}\, p \frac{L_m}{L_s}\, (-\psi_{ds} i_{qr}) \tag{4.58}$$

Substituting the value of stator flux

$$T_{em} = -\frac{3}{2}\, p\, \frac{L_m}{L_s}\, \frac{\widehat{V_g}^2}{\omega_s}\, i_{qs} \tag{4.59}$$

Thus we can see that the electromagnetic torque can be controlled by quadrature axis current[63, 68].

4.4.2 Current Control Loops

The rotor converter ensures that the actual currents must track these references. It is possible to implement these control loops in any reference frame but will use the same reference frame as the commands, that are, aligned with the stator flow d-axis also known as synchronous reference system. The rotor voltages of the three phases have to be

calculated by the rotor inverter from v_{dr} and v_{dq} by Parks inverse transform. The currents i_{dr} and i_{qr} are also calculated by the Park's transformation according to the three phase currents. θ_r must be known and to find θ_r , θ_m the angular position of the rotor has to be known.

There are a lot of controllers which can be used for the control loop but the most widely used current loop controller is the Proportional Integral (PI) controller. To calculate the PI regulator parameters we can use the dq model[60-62]. In the dq model, the voltage is aligned with the q axis, so its d component is zero. Also the d axis is aligned with the flux, so the flux along the q axis is null. The voltage in the rotor terminals is nothing but the voltage drop in the resistance R_r and the voltage induced by the flux rotor.

$$v_{dr} = R_r i_{dr} - \omega_r \psi_{qr} + \frac{d}{dt}\,\psi_{dr} \tag{4. 60}$$

$$v_{qr} = R_r i_{qr} - \omega_r \psi_{qr} + \frac{d}{dt}\,\psi_{qr} \tag{4. 61}$$

The relationship between this rotor flux and the rotor currents is

$$\psi_{dr} = \left(L_r - \frac{L_m^2}{L_s}\right) i_{dr} + \frac{L_m}{L_s}\psi_{ds} \tag{4. 62}$$

$$\psi_{qr} = \left(L_r - \frac{L_m^2}{L_s}\right) i_{qr} \tag{4. 63}$$

The proportionality ratio between these fluxes and the currents is referred to as the transitory inductance of the rotor, σL_r and is the result of adding in series the rotor leakage inductance with parallel magnetizing and the stator leakage inductance:

$$\left(L_r - \frac{L_m^2}{L_s}\right) = L_{\sigma r} + \frac{L_m}{L_{\sigma s}} = \sigma L_r \tag{4. 64}$$

From the above expressions, the relationship between the rotor voltages and the currents is obtained.

$$V_{dr} = R_r i_{dr} - \omega_r \sigma L_{r i_{qr}} + \sigma L_r \left(\frac{d i_{dr}}{dt}\right) + \frac{L_m}{L_s}\frac{d}{dt}\,\psi_{ds} \tag{4. 65}$$

$$V_{qr} = R_r i_{qr} - \omega_r \sigma L_{r i_{qr}} + \sigma L_r \left(\frac{d i_{qr}}{dt}\right) + \frac{L_m}{L_s} \frac{d}{dt} \psi_{ds} \quad (4.66)$$

During the regular operation, the grid voltage is constant and hence the derivative of the stator flux is zero and it disappears. From the control point of view the term $\omega_r \left(\frac{L_m}{L_s}\right) \psi_{ds}$ is a constantperturbation. Than can be easily compensated by the controller[63, 68].

4.4.3 Reference Frame Orientation

The basis of vector control is to refer the rotor currents in a synchronous reference frame, oriented so that its *d* axis is aligned with the stator flux. This is almost equivalent of aligning *q* axis with the stator voltage. So, there are two options to align the axis: to estimate the flux and align the *d* axis to it, or to align the *q* axis with the voltage and delay by 90deg the *d* axis[61].

4.4.4 Complete Control System

Classical Vector control includes the

- Generation of reference: reference current calculation from the desired stator active and reactive powers
- Current Control loops
- Reference Frame transformations

Figure 4.22 shows a schematic of the vector control systems

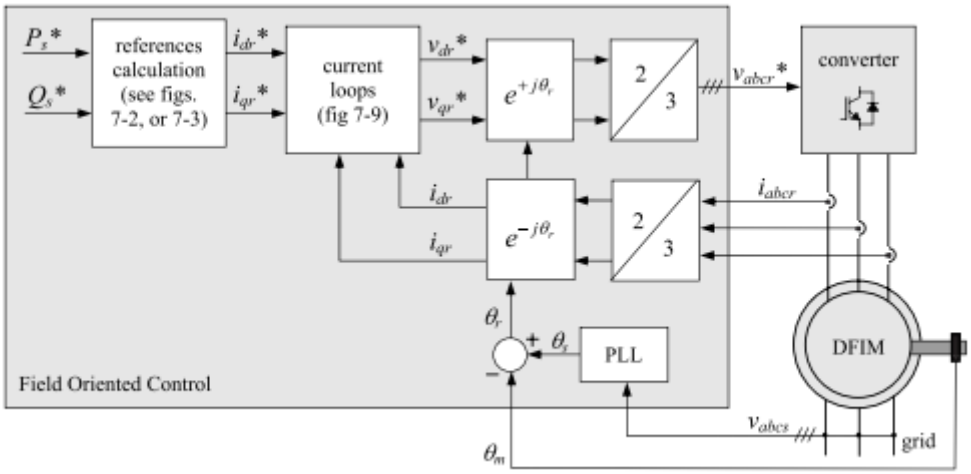

Figure 4.22. Schematic of the vector control system [61].

4.5 Direct Control of DFIG based Wind Energy Systems

This section discusses the equivalent exposition for DFIG based wind turbines: direct control techniques. Direct control techniques are an alternative solution to vector control for control principles and performance features. First principles of direct control techniques are presented; by analyzing (a) direct torque control (DTC) and (b) direct power control (DPC). Both controls share a common basic structure and philosophy but they are oriented to directly control different magnitudes of the machine. DTC seeks to control the torque and the rotor flux amplitude of the machine, while DPC controls the stator active and reactive powers.

4.5.1 DTC Control of the DFIG

This version of DTC is also called as “classic DTC”. It has the following general characteristics.

- Fast Dynamic Response
- On-line implementation simplicity
- Robustness against model uncertainties
- Reliability
- Good perturbation rejection

- Non-constant switching frequency behavior

Out of these only the non-constant switching frequency is its main drawback. These non-linear behaviors also need special attention and this behavior also affects other system variables such as torque, current and fluxes, leading in non-uniform ripples of these variables. The DTC is based on the direct control of electromagnetic torque and rotor flux amplitude of the machine. However, these particular characteristics of direct control techniques can be eliminated and are discussed in the Sections 4.5.1.2. [61]

The DTC is based on a direct control of control of two magnitudes of the DFIG, the electromagnetic torque and rotor flux amplitude of the machine. We will first review the background theory of DTC and then discuss control strategies later.

4.5.1.1 Basic Control Principle

The DTC is based on space vector representation of the achievable output of the two level VSC.

- There are two variables of the DFIG that are directly controlled: the torque and the rotor flux amplitude.
- The rotor flux and the stator flux rotate clockwise or anticlockwise to a distance noted by an angle δ.
- By controlling the distance between the space vectors it is possible to control the torque.
- Different voltage vectors need to be injected into the rotor of the machine in order to influence the rotor flux of the machine.
- DTC creates the pulses for the controlled semiconductors of the converter.

We know that torque can be expressed as

$$T_{em} = \frac{3}{2}\, p \frac{L_m}{\sigma L_r L_s} \left|\overrightarrow{\Psi_r}\right| \left|\overrightarrow{\Psi_s}\right| sin\delta \tag{4.67}$$

It is obvious from the relation that torque depends on the stator and rotor flux amplitudes and the angle between δ. Since the stator is directly connected to the grid the stator flux vector has constant amplitude and rotating speed (depending on the stator voltage

applied). Also, we can deduce that by controlling the rotor flux amplitude and the angle δ it is possible to control the torque magnitude. Hence we need to create a rotor flux space vector that rotates at the same angular speed as the stator flux to a distance δ to control the machine, since the torque is controlled.

We use the rotor voltage equation in the dq reference frame to create the desired rotor flux.

$$\overrightarrow{V_r^r} = R_r \overrightarrow{i_r^r} + \frac{d\overrightarrow{\Psi_r}}{dt} \tag{4. 68}$$

Neglecting the voltage drop in the rotor resistance gives

$$\overrightarrow{V_r^r} = \frac{d\overrightarrow{\Psi_r}}{dt} \tag{4. 69}$$

It is absolutely clear by this expression that by applying a necessary voltage to the rotor it is possible to directly influence the rotor flux. Considering constant rotor voltage injection during h, we find

$$\left|\overrightarrow{\Psi_r}\right|_{fin} = \left|\overrightarrow{\Psi_r}\right|_{ini} + \overrightarrow{V_r^r}\, h \tag{4. 70}$$

Now we will see, by injecting different rotor voltages, rotor flux amplitude is controlled.

Assuming that the rotor flux vector and the rotor flux vector are rotating in synchronous speeds, there are eight different voltage possibilities, when the rotor of the machine is fed by a two-level voltage source converter. Out of the eight only some are permitted depending on where the rotor flux space vector is located. Fig 4-23 shows that when the rotors flux space vector is located in sector 1 the four possible voltage vector injections are V2, V3, V5, V6. For example we inject voltage vector V3 and assuming that the stator flux vector rotates very slow, so that during the time h time interval the stator flux has not moved, the following are consequences –

- The rotor flux amplitude has been reduced
- The angle δ has been reduced
- Both magnitude reductions yield a reduction in the torque

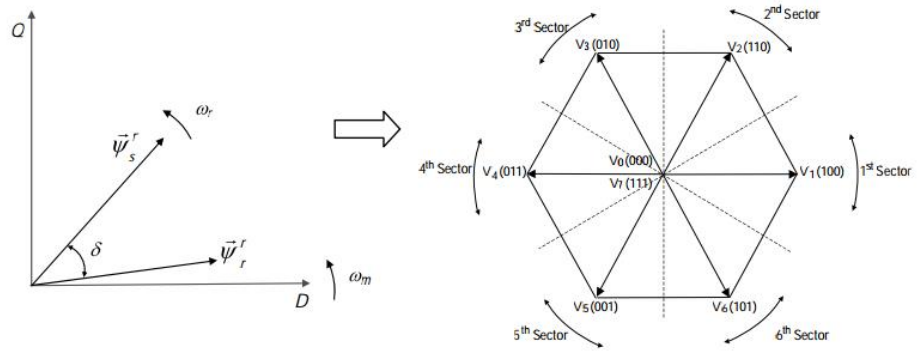

Figure 4.23. Space vector representation of stator and rotor flux
(a) Initial stator and rotor flux locations, (b) Hexagon values of the two-level converter..

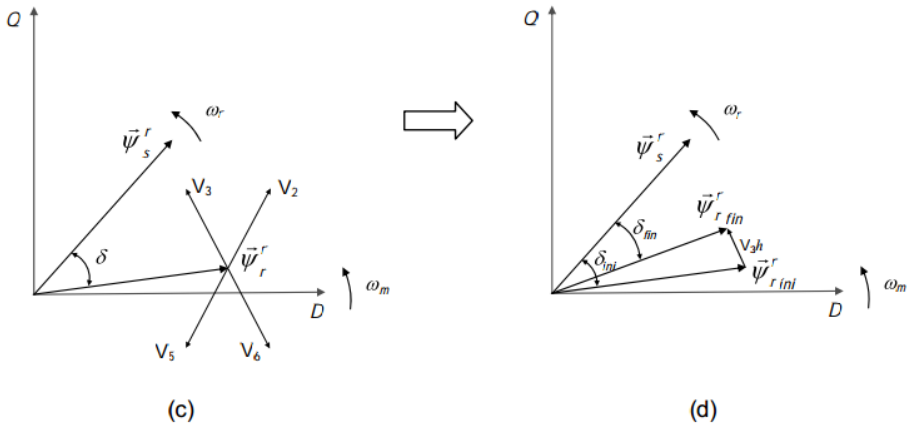

Figure 4.24. Space vector representation of stator and rotor flux
(c) four possible voltage vectors to modify the rotor flux (d) rotor flux variation with V_3[61].

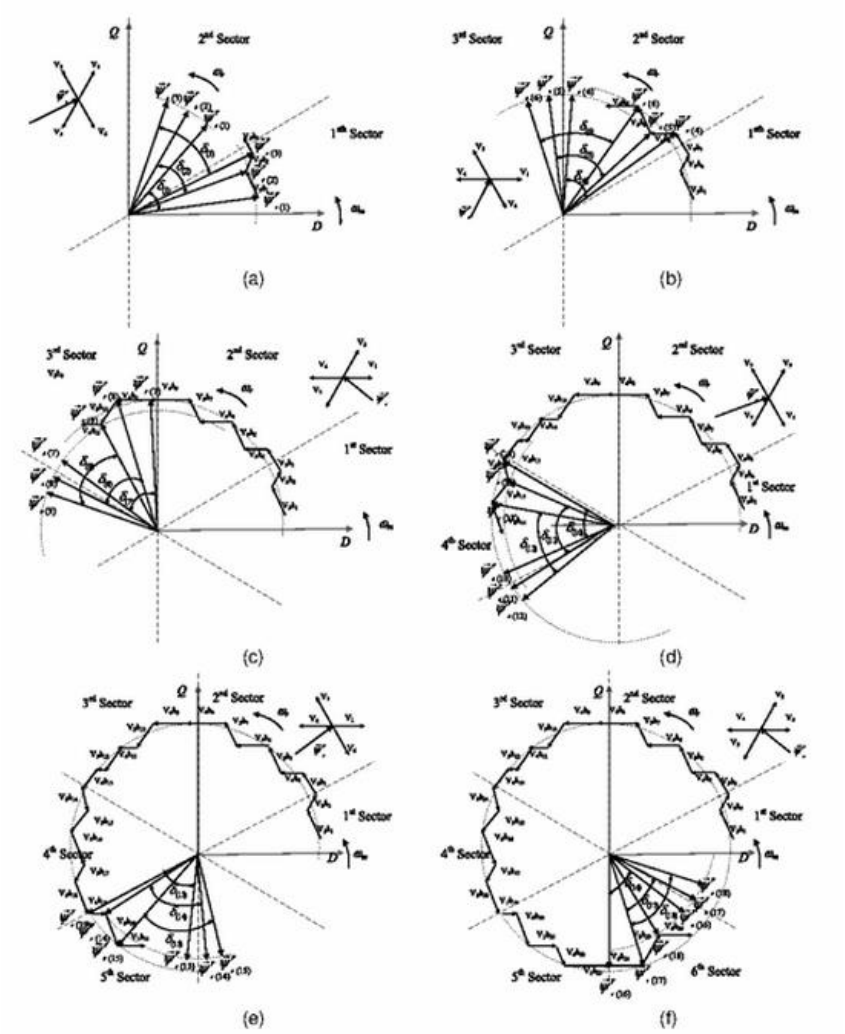

Figure 4.25. Trajectory representation of stator and rotor flux with different voltage vector injections [61].

Repeating a large sequence of different voltage injections, with different application time $h1, h2$ etc. and now considering that the stator flux is rotating, we see that the rotor flux a circular trajectory behind the stator flux.

From the Figure 4.25, we can see that by injecting different voltage vectors, the rotor flux describes a nearly circular trajectory and smaller the injection time , "h" , the more circular trajectory appears.

4.5.1.2 Control Block Diagram

The control block diagram is as shown in Figure 4-26

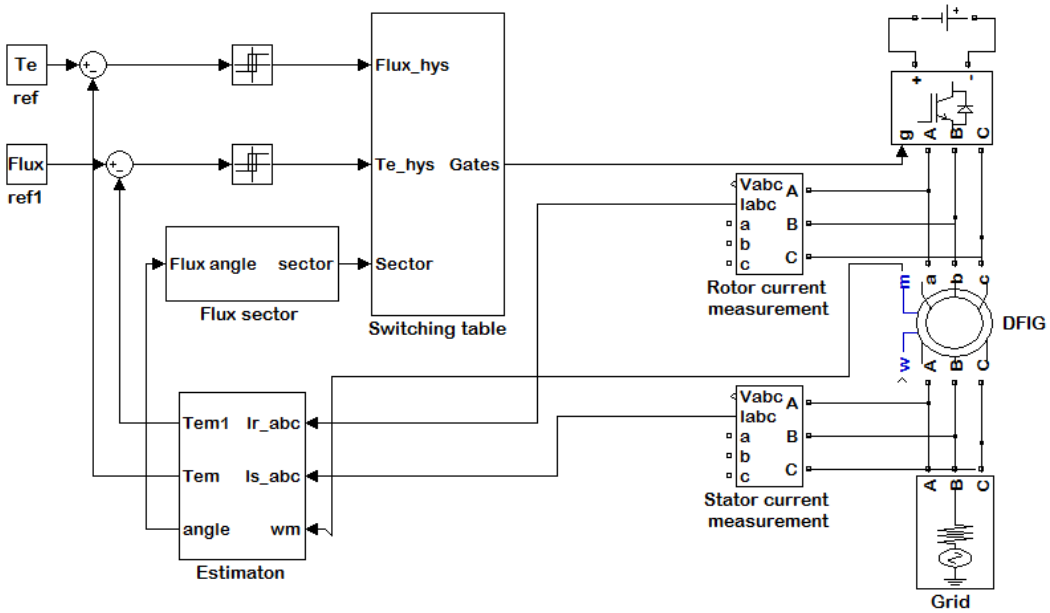

Figure 4.26. Direct torque control (DTC) block diagram.

Since the directly controlled variables are the electromagnetic torque and rotor flux vector, the control strategy calculates the pulses (S_a, S_b, S_c) for the controlled semiconductors of the two level VSC.

The control strategy is divided into 5 different blocks

- Estimation block
- Torque ON-OFF controllers
- Flux ON-OFF controller
- Voltage vector selection
- Pulse generation block

Estimation Block

As mentioned before the directly controlled vectors are torque and rotor flux and these variables cannot be easily measured and must be estimated from the measurements of the machine. Figure 4-27 for estimation is shown. From the rotor and the stator current measurements together with the angular position θ_m, the stator and rotor flux $\alpha\beta$ components are estimated. After calculating the the rotor flux $\alpha\beta$ components are

estimated, it is necessary to calculate the position where the rotor flux lies, that is the rotor flux angle, with this rotor flux angle we can derive the sector using the Table 7.

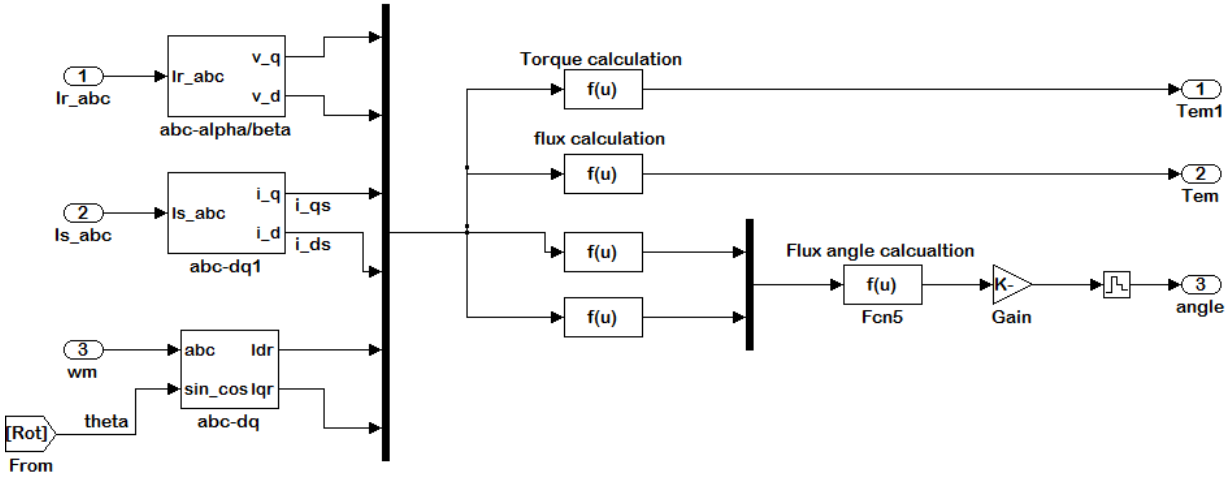

Figure 4.27. Estimation block diagram.

Table 6. Sector selection according to rotor flux angle

Rotor Flux angle	**Sector**
$(270^o, 30^o)$	1
$(30^o, 90^o)$	2
$(90^o, 150^o)$	3
$(150^o, 210^o)$	4
$(210^o, 270^o)$	5
$(270^o, 30^o)$	6

Voltage Vector Selection and ON-OFF Hysteresis Controllers

The DTC selects the required rotor voltage vector directly from the rotor flux and electromagnetic torque and rotor flux errors using hysteresis ON-OFF controllers. The flux controller is based on a two-level hysteresis comparator with H_F hysteresis band, while the torque controller uses a three-level hysteresis controller with H_T band. The figures are as follows. Depending on the value of the torque error, the output uT_{em} can take value -1, 0, or 1. Also depending on the value of the flux error, the output $u|\vec{\psi}\_r|$ can take value of -1 or 1 (not 0). Once the values of uT_{em} and $u|\vec{\psi}\_r|$ are defined by means of the ON-OFF

controllers together with the information of the rotor flux vector position it is possible to select the rotor voltage vector using the table.

Table 7. Voltage vector selection according to comparator output

		uT_{em}		
		1	**0**	**-1**
$u\|\vec{\psi}_r\|$	**1**	$V_{(k-1)}$	V_0, V_7	$V_{(k+1)}$
	- 1	$V_{(k-2)}$	V_0, V_7	$V_{(k+2)}$

For example. if the rotor flux vector is located in sector 5, $uT_{em} = 1$ and $u|\vec{\psi}\_r|$ = -1 the selected voltage vector is V_3. The zero vectors produces nearly zero rotor flux variation and very small positive or a negative torque variation.

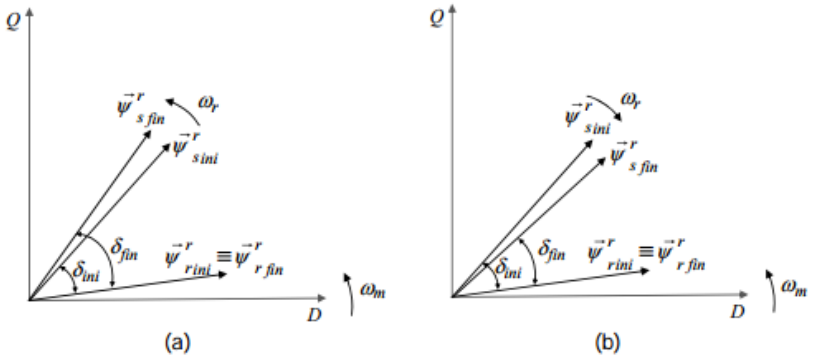

Figure 4.28. Change in value of T_{em} due to zero vector injection.

From Figure 4.28 we see that since the zero vector leaves the rotor flux vector unaltered, the stator flux movement produces an angle δ increase or decrease provoking an increase or decrease in the torque. Zero vector is generally not used to control the torque or the flux but it is used to reduce the torque and flux ripples at steady state operation. It is obvious that it is advantageous if the torque and flux ripples are minimized.

Pulse Generation

Once the vector is that will correct the torque and flux error is selected, the next task is to create or generate the pulses for the controlled semiconductors of the two-level converter. We use the following Table 8 to determine the voltage vector injected.

Table 8. Switching pattern according to the voltage vector

Vector	S_a	S_a	S_a
V_0	0	0	0
V_1	1	0	0
V_2	1	1	0
V_3	0	1	0
V_4	0	1	1
V_5	0	0	1
V_6	1	0	1
V_7	1	1	1

Torque and Flux Waveforms

In Figure 4.29 we see the steady state behavior of the directly controlled variables is shown under DTC. The figure shows the torque and rotor flux amplitude waveforms when the machine operates at hypersynchronous speed. If a reduction of torque and flux ripples is required to improve accuracy, we need to set the bandwidths of both the controllers (H_T and H_F). For every active vector we can see that the rotor flux changes but for the zero vector remains the same.

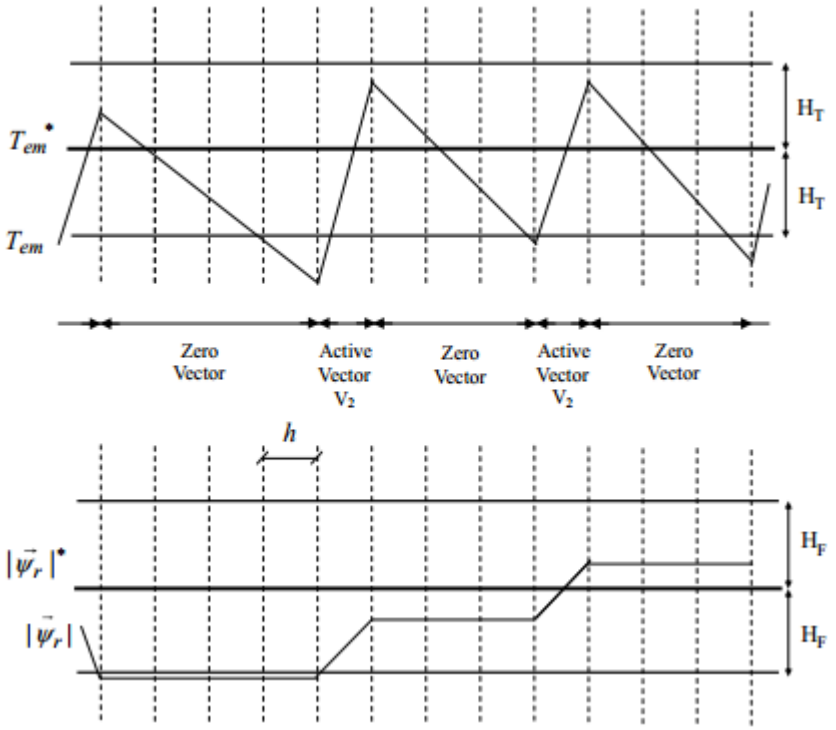

Figure 4.29. Steady state torque and flux waveforms [61].

CASE STUDY

This case study shows a 2 MW DFIG, controlled by the DTC technique described in this section. The hysteresis band of the ON-OFF controllers is set to 5% of the rate torque while the flux hysteresis is set to 1.5% of the rated flux. The machine is operating at 1125 rev/min. The DC bus voltage is controlled to 1000 V by the grid side converter. At the beginning of the experiment the machine operates at nominal torque and in the middle of the experiment of the torque is revers to positive so the machine operates as generator. Hence in this experiment we can observe both the steady state and the transient performances with the DTC. The following Figures 4.30-4.36 display the characteristic variables of the machine. We can observe that, when the DFIG is directly connected to the grid through the stator and when the torque is reversed from negative (generating) to positive (motor), a very quick transient response is seen. The torque reaches to a new reference value without a further overshoot than that defined by the torque hysteresis

comparator. Also the flux is also not affected by the transient and in the Figure 4.33 sector we can see that where the rotors flux vector is present.

Also shown in the Figure 4.30 to Figure 4.36 are the stator and rotor current behaviors demonstrating that despite a sever change of torque, the currents do not overshoot but we can see a dip in the rotor currents. The ripple present in the currents at steady state is due to ripple in the torque and the flux.

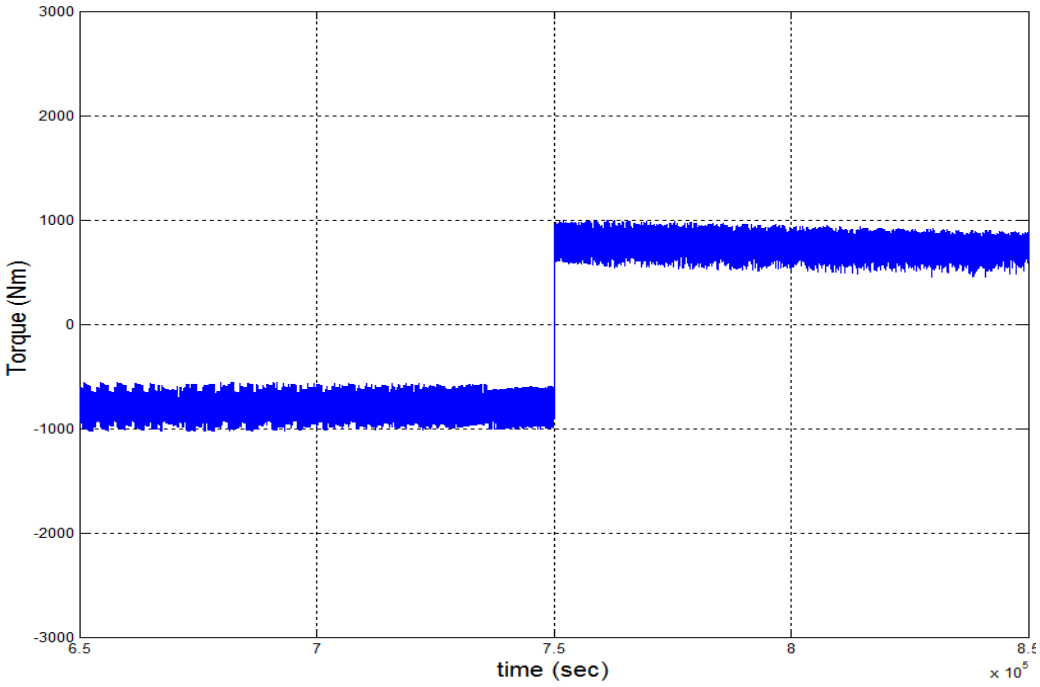

Figure 4.30. Torque amplitude.

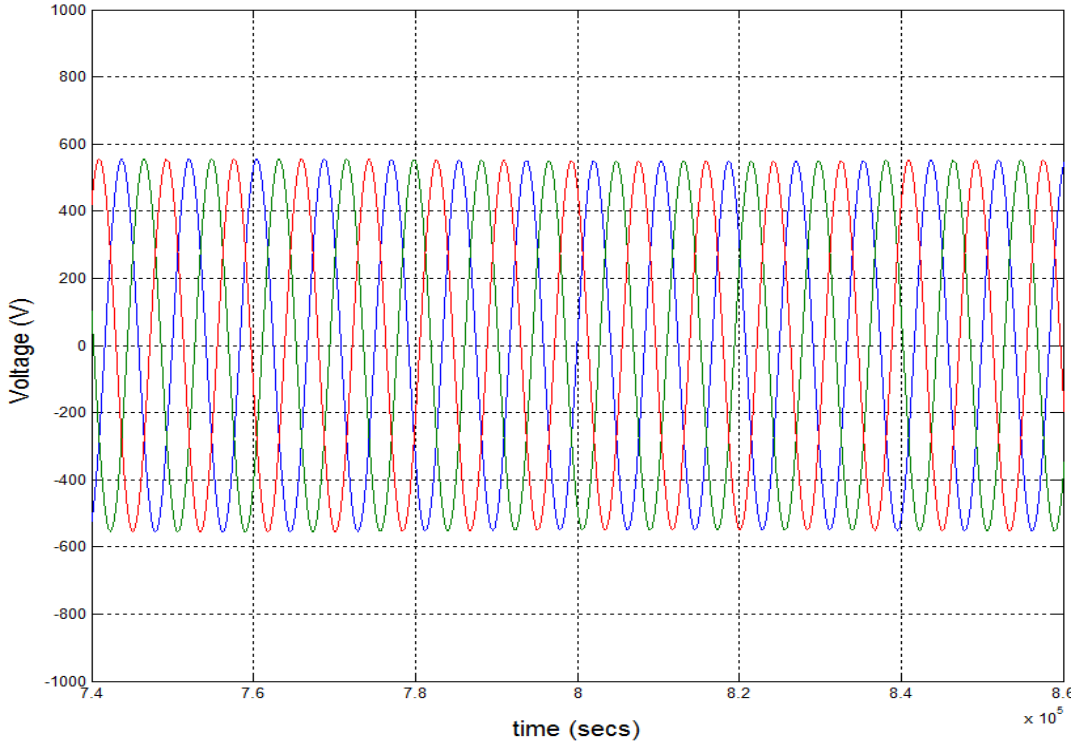

Figure 4.31. *abc* stator voltages.

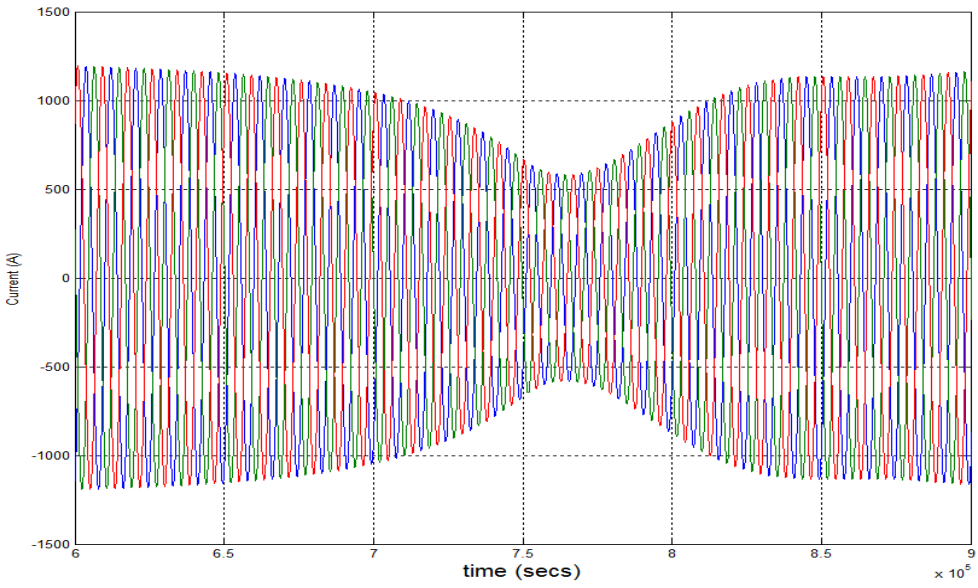

Figure 4.32. *abc* stator currents.

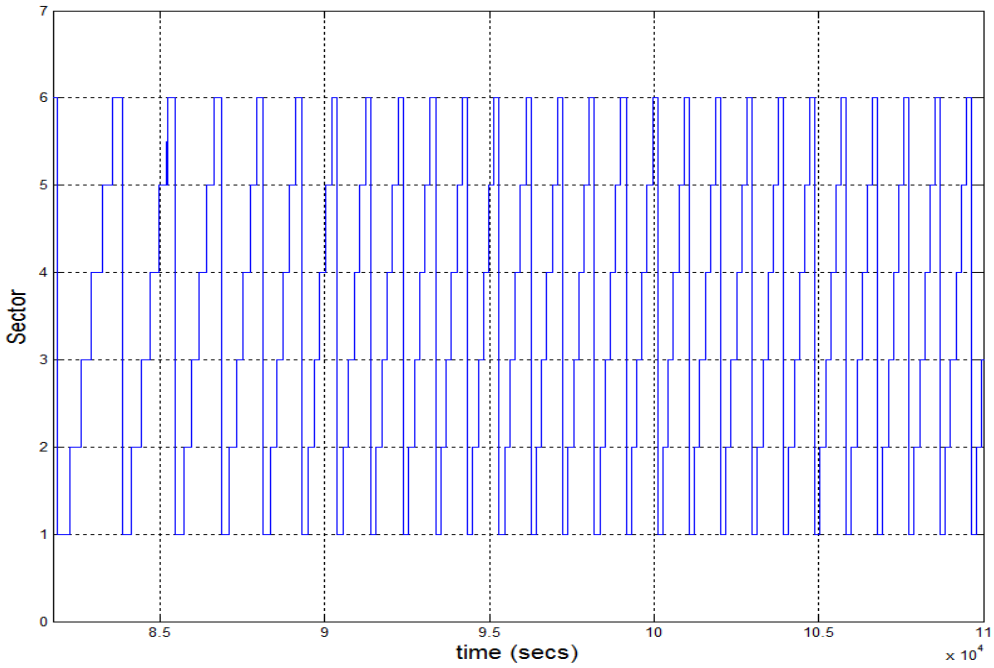

Figure 4.33. Sector.

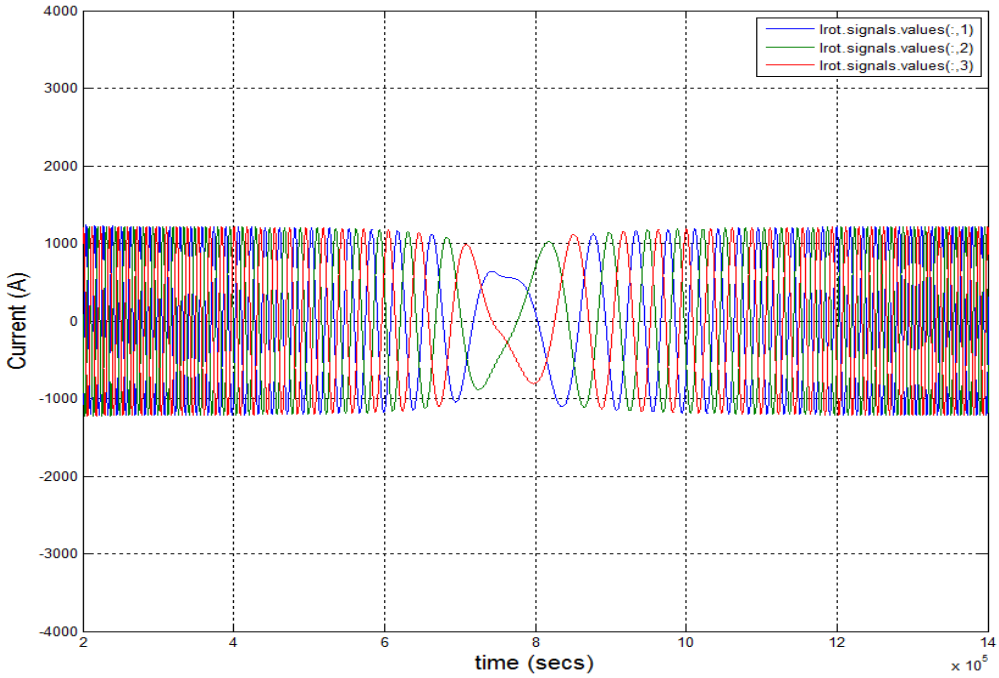

Figure 4.34. *abc* rotor currents.

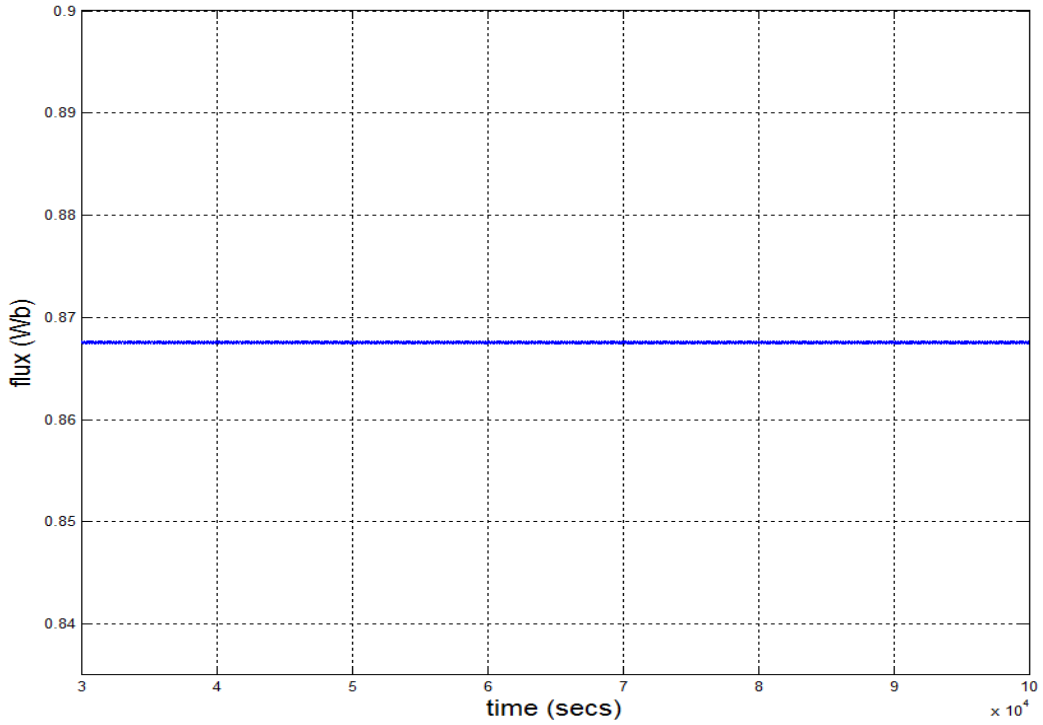

Figure 4.35. Rotor flux amplitude.

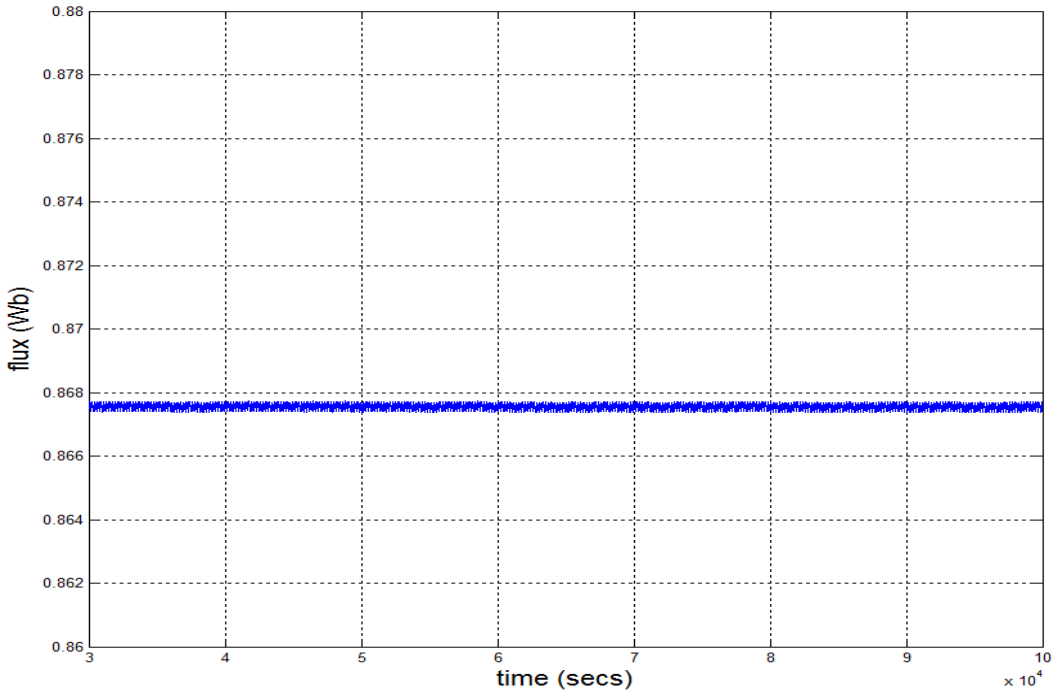

Figure 4.36. Rotor flux amplitude (zoom).

4.5.2 Direct Power Control of DFIG

Direct power control of is based on the same principles as the direct torque control technique only difference is that the directly controlled variables here are stator active and reactive power instead of electromagnetic torque and rotor flux.

4.5.3 Basic Control Principle

As mentioned before the, the DPC technique is based on directly control of the stator active and reactive power of the DFIG. We know that

$$P_s = \frac{3}{2}\mathrm{Re}\{\overrightarrow{v_s} * \overrightarrow{\imath_s}\} \tag{4. 71}$$

$$Q_s = \frac{3}{2}\mathrm{Im}\{\overrightarrow{v_s} * \overrightarrow{\imath_s}\} \tag{4. 72}$$

As done in DTC, by injecting directly rotor voltage vectors, the stator active and reactive powers are controlled, achieved by DPC with the necessary creation of a rotatory rotor flux space vector. From the equations (4. 73) and (4. 74) it is impossible to know how injection of different voltage vectors can influence the creation of $P_s$and Q_s.

But we know that ,

$$P_s = \frac{3}{2}\frac{L_m}{\sigma L_r L_s}\,\omega_s\left|\overrightarrow{\Psi_r}\right|\left|\overrightarrow{\Psi_s}\right| sin\delta \tag{4. 75}$$

$$Q_s = \frac{3}{2}\frac{1}{\sigma L_s}\,\omega_s\left|\overrightarrow{\Psi_s}\right|\left[\frac{L_m}{L_r}\left|\overrightarrow{\Psi_s}\right| - \left|\overrightarrow{\Psi_r}\right| cos\delta\right] \tag{4. 76}$$

where δ is the phase shift between the rotor flux space vectors. We can show from the last two expressions that

- The stator active power depend upon stator and rotor flux vectors
- The stator active and reactive power can be controlled by modifying $\boldsymbol{\delta}$and their amplitudes

Similar to the basic control principle of DTC, since it is possible to know how the injected rotor voltage vector influence the rotor flux and its relative distance to the stator flux, it is possible to know their influence on the stator active and reactive power as well. More specifically by checking the terms $|\overrightarrow{\Psi_r}|sin\delta$ and $|\overrightarrow{\Psi_r}|cos\delta$, it is possible to modify P_s and Q_s. Figure 4.37 illustrates the space vector representation of stator and rotor fluxes.

Since a two level converter feeds the rotor of the DFIG there are several rotor voltage injection possibilities as shown in figure (a) and (b). Similar to the DTC scheme if voltage vector V_3 is applied during a time interval h the rotor flux vector moves from its initial position to final position (Assuming that for the time interval h that the stator flux vector position is unaltered). Fig C illustrates the rotor flux space vector movement. Fig D illustrates the changes in the $|\overrightarrow{\Psi_r}|sin\delta$ term and changes in the $|\overrightarrow{\Psi_r}|cos\delta$ term due to voltage vector V_3 injection.

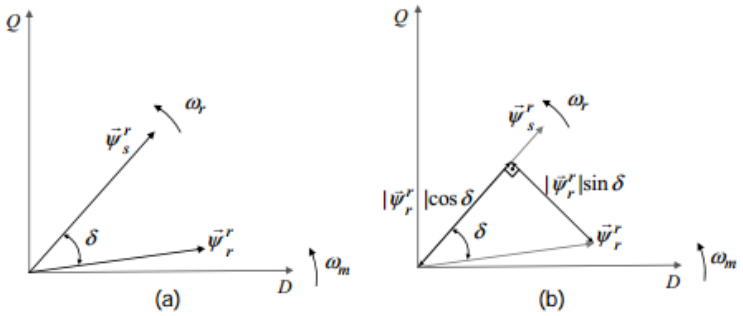

Figure 4.37. Space vector representation of stator and rotor fluxes.

Observing Figure 4.37 we see that the term $|\overrightarrow{\Psi_r}|sin\delta$ has slightly decreased and the term $|\overrightarrow{\Psi_r}|cos\delta$ has slightly increased and hence due to this

$$V_3 \Rightarrow \begin{cases} |\overrightarrow{\Psi_r}|cos\delta \uparrow \\ |\overrightarrow{\Psi_r}|sin\delta \downarrow \end{cases} \quad (4.77)$$

Similar to the DTC philosophy, repeating a large sequence of different voltage injections (with different time intervals (h_1, h_2etc.) and now considering that the stator flux is rotating, the rotor flux follows a circular trajectory behind the stator flux as shown in the Figure 4.38.

From a different perspective, it can be said that although the direct power control technique does not impose direct rotor flux control, indirectly by controlling the stator active and reactive power, it imposes amplitude for the rotor flux space vector and its rotation to a distance δ from the stator flux space vector.

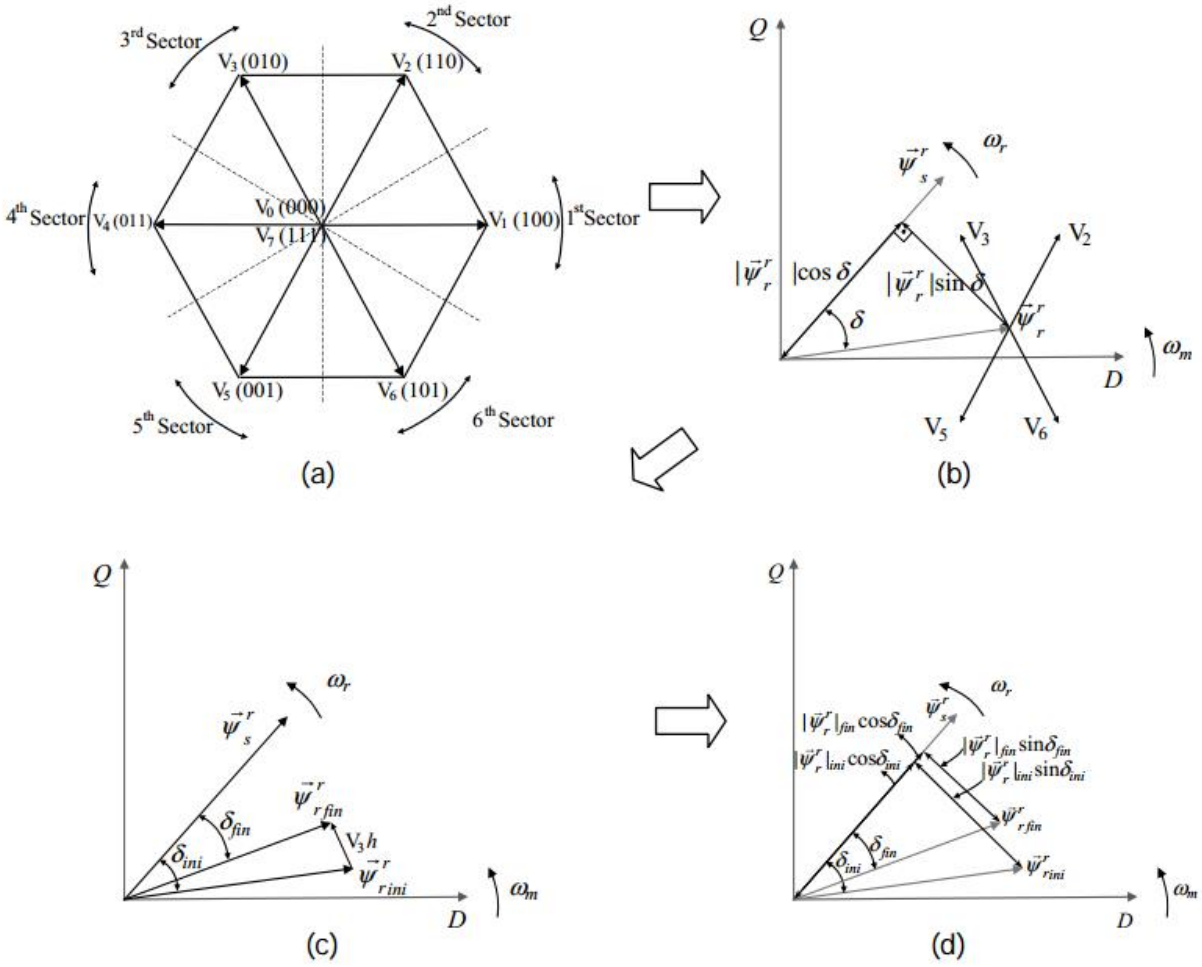

Figure 4.38. Space vector representation of stator and rotor fluxes (a) hexagon voltages of two-level VSC, (b) four possible voltage vectors to modify rotor flux location, (c) rotor flux variation with V_3 injection, (d) Term variations [61].

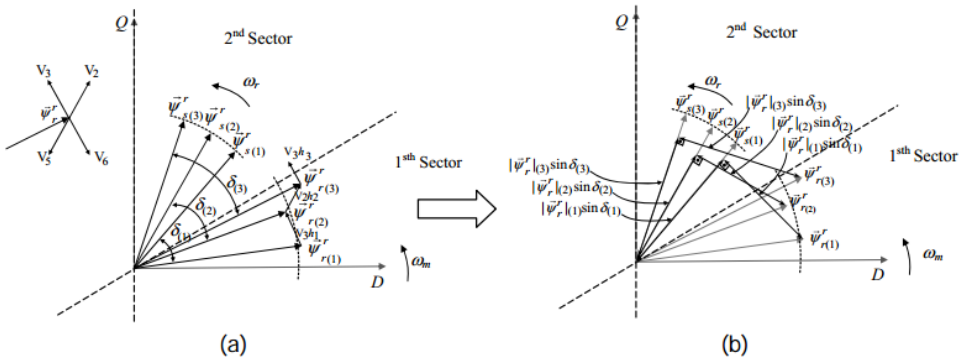

Figure 4.39. Trajectory representation of stator fluxes with different voltage vector [61].

4.5.4 Control Block diagram

The control block diagram of the direct power control (DPC) strategy is shown the Figure 4.40 and we can see that if follows an exact same philosophy of the DTC. The directly controlled variables are the stator active and reactive powers. From the P_s and$Q_s$references, the control strategy calculates the pulses (S_a, S_b, S_c) for the controlled semiconductors of the two-level VSC.

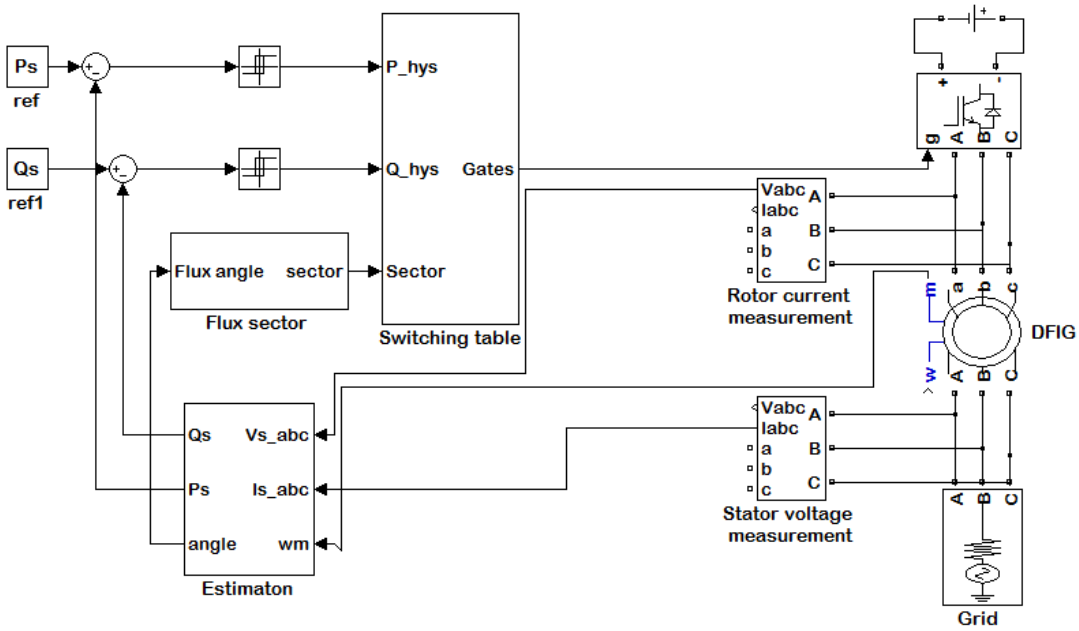

Figure 4.40. Direct power control (DPC) block diagram.

Similar to the DPC scheme the control strategy is divided into 5 different blocks

- Estimation block
- Torque ON-OFF controllers
- Flux ON-OFF controller
- Voltage vector selection
- Pulse generation block

Estimation Block

Since the directly controlled variables P_s and Q_s can be directly calculated from the measured stator voltage and currents the estimation block, shown in Figure 4.41 is slightly different from the DTC.

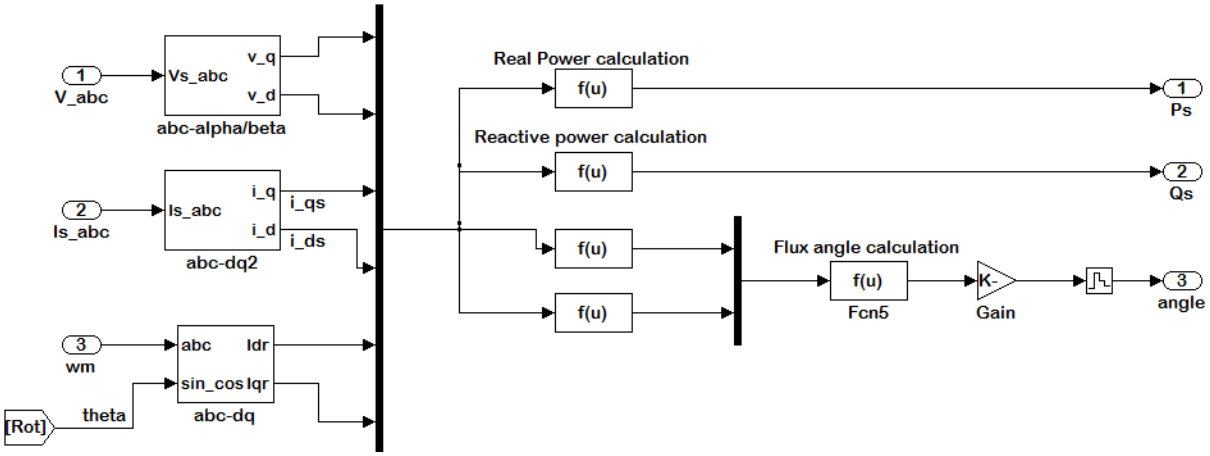

Figure 4.41. Estimation block diagram.

The rotor and the stator current measurement together with the rotor angular measurement θ_m, the rotor flux $\alpha\beta$ components are calculated for sector calculation. On the other hand the measurements of stator voltages and currents, the actual values of P_s and Q_s.

Voltage Vector Selection and ON-OFF Hysteresis Controllers

The DPC technique also selects the required voltage vector directly from P_s and Q_s errors, using hysteresis ON-OFF controllers. It chooses the needed voltage vector to correct the errors in the controlled variables. The ON-OFF controller structure is equivalent to DTC. The Q_s controller is based on a two-level hysteresis comparator with H_Q hysteresis band,

while the P_s controller uses a three-level hysteresis comparator $H_P$hysteresis band. The schematics are shown in the Figure 4.42.

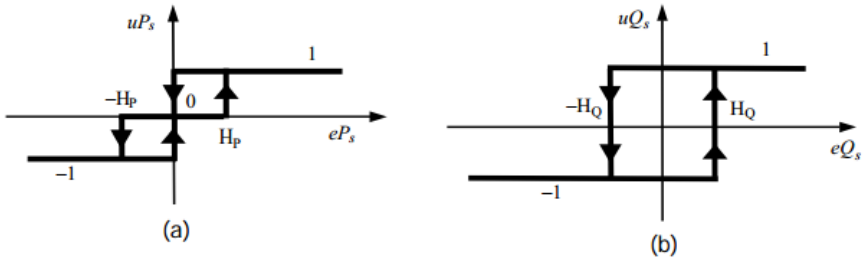

Figure 4.42. ON-OFF P_s and Q_s controller with hystersis band.

Once the uP_s and uQ_s signals are defined by means of the ON-OFF controllers, together with the information about the rotor flux space vector position it is possible to select the rotor voltage vector using the look up table

Table 9. Voltage vector selection according to compartor output

		uP_s		
		1	**0**	**1**
uQ_s	**1**	$V_{(k-2)}$	V_0, V_7	$V_{(k+2)}$
	-1	$V_{(k-1)}$	V_0, V_7	$V_{(k+1)}$

The voltage vectors are selected from the ON-OFF controllers and the sector in which the rotor space vector is located and similar to the DTC only four active vectors are permitted $(V_{(k-2)}, V_{(k-1)}, V_{(k+1)}, V_{(k+2)})$ and the zero vector (V_0, V_7). However DPC produces both P_s and $Q_s$variation as shown in Figure 4.43.

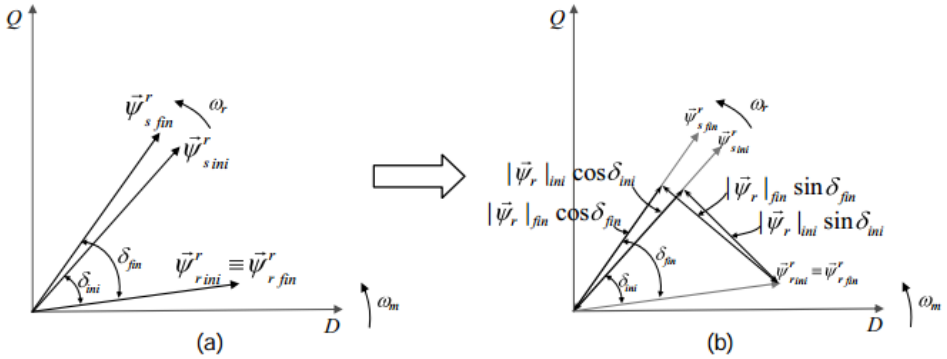

Figure 4.43. P_s and Q_s increase due to zero vector insertion [67].

Pulse Generation

Similar to DTC, once the vector that corrects the stator power error is selected, and the pulses for the controlled semiconductors of the two-level VSC are created according to the table.

Table 10. Pulse generation according to voltage vector.

Vector	S_a	S_a	S_a
V_0	0	0	0
V_1	1	0	0
V_2	1	1	0
V_3	0	1	0
V_4	0	1	1
V_5	0	0	1
V_6	1	0	1
V_7	1	1	1

Stator Power Waveforms

Figure 4.44 illustrates the stator active and reactive power waveforms. One major difference from the DTC scheme is that when zero vector is injected the reactive power varies.

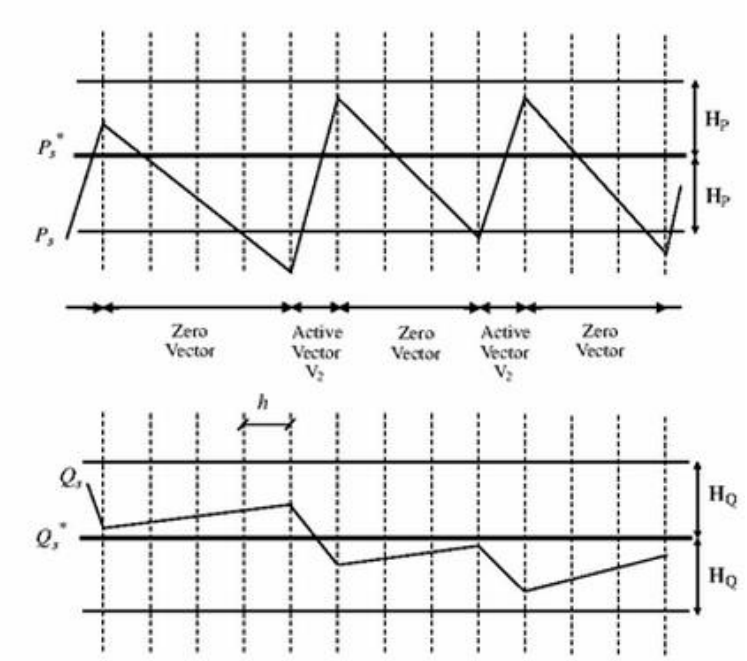

Figure 4.44. Steady state P_s and Q_s waveforms [61].

Case Study

This example shows a 2 MW DFIG, controlled by the DPC technique described in this section. Both the hysteresis band of the ON-OFF controllers is set to 2.5% of the rated power. The machine operates ate hypersynchronous speed of 1875 rev/min (synchronous speed is 1550 rev/min). The DC bus voltage of the back-to-back converter is controlled to 1000 V by the grid side converter.

At the beginning of the experiment the machine operates as a generator delivering nominal active power. The reactive power reference is set to zero. At 4.5 secs of the experiment the, the active power is reversed to positive, so that the machine begins to operate as a motor. This experiment shows the steady and transient performances with the DPC. The following Figures 4.45 to 4.50 illustrate P_s and Q_s behavior, when the DFIM is connected directly to the grid through the stator. In the middle of the experiment, P_s is reversed from negative (generator) to positive (motor). A very quick and safe response is seen, since P_s reaches the new reference value without further overshoot than that defined by the hysteresis band. Finally the stator and rotor current behaviors are shown. The rotor current in Figure 4.45 shows a tiny overshoot but the stator voltages and current do not show any overshoot despite the severe change in power demand.

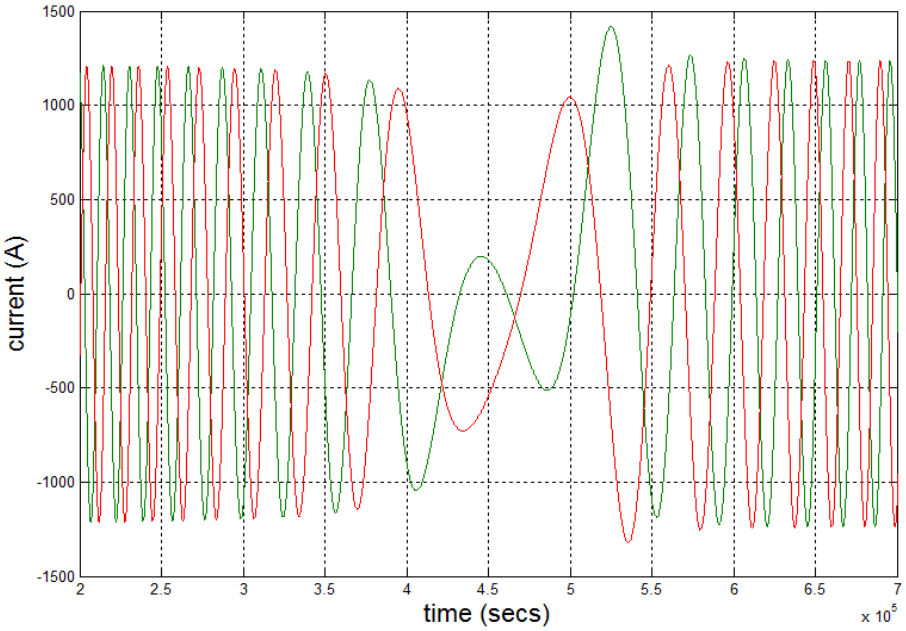

Figure 4.45. *ab* rotor currents.

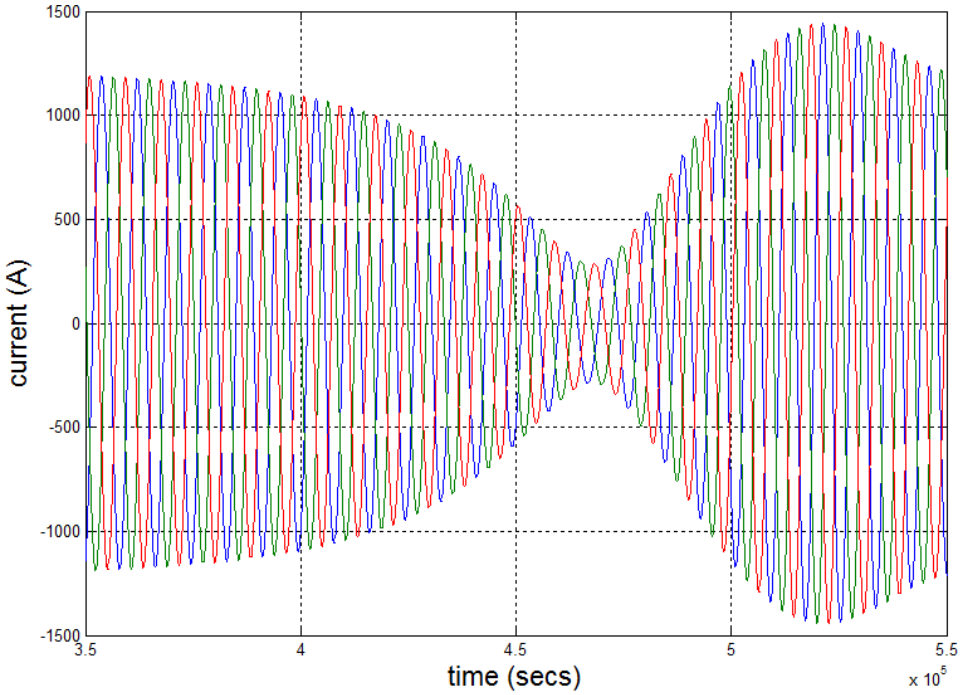

Figure 4.46. *abc* stator current.

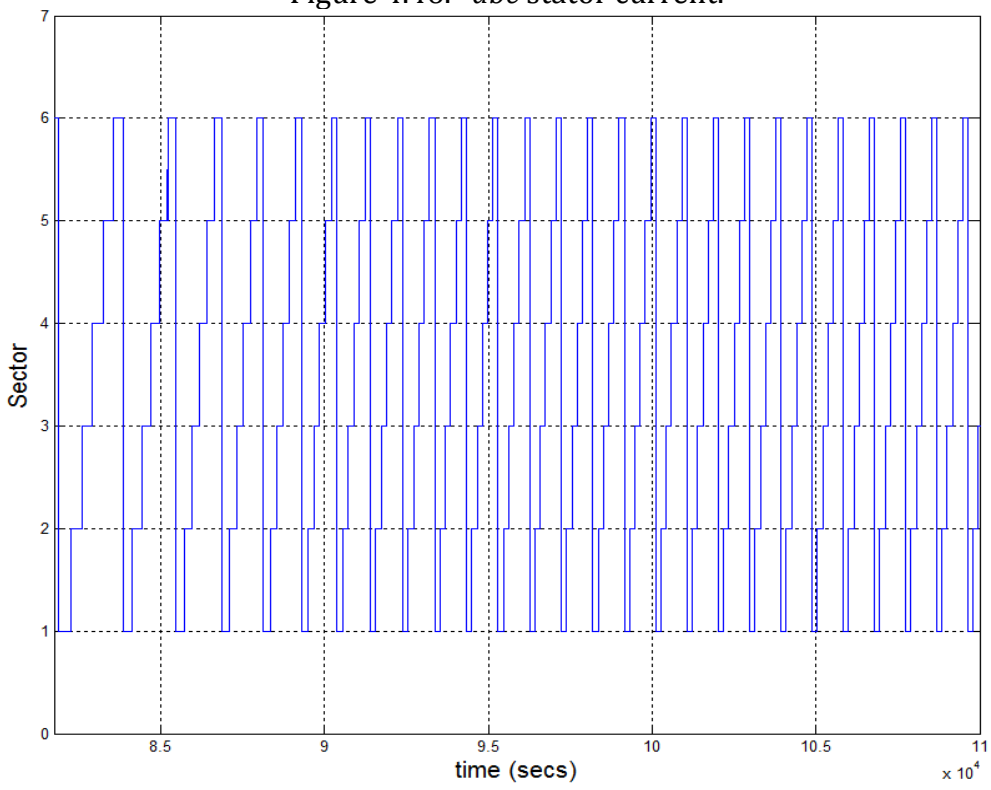

Figure 4.47. Sector.

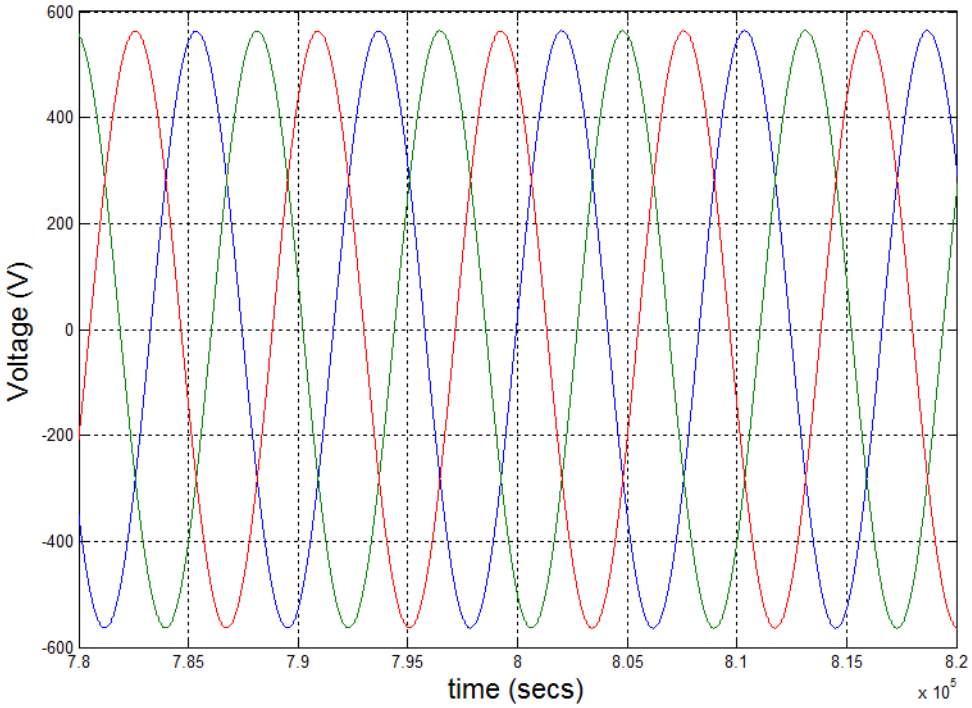

Figure 4.48. *abc* stator voltages.

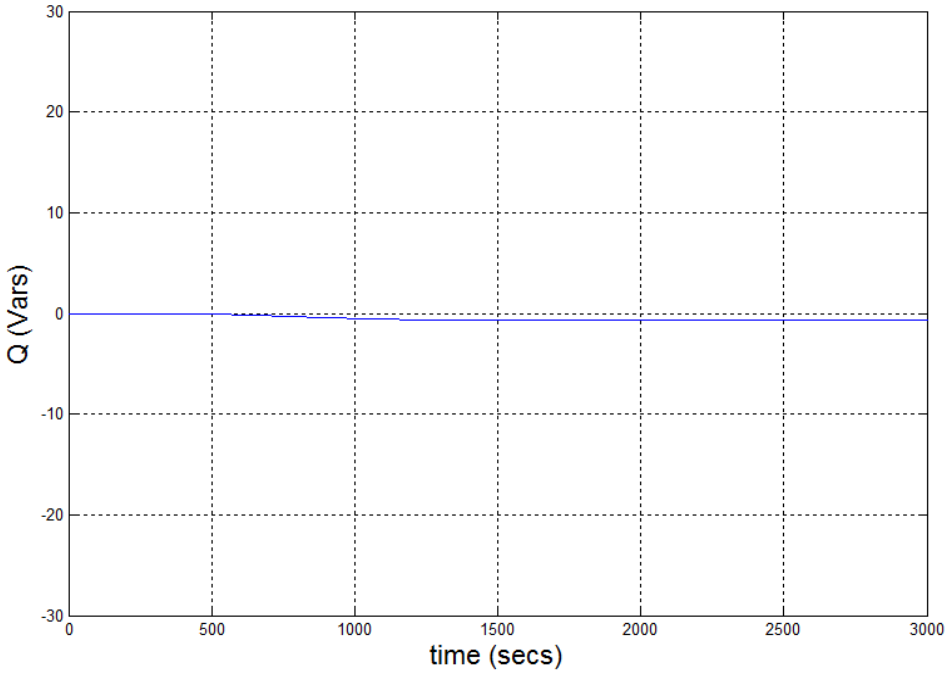

Figure 4.49. Reactive power.

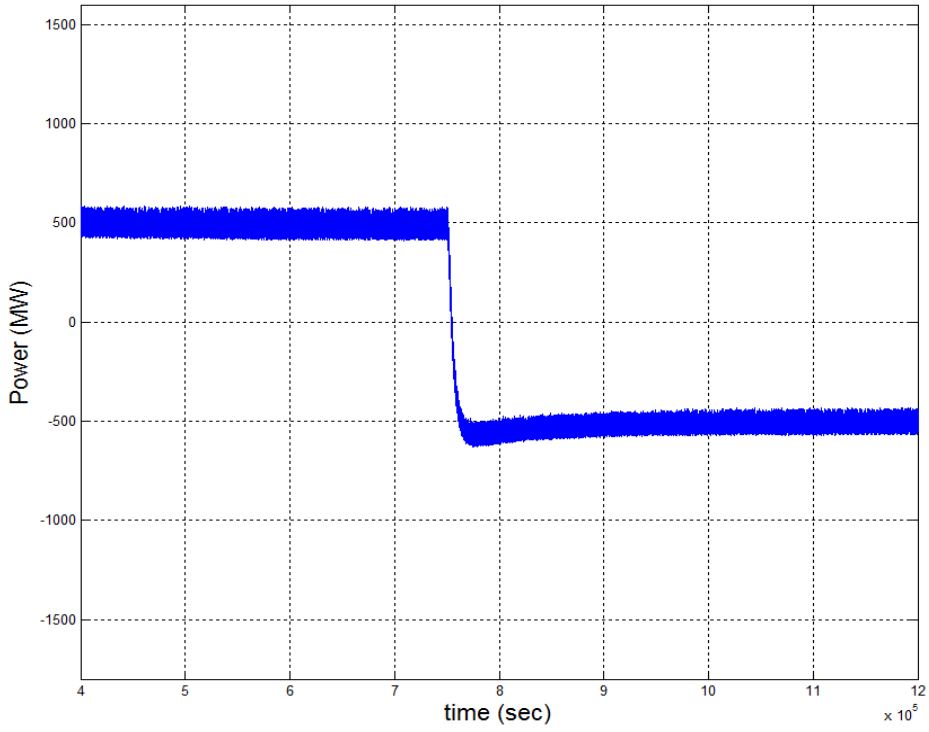

Figure 4.50. Stator active power.

4.6 Summary

In this chapter we introduced the work-horse of the wind energy industry, the doubly-fed induction generator. The DFIG has several advantages over the regular squirrel cage induction generator and hence it is widely used in today's industry. The main advantages include reduced capacity converters used in the DFIG systems and direct interconnection of the stator to the grid. Another advantage of the DFIG was the constant voltage and frequency of the stator irrespective of the wind speed.

Further the back-to-back converter used in the DFIG systems based on the two level topology and multilevel topology was explained. The complete grid side system was explained and analyzed with modelling of the back-to-back converter was done with an analysis of the switching strategy of the converter.

The steady state model of the DFIG was developed further in this chapter and it was analyzed through investigating the equivalent circuit of the machine. The operating modes

and the power flows were understood by learning about the basic power, torque the four quadrant operations.

Ahead, the most important dynamic model of the doubly fed induction machine was developed in the three reference frames namely, the $\alpha\beta$ (stationary), dq (synchronous) and the DQ (rotor) reference frame and these models were tested by simulating them on Simulink platform. Control of the grid connected DFIG is mandatory and hence vector control strategies were developed by introducing vector control for the DFIG. The current loops and calculation of the current references were explained and the direct control strategies namely the direct torque control (DTC) and the direct power control (DPC) were developed. The complete systems are thoroughly explained by developing the models and simulation results confirm that these strategies work well during the steady state and the dynamic operation of the DFIG.

CHAPTER 5 Summary

This thesis presents important aspects of integrating the wind energy systems with the grid. The specific goals of this study, based on chapters 1 to 5, can be summarized as follows:

- Explaining the basics of wind energy systems with advantages and disadvantages and stressing on the importance of wind energy systems.
- Introducing different wind energy system topologies to explore more opportunities of wind energy systems.
- Elaborating on the power electronics converters which are used to interface wind energy generators with the grid.
- Suggesting a ideal topology of the converter based on the rating of the generators used in the wind energy system and type of conversion needed.
- Suggesting switching strategies for the converters described which give optimum switching and best output.
- Simulating the working of the converters using MATLAB/SIMULINK software and comparing the switching strategies by observing and analyzing the output waveforms.
- Developing a model for the grid connected inverter using the space vector modulation technique based on the voltage oriented control strategy.
- Developing a dynamic model for the squirrel cage induction generator based on the linear dynamic model of the generator.
- Developing a dynamic flux and torque equations for the induction generator.
- Introducing a vector control for the induction generators and stating its advantages over the regular scalar (v/f) control.
- Explaining the field oriented control strategy used for the induction generators based on the direct and indirect detection of the rotor flux angle.

- Developing the simulation models for the both direct and indirect field oriented control strategies and investigating the behavior of the strategies under steady state and transient state.
- Introducing the direct torque technique for the induction generator and explaining the complete control strategy.
- Developing the simulation model for the direct torque control technique and simulation the system under steady and transient state and analyzing the behavior of the system.
- Introducing the doubly-fed induction generators used in the wind energy systems and explaining the operation of the generators and specifying the specific advantages if has over the squirrel cage generators.
- Explaining the operation of the two-level back to back converter with modeling the converter with its interface with the DFIG
- Developing the dynamic model for the DFIG based on the equivalent circuit in stationary, rotor and synchronous reference frame and analyzing the performance of a 2MW DFIG in the different reference frames.
- Explaining the vector control of the DFIG.
- Describing the direct control techniques, namely the direct torque control and the direct power control and developing simulation models for the control strategies and analyzing the behavior of the system under steady and transient conditions.

The most significant achievements of this thesis can be summarized as follows:

- After analyzing the operation of power converters namely, AC voltage controllers, DC/DC converters and voltage source converters, it was seen that using power electronics for interfacing the wind energy systems into the grid provides a lot of advantages over direct connection to the grid.
- Using power converters provides advantages like low inrush current, adjusting the voltage level for the grid tied inverter, constant frequency voltage and constant voltage amplitude, active and reactive power control.

- Choosing the space vector modulation strategy ensures minimum amount of switching, thus reducing the switching loses and providing least harmonic distortion.
- Simulated waveforms of the direct and indirect field oriented control of prove that the steady and transient operation results are both exactly similar to each other and both the strategies perform well under transients without overshoot of any parameters.
- The values obtained through theoretical analysis and simulation results match, which proves that the simulation results obtained are correct.
- Analysis of the waveforms obtained through DTC strategy proves that the strategy performs well under steady and transient situations and the parameters fixed by the hysteresis comparators prevent any overshoot of parameters and values obtained through theoretical analysis and simulation results match, which proves that the simulation results obtained are correct.
- The developed $\alpha\beta$ and the dq dynamic models in the form of differential equations and the state-space representation, used for simulation models emphasized the different peculiarities and characteristic aspects of the DFIG.
- The vector control showed how active and reactive power regulated by the control strategy. The currents were perfectly regulated by the current control loops.
- The performance of the direct control technique's, which is a valid alternative to vector control is, was very similar to each other and hence making both these strategies a very valid controls for a realistic wind generation environment.
- The output waveforms of the DTC and DPC strategies show that the system works well under steady state and transient conditions without the overshoot of any parameters and hence prototyping can be done based on these strategies.

5.1 Future work

The only shortcomings of field oriented control and the direct control methods are the non-constant switching pattern. This can be overcome by advanced and more complicated control strategies like Predictive Direct Torque Control (PDTC) and Predictive Direct Power Control (PDPC). Also predictive techniques can be designed in such a way that the converters operate at a considerably low switching frequency, reducing the electromagnetic ripples and rotor flux ripples.

Appendix

Dynamic Modeling of DFIG

Here we will model the DFIG dynamically and examine the transient behavior for in-depth machine control. In order to control the machine in all states, it is mandatory to bring the machine back to the steady state when the machine is in a different state. The dynamic behavior of the machine explains the machines variables in transition periods and this dynamic behavior is studied by a dynamic model. By means of the dynamic model it is possible to know the continuous performance of the variables of the machine such as torque, current, and flux. We will use this dynamic model represented in differential equations as compact set of model equations for our simulation study[61].

The simplified and idealized stator voltages

$$v_{as} = R_s i_{as}(t) + \frac{d\Psi_{\mathrm{as}}(t)}{dt} \quad \text{(A. 1)}$$

$$v_{as} = R_s i_{bs}(t) + \frac{d\Psi_{\mathrm{bs}}(t)}{dt} \quad \text{(A. 1)}$$

$$v_{as} = R_s i_{cs}(t) + \frac{d\Psi_{\mathrm{cs}}(t)}{dt} \quad \text{(A. 3)}$$

Where

$R_s$is the Stator Resistance

$i_{as}(t), i_{bs}(t), i_{cs}(t)$ are the stator currents of phases a, b, c

$v_{as}(t), v_{bs}(t), v_{cs}(t)$ are the applied stator voltages

$\Psi_{as}, \Psi_{bs}, \Psi_{cs}$ are the stator fluxes

Similarly, the rotor magnitudes are described by

$$v_{ar} = R_s i_{ar}(t) + \frac{d\Psi_{\mathrm{ar}}(t)}{dt} \quad \text{(A. 4)}$$

$$v_{br} = R_s i_{br}(t) + \frac{d\Psi_{\mathrm{br}}(t)}{dt} \quad \text{(A.5)}$$

$$v_{cr} = R_s i_{cr}(t) + \frac{d\Psi_{\mathrm{cr}}(t)}{dt} \quad \text{(A. 6)}$$

$R_r$is the Rotor Resistance

$i_{ar}(t), i_{br}(t), i_{cr}(t)$ are the rotor currents of phases a, b, c

$v_{ar(t)}, v_{br(t)}, v_{cr(t)}$ are the applied Rotor voltages

$\Psi_{ar}, \Psi_{br}, \Psi_{cr}$ are the Rotor fluxes[57, 60, 64]

α-β Model

The differential equations representing the model of the DFIG using the Space vector notation are derived in the Stator Reference Frame

Multiplying equations (1) and (4) by $\frac{2}{3}$,(2) and (5) by $\frac{2}{3}a$ and (3) and (6) by $\frac{2}{3}a^2$

We get the voltage equations in space vector form

$$\overrightarrow{v^s}_s = R_s \vec{i}^s{}_s + \frac{d\overrightarrow{\Psi_{\mathrm{s}}^s}}{dt} \quad \text{(A. 7)}$$

$$\overrightarrow{v^r}_r = R_r \vec{i}^r{}_r + \frac{d\overrightarrow{\Psi_{\mathrm{r}}^r}}{dt} \quad \text{(A. 8)}$$

The correlation between the fluxes and the currents is given by

$$\overrightarrow{\Psi}_{\mathrm{s}}^s = L_s \vec{i}^s{}_s + L_m \vec{i}^r{}_r \quad \text{(A. 8)}$$

$$\overrightarrow{\Psi}_{\mathrm{r}}^r = L_m \vec{i}^r{}_s + L_r \vec{i}^r{}_r \quad \text{(A. 10)}$$

Where L_s *and* L_r are stator and rotor inductances

$$L_s = L_{\sigma s} + L_m \quad \text{(A. 11)}$$

$$L_r = L_{\sigma r} + L_m \tag{A. 12}$$

Substituting the values of Stator and Rotor Inductances values in the values of the fluxes

$$\overrightarrow{\Psi}_s^s = L_s \vec{\imath}^s{}_s + L_m \vec{\imath}^r{}_r = L_s \vec{\imath}^s{}_s + L_m \, e^{j\theta_m} \vec{\imath}^r{}_r \tag{A. 13}$$

$$\overrightarrow{\Psi}_r^r = L_m \vec{\imath}^r{}_s + L_r \vec{\imath}^r{}_r = L_m e^{-j\theta_m} \vec{\imath}^r{}_s + L_r \vec{\imath}^r{}_r \tag{A. 14}$$

Thus the $\alpha\beta$ model is obtained by the following equations in the stator coordinates

$$\vec{v}_s^s = R_s \vec{\imath}^s{}_s + \frac{d\overrightarrow{\Psi_s^s}}{dt} \tag{A. 15}$$

$$\vec{v}_r^s = R_r \vec{\imath}^s{}_r + \frac{d\overrightarrow{\Psi_r^s}}{dt} - j\omega_m \overrightarrow{\Psi_r^s} \tag{A. 16}$$

$$\overrightarrow{\Psi}_s^s = L_s \vec{\imath}^s{}_s + L_m \vec{\imath}^s{}_r \tag{A. 17}$$

$$\overrightarrow{\Psi}_r^r = L_m \vec{\imath}^r{}_s + L_r \vec{\imath}^r{}_r \tag{A. 18}$$

Deriving the electric powers on the stator and rotor side for the model

$$P_s = \frac{3}{2} \mathrm{Re}\,\{\overrightarrow{v_s} * \overrightarrow{\imath_s}\} = \frac{3}{2}\,(v_{\alpha s} i_{\alpha s} + v_{\beta s} i_{\beta s}) \tag{A. 19}$$

$$P_r = \frac{3}{2} \mathrm{Re}\,\{\overrightarrow{v_r} * \overrightarrow{\imath_r}\} = \frac{3}{2}\,(v_{\alpha r} i_{\alpha r} + v_{\beta r} i_{\beta r}) \tag{A. 20}$$

$$Q_s = \frac{3}{2} \mathrm{Im}\,\{\overrightarrow{v_s} * \overrightarrow{\imath_s}\} = \frac{3}{2}\,(v_{\alpha s} i_{\alpha s} + v_{\beta s} i_{\beta s}) \tag{A. 21}$$

$$P_s = \frac{3}{2} \mathrm{Im}\,\{\overrightarrow{v_r} * \overrightarrow{\imath_r}\} = \frac{3}{2}\,(v_{\alpha r} i_{\alpha r} + v_{\beta r} i_{\beta r}) \tag{A. 23}$$

Finally the electromagnetic torque can be found from

$$T_{em} = \frac{3}{2}\, p\, \mathrm{Im}\left\{\overrightarrow{\Psi}_r^r * \overrightarrow{\imath_r}\right\} = \frac{3}{2}\,(\Psi_{\beta r} i_{\alpha r} + \Psi_{\alpha r} i_{\beta r}) \tag{A. 24}$$

d-q Model

In Contrast to the $\alpha\beta$ model the equations representing the model of the DFIG are derived in the synchronous reference frame. From the original voltage equations, multiplying them by $e^{-j\theta_s}$and $e^{-j\theta_r}$ the stator and rotor equations yields

$$\vec{V}_s^a = R_s\vec{i_s^a} + \frac{d\overrightarrow{\Psi_s^a}}{dt} + j\omega_s\overrightarrow{\Psi_s^a} \tag{A. 25}$$

$$\vec{V}_r^a = R_r\vec{i_r^a} + \frac{d\overrightarrow{\Psi_r^a}}{dt} + j\omega_r\overrightarrow{\Psi_r^a} \tag{A.26}$$

The subscript "a" denotes space vectors referred to a synchronously rotating

Using the same flux expression we find

$$\overrightarrow{\Psi_s^a} = L_s\vec{i}^a{}_s + L_m\vec{i}^a{}_r \tag{A. 27}$$

$$\overrightarrow{\Psi_r^a} = L_m\vec{i}^a{}_s + L_r\vec{i}^a{}_r \tag{A. 28}$$

The dq components have constant values for sinusoidal voltages where as the $\alpha\beta$ components that are sinusoidal magnitudes.

The torque and power expressions in the dq reference frame are equivalent to the $\alpha\beta$ equations [57, 60, 64]

$$P_s = \frac{3}{2}\mathrm{Re}\,\{\overrightarrow{v_s} * \overrightarrow{i_s}\} = \frac{3}{2}\,(v_{ds}i_{\alpha ds} + v_{qs}i_{qs}) \tag{A. 29}$$

$$P_r = \frac{3}{2}\mathrm{Re}\,\{\overrightarrow{v_r} * \overrightarrow{i_r}\} = \frac{3}{2}\,(v_{dr}d + v_{qr}i_{qr}) \tag{A. 30}$$

$$Q_s = \frac{3}{2}\mathrm{Im}\,\{\overrightarrow{v_s} * \overrightarrow{i_s}\} = \frac{3}{2}\,(v_{qs}i_{ds} + v_{ds}i_{qs}) \tag{A. 31}$$

$$P_s = \frac{3}{2}\mathrm{Im}\,\{\overrightarrow{v_r} * \overrightarrow{i_r}\} = \frac{3}{2}\,(v_{qr}i_{dr} + v_{dr}i_{qr}) \tag{A. 32}$$

And the torque expressions also yields

$$T_{em} = \frac{3}{2}\, p\, \frac{L_m}{L_s}\, \mathrm{Im}\left\{\vec{\Psi}_s * \vec{i_r}\right\} = \frac{3}{2}\, p\, \frac{Lm}{Ls}\left(\Psi_{qr} i_{dr} + \Psi_{dr} i_{qr}\right) \tag{A. 33}$$

For the sake of simplicity the subscripts have been omitted

State Space Representation of the *α-β* Model and Simulation Block Diagram

The state space model which we are going to use for our computer simulation is as follows.

$$\frac{d}{dt}\begin{bmatrix}\vec{\psi_S^s}\\ \vec{\psi_r^s}\end{bmatrix} = \begin{bmatrix} -\frac{R_s}{\sigma L_s} & \frac{R_s L_m}{\sigma L_s L_r} \\ \frac{R_s L_m}{\sigma L_s L_r} & -\frac{R_r}{\sigma L_r} + j\omega_m \end{bmatrix} \cdot \begin{bmatrix}\vec{\psi_S^s}\\ \vec{\psi_S^s}\end{bmatrix} + \begin{bmatrix}\vec{v_S^s}\\ \vec{v_r^s}\end{bmatrix} \tag{A. 34}$$

Expanding this expression in the $\alpha\beta$ components

$$\frac{d}{dt}\begin{bmatrix}\psi_{\alpha s}\\ \psi_{\beta s}\\ \psi_{\alpha r}\\ \psi_{\beta r}\end{bmatrix} = \begin{bmatrix} -\frac{R_s}{\sigma L_s} & 0 & \frac{R_s L_m}{\sigma L_s L_r} & 0 \\ 0 & -\frac{R_s}{\sigma L_s} & 0 & \frac{R_s L_m}{\sigma L_s L_r} \\ \frac{R_s L_m}{\sigma L_s L_r} & 0 & -\frac{R_s}{\sigma L_s} & 0 \\ 0 & \frac{R_s L_m}{\sigma L_s L_r} & 0 & -\frac{R_s}{\sigma L_s} \end{bmatrix} \cdot \begin{bmatrix}\psi_{\alpha s}\\ \psi_{\beta s}\\ \psi_{\alpha r}\\ \psi_{\beta r}\end{bmatrix} + \begin{bmatrix}v_{\alpha s}\\ v_{\beta s}\\ v_{\alpha r}\\ v_{\beta r}\end{bmatrix} \tag{A. 35}$$

If, instead of the fluxes the currents are chosen as state space magnitudes, the equivalent model of the DFIM is derived as follows [67]

$$\begin{aligned}\frac{d}{dt}\begin{bmatrix}\vec{i_S^s}\\ \vec{i_r^s}\end{bmatrix} = &\left(\frac{1}{\sigma L_s L_r}\right)\begin{bmatrix} -R_s L_r - j\omega_m L_m^2 & -R_r L_m - j\omega_m L_m L_r \\ R_s L_m + j\omega_m L_m L_s & -R_s L_r - j\omega_m L_r\, L_s \end{bmatrix} \cdot \begin{bmatrix}\vec{i_S^s}\\ \vec{i_r^s}\end{bmatrix} \\ &+ \left(\frac{1}{\sigma L_s L_r}\right)\begin{bmatrix} L_r & -L_m \\ -L_m & L_s \end{bmatrix} \cdot \begin{bmatrix}\vec{v_S^s}\\ \vec{v_r^s}\end{bmatrix}\end{aligned} \tag{A. 36}$$

Expanding this expression in the $\alpha\beta$ components

$$\frac{d}{dt}\begin{bmatrix} i_{\alpha s} \\ i_{\beta s} \\ i_{\alpha r} \\ i_{\beta r} \end{bmatrix} = \left(\frac{1}{\sigma L_s L_r}\right)\begin{bmatrix} -R_s L_r & \omega_m L_m^2 & R_r L_m & \omega_m L_m L_r \\ -\omega_m L_m^2 & -R_s L_r & -\omega_m L_m L_r & R_r L_m \\ R_s L_m & -\omega_m L_m L_s & -R_s L_r & -\omega_m L_r\, L_s \\ \omega_m L_m L_s & R_s L_m & \omega_m L_r\, L_s & -R_s L_r \end{bmatrix}.\begin{bmatrix} i_{\alpha s} \\ i_{\beta s} \\ i_{\alpha r} \\ i_{\beta r} \end{bmatrix} + \left(\frac{1}{\sigma L_s L_r}\right)\begin{bmatrix} L_r & 0 & -L_m & 0 \\ 0 & L_r & 0 & L_m \\ -L_m & 0 & L_s & 0 \\ 0 & L_m & 0 & L_s \end{bmatrix} \quad \text{(A. 37)}$$

Depending upon choice of the state space magnitudes, different state-space models can be obtained.

Bibliography

[1] T. Ackermann, *Wind power in power systems*: Wiley Online Library, 2005.

[2] S. Heier, and R. Waddington, *Grid integration of wind energy conversion systems*: Wiley New York, 1998.

[3] M. R. Patel, *Wind and solar power systems: design, analysis, and operation*: CRC press, 2005.

[4] M. Liserre, T. Sauter, and J. Y. Hung, "Future energy systems: Integrating renewable energy sources into the smart power grid through industrial electronics," *Industrial Electronics Magazine, IEEE*, vol. 4, no. 1, pp. 18-37, 2010.

[5] B. Wu *et al.*, *Power conversion and control of wind energy systems*: Wiley. com, 2011.

[6]

[7] E. Hau, and H. Platz, "Wind Turbines-Fundamentals, Technologies, Application, Economics," 2000.

[8] E. Hau, *Windturbines*: Springer Berlin etc., 2000.

[9] EnergyBC, "Darrieus Wind turbine."

[10] M. Ragheb, "COMPONENTS OF WIND MACHINES," 2014.

[11] D. McGahn, "Direct Drive Generators," *High Temperature Superconductor Based Machines*, American Superconductor.

[12] A. Ragheb, and M. Ragheb, "Wind turbine gearbox technologies." pp. 1-8.

[13] F. Iov, and F. Blaabjerg, "Power electronics for renewable energy systems." pp. 9-12.

[14] F. Blaabjerg *et al.*, "Power electronics in renewable energy systems." pp. 1-17.

[15] F. Blaabjerg *et al.*, "Power electronics in wind turbine systems." pp. 1-11.

[16] B. Wu, *High-power converters and AC drives*: Wiley. com, 2006.

[17] M. H. Rashid, *Power electronics handbook*: Academic Pr, 2001.

[18] N. Yamamura, M. Ishida, and T. Hori, "A simple wind power generating system with permanent magnet type synchronous generator." pp. 849-854.

[19] A. Faulstich, J. Stinke, and F. Wittwer, "Medium voltage converter for permanent magnet wind power generators up to 5 MW." pp. 9 pp.-P. 9.

[20] J. Birk, and B. Andresen, "Parallel-connected converters for optimizing efficiency, reliability and grid harmonics in a wind turbine." pp. 1-7.

[21] A. S. Mikhail *et al.*, "Variable speed distributed drive train wind turbine system," Google Patents, 2006.

[22] B. K. Bose, *Modern power electronics and AC drives*: Prentice hall USA, 2002.

[23] F. Blaabjerg, and Z. Chen, "Power electronics for modern wind turbines," *Synthesis Lectures on Power Electronics,* vol. 1, no. 1, pp. 1-68, 2005.

[24] A. M. Trzynadlowski, *Introduction to modern power electronics*: John Wiley & Sons, 2010.

[25] P. H. Tran, "MATLAB/SIMULINK Implementation and Analysis of Three Pulse-width-modulation (PWM) Techniques," Boise State University, 2012.

[26] H. Abu-Rub, A. Iqbal, and J. Guzinski, *High performance control of AC drives with Matlab/Simulink models*: Wiley-Interscience, 2012.

[27] R. Melício, V. Mendes, and J. Catalão, "Modeling and simulation of wind energy systems with matrix and multilevel power converters," *Latin America Transactions, IEEE (Revista IEEE America Latina),* vol. 7, no. 1, pp. 78-84, 2009.

[28] "Current Source Inverter ".

[29] B. Wu, "Current Source Rectifiers," 2006

[30] L. Xu, "Control of power converter for grid integration of renewable energy conversion and STATCOM systems," The University of Alabama TUSCALOOSA, 2009.

[31] S. Nath, and S. Rana, "The Modeling and Simulation of Wind Energy Based Power System using MATLAB," *International Journal of Power System Operation and Energy Management,* vol. 1, 2011.

[32] S.-H. Song, S.-i. Kang, and N.-k. Hahm, "Implementation and control of grid connected AC-DC-AC power converter for variable speed wind energy conversion system." pp. 154-158.

[33] P. Matić, A. Rakić, and S. N. Vukosavić, "Space vector representation of induction motor model in field weakening regime," *Serbian Journal of Electrical Engineering,* vol. 9, no. 1, pp. 53-61, 2012.

[34] J. L. Dominguez Garcia, "Modeling and control of squirrel cage induction generator with full power converter applied to windmills," 2010.

[35] A. Kishore, and G. S. Kumar, "A Generalized State-Space Modeling of Three Phase Self-Excited Induction Generator For Dynamic Characteristics and Analysis." pp. 1-6.

[36] M. Pucci, "State space-vector model of linear induction motors." pp. 2654-2661.

[37] J. Domínguez-García *et al.*, "Vector control of squirrel cage induction generator for wind power." pp. 1-6.

[38] T. A. Lipo, *Vector control and dynamics of AC drives*: Oxford University Press, 1996.

[39] W. Emar *et al.*, “V/F Control of Squirrel Cage Induction Motor Drives Without Flux or Torque Measurement Dependency,” *International Journal of Robotics and Automation (IJRA),* vol. 2, no. 2, pp. 77, 2011.

[40] A. M. Trzynadlowski, *The field orientation principle in control of induction motors*: Springer, 1993.

[41] A. M. Trzynadlowski, *Control of induction motors*: Academic Pr, 2001.

[42] H. Kubota, K. Matsuse, and T. Nakano, “DSP-based speed adaptive flux observer of induction motor,” *Industry Applications, IEEE Transactions on,* vol. 29, no. 2, pp. 344-348, 1993.

[43] J. L. Domínguez-García *et al.*, “Indirect vector control of a squirrel cage induction generator wind turbine,” *Computers & Mathematics with Applications,* vol. 64, no. 2, pp. 102-114, 2012.

[44] D. Fu, and Y. Xing, "Study on linear dynamic model and analysis of operating characteristics of high-power vscf wind energy conversion system." pp. 1-6.

[45] R.-J. Wai, and K.-M. Lin, “Robust decoupled control of direct field-oriented induction motor drive,” *Industrial Electronics, IEEE Transactions on,* vol. 52, no. 3, pp. 837-854, 2005.

[46] P. A. De Wit, R. Ortega, and I. Mareels, “Indirect field-oriented control of induction motors is robustly globally stable,” *Automatica,* vol. 32, no. 10, pp. 1393-1402, 1996.

[47] G. Singh, K. Nam, and S. Lim, “A simple indirect field-oriented control scheme for multiphase induction machine,” *Industrial Electronics, IEEE Transactions on,* vol. 52, no. 4, pp. 1177-1184, 2005.

[48] H. Le-Huy, "Comparison of field-oriented control and direct torque control for induction motor drives." pp. 1245-1252.

[49] P. Vas, *Vector control of AC machines*: Clarendon press Oxford, 1990.

[50] P. Vas, “Sensorless vector and direct torque control,” 1998.

[51] T. G. Habetler *et al.*, “Direct torque control of induction machines using space vector modulation,” *Industry Applications, IEEE Transactions on,* vol. 28, no. 5, pp. 1045-1053, 1992.

[52] G. S. Buja, and M. P. Kazmierkowski, “Direct torque control of PWM inverter-fed AC motors-a survey,” *Industrial Electronics, IEEE Transactions on,* vol. 51, no. 4, pp. 744-757, 2004.

[53] J. N. Nash, “Direct torque control, induction motor vector control without an encoder,” *Industry Applications, IEEE Transactions on,* vol. 33, no. 2, pp. 333-341, 1997.

[54] C. G. Mei *et al.*, "Direct torque control of induction motor-variable switching sectors." pp. 80-85.

[55] R. Gabriel, W. Leonhard, and C. J. Nordby, “Field-oriented control of a standard AC motor using microprocessors,” *Industry Applications, IEEE Transactions on*, no. 2, pp. 186-192, 1980.

[56] b. t. s. o. L.-V. Ltd., "Principles of Doubly-Fed Induction Generators (DFIG) ", May 2011.

[57] A. P. Lozano, “ANALYSIS, MODELLING AND CONTROL OF A DOUBLY-FED INDUCTION GENERATOR FOR LARGE WIND TURBINES.”

[58] S. Muller, M. Deicke, and R. W. De Doncker, “Doubly fed induction generator systems for wind turbines,” *Industry Applications Magazine, IEEE,* vol. 8, no. 3, pp. 26-33, 2002.

[59] H. Ø. Røstøen, T. M. Undeland, and T. Gjengedal, "Doubly-fed induction generator in a wind turbine."

[60] A. Petersson, “Analysis, modeling and control of doubly-fed induction generators for wind turbines,” Chalmers University of Technology, 2005.

[61] G. Abad, L. Marroyo, and G. Iwanski, *Doubly fed induction machine: modeling and control for wind energy generation*: Wiley. com, 2011.

[62] R. Pena, J. Clare, and G. Asher, “Doubly fed induction generator using back-to-back PWM converters and its application to variable-speed wind-energy generation,” *IEE Proceedings-Electric Power Applications,* vol. 143, no. 3, pp. 231-241, 1996.

[63] A. Tapia *et al.*, “Modeling and control of a wind turbine driven doubly fed induction generator,” *Energy Conversion, IEEE Transactions on,* vol. 18, no. 2, pp. 194-204, 2003.

[64] Y. Lei *et al.*, “Modeling of the wind turbine with a doubly fed induction generator for grid integration studies,” *Energy Conversion, IEEE Transactions on,* vol. 21, no. 1, pp. 257-264, 2006.

[65] S. M. Skeist, and R. H. Baker, "Doubly fed induction machine," Google Patents, 2005.

[66] J. Yao *et al.*, “An improved control strategy of limiting the DC-link voltage fluctuation for a doubly fed induction wind generator,” *Power Electronics, IEEE Transactions on,* vol. 23, no. 3, pp. 1205-1213, 2008.

[67] G. Abad *et al.*, “Direct power control of doubly-fed-induction-generator-based wind turbines under unbalanced grid voltage,” *Power Electronics, IEEE Transactions on,* vol. 25, no. 2, pp. 442-452, 2010.

[68] D. Xiang *et al.*, “Control of a doubly fed induction generator in a wind turbine during grid fault ride-through,” *Energy Conversion, IEEE Transactions on,* vol. 21, no. 3, pp. 652-662, 2006.